Structure-function analysis of centromeres in the *Cryptococcus* species complex

A thesis submitted for the degree of

Doctor of Philosophy

By

Vikas Yadav

Molecular Biology and Genetics Unit

Jawaharlal Nehru Centre for Advanced Scientific Research

Jakkur, Bangalore

560064

August 2017

Dedicated to my parents and sister

DECLARATION

I do hereby declare that the work described here in this thesis titled '**Structure-function analysis of centromeres in the *Cryptococcus* species complex**' has originally been carried out by myself under the guidance and supervision of **Kaustuv Sanyal**, Professor, Molecular Biology and Genetics Unit, Jawaharlal Nehru Centre for Advanced Scientific Research, Bangalore-560064, India. In keeping with the norm of reporting the scientific observations, due acknowledgements have been made whenever the work described was carried out in collaboration with other researchers. Any omission, which might have occurred by oversight or misjudgement, is regretted.

Vikas Yadav

Place: Bangalore

Date: 28/6/17

Jawaharlal Nehru Center for Advanced Scientific Research

Jakkur Post
Bangalore 560 064
INDIA

Tel: +91 (80) 2208 2878
Fax: +91 (80) 2208 2766

Kaustuv Sanyal *PhD, FASc, FNASc*
Professor
Molecular Mycology Laboratory
Molecular Biology & Genetics Unit

Email: sanyal@jncasr.ac.in
Web: http://www.jncasr.ac.in/sanyal/

28 August 2017

Certificate

This is to certify that the work described in this thesis titled '**Structure-function analysis of centromeres in the *Cryptococcus* species complex**' is the result of investigations carried out by **Mr. Vikas Yadav** in the Molecular Biology and Genetics Unit, Jawaharlal Nehru Centre for Advanced Scientific Research, Bangalore, India, under my supervision and guidance. The results presented here have not previously formed the complete basis for the award of any other diploma or degree.

Kaustuv Sanyal.

Kaustuv Sanyal

Kaustuv Sanyal, Ph.D
Professor
Molecular Mycology Laboratory
Molecular Biology and Genetics Unit
Jawaharlal Nehru Centre for
Advanced Scientific Research
Jakkur Post, Bangalore - 560 064, India.
Ph :+91-80-22082878, Email: sanyal@jncasr.ac.in

Acknowledgement

This thesis has had inspiration and mentorship from numerous outstanding individuals whose contributions were important to the successful realization of this thesis. I take this opportunity to convey my gratitude to them as well as to express my sincere apology to those I may not mention individually.

I take pleasure in expressing my sincere gratitude to my advisor, Prof. Kaustuv Sanyal. I am deeply indebted to him for his encouragement, wisdom, enthusiasm, and his great efforts to explain things clearly and simply. It is because of him that during my tenure here, I learnt not only about my work or project but also about management, team work. All the lessons learnt in the lab enriched my growth as a researcher, a scientist and as a human being.

I gratefully thank the Hon. Faculty Fellow, Dr. G. R. Ramesh for all the things he taught during the first year of my program. He was the first person to teach us the basics of scientific experiments and his teachings proved as an advantage during the work of my PhD.

I am also grateful to all the faculty members of Molecular Biology and Genetics Unit, Prof. Anuranjan Anand, Prof. Uday Kumar Ranga, Prof. Namita Surolia, Prof. Maneesha Inamdar, Prof. Tapas Kundu, Prof. Hemalatha Balaram, Dr. Ravi Manjithaya and Dr. James Chelliah, for various courses they taught and discussions during the departmental work presentations.

I was involved in a number of collaborations during my PhD and all these collaborations have resulted in fruitful results for me. I am extremely obliged to Joseph Heitman, Duke University, USA and his lab members, specifically Lukasz Kozubowski, Sheng Sun and Blake Billmyre for all the help. The collaboration with these people made my work very interesting and exciting. I appreciate their contributions of time and ideas to make my research experience productive and stimulating. I thank Guus Bakkeren, Summerland Research & Development Centre, Canada for sending *Ustilago hordei* BAC clones. I would like to express my gratitude towards Raja Paul, IACS, Kolkata and his student Sabyasachi Sutradhar for the mathematical model work. I would like to sincerely thank Dr. Jayanta Haldar, NCU, JNCASR and his lab members Jiaul Hoque and Chandradhish Ghosh. This collaboration helped me learn new aspects of research and allowed me to work on anti-microbial compounds, an area which is of specific interest for me. I also thank Anirban Bhunia, Bose Institute, Kolkata and his student Aritreyee Datta for the collaboration work on anti-cryptococcal peptide.

I thank Ms. Suma and Mr. Sunil of confocal facility, MBGU, JNCASR for the imaging and discussions about image processing. I would also like to thank members of the Autophagy laboratory, MBGU for the microscopy help. I would like to acknowledge JNC sequencing facility (Ms. Anitha and Ms. Greeshma), MBGU office staff, JNC animal facility (Dr. Prakash), JNC admin staff and academic staff.

I thank all the past and present lab members of Molecular Mycology Lab - Tanmoy, Jitendra, Sreyoshi, Laxmi, Gautam, Arti, Abhishek, Neha, Lakshmi, Shreyas, Sundar, Rima, Krishnendu, Radha, Priya J, Priya B, Aditi, Jigyasa, Satya, Bornika, Hashim, Shweta,

Ashwathy and Bhagya for timely help, various discussions and good times in the lab. In particular, I gratefully recognize Gautam Chatterjee who was my mentor in the initial days of my lab work. He provided lots of insights that greatly improved my work and patiently taught me all the required techniques. I am so grateful to Arti for all the support and help during the tough times. I thank Nagaraja, our lab helper for all the efforts he has put to make reagents available.

My stay in JNC was a pleasant one and a number of people outside the lab made that happen. My batch mate group involving, Sunaina, Lakshmi, Surabhi, Shveta, Avani, Manaswini, Suresh, Amrutha, Malini, Arpit and Vaijayanthi, was the first group of people I met here. In all these years, these people provided a stimulating and fun environment to learn and grow. I would like to take this opportunity to thank them for all the good time. I am grateful to Shri, Pooja, Sambhavi, Piyush, Rafi, Achal, Raaghesh, Atif, Aishwarya, Vybhav for all the good times in and around the campus. All these people have given me a lot to cherish. I would also like to acknowledge my school and college friends Pooja, Richa, Sachin and Silky.

This has been a long journey, and I could not have done it without my family. I owe everything to my Papaji and Mummy without whom I won't have been where I am today. They have taught me to look at the best in everything and everyone. The love from my sister Jyoti has been unconditional all this time. No acknowledgement will be ever enough to expresses my gratitude towards them.

Vikas

Table of contents

List of figures and tables

Introduction

Results

Discussion

Materials and Methods

Abbreviations

°C	-	degree Celsius
µg	-	microgram
µl	-	microliter
ARS	-	autonomously replicating sequence
BAC	-	Bacterial artificial chromosome
BLAST	-	Basic Local Alignment Search Tool
BLASTn	-	Nucleotide blast
bp	-	base pair
CCAN	-	Constitutive centromere associated network
ChIP	-	Chromatin immunoprecipitation
ChIP-seq	-	ChIP sequencing
Chr	-	chromosome
cm	-	centimetre
cMT	-	cytoplasmic microtubule
DMSO	-	Dimethyl sulfoxide
DNA	-	deoxyribonucleic acid
dsRNA	-	double stranded RNA
DTT	-	Dithiothreitol
EDTA	-	Ethylenediaminetetraacetic acid
EGTA	-	ethylene glycol tetra acetic acid
G-418	-	Genticin-418
GFP	-	green fluorescent protein
h	-	hour
Hyg	-	hygromycin
INM	-	inner nuclear membrane
kb	-	kilo base
LINE	-	Long interspersed nuclear elements
LTR	-	long terminal repeat
M	-	molar
Mb	-	mega base
mg	-	milligram
min	-	minute
ml	-	millilitre

mM	-	mill molar
MT	-	microtubule
MTOC	-	microtubule organising center
MYA	-	million years ago
N	-	normal
NAT	-	Nourseothricin
ncRNA	-	non coding RNA
NE	-	nuclear envelope
Noc	-	Nocodazole
NPC	-	nuclear pore complex
OD600	-	optical density at 600 nm wavelength
ONM	-	outer nuclear membrane
ORF	-	open reading frame
PAGE	-	Polyacrylamide gel electrophoresis
PBS	-	phosphate buffer saline
PCR	-	Polymerase chain reaction
psi	-	pounds per square inch
RNA	-	ribonucleic acid
RNAi	-	RNA interference
RNA-seq	-	RNA sequencing
rpm	-	revolutions per minute
RT	-	room temperature
s	-	second
Sc	-	scaffold
SC	-	supercontig
SDS	-	Sodium dodecyl sulfate
siRNA	-	small interfering RNA
SPB	-	Spindle pole body
TE	-	transposable element
UTR	-	untranslated region

1. INTRODUCTION

Mitosis

Mitosis is a form of eukaryotic cell division that gives rise to two daughter cells with identical genetic makeup as the parent cell. The mitotic cell cycle is broadly divided into two major phases: interphase and mitosis. During interphase, a cell prepares itself for division by increasing its size and synthesizing necessary components required for its division. Interphase is further divided into three stages: gap1 (G1), synthesis (S) and gap2 (G2) phase. In G1 and G2 phases, a cell grows by increasing its cytoplasmic content, synthesizes a number of proteins and also duplicates organelles for the division. In the S phase, each chromatid is duplicated by DNA replication. The mitotic (M) phase is the stage when duplicated sister chromatids segregate equally into daughter cells. The M phase is subdivided into prophase, metaphase, anaphase, and telophase. Once chromosomes completely segregate, cytokinesis takes place which physically divides a single cell into two separate identical daughter cells. This event also marks the end of the cell cycle. Though the outcome of the mitotic cell cycle is the same in yeasts and metazoans, many subtle differences exist (Wang *et al.* 2003). The stages of the cell cycle have clear boundaries in metazoans but not in yeasts. Unlike metazoans, G2 and mitotic phases are overlapping and usually defined as the G2/M stage in yeasts. Many yeast species undergo "closed" mitosis as the nuclear envelope (NE) never breaks down unlike "open" mitosis in metazoan cells where the NE completely breaks down at the onset of mitosis. Moreover, yeast chromosomes do not condense as much as those of metazoans during mitosis. In addition, formation of the metaphase plate where chromosomes align on one plane is absent in yeast.

The foundation for the process of chromosome segregation is provided by a specialized chromatin structure, the centromere, upon which > 80 proteins assemble to form the kinetochore. The kinetochore connects chromosomes to the mitotic spindle through centromeric chromatin (Figure 1.1). The mitotic spindle, nucleated by the microtubule

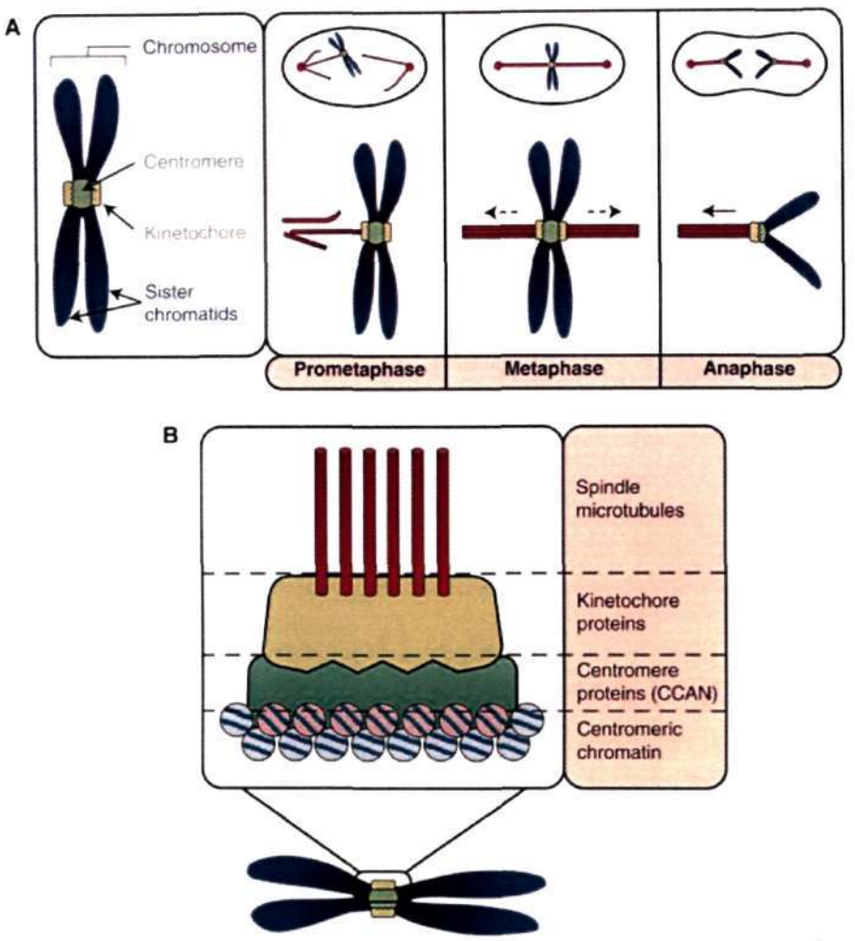

Figure 1.1 Organization of chromosome segregation machinery during mitosis. (A) A cartoon depicting the key protein complexes involved in chromosome segregation. During the early stages of mitosis, centromeres recruit kinetochore proteins. The kinetochore forms the attachment site for spindle microtubules. During metaphase, both kinetochores of all sister chromatid pairs are stably and correctly attached to microtubules, and form metaphase plate. The sister chromatids are then segregated during anaphase to two opposite poles. **(B)** Centromeric chromatin consists of specialized nucleosomes containing the histone H3 variant centromere protein (CENP-A). This is followed by assembly of a network of kinetochore proteins that are collectively known as the constitutive centromere associated network (CCAN). Kinetochore proteins, specifically recruited on the CCAN for mitosis, attach to spindle microtubules. [Figure adapted from (Westhorpe and Straight 2014)]

organizing centres (MTOCs), is a bipolar array of microtubules (MTs) that provides the force required to segregate chromosomes. The unequal rate of MT polymerization and depolymerization provides the push-pull forces that mediate pole-ward movement of segregated chromosomes into two daughter cells (See section 1.6 for details). Any defects in proper chromosome segregation can cause various types of complications leading to the onset of diseases (Potapova and Gorbsky 2017). Most of these defects because of improper

kinetochore-microtubule attachments and are sensed by the spindle assembly checkpoint resulting in delay for the cell cycle completion. This delay leads to either resolution of the defects or cell death by apoptosis in case the damage is not repairable. Cells with chromosome segregation errors that escape the spindle assembly checkpoint gives rise to progeny with altered chromosome content causing aneuploidy or micronuclei formation. Aneuploidy affects cellular fitness and hence acts as driver for genomic and chromosomal instability. Aneuploidy is correlated with a number of cancers in humans and has been implemented in development of drug resistance in pathogenic fungi (Kwon-Chung and Chang 2012, Giam and Rancati 2015, Wertheimer *et al.* 2016, Sansregret and Swanton 2017). Thus, precise chromosome segregation is crucial for proper accomplishment of the cell cycle and survival of an organism.

Centromere

The centromere is a specialized chromosomal locus that helps in separation of sister chromatids during the mitotic cell division. The centromere was first defined as the primary constriction of a metaphase chromosome that holds the sister chromatids together and binds to spindle MTs to bring about the movement of chromatids to opposite poles during anaphase. At the molecular level, the centromere is defined as a site of a chromosome on which a large number of proteins assemble to form the kinetochore to help in faithful chromosome segregation. The first functional centromere DNA sequence was identified several decades ago in the budding yeast *Saccharomyces cerevisiae* (Clarke and Carbon 1980). It was described as a region whose presence on a plasmid with a replication origin allows it to be stably propagated both in mitosis and meiosis. In humans, anti-centromere antibodies could be isolated from a human patient with an autoimmune disease called CREST (Moroi *et al.* 1980, Earnshaw and Rothfield 1985). These studies led to the identification of

several centromere-associated proteins like CENP-A, CENP-B, and CENP-C. Discovery of centromeres in a large number of species over the last few years revealed that the length of centromere DNA is highly variable and ranges from 125 bp to a few megabases.

Types of centromeres

Centromeres usually form on a localised place to form a eukaryotic monocentric chromosomes (Figure 1.2). Ocassionally in some plants and animals, centromeres can be diffuse and run along the entire chromosomomal length to form holocentric chromosome (Mandrioli and Manicardi 2012, Melters *et al.* 2012). However, holocentric chromosomes are not yet reported in fungi. Localized centromeres can be further classified into point and regional, based on the length of centromere DNA (Figure 1.2).

Point centromere

Point centromeres form on a short stretch of DNA (usually <400 bp) and are found in some budding yeast species, belonging to the subphylum of Hemiascomycota. The characteristic feature of the point centromere is the presence of conserved DNA sequence motifs, which are essential for centromere formation and thus, are known as genetically defined centromeres (Talbert *et al.* 2009, Roy and Sanyal 2011). The best studied organism harbouring point centromere is *S. cerevisiae* with a 125 bp centromere DNA. The budding yeast centromere DNA comprises of three consensus Centromeric DNA Elements (*CDE*s). The first domain, *CDEI*, is an evolutionarily conserved 8 bp DNA sequence and is not absolutely essential for the centromere function (Cumberledge and Carbon 1987). The central element *CDEII* is a nonconserved, AT-rich (>86%) 78-86 bp long DNA sequence (Fitzgerald-Hayes *et al.* 1982, Hieter *et al.* 1985). The AT-richness and the length of *CDEII* have been shown to be important for the centromere function. The third element, *CDEIII* is a 25 bp long imperfect palindromic sequence. This element is the most conserved one, and a deletion or substitution of a single base in the central CCG sequence completely disrupts

centromere formation in this organism (McGrew *et al.* 1986, Ng and Carbon 1987). The centromeres with similar *CDEI*, *CDEII* and *CDEIII* elements have also been identified and isolated in several other budding yeasts, such as *Saccharomyces bayanus*, *Saccharomyces mikatae*, *Saccharomyces paradoxus*, *Candida glabrata*, *Kluyveromyces lactis*, *Ashbya gossypii* etc (Heus *et al.* 1993, Heus *et al.* 1993, Meraldi *et al.* 2006, Lynch *et al.* 2010). However, the centromeres of *K. lactis* and *A. gossypii* comprise of an atypical longer *CDEII* element (160 bp in length). Other hemiascomycetous budding yeasts, *Naumovozyma castellii*, *Candida maltosa* and *Yarrowia lipolytica*, also possess point centromeres which comprise of slightly different features. In *N. castellii*, the centromeres are defined by an 110 bp consensus sequence and do not have conventional conserved *CDEI*, *II* and *III* elements (Kobayashi *et al.* 2015). Rather it is made up of a novel set of conserved domains, defined as *NaCDEI*, *II* and *III*. Centromeres in *C. maltosa* are 325 bp in length, which is sufficient to confer mitotic stability. However, the centromere in this organism strikingly lacks point centromere specific and essential *CDEIII* element (Ohkuma *et al.* 1995). The centromere of *Y. lipolytica* spans 200 bp which provides centromere function but does not possess the consensus *CDEI* and *CDEIII* elements (Fournier *et al.* 1993, Vernis *et al.* 2001).

Regional centromere

The centromeres of most other organisms are longer (often few kb to Mbs long) and are usually repetitive and heterochromatic in nature (Figure 1.2). The centromere formation in this class is primarily governed by epigenetic factors (see section 1.2.3). In fungi, pathogenic budding yeasts *Candida albicans*, *Candida tropicalis*, *Candida lusitaniae* and *Candida dubliniensis* harbour short regional centromeres with varying length ranging from 4 to 18 kb (Sanyal *et al.* 2004, Padmanabhan *et al.* 2008, Kapoor *et al.* 2015, Chatterjee *et al.* 2016). In *C. albicans*, *C. lusitaniae* and *C. dubliniensis*, each centromere is unique and different in DNA sequence. While the centromeres in these three species are mostly repeat-

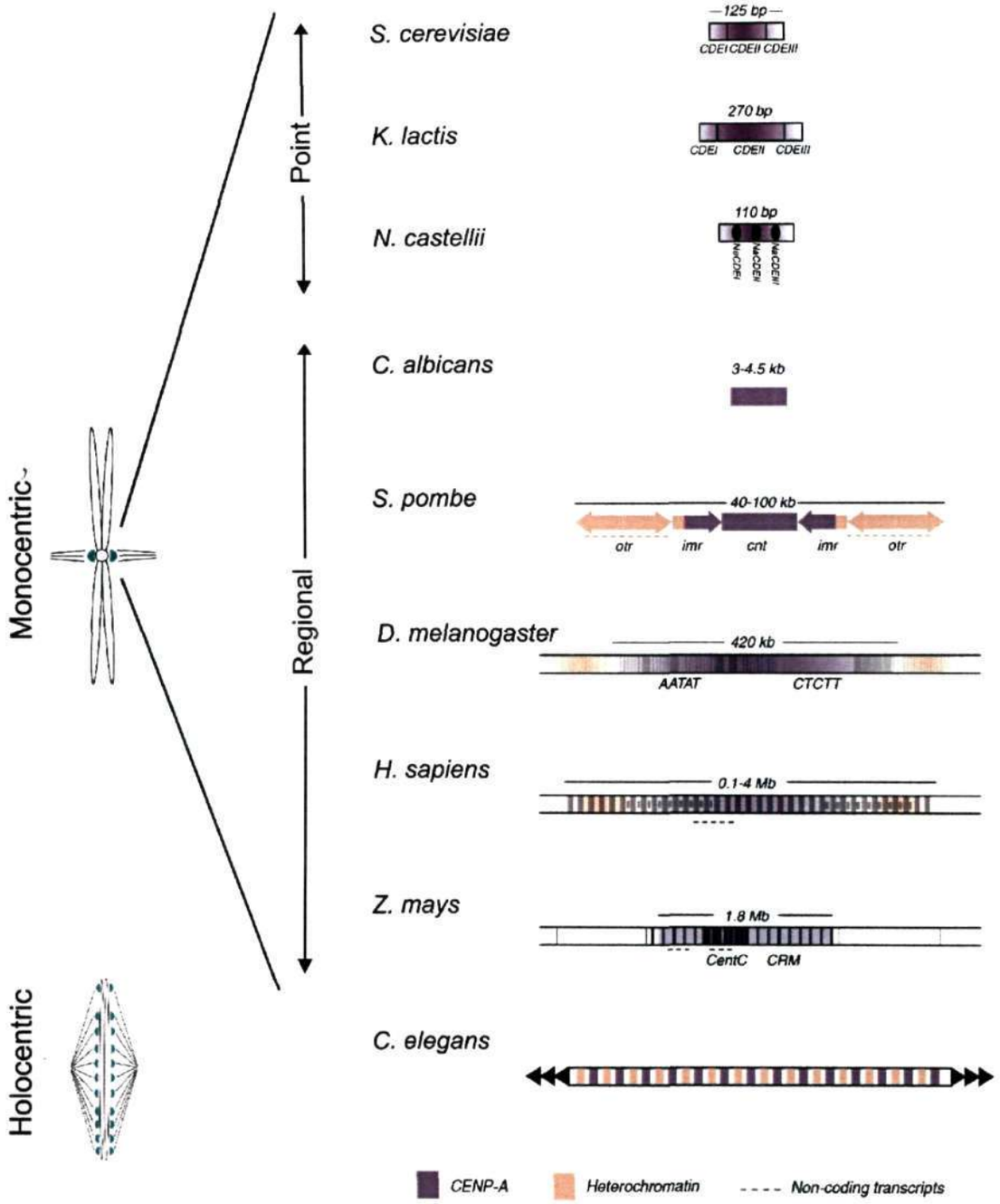

Figure 1.2 Organization of centromeres in various organisms. The chromosome can be monocentric and polycentric based on the number of functional kinetochore formation sites. The centromeres in monocentric chromosomes are classified further into "point" or "regional" centromeres based on the length of centromere DNA. [Figure modified from (Buscaino *et al.* 2010)]

less, they do not show any sequence similarities between centromeres of the same or the other species. It is important to note that some chromosomes show the presence of chromosome-

specific short repeats or remnants of transposable elements in *C. albicans* and *C. dubliniensis* (Padmanabhan *et al.* 2008). In contrast, *C. tropicalis* harbours repeat-rich centromeres. Each of the seven centromeres in *C. tropicalis* consists of a mid-core flanked by inverted repeats on both sides (Chatterjee *et al.* 2016). Both the mid-core and inverted repeats are highly homogeneous among different centromeres, unlike other *Candida* species. These studies show that centromere DNA properties can significantly differ between species of the same complex. A distantly related ascomycete, the fission yeast *Schizosaccharomyces pombe*, has centromeres that are repeat-rich, similar to *C. tropicalis*. Centromeres in *S. pombe* are 40-110 kb long and composed of the non-repetitive central core (*cnt*) flanked by pericentric repeats (Clarke *et al.* 1986, Chikashige *et al.* 1989, Clarke and Baum 1990, Steiner *et al.* 1993, Wood *et al.* 2002). The pericentric repeats are longer than the ones in *C. tropicalis* and are further divided into innermost (*imr*) and outer (*otr*) repeats. The *otr* includes two distinct elements - *dg* and *dh* (Chikashige *et al.* 1989, Pidoux and Allshire 2004). The *cnt* sequences of chromosome 1 and chromosome 3 share a considerable homology, whereas *cnt* of the third chromosome, chromosome 2, is heterogeneous in sequence. The *imr* in all three centromeres is unique while the *dg* and *dh* repeats are 97% and 48% identical in sequence among centromeres (Grewal and Klar 1997, Wood *et al.* 2002). The centromeres of a filamentous ascomycete *Neurospora crassa* are AT-rich, ~150-300 kb long and composed of repetitive DNA elements (Cambareri *et al.* 1998, Smith *et al.* 2011). The repeats at *CEN7* are mostly a cluster of inactive retrotransposable-like elements (*Tcen*, *TglI*, *Tgl2*, and *Tad*). Similarly, the centromeres of another fungus, *Aspergillus niger*, are found to be enriched with two degenerate LTR retrotransposable elements (*Dane1* and *Dane2*) in *CENIV* (Aleksenko *et al.* 2001, Nielsen *et al.* 2001). Enrichment of retrotransposable elements at centromeres in higher fungi is one of the characteristic features, perhaps to protect host genome against the foreign, selfish retrotransposable elements. Besides fungi, the centromeres of the higher eukaryotes

are highly repetitive in nature and in many cases, these comprise of transposons or satellite DNA.

The centromere in *Drosophila melanogaster* comprises of tandem repeats of pentameric AATAT and TTCTC sequences, interspersed with more complex transposable elements (Sun *et al.* 1997). However, the simple repeats or transposable elements are neither centromere specific nor universal to all the centromeres. The centromeres of most chromosomes in chicken contain homogeneous arrays, which are largely chromosome-specific (Shang *et al.* 2010). However, the centromeres in chromosome 5, chromosome 27 and chromosome Z are strikingly non-repetitive in nature. The centromeres in the mouse are composed of two tandemly arranged conserved elements known as major and minor satellite DNAs. The minor satellite DNAs are AT-rich, comprised of 120 bp monomers, and arranged over a 300-600 kb centromeric region. Adjacent to these minor repeats are the major satellite DNA repeats that can span up to 2 Mb. Each unit of this major satellite DNA is of 234 bp long, and tandemly arranged and has a role in heterochromatin formation (Wong and Rattner 1988, Vissel and Choo 1989, Zeng *et al.* 2004). The centromeres in humans and primates span over a few Mb and are composed mostly of nearly one nucleosome-length long 171 bp sequence arrays known as alpha satellite DNA (Giannuzzi *et al.* 2012). The average length of the satellite monomer varies between 168 to 172 bp. However, it can go upto 340 to 550 bp in length as seen in certain primates. Despite the difference in length, this satellite element is arranged in a head to tail orientation in tandem, but the number of repeats is chromosome-specific.

Like metazoan centromeres, the centromeres of most plants harbour highly repetitive DNA elements and span 420 kb to 4 Mb in length. The repeats in most cases are derived from transposable elements. The 155 bp CentO repeat of rice, *Oryza sativa, (Cheng et al. 2002),* the 156 bp CentC repeat of maize, *Zea mays, (Zhong et al. 2002)* and the 178 bp repeat of

Arabidopsis thaliana (Arabidopsis Genome 2000, Simon *et al.* 2015) are all a nucleosome length long. This conservation of the repeat length in both animal and plants has been proposed to be important for uniform nucleosome phasing and subsequent propagation of centromeric chromatin. In contrast to widespread belief of repeat conservation among the centromeres in a species, a recent study in potato (*Solanum tuberosum*) showed the presence of both repetitive and repeatless centromeres in the same species. The authors found that while half of the centromeres harbour repeats, the remaining centromeres are devoid of any higher order architecture (Gong *et al.* 2012). One of the centromeres was found to have a mix of single copy sequences and repeats. Another study indicated that the centromere length is actively regulated in a species. Wang and co-workers transferred nine maize centromeres into oat by performing inter-species cross between maize (*Zea mays*) and oat (*Avena sativa*) (Wang *et al.* 2014). The authors found that maize centromeres expand themselves to encompass a larger area in oat background and attain the size of a typical oat centromere.

Holocentromere

In several eukaryotes, an entire chromosome may serve as a site for the kinetochore formation (Figure 1.2). These chromosomes, known as the holocentric chromosomes, are found in nematodes, insects and a few plant species (Melters *et al.* 2012, Cuacos *et al.* 2015). The most studied organism with holocentric chromosomes is a nematode, *Caenorhabditis elegans*. It was considered for a long time that the kinetochore proteins localize along the entire length of a chromosome in this organism (Talbert *et al.* 2009). However, a recent study proposed that the holocentric chromosomes in *C. elegans* are polycentric in nature with discrete centromeric sites along the chromosomes (Steiner and Henikoff 2014). Similarly in a sedge, *Rhyncospora pubera*, multiple centromeric units assemble along the chromosome instead of a diffuse organization (Marques *et al.* 2015). These studies indicate that the holocentromeric chromosomes are probably polycentric in nature with multiple centromeres

forming along the chromosome.

Rapid evolution of centromeres among closely related species

Centromeres are the fastest evolving loci in the genome despite having a conserved function, a phenomenon termed as the 'centromere paradox' (Henikoff *et al.* 2001). A recent study analyzed the centromere sequences in 282 species of plants and animals and showed the divergence of the centromeric repeat sequences among these organisms (Melters *et al.* 2013). This rapid evolution of the centromere DNA is not limited to centromeres between two distantly related organisms, but even closely related species can have different types of centromeres. Two of such well studied species complexes belong to the Ascomycota group of fungi, *Schizosaccharomyces*, and *Candida*. The centromeres in three species of *Schizosaccharomyces* clade, *S. pombe*, *Schizosaccharomyces japonicus* and *Schizosaccharomyces octosporus,* show divergence in organization of DNA sequence elements (Rhind *et al.* 2011). *S. japonicus* contains mostly transposons in the centromere whereas *S. pombe* and *S. octosporus* contain repeat-rich centromeres and have lost most of the active transposons (Rhind *et al.* 2011). Two CTG clade species *C. albicans* and *C. dubliniensis*, which diverged from a common ancestor around 50 million years ago (MYA) harbour repeat-less centromeres. These two species differ in their centromere DNA sequences while the rest of genome is well-conserved and syntenous between two species (Padmanabhan *et al.* 2008, Jackson *et al.* 2009). Further, *C. albicans* and *C. dubliniensis* differ from another related species, *C. tropicalis*, which diverged 150 MYA and contains repetitive centromeres (Chatterjee *et al.* 2016). These studies show that the centromere evolves rapidly among closely related species in fungi. This rapid evolution of centromeres is also seen in plants and animals. Multiple studies described the evolution of centromeric regions among closely related species of plants like rice, maize, and potato (Zhang *et al.* 2014, Gao *et al.* 2015, Schneider *et al.* 2016). Similarly, a number of closely related primates

show the divergence in the sequence, length, and arrangement of centromeric alpha-satellites repeats (Giannuzzi *et al.* 2012).

Determinants of centromere identity

The loss of a centromere or the presence of more than one centromere in a chromosome (barring holocentric chromosomes) may lead to genome instability. Thus, formation and maintenance of a centromere at a specific location as well as prevention of more than one centromere on a chromosome is critical for chromosome stability. The factors that maintain the site of the kinetochore formation on a specified locus are not well understood and may differ among organisms. Broadly, these factors can be classified into two groups, genetic and epigenetic (Figure 1.3).

Genetic centromeres

As the name suggests, genetic centromeres are defined by the presence of a specific DNA sequence which acts as the binding sites of kinetochore proteins (Talbert *et al.* 2009, Roy and Sanyal 2011). Typically, point centromeres have specific DNA sequence motifs that make these centromeres genetically defined. When cloned into a plasmid with an autonomously replicating sequence (ARS), a genetically defined centromere could stabilize these ARS plasmids as minichromosomes both in mitotic and meiotic division (Talbert *et al.* 2009, Roy and Sanyal 2011). Centromeres of *S. cerevisiae* is an ideal example of a point centromere.

Epigenetic centromeres

In most organisms, centromeres are not defined by the underlying DNA sequence but specified by the presence of CENP-A – the centromere specific histone H3 variant. The factors required for the assembly of CENP-A at a locus differ among organisms studied (Dawe and Henikoff 2006, Gieni *et al.* 2008, Roy and Sanyal 2011). While point centromeres are genetic in nature, all studied regional centromeres are defined epigenetically with a little

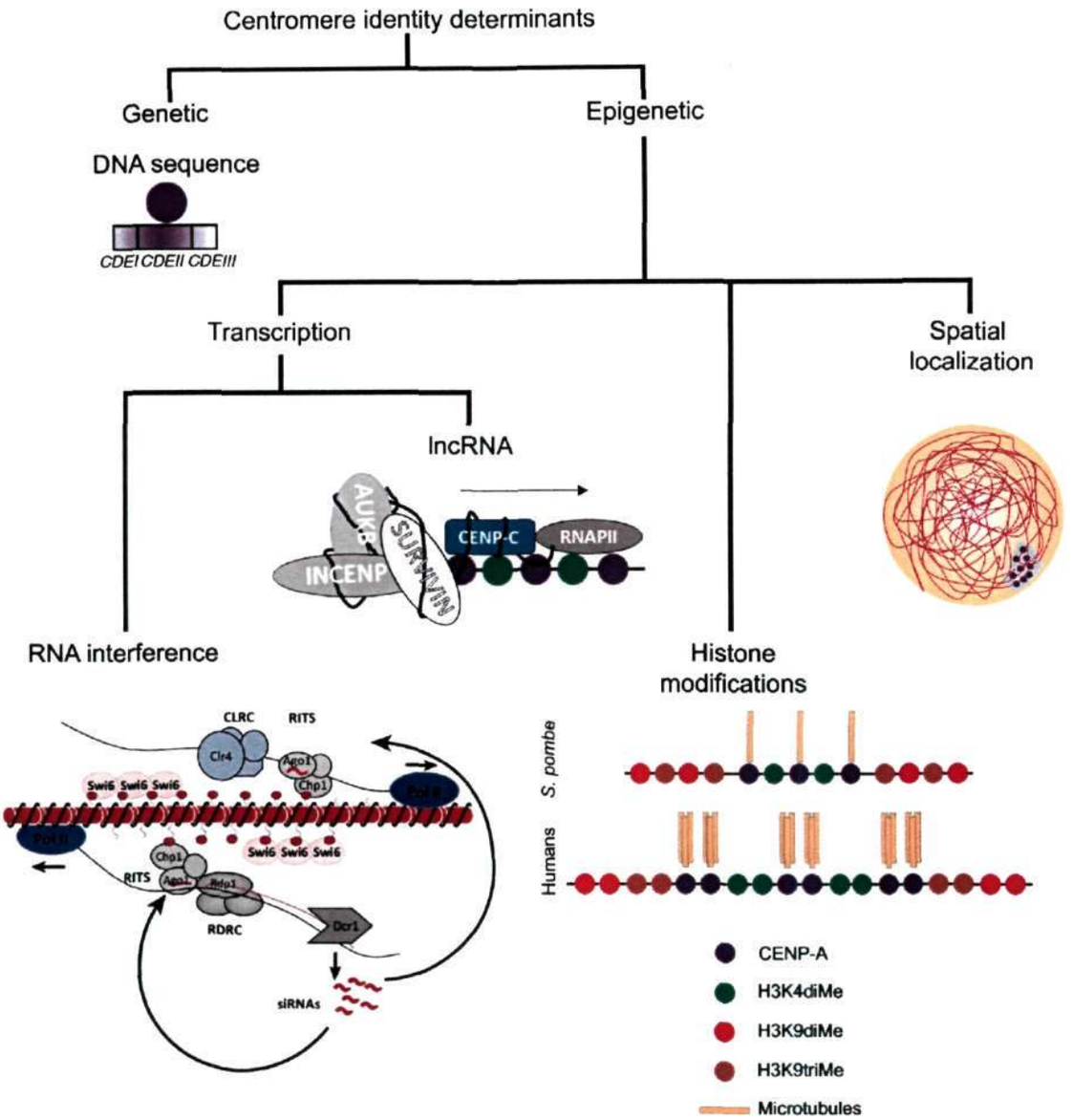

Figure 1.3. A flowchart showing key molecular players involved in centromere identity and maintenance. Centromeres can be defined in either genetic or epigenetic manner. The position of genetically defined centromeres is defined by DNA sequence element/s whereas the epigenetically defined centromere formation is regulated by a number of factors. Some of the well studied epigenetic determinants include centromere transcription, presence of specific histone modifications and spatial localization of centromeres.

or no contribution from the centromere DNA sequence. The important epigenetic factors studied in this aspect include centromeric transcription, chromatin modifications, and spatial localization of centromeres (Figure 1.3).

Centromere transcription

For a very long time, the centromere was considered to be heterochromatic in nature, and it

was assumed to be transcriptionally inert. However, landmark studies in the fission yeast, *S. pombe*, showed that siRNA derived from pericentromeric regions (*dg-dh* repeats) are necessary for the centromere function (Hall *et al.* 2002, Volpe *et al.* 2002, Volpe *et al.* 2003). These studies indicated that the centromere transcription is permissible and has functional significance. Later studies probing the origin of these siRNAs showed that the pericentromeric repeats are transcribed by RNA polymerase II to generate double stranded RNA, a substrate for the RNAi machinery (Figure 1.3 and section 1.3) (Reinhart and Bartel 2002, Volpe *et al.* 2003). Since then, centromere transcription has been studied in several organisms and was found to be essential for the centromere function (Chan and Wong 2012, Hall *et al.* 2012, Scott 2013). In budding yeast, *S. cerevisiae*, Cbf1, a transcription factor, binds to the centromere DNA and required for centromeric transcript production (Hemmerich *et al.* 2000, Ohkuni and Kitagawa 2011). Loss of Cbf1 along with its regulatory proteins Ste12 and Dig1 leads to chromosome instability. In *S. pombe*, a GATA-type zinc finger transcription factor, Ams2, was found to be necessary for CENP-A association at the centromere (Chen *et al.* 2003). Another study in *S. pombe* also reported ncRNA emanating from the centromere core regions (Choi *et al.* 2011). In maize, transcripts from CentC repeats as well as CRM (centromeric retrotransposons of maize) retrotransposons are tightly bound to maize CENP-A (Topp *et al.* 2004). However, these transcripts did not resemble siRNA, and their exact function is not yet well understood. Similarly, in mouse cell lines, centromere core minor satellite transcripts were found to be a part of centromere core chromatin (Bouzinba-Segard *et al.* 2006). These studies suggest the centromere core derived ncRNA as the critical determinant of centromeric chromatin assembly. Centromeric RNA has also been shown to interact with other kinetochore proteins besides CENP-A. A few studies in mouse and human cells depicted the necessity of centromere core transcripts for loading of CENP-C and chromosome passenger complex (CPC) (Wong *et al.* 2007, Ferri *et al.* 2009). Studies using

the human artificial chromosome depicted that a dynamic balance between permissive and repressive chromatin maintains proper centromere function (Nakano *et al.* 2008). A completely open or closed conformation for transcription can lead to loss of kinetochore function resulting in chromosome mis-segregation. Overall, these studies provide evidence that a low level of centromeric transcription is essential for centromere function in almost all organisms. Indeed, active genes have been found to be present in rice centromeres suggesting centromeric chromatin is not transcriptionally silent in nature (Nagaki *et al.* 2004).

Chromatin modifications

Centromeres were identified as a darkly stained region of the chromosome indicating its heterochromatic nature (Flemming 1882). A series of studies across several organisms confirmed the heterochromatic nature of centromeres. Recent studies on the presence of histone marks in centromeres in *S. pombe* and *N. crassa* revealed their association with heterochromatin marks H3K9diMe and H3K9triMe, respectively (Volpe *et al.* 2002, Cam *et al.* 2005, Smith *et al.* 2011). A study in *Drosophila melanogaster* revealed that centromeric H3 is not methylated at H3K9 but are instead H3K4 di-methylated, a modification associated with transcriptionally silenced euchromatin (Sullivan and Karpen 2004). By contrast in maize, instead of H3K4diMe, H3K9diMe was found to be present in centromeres (Jin *et al.* 2008). In humans and *D. melanogaster*, both H3 and H4 at the centromere were shown to be hypoacetylated, as observed in heterochromatin (Gieni *et al.* 2008). All these modifications corroborate with a low level of transcription from the centromeres. More studies in a number of model systems revealed several post-translational modifications of histone H3, H4 and CENP-A, and their roles in the centromere specification to kinetochore assembly (Fukagawa 2017). Apart from histones, DNA methylation has also been observed at the centromeres in a few organisms (Chen *et al.* 2003, Zhang *et al.* 2006, Yamagata *et al.* 2007, Smith *et al.* 2011). Centromeres in maize and *A. thaliana* show hypomethylation in centromere

chromatin as compared to hypermethylation in flanking pericentromeres (Zhang *et al.* 2008, Koo *et al.* 2011). The level of DNA methylation at centromeres is also found to be directly related to H3K9di-methylation in these organisms. Despite this long known presence of DNA methylation at centromeres, its role at the centromere is not well understood in any organism.

Spatial localization

In most of the yeast species studied, centromeres are clustered at one location within the nucleus (Figure 1.3 and section 1.5.5) (Jin *et al.* 2000, Sanyal and Carbon 2002, Anderson *et al.* 2009). It has been proposed that this clustering of centromeres aids in determining the site of centromere formation in these organisms. According to this hypothesis, a part of the nucleus is enriched with a pool of CENP-A protein to form a CENP-A cloud (Shang *et al.* 2013, Thakur and Sanyal 2013, Fukagawa and Earnshaw 2014, Scott and Bloom 2014). It was proposed that the region of a chromosome that is in close proximity to this CENP-A cloud would attract a higher level of CENP-A and thus serves as a preferred site for centromere formation. Evidence for this hypothesis stems from studies in *C. albicans* and chicken cells where neocentromere formation was found to be close to the native centromere when the native centromere was deleted or inactivated (Shang *et al.* 2013, Thakur and Sanyal 2013).

RNA interference (RNAi)

RNA interference (RNAi) is a post-transcriptional gene silencing mechanism mediated by small RNAs. RNAi regulates gene expression by inhibiting either translation or directly degrading the target transcripts (Dumesic and Madhani 2014, Villalobos-Escobedo *et al.* 2016). RNAi is mediated by small non-coding RNAs with a size range of 20-32 nucleotides. This mechanism allows fast but specific changes in gene expression essential for processes such as development and immunity.

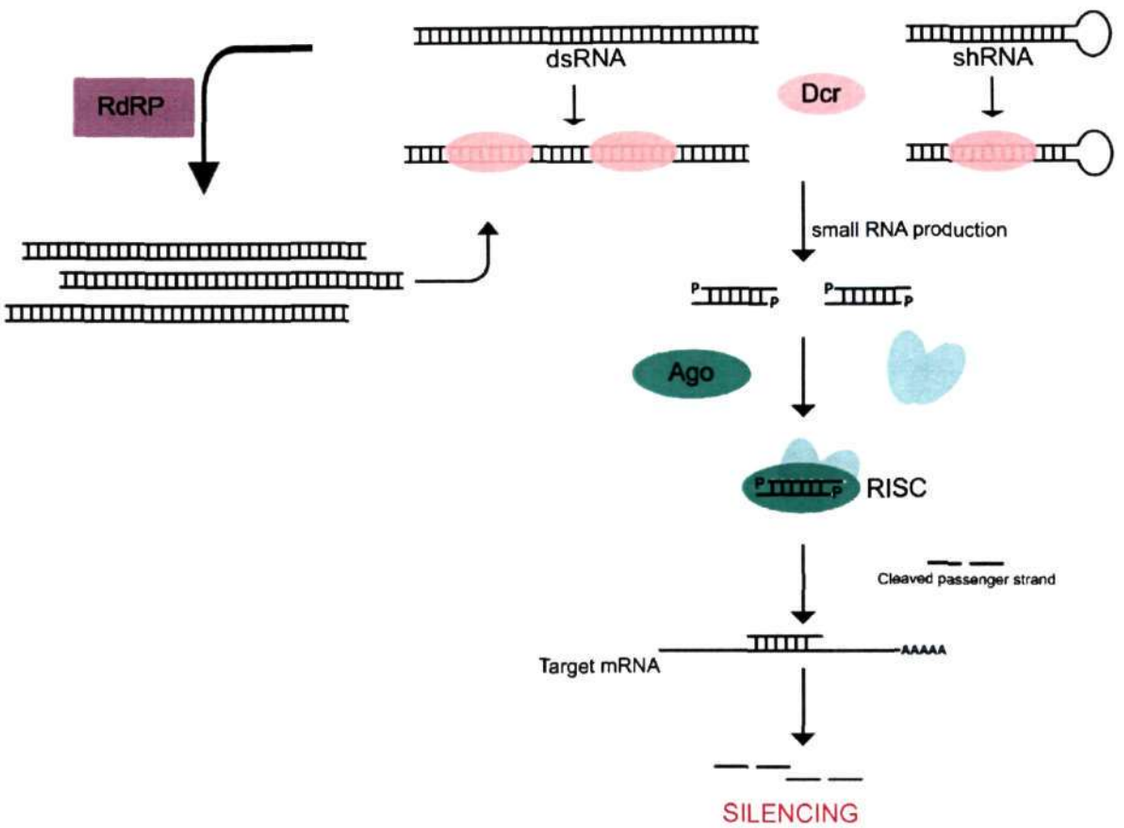

Figure 1.4 Schematic describing the key events in RNA interference (RNAi). Double stranded RNA generated from repeats or transposons or hairpin structures is processed by Dicer (Dcr) to produce small RNAs. These small RNAs are recognised by Argonaute (Ago) along with other adapter proteins (shown here in light blue). The complex thus formed (RISC complex) cleaves the passenger strand and recognises the target mRNA with the help of the guide strand. The target mRNA is then cleaved into smaller pieces and thus inhibiting the translation of the mRNA. In most cases, RNA-dependent RNA polymerase (RdRP) helps in amplification of the signal for RNAi machinery by producing more double stranded RNAs from the target RNA.

RNAi requires the dsRNA as a template to work on and successfully silence a region (Figure 1.4). This process involves a few key proteins along with their accessory proteins. RNAi acts on dsRNAs that are produced in a cell as a result of bidirectional transcription of a region or by formation of the hairpin structure by long ncRNA (Ghildiyal and Zamore 2009, Fellmann and Lowe 2014). The first step of RNAi is the cleavage of dsRNA or hairpin RNA in smaller dsRNA moieties. This step is carried out by an RNase-III like endonuclease protein Dicer (Dcr) to produce small RNAs of 20-25 nucleotides in length. These small RNAs bind to Argonaute (Ago), which is part of the RNA-induced transcriptional silencing

(RITS) complex consisting of Tas3 and Chp1. One strand from these small RNA duplex molecules directs silencing and is called the guide strand. The other strand, that is eventually destroyed, is called the passenger strand. The RITS complex recognizes the target RNA or DNA based on the complementarity of the guide RNA strand. The complex also includes proteins that redirect the target mRNA to the site of degradation. Another enzyme, RNA-dependent RNA polymerase (RdRP), amplifies the signal by producing more dsRNA from precursor RNA using small RNA as the primers. This cascade of events leads to degradation of target mRNAs resulting in transcriptional silencing. In some cases, the RNAi machinery also recruits heterochromatic proteins onto the target DNA and causes further repression at the post-transcriptional level (Matzke and Birchler 2005, Volpe and Martienssen 2011).

Small RNAs can be classified into small interfering RNA (siRNA), microRNA (miRNA), and Piwi-interacting (piRNA) based on the precursor long RNA (Ghildiyal and Zamore 2009). Though the overall process of RNAi remains conserved, the biogenesis of these small RNAs shows some differences in the proteins involved in this process.

piRNA

piRNAs are the most recently discovered small RNAs and have been found only in animals. These are also the longest small RNAs with a length of 26-31 nucleotides (Aravin *et al.* 2001, Vagin *et al.* 2006). The piRNAs have emerged as a complex population of small RNAs that are highly enriched in the germline tissues of the majority of metazoans (Weick and Miska 2014, Iwasaki *et al.* 2015). piRNAs regulate the activity of transposons and hence preserving normal gametogenesis and reproduction. However, the mechanisms by which piRNAs play their role in germ cell development remain largely unknown.

miRNA

miRNAs are encoded within the genome and are transcribed to give rise to a hairpin structure which is then processed by Dcr. Many miRNAs are known to reside in introns of their pre-

mRNA host genes and share their regulatory elements. The final small RNAs are ~22 nucleotides in length and are involved in processes like normal development, host pathogen interactions and stress tolerance (He and Hannon 2004, Wienholds and Plasterk 2005, Cai *et al.* 2009). Unlike other small RNA species, miRNAs can target and regulate a set of mRNAs instead of a specific mRNA substrate. Also, a single mRNA can be targeted by multiple miRNAs providing additional level of complexity to their biology. The miRNA regulation is not well understood in fungi and was considered absent in fungi until recent studies proved otherwise (Lee *et al.* 2010, Zhou *et al.* 2012, Zhou *et al.* 2012).

siRNA

siRNAs are derived from dsRNAs originating from transposons, DNA repeats or viral DNA sequences integrated into the host genome. Thus, siRNAs are usually involved in the genome protection and prevention of viral infection (Obbard *et al.* 2009, Dumesic and Madhani 2014). The length of siRNAs varies from 20 to 25 nucleotides and are well studied in fungi, animals, and plants. Due to their nature of degrading the target mRNA, these RNAs have also been exploited as a tool to study gene function by lowering the gene expression levels and for developing the siRNA based therapeutics (Kim and Rossi 2008, Ambesajir *et al.* 2012, Chery 2016).

RNAi in fungi

The process of RNAi, mediated by siRNAs, has been well studied in all three kingdoms of life: fungi, animals, and plants. While RNAi is shown to be present in all animals and plants studied till date, fungal kingdom presents a scenario where RNAi was lost multiple times during evolution (Figure 1.5) (Drinnenberg *et al.* 2009, Billmyre *et al.* 2013).

In fungi, RNAi-mediated gene silencing was first studied in a filamentous fungus, *N. crassa* (Romano and Macino 1992, Shiu *et al.* 2001). Two of the well characterized processes, quelling and meiotic silencing by unpaired DNA (MSUD), are employed by this

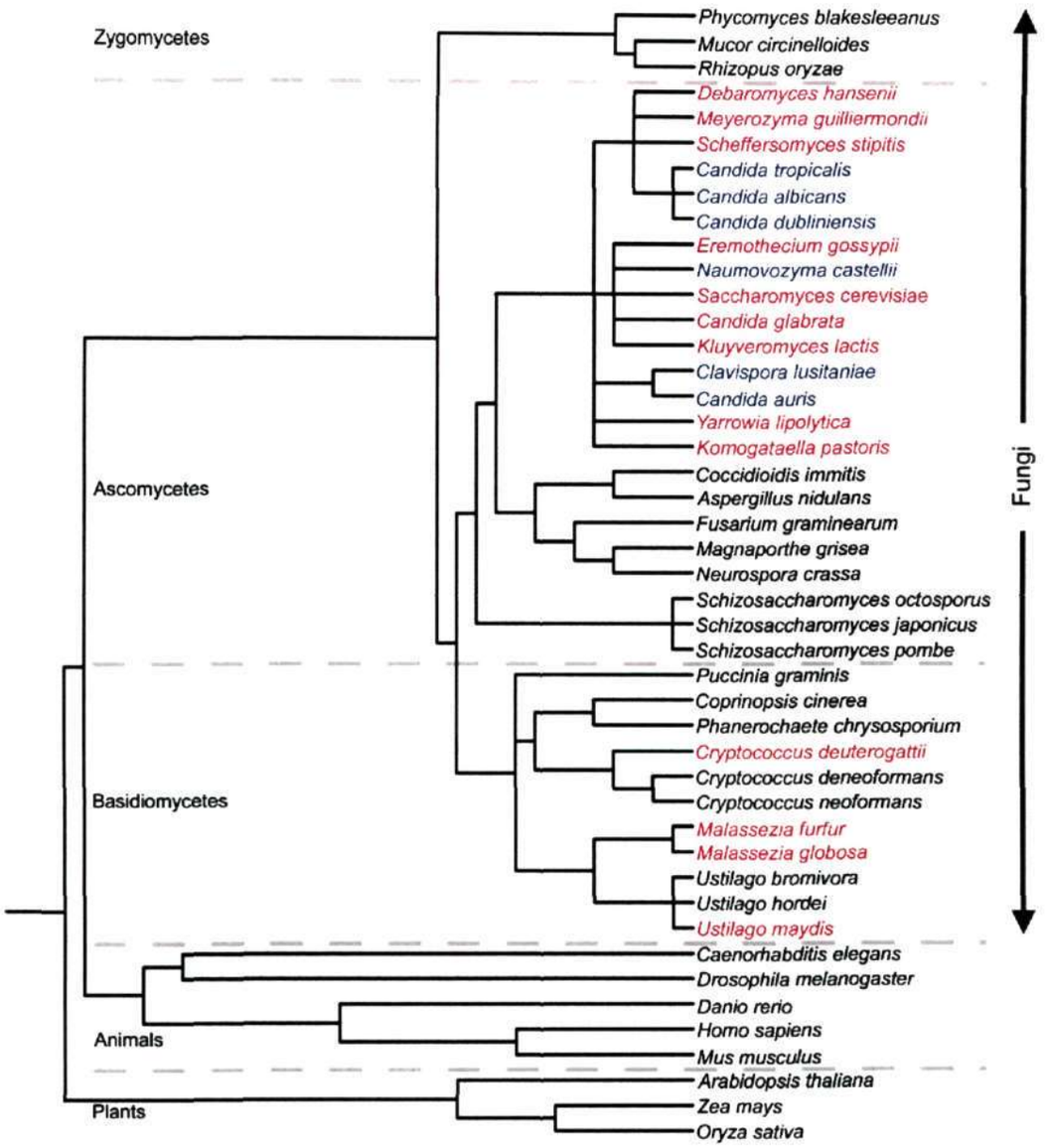

Figure 1.5 Phylogeny showing the status of RNAi machinery across fungi. The species listed in red colour have lost functional RNAi while it is retained in the species listed in black. The species in blue possess a cryptic RNAi machinery.

organism for genome defence (Nakayashiki 2005, Billmyre *et al.* 2013). Both these processes involve a molecular mechanism similar to the RNAi silencing. All the key RNAi proteins namely Dcr, Ago, and RdRP, have been shown to play a major role in both quelling and MSUD. Another fungal species where RNAi has been well studied is the fission yeast, *S. pombe*. In this organism, RNAi plays a critical role in centromere function and heterochromatin formation (Volpe *et al.* 2003, Volpe and Martienssen 2011). The loss of

RNAi proteins in *S. pombe* leads to chromosome mis-segregation and abnormal centromere function. In the past decade, RNAi has been studied in *Magnaporthe oryzae*, *Cryptococcus neoformans*, *Mucor circinelloides* and *Aspergillus nidulans* (Kadotani *et al.* 2003, Mouyna *et al.* 2004, Janbon *et al.* 2010, Torres-Martinez and Ruiz-Vazquez 2016). In all these fungi, RNAi was found to be involved in regulation of transposons and hence plays a critical role in genome defence.

Despite having such an essential function, RNAi machinery has been lost in some fungal species (Billmyre *et al.* 2013). A landmark study explored the status of proteins involved in RNAi among ascomycetes, basidiomycetes, and zygomycetes (Nakayashiki *et al.* 2006). The study revealed that a few species like *S. cerevisiae*, *C. glabrata*, and *Ustilago maydis* have lost all the proteins required for functional RNAi. Another class of organisms including *C. albicans*, *C. tropicalis* and *N. castellii* harbour some of the proteins (Ago and Dcr), but have lost others (RdRP) indicating the presence of cryptic RNAi machinery in these species. However, the cryptic RNAi machinery was shown to be functional to give rise to small RNAs (Drinnenberg *et al.* 2009). Since the loss of RNAi was found to be in taxonomically distinct species, it was proposed that the loss of RNAi took place a few times during evolution. The loss of RNAi in the fungal species was further correlated with the presence of "killer" virus, an endemic viral system that is cytoplasmically inherited as a double stranded RNA (Drinnenberg *et al.* 2011). The "killer" virus was found to be present in *S. cerevisiae* and its close relatives that have lost RNAi but not in *N. castellii*, a budding yeast, which has the functional RNAi machinery. The "killer" positive cells kill the neighbouring "killer" negative cells, including the RNAi positive cells, providing clear growth advantage in the environment. It has been suggested that maintenance of "killer" virus led to evolution of RNAi-deficient fungal species, not just in Ascomycota but also in Basidiomycota like in *U. maydis*, a species that has lost RNAi but harbours the killer virus.

RNAi and centromere function

Study by Volpe *et al.* in the fission yeast, *S. pombe*, revealed that the siRNA derived from pericentromeric regions are necessary for the centromeric heterochromatin formation (Figure 1.3) (Volpe *et al.* 2003). This study indicated that the centromere transcription was permissible and has functional significance. The pericentromere in *S. pombe* comprises of *dg-dh* repeats. These repeats are transcribed by RNA polymerase II and generate pre-siRNA transcripts. These dsRNA transcripts are cleaved and processed by the RNAi machinery to suppress the transcription from these regions (Reinhart and Bartel 2002, Djupedal *et al.* 2009). The RNAi machinery also recruits heterochromatic proteins like Clr4, Swi6 (homolog of heterochromatin protein 1, HP1) leading to further transcriptional suppression of these regions (Volpe and Martienssen 2011). Though the role of RNAi in pericentric heterochromatin assembly in *S. pombe* is well established, the same is less explored in vertebrates. Since Dcr is essential for survival in vertebrates, studies are limited to cell culture based systems. A study in DT40 chicken cells showed Dcr is required for normal chromosome segregation (Fukagawa *et al.* 2004). Similar to *S. pombe*, pericentric transcript accumulation was observed along with the loss of HP1 binding from these regions. However, a few studies in mouse embryonic stem (ES) cells showed varying results regarding essentiality of Dcr/RNAi for heterochromatin assembly in these cells (Kanellopoulou *et al.* 2005, Murchison *et al.* 2005). While these studies indicate a role of Dcr in repression of the pericentric region, no aneuploidy is observed in Dcr depleted cells.

Transposons

Transposons or transposable elements (TE) are ubiquitous genetic elements that occur both in prokaryotes and eukaryotes. These elements are considered to be selfish, independently replicating entities in the host genome (Hua-Van *et al.* 2005). They constitute

significant part of the genome in many organisms accounting for as high as 85% of the genome in maize (Schnable *et al.* 2009). While transposons amount to 40-45% of the human genome, only 3% of the *S. cerevisiae* genome represents transposons (Hua-Van *et al.* 2005). In the past two decades, numerous studies suggested both positive and negative impacts of TEs on the genome structure evolution (Goodier and Kazazian 2008, Chuong *et al.* 2017). These studies imply that transposons can play important roles in a cell contrary to the belief that they are "junk DNA" (Biemont 2010). One of the most widely understood roles of TEs is in the regulation of gene expression by providing transcription factor binding sites. Two other well known functions of transposons include telomerase activity and immunoglobulin recombination. As transposons act as insulators, they have also been proposed to play a significant role as a barrier element to mark the genome into distinct chromatin loops domains (Hua-Van *et al.* 2005). The process by which TEs move from one place to the other in the genome is known as transposition. Based on the mode of transposition, the transposons can be broadly divided into two classes – retroelements or RNA transposons (Class II) and DNA transposons (Class I) (Figure 1.6) (Hua-Van *et al.* 2005, Piegu *et al.* 2015).

RNA transposons

Retrotransposons involve an intermediate RNA moiety and use the "copy-paste" mechanism for transposition (Goodier and Kazazian 2008, Muszewska *et al.* 2011). These elements are transcribed from the donor site followed by reverse transcription to give rise to double stranded molecules which are then inserted into the target locus. Most of the retroelements belong to either LTR retrotransposons or LINEs. These elements differ from each other in their structures. Retroelements consist of three ORFs – Gag, Pol, and Env. The role of Gag-like protein is not well understood, and the env is not found in most of these elements. The 'Pol' ORF codes for a polypeptide consisting of four domains – PR (protease), RT (reverse transcriptase), RH (RNase H) and IN (Integrase). LTR retroelements comprise of two or three

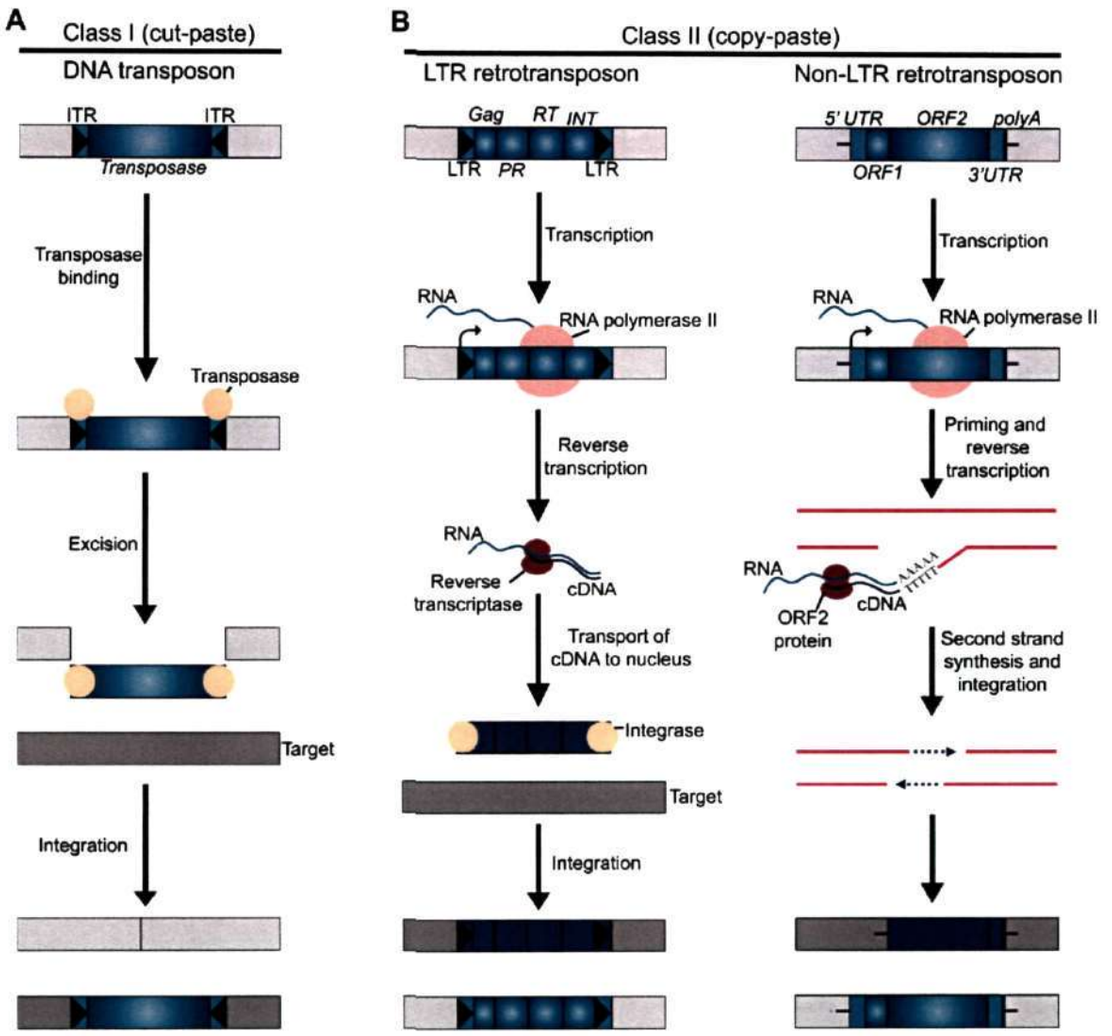

Figure 1.6 Types of transposons and their mode of mobilization. **(A)** DNA transposons are flanked by inverted terminal repeats (ITRs) and encode a transposase. These transposons mobilize by a 'cut and paste' mechanism. The transposase binds at the ITRs, excises the transposon from its existing genomic location (light grey bar) and pastes it into a new genomic location (dark grey bar). **(B)** Class II transposons also known as retrotransposons mobilize by replicative mechanisms that require the reverse transcription of an RNA intermediate. They are of two types - LTR retrotransposons and non-LTR retrotransposons. LTR elements contain two long terminal repeats (LTRs) and encode Gag, protease (PR), reverse transcriptase (RT) and integrase (INT) proteins. The 5′ LTR contains a promoter and produces the mRNA using the host RNA polymerase II. The reverse transcriptase copies the TE mRNA into a full-length cDNA. In the second step, integrase inserts the cDNA into the new target site (dark grey bar). Non-LTR retrotransposons lack LTRs and encode either one or two ORFs. Similar to LTR retrotransposons, the transcription of non-LTR retrotransposons generates a full-length mRNA. Further, these elements mobilize by target-site-primed reverse transcription. In this mechanism, an endonuclease generates a single-stranded 'nick' in the genomic DNA that is used to prime reverse transcription of the RNA. Many a times, the integration events are not complete and end up with truncated integration of non-LTR retrotransposon. The new element shown here (dark blue rectangle in grey bar) is 5′ truncated and is retrotransposition-defective. It is important to note that some non-LTR retrotransposons lack polyA tails at their 3′ ends.

of these ORFs flanked by LTR elements on both sides. The LTR regions provide binding sites for some transcription factors and hence play a significant role in the transposition of these elements. LINE elements consist of two ORFs with a 5' ÚTR and 3' UTR. The 5' UTR provides binding sites for the transcription factors. Due to the presence of conserved domains in all these elements, a high level of similarity exists at the DNA sequence level making them prone to recombination. A study also proposed that recombination among retroelements leads to truncation of these elements rendering them inactive for further transposition (Devos *et al.* 2002).

DNA transposons

Unlike retroelements, DNA transposons are not able to copy themselves from the target site, rather they jump from one place to other in the "cut-paste" mode (Sinzelle *et al.* 2009). The only encoded protein, transposase, excises these elements from the donor site and integrates into the target site. DNA transposons are structurally more homogeneous than retroelements and usually flanked by inverted terminal repeats (ITRs). The excision involves recombination between ITRs leaving a copy of ITR in the donor site as the footprint of the transposon. DNA transposons are usually shorter (less than 3 kb) than retroelements (5 kb or more) (Hua-Van *et al.* 2005) and are also the less abundant type of TEs than retroelements. The difference in the relative abundance of these two elements could be due to a larger size and copy-paste based mechanism of retroelements.

Transposons distribution across genome and their regulation

Transposons, contributing a considerable proportion of a genome, may or may not have a preferred site of accumulation. Many of the TEs seem to have evolved mechanisms that favor their integration into those regions which maximize their chances of survival and propagation (Servant and Deininger 2015, Sultana *et al.* 2017). While some elements target gene-poor, heterochromatic regions, others prefer transcriptionally active 5' UTR regions of

genomes. The distribution of TEs also differs based on the type of elements and the host organism under study. While in some organisms they are limited to a specific region like the centromere or telomere, they can be present throughout the genome in others (Fedoroff 2012, Biscotti *et al.* 2015, Chuong *et al.* 2017). Overall, in most organisms, TEs are more abundant within the heterochromatin including centromeres. Based on a number of studies in a diverse group of organisms, three different models have been proposed to explain the accumulation of TEs in heterochromatic regions (Hua-Van *et al.* 2005). The first model states that low recombination rates in heterochromatin provide safety to TEs. According to the second model, low gene density in heterochromatic regions makes these regions more successful targets since the chances of interfering with the host machinery are minimal. A third model suggests that a low level of expression in the heterochromatin allows them to replicate and hence helps in the proliferation of these elements.

Transposons and centromere evolution

Centromeres, including pericentromeres, in most organisms (including plants, animals, and fungi) are enriched with TEs (Dawe 2003, Wong and Choo 2004, Neumann *et al.* 2011). A number of hypotheses have been proposed suggesting a role of transposons in the evolution of centromeres (Wong and Choo 2004). Some of the TEs are exclusive to the centromeres and form the basis of the first hypothesis. For example, some grass species harbour Ty3-gypsy elements specifically at their centromeres (Cheng *et al.* 2002, Neumann *et al.* 2011). These elements show more than 80% identity among different species. Further, these are also found at centromeres of cereals. The second hypothesis suggests that TEs are used as a template to evolve centromeric and pericentromeric repeats. Evidence for this hypothesis comes from studies showing that centromere repeats in some organisms show similarity to retroelements (Heikkinen *et al.* 1995, Kapitonov and Jurka 1999, Cheng and Murata 2003). The third school of thoughts towards the role of retroelements in centromere

evolution stems from the presence of kinetochore proteins like CENP-B that show homology to transposases. CENP-B associates directly with α-satellites in humans and *dg-dh* repeats in *S. pombe* (Sullivan and Glass 1991, Kipling and Warburton 1997, Nakagawa *et al.* 2002, Masumoto *et al.* 2004). Both these types of repeats show similarities to transposons indicating the presence of a remnant system consisting of transposons and their binding sites. Further evidence towards the role of transposons in the centromere evolution comes from neocentromere studies. Human neocentromeres form ectopically in euchromatin regions that have a high level of LINEs (Lo *et al.* 2001, Alonso *et al.* 2003, Saffery *et al.* 2003). In certain cases, the transposons present in the centromeres are essential for the centromere function. For example, retrotransposons present in cereal centromeres, known as CR retroelements, interact strongly with CENP-A (Zhong *et al.* 2002). Reactivation of the otherwise suppressed centromere transposons leads to meiotic failure in mice (Bourc'his and Bestor 2004). These studies are complemented by the observations that the heterochromatin formation constitutes an important part of centromere assembly and function. The double-stranded RNA generated from retrotransposons is an ideal target for the RNAi machinery leading to dsRNA degradation and in some cases causing heterochromatinization through repressive histone modifications (such as H3K9 dimethylation as seen in *S. pombe*) and/or DNA methylation (Volpe and Martienssen 2011, Matzke and Mosher 2014). The deployment of such a system, such as TEs, to initiate heterochromatin formation at the centromere could have happened during evolution. Also, it is speculated that by regulating transposons at centromeres, RNAi may play an important regulatory role in the structural evolution of centromeres. However, such studies to explore the role of RNAi and its effect on the centromere structure/function have not been attempted.

Kinetochore

The kinetochore is a complex macromolecular structure that assembles on the centromere DNA to facilitate attachment of chromosomes to the mitotic spindle. It consists of more than 80 proteins which form a compact complex structure onto DNA (Table 1.1). These proteins are largely conserved from yeasts to humans except a few which are species specific. Based on electron microscopy and their closeness to centromeric DNA, all the proteins are placed into two distinct layers in the kinetochore. The proteins which directly interact with centromere DNA form the inner layer and the proteins which interact with microtubules constitute the outer layer (Figure 1.7A) (Brinkley BR and Stubblefield 1966, Cleveland *et al.* 2003, Cheeseman 2014, Musacchio and Desai 2017).

Inner kinetochore

The proteins in the inner layer interact directly with specialized centromeric chromatin and are known as constitutive centromere associated network (CCAN). The foundation for CCAN is laid by the presence of CENP-A, followed by CENP-C, two of the evolutionary conserved kinetochore proteins. The remaining proteins are grouped in 4 different sub-complexes: the CENP-LN complex, the CENP-HIKM complex, the CENP-OPQRU complex and the CENP-TWSX complex (Westermann and Schleiffer 2013, Musacchio and Desai 2017). Most of the CCAN proteins have their orthologs in the budding yeast *S. cerevisiae* and are identified as the Ctf19 complex.

CENP-A is a histone H3 variant and the hallmark of centromere identity (Meluh *et al.* 1998, Takahashi *et al.* 2000, Sanyal and Carbon 2002). Human CENP-A homologs are known as Cse4 in *S. cerevisiae*, Cnp1 in *S. pombe* and CID in *D. melanogaster*. CENP-A has a centromere targeting domain (CATD) and a conserved histone fold domain (HFD) (Figure 1.7B) (Malik and Henikoff 2003, Roy and Sanyal 2011, Musacchio and Desai 2017). The N-

Layer in kinetochore structure	Kinetochore protein	Complex	Organism		
			H. sapiens	*S. cerevisiae*	*S. pombe*
INNER	Ndc10	CBF3	-	Ndc10	-
	Scm3	#	HJURP	Scm3	Scm3
	CENP-A	#	CENP-A	Cse4	Cnp1
	CENP-C	#	CENP-C	Mif2	Cnp3
	CENP-T	CENP-T	CENP-T	Cnn1	Cnp20
	CENP-W	CENP-T	CENP-W	Wip1	SPAC17G8.15
	CENP-S	CENP-T	CENP-S	Mhf1	SPBC2D10.16
	CENP-X	CENP-T	CENP-X	Mhf2	Mhf2
	Ctf19	Ctf19 super complex (COMA complex)	CENP-P	Ctf19	Fta2
	Okp1	-do-	CENP-Q	Okp1	Fta7
	Mcm21	-do-	CENP-O	Mcm21	Mal2
	Ame1	-do-	CENP-U	Ame1	Mis17
	Mis6	-do-	CENP-I	Ctf3	Mis6
	Sim4	-do-	CENP-K	Mcm22	Sim4
	Mis15	-do-	CENP-N	Chl4	Mis15
	Fta1	-do-	CENP-L	Iml3	Fta1
OUTER	Mis12	Mis12/ MIND	Mis12	Mtw1	Mis12
	Dsn1	-do-	Dsn1	Dsn1	Mis13
	Nsl1	-do-	Nsl1	Nsl1	Mis14
	Nnf1	-do-	Nnf1	Nnf1	Nnf1
	Spc105	Spc105	Knl1	Spc105	Spc7
	Kre28	-do-	Zwint1	Kre28	-
	Sos7	-do-	-	-	Sos7
	Ndc80	Ndc80	Hec1	Ndc80	Ndc80
	Nuf2	-do-	Nuf2	Nuf2	Nuf2
	Spc24	-do-	Spc24	Spc24	Spc24
	Spc25	-do-	Spc25	Spc25	Spc25
	Dam1	Dam1/DASH	-	Dam1	Dam1
	Duo1	-do-	-	Duo1	Duo1
	Dad1	-do-	-	Dad1	Dad1
	Dad2	-do-	-	Dad2	Dad2
	Dad3	-do-	-	Dad3	Dad3
	Dad4	-do-	-	Dad4	Dad4
	Spc34	-do-	-	Spc34	Spc34
	Ask1	-do-	-	Ask1	Ask1
	Hsk3	-do-	-	Hsk3	Hsk3
	Spc19	-do-	-	Spc19	Spc19
	Ska1	Ska complex	Ska1	-	-
	Ska2	-do-	Ska2	-	-
	Ska3	-do-	Ska3	-	-

Table 1.1 Kinetochore proteins/protein complexes in yeasts.
#, Not applicable, -, absent in the respective organism

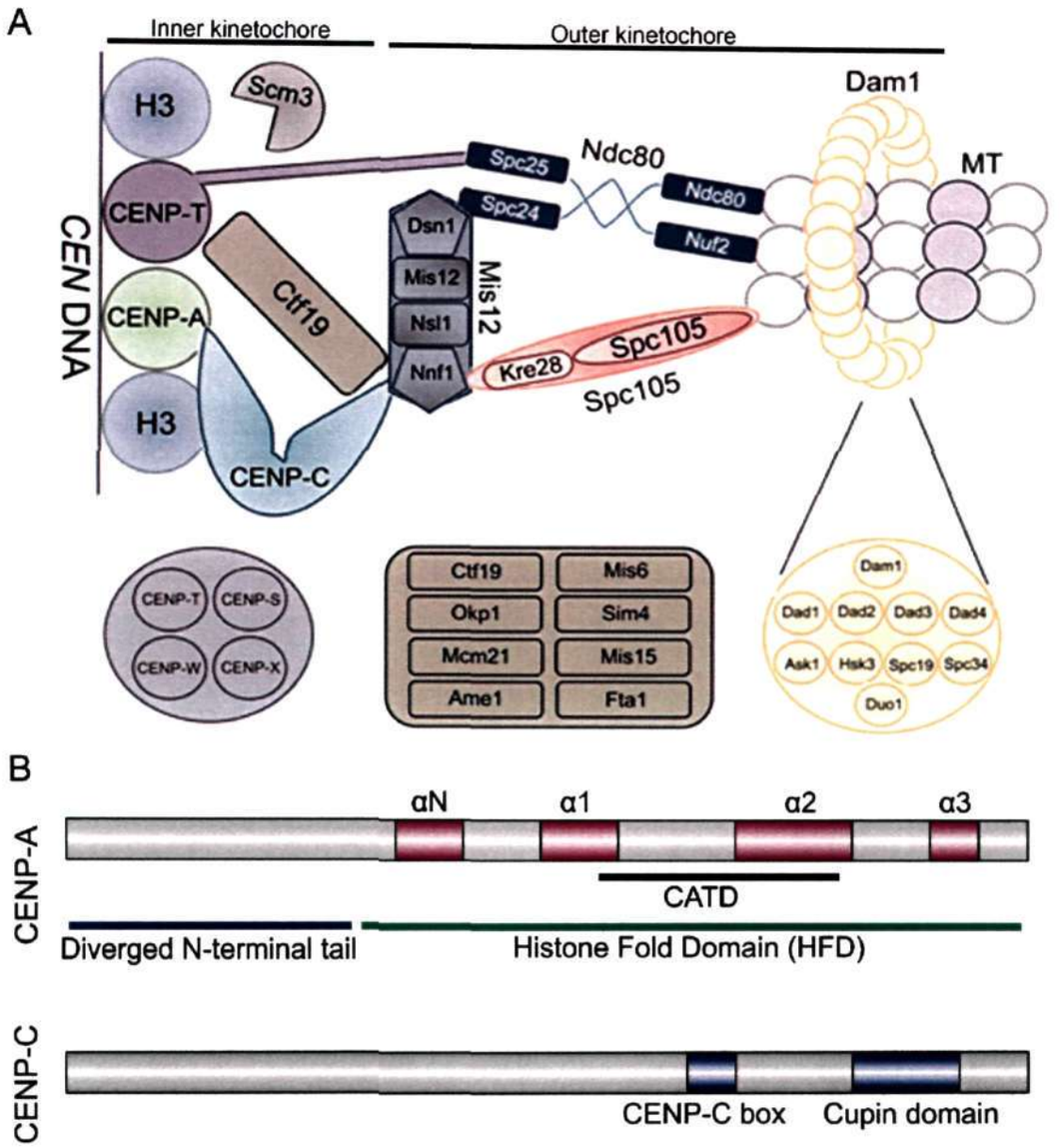

Figure 1.7 Kinetochore proteins in yeasts. (A) A cartoon depicting various proteins present in the budding yeast kinetochore. The constituent proteins of the CENP-T complex, the Ctf19 complex and the Dam1 complex are shown separately. [Figure adapted from (Roy *et al.* 2013)] **(B)** Line diagrams showing the presence of conserved domains of CENP-A and CENP-C. Presence of CATD and diverged N-terminal tail defines the identity of CENP-A and separates it from canonical histone H3. CENP-C harbors two conserved domains, CENP-C box and a DNA binding domain "cupin" domain. These two domains can be used to identify the CENP-C in a species.

terminal of this protein is hyper-variable and its exact role is not yet defined though it is essential in *S. cerevisiae* (Henikoff and Dalal 2005). Since CENP-A forms the foundation of the kinetochore in most of the organisms, its depletion results in cell death. Assembly of CENP-A is regulated by other kinetochore proteins in some of the organisms like *S.*

cerevisiae and *C. albicans* but not in others (Ortiz *et al.* 1999, Tanaka *et al.* 2009, Thakur and Sanyal 2012). A chaperone known as Scm3 in yeast or HJURP in humans helps in the recruitment of CENP-A at the centromere (Camahort *et al.* 2007, Stoler *et al.* 2007, Pidoux *et al.* 2009, Williams *et al.* 2009, Barnhart *et al.* 2011, Zhou *et al.* 2011).

The other evolutionarily conserved inner kinetochore protein is CENP-C. The CENP-C protein family includes CENP-C in humans, Mif2 in *S. cerevisiae*, Cnp3 in *S. pombe*, and many others. This protein family contains a ~25 amino acid long conserved region, known as the CENP-C box, which is essential for its kinetochore localization (Figure 1.7B) (Meluh and Koshland 1995, Milks *et al.* 2009). The presence of C-terminal "cupin" domain helps in dimerization for CENP-C, which is important for its recruitment onto the kinetochore. CENP-C interacts with the C-terminal of CENP-A, an essential prerequisite for its recruitment onto the kinetochore (Westhorpe and Straight 2013, Musacchio and Desai 2017).

Among the other complexes present in CCAN, the CENP-TWSX complex has been well characterized and is proposed to form a nucleosome-like structure (Nishino *et al.* 2012). All four proteins belonging to this complex possess histone fold domain. CENP-T has a long N-terminal tail which can directly interact with the Ndc80 complex present at the outer layer of the kinetochore. Unlike CENP-A and CENP-C, which are conserved in most organisms, a group or all other proteins of the CCAN complex are lost in a number of organisms (Westermann and Schleiffer 2013, Drinnenberg *et al.* 2016, Freitag 2016). Since the loss of these proteins is tolerated, the exact structural and functional contributions of these CCAN complexes remains to be understood. In organisms with point centromeres, the inner kinetochore also includes the point centromere specific CBF3 complex which also binds to the centromere DNA using one of its subunits, Ndc10 (Lechner and Carbon 1991, McAinsh *et al.* 2003).

Outer kinetochore

The outer kinetochore layer includes the proteins which interact with microtubules. Some of these proteins interact with inner kinetochore proteins and form a scaffold on to which the microtubule binding proteins assemble. These proteins include the KNL1-MIS12-NDC80 (KMN) network, the Dam1 complex and the Ska complex.

KMN network

It includes the Ndc80 complex, the Mis12 complex and the Spc105 complex in yeast. In metazoans, this is formed by KNL1-MIS12-NDC80 (KMN) network. The Ndc80 complex is a hetero-tetrameric complex consisting of four conserved subunits: Ndc80, Nuf2, Spc24, and Spc25 (Wigge and Kilmartin 2001). These subunits arrange themselves in a long X-shaped structure which interacts with the proteins from the inner kinetochore on one side and the MTs on the other side (Ciferri *et al.* 2008, Musacchio and Desai 2017). The N-terminal tails of Ndc80 and Nuf2 comprises of the calponin-homology (CH) domain which directly binds to microtubules (Wei *et al.* 2007, Valverde *et al.* 2016). On the other hand, C-terminal tails of Spc24 and Spc25 bind to the inner kinetochore protein, CENP-T. The Ndc80 complex also binds to another outer kinetochore complex, the Mis12/MIND complex. The Mis12 complex is also comprised of four evolutionary conserved and essential kinetochore proteins: Mis12/Mtw1, Dsn1/Mis13, Nsl1/Mis14, and Nnf1 (Goshima *et al.* 1999, Venkei *et al.* 2011, Petrovic *et al.* 2016). Among these proteins, Mis12 in *S. pombe* and its homolog Mtw1 in *S. cerevisiae*, have been studied more extensively than other proteins. Sequence analysis predicted the presence of two conserved amino-acid stretches at the N-terminal of this protein. These two conserved motifs are present in the Mis12 family proteins in all studied organisms ranging from yeasts to humans (Meraldi *et al.* 2006). The Spc105 complex consists of a conserved protein Spc105 (*S. cerevisiae*) or Spc7 (*S. pombe*). KNL1 present in humans is homologous to yeast Spc105 protein. In *S. cerevisiae*, the Spc105 protein interacts

with another protein Kre28 which is a point centromere-specific protein while in *S. pombe*, Spc7 interacts with Sos7, a recently identified protein in the complex (Nekrasov *et al.* 2003, Pagliuca *et al.* 2009, Jakopec *et al.* 2012). In humans, KNL1 is found to be associated with Zwint-1, the functional homolog of Sos7 (Starr *et al.* 2000, Jakopec *et al.* 2012, Varma and Salmon 2012).

Dam1 complex

The Dam1 complex or DASH complex directly interacts with MTs, and is formed by a ten-subunit protein complex. A number of biochemical and genetic screens identified 10 proteins in this complex: Dam1, Duo1, Dad1, Dad2, Dad3, Dad4, Spc34, Ask1, Spc19, and Hsk3. These proteins have been shown to be conserved and fungus specific (Hofmann *et al.* 1998, Cheeseman *et al.* 2001, Enquist-Newman *et al.* 2001, Liu *et al.* 2005, Sanchez-Perez *et al.* 2005, Burrack *et al.* 2011, Thakur and Sanyal 2011). Though this complex is found in all fungi, the essentiality of this complex differs. This complex is essential in *S. cerevisiae* and *C. albicans* but not in *S. pombe*. This complex also differs in the timing of its recruitment at the kinetochore. It is present onto the kinetochore throughout the cell cycle in *S. cerevisiae* and *C. albicans*, but most of the proteins of the Dam1 complex are recruited onto the kinetochore only during mitosis in *S. pombe* (Hofmann *et al.* 1998, Cheeseman *et al.* 2001, Liu *et al.* 2005, Sanchez-Perez *et al.* 2005, Thakur and Sanyal 2011). While the *in vivo* structural assembly of the Dam1 complex remains unknown, this complex has been shown to form a ring around MTs *in vitro* in *S. cerevisiae* (Miranda *et al.* 2005).

Ska complex

In humans, the Dam1 complex is replaced by the Ska complex which comprises of three subunits and shares no sequence similarity with proteins of the Dam1 complex. It consists of three subunits; Ska1, Ska2, and Ska3. All these proteins interact with the MTs and the Ndc80

complex (Hanisch *et al.* 2006, Schmidt *et al.* 2012, Ye and Maresca 2013). This complex in humans is thought to be a functional homolog of the Dam1 complex in yeasts.

Kinetochore assembly

Most of the proteins at the various layers of a kinetochore are conserved but steps that lead to their assembly vary. In *S. cerevisiae* and *C. albicans*, the proteins from both layers are present throughout the cell cycle (Meluh *et al.* 1998, Goshima and Yanagida 2000, Sanyal and Carbon 2002, Roy *et al.* 2011, Thakur and Sanyal 2011). In fission yeast, *S. pombe* most of the Dam1 complex proteins are loaded onto the kinetochore only during mitosis (Liu *et al.* 2005, Sanchez-Perez *et al.* 2005). The process of kinetochore assembly is completely different in humans where most of the outer kinetochore proteins are loaded onto the kinetochore only during mitosis in an ordered manner (Liu *et al.* 2006, Cheeseman and Desai 2008). The regulation of assembly of kinetochore proteins also differs among the yeasts. In *S. cerevisiae*, assembly of a kinetochore is regulated by a point centromere specific protein, Ndc10 which is not present in *C. albicans* and *S. pombe*. In *S. pombe*, the outer kinetochore proteins like Spc7 and Mis6 sub-complexes play important roles in the assembly of the complete kinetochore. This regulation is different in *C. albicans*, where the complete process of assembly is an interdependent process in which proteins from multiple complexes affect each other (Roy *et al.* 2013). This basic difference in the presence of kinetochore proteins onto the centromere DNA between metazoans and yeasts is related to many cytological events in these organisms. The presence of the outer kinetochore is a prerequisite for the kinetochore-MT interaction to take place, hence assembly of the outer kinetochore determines the timing of the kinetochore-MT attachment.

Kinetochore – microtubule attachment

The kinetochore-MT interaction is a conserved process which is essential for proper chromosome segregation. The process of kinetochore-MT attachment depends on forces

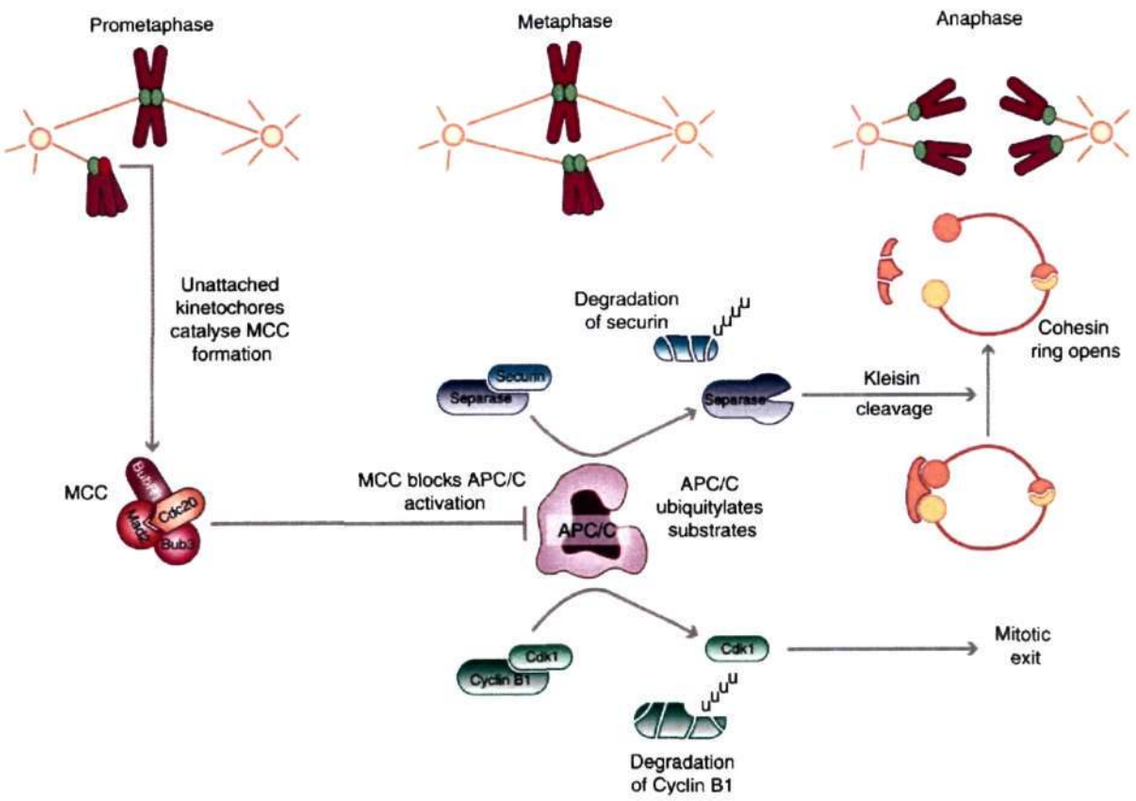

Figure 1.8 A cartoon representing the process of spindle assembly checkpoint (SAC). In prometaphase, unattached kinetochores form the base for the formation of the mitotic checkpoint complex (MCC) leading to inhibition of the APC/C. This results in halting the cell cycle and allows the cell to perform necessary actions to correct the kinetochore microtubule attachment. Once all the chromosomes are attached and aligned (metaphase), Cdc20 activates the APC/C leading to the ubiquitylation and degradation of securin and cyclin B1. Degradation of securin releases separase which then cleaves the Scc1 kleisin subunit of the cohesion ring structure. This allows sister chromatids to separate during anaphase. [Figure adapted from (Lara-Gonzalez *et al.* 2012)]

generated by MT pulling on the kinetochore (Tanaka 2010). First, the MTs emanating from the spindle pole bodies (SPBs) attach to the kinetochores by a search and capture mechanism. This initial attachment is mediated by proteins from the outer kinetochore like the Dam1 complex, the Ska complex and the Ndc80 complex. The capturing of one side of a kinetochore by the spindle MTs generates force imbalance due to one-sided pulling force. The force is balanced when MTs emanating from the opposite pole capture the other side of the monopolar chromosome. The kinetochore capturing by MTs from both sides balances tension and stabilizes the chromosomes movement. The poleward forces on the chromosome are stabilized by inward forces exerted by cohesins that prevent poleward movement and thus

separation of chromosomes until the onset of anaphase. In the absence of the bipolar attachment of each chromosome, the cell cycle halts for correcting the attachment. The force imbalance is sensed by the checkpoint proteins belonging to spindle assembly checkpoint (Figure 1.8) which arrests the cell cycle progression until errors are corrected (Lara-Gonzalez *et al.* 2012, Foley and Kapoor 2013). Most often, the regulatory proteins present in the cell, including the proteins from the spindle assembly checkpoint, help in achieving the biorientation. Once chromosomes are bi-oriented and tension on the chromosome is balanced, checkpoint proteins allow the cell cycle to continue which leads to proper chromosome segregation. The kinetochore-MT interaction depends on the presence of a fully assembled kinetochore and also the dynamics of the NE (Guttinger *et al.* 2009).

Kinetochore clustering

Centromeres/kinetochores are clustered at the nuclear periphery in yeasts (Figure 1.9). The kinetochore clustering helps in organization of yeast chromosomes in the Rabl configuration so that chromosome arms lie freely in the nucleoplasm (Taddei and Gasser 2012). This arrangement facilitates compartmentalization such as repair foci, high transcription foci etc. in the interphase nucleus (Taddei *et al.* 2010, Zimmer and Fabre 2011, Taddei and Gasser 2012). In budding yeast, *S. cerevisiae*, kinetochores are always clustered (Jin *et al.* 2000, Anderson *et al.* 2009). However, in *S. pombe*, kinetochores are clustered in interphase cells but de-cluster during mitosis (Takahashi *et al.* 2000). This phenomenon aids in the kinetochore attachment to MTs during the onset of mitosis in both the yeast species (Jin *et al.* 2000, Hou *et al.* 2012, Richmond *et al.* 2013). Several studies revealed a diverse group of proteins playing an important role in kinetochore clustering and helping in proper chromosome segregation. In *S. cerevisiae*, where clustered kinetochores are always attached to the SPB directly through MTs (Tanaka *et al.* 2010); the presence of Slk19 is required even when MTs are depolymerized (Richmond *et al.* 2013). Whereas in *S. pombe*, the kinetochores

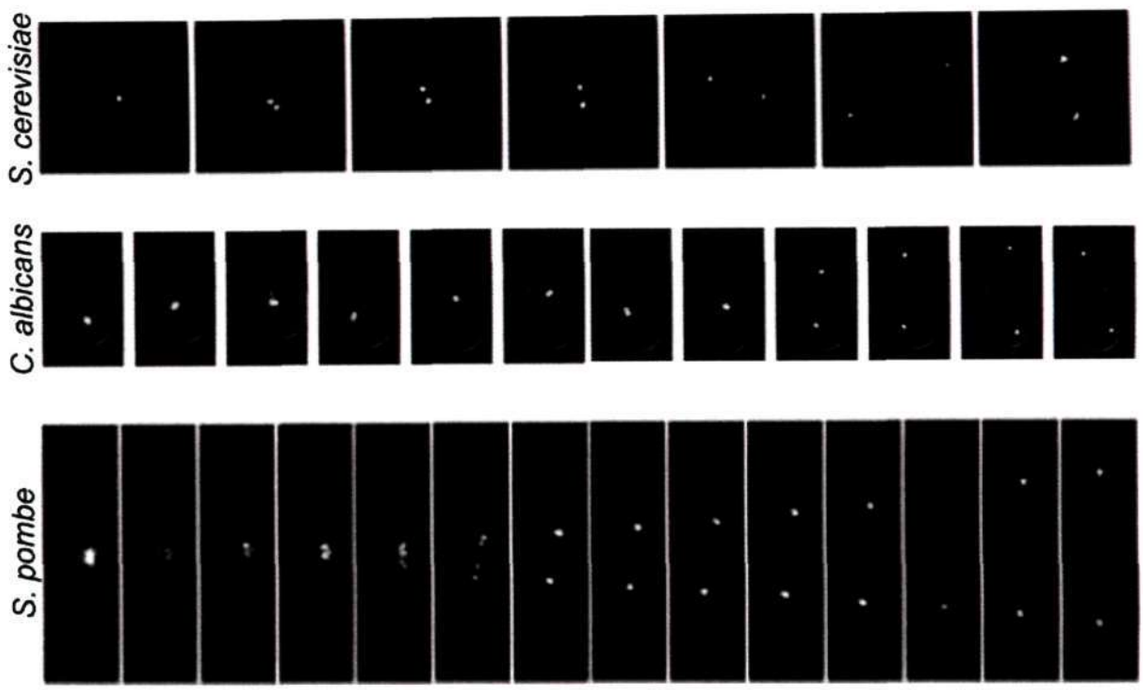

Figure 1.9 Kinetochore clustering dynamics in fungi. Kinetochores are clustered in most of the fungi studied as shown here for the budding yeast *S. cerevisiae* (Ndc80), *C. albicans* (CaMtw1) and the fission yeast *S. pombe* (Mis12). The kinetochores remain clustered through the cell cycle in both *S. cerevisiae* and *C. albicans* whereas they uncluster during mitosis in *S. pombe*. [Figures modified from (Aoki *et al.* 2006, Roy *et al.* 2011, Suzuki *et al.* 2016)]

are held close to the SPB by an indirect link involving proteins like Csi1 (Hou *et al.* 2012). Deletion of Csi1 leads to defects in clustering and chromosome segregation. However, MTs disruption directly does not show any defects in the kinetochore clustering in this organism (Castagnetti *et al.* 2010). A recent report in *S. pombe* revealed that another protein Sad1, an inner nuclear envelope protein, also plays an important role in the kinetochore clustering (Fernandez-Alvarez *et al.* 2016). Sad1 forms a link between the SPB and the kinetochore cluster. Using a specific mutant of this protein, authors provided evidence that an interaction between the kinetochore and the SPB is required for normal spindle nucleation (Fernandez-Alvarez *et al.* 2016). The kinetochore clustering in also seen in mitotic cells of *Drosophila* where they are present close to the nucleolus and play an important role in heterochromatin organization (Marshall *et al.* 1996, Padeken *et al.* 2013). A nucleoplasmin homolog, NLP, is required for maintaining the kinetochore cluster close to the nucleolus in this organism

(Padeken *et al.* 2013). During *Drosophila* meiosis, the kinetochore cluster also helps in proper synapse formation at early stages (Takeo *et al.* 2011, Tanneti *et al.* 2011). Metazoans do not show kinetochore clustering at any stage of the cell cycle where the metaphase plate, a mitotic structure analogous to the kinetochore cluster, is present.

Microtubules and microtubule organizing centres

Microtubule organizing centres (MTOCs) are the primary MT nucleating centres and consist of a core complex consisting of three proteins namely γ-tubulin, Spc98 and Spc97 (Kollman *et al.* 2008). These three proteins form a small complex known as γ-tubulin small complex (γ-TuSC), which can then associate with more proteins to form the γ-tubulin ring complex, γ-TuRC (Figure 1.10A) (Lin *et al.* 2015). The ring complex also forms the foundation for the assembly of α-β tubulin dimers and initiate polymerization of MTs. By nucleating MTs, the γ-tubulin complex determines the tracks along which different cellular components are transported. In most organisms including *S. pombe*, *Drosophila* and other animals, proteins like GCP4-6 (γ-TuRC specific proteins) associate with γ-TuSC and form a part of γ-TuRC (Gunawardane *et al.* 2000, Murphy *et al.* 2001, Anders *et al.* 2006). While the exact role of GCP4-6 remains largely unknown, these proteins are found to be important for microtubule nucleation from γ-tubulin complex. In all these organisms, MTOCs are present in the cytoplasm during interphase. These MTOCs cluster during mitosis onto a structure known as the spindle pole body (SPB) in yeast and the centrosome in animals (Figure 1.10B and C) (Luders and Stearns 2007, Bettencourt-Dias 2013). In contrast, budding yeast *S. cerevisiae* harbors only γ-TuSC, which organizes itself in a ring structure and thus works as γ-TuRC as well (Kollman *et al.* 2010). Interestingly, the genes coding of GCP4-6 are absent from *S. cerevisiae* genome. Also there is only one MTOC in S. cerevisiae, which duplicates to form SPBs during mitosis. Spc110 and Spc72 present in the SPB act as the binding site for

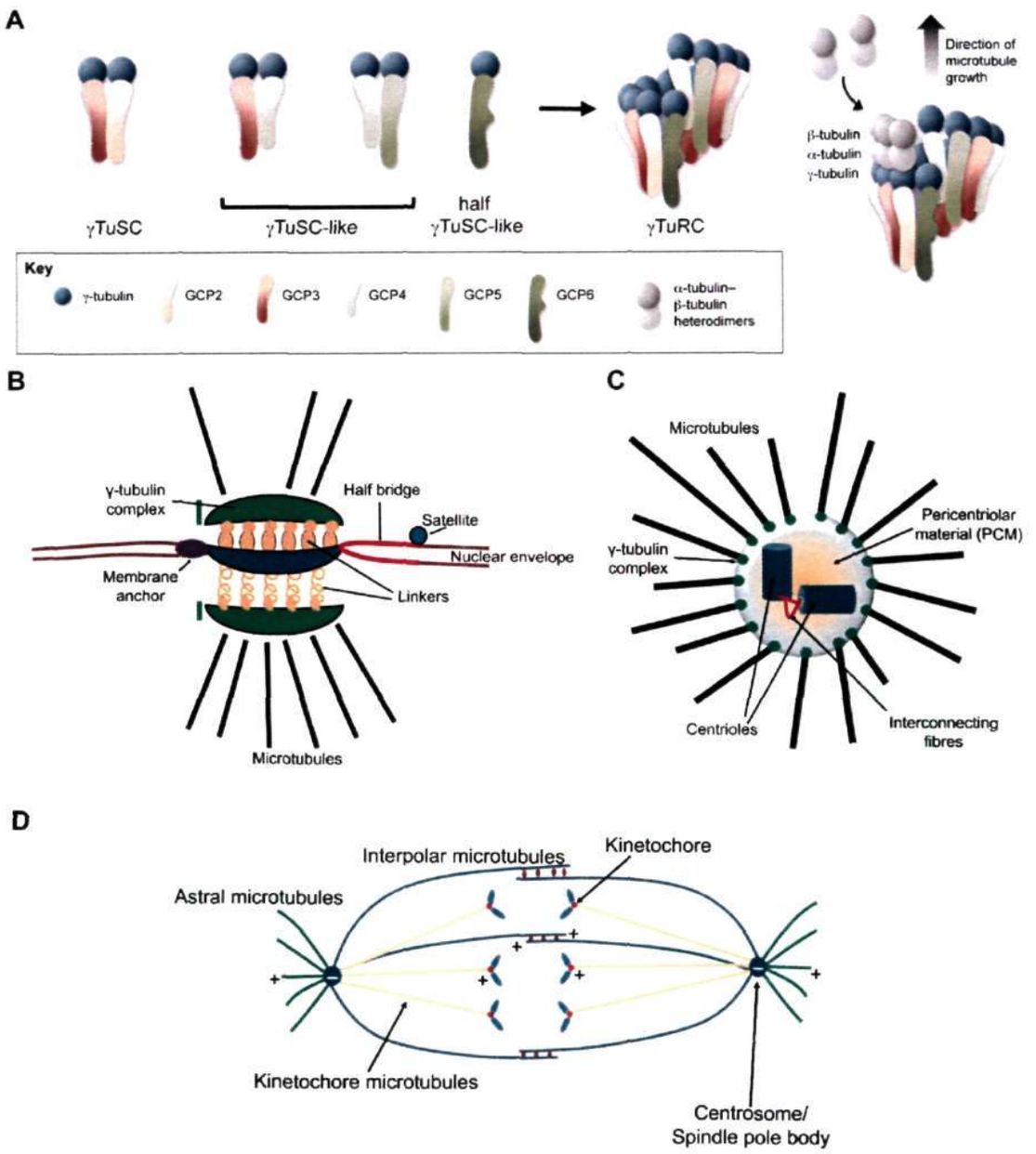

Figure 1.10 Microtubule organizing centre and microtubules. **(A)** A model showing the assembly of γ-tubulin ring complex (γ-TuRC). γ-tubulin small complex (γTuSC) like complexes are assembled by replacement of GCP2 and/or GCP3 with GCP4, GCP5 and/or GCP6. Sometimes, half complexes are observed that contain a single molecule of GCP4, GCP5 or GCP6 interacting with γ-tubulin. Microtubule polymerization from γTuRC involves interactions of α–β-tubulin heterodimers with γ-tubulin in the γTuRC.[Figure adapted from (Teixido-Travesa *et al.* 2012)] **(B)** A schematic representation of spindle pole body showing all major components including the γ-tubulin complex. **(C)** A simplified view of centrosomes describing microtubule nucleation. While the γ-tubulin complex remains conserved in centrosomes, rest of the constituents components are different. **(D)** A cartoon representing the various types of microtubules present in a mitotic cell. The centrosome or spindle pole body is the nucleation centre for various microtubules which interact with kinetochore (kinetochore microtubules) or cortex (astral microtubules) or microtubules originating from other poles (interpolar microtubules). The microtubules interact with each other with help of motor proteins (brown circles).

γ-TuSC and initiate MT nucleation (Lin *et al.* 2014).

MTs are polarized, hollow cylinders that are formed by polymerization of α/β-tubulin heterodimers. The plus end of these polar MT strands is highly dynamic and undergo growth as well as shrinkage at a faster rate than the less dynamics minus end. The minus end is anchored to MTOCs. In non-proliferating cells, MTs carry out a variety of processes including cell motility, organelle trafficking, cell signalling and adhesion. MTs are synergistically modulated by motor proteins: the plus-end directed kinesins, the minus-end directed dyneins, and MAPs which dynamically alter the rate of MT stability (Mallik and Gross 2004, Wade 2009). During interphase, MTs are largely localized to the cytoplasm in most organisms. The cytoplasmic microtubules (cMTs) along with motor proteins influence nuclear positioning and movement (Lee *et al.* 2000, Fink *et al.* 2006, Ten Hoopen *et al.* 2012). Upon the onset of mitosis, cMTs reorganize themselves to form the mitotic spindle between the two poles (SPBs in yeast or centrosomes in metazoans). The minus ends of MTs are anchored to the SPBs, while the more dynamic plus ends radiate outward to facilitate interactions with other cellular components (Figure 1.10D). Some of these MTs interact with kinetochores to become kinetochore microtubules (kMTs) and provide the pulling force on chromosomes during anaphase. Astral MTs make contact with the cell cortex aiding in spindle positioning, while inter-polar microtubules (ipMTs) are formed when the plus ends of MTs originating from opposite poles interact via sliding, resulting in an anti-parallel array at the mid-zone. The combination of pushing force provided by ipMTs on SPBs along with the pulling force from kMTs and astral MTs aids in segregation during anaphase.

Combined together, MTs and MTOCs lead to mitotic spindle formation and its proper alignment during mitosis. The spindle positioning is not only crucial for proper chromosome segregation but also defines the site of nuclear division. In general, the spindle is positioned centrally in a dividing cell and thus a mother cell gives rise to two identical daughter cells by

the fission mode of division. While most organisms undergo this type of division, few others show variations in spindle positioning and hence give rise to cell polarity (Horvitz and Herskowitz 1992, Neumuller and Knoblich 2009). This type of division is observed during developmental stages of multicellular organisms and in stem cells (Knoblich 2008, Neumuller and Knoblich 2009). Budding yeasts also undergo a similar unequal cell division where the site of the division is defined prior to spindle positioning (Fraschini *et al.* 2008). Some studies have been carried out to identify the factors to understand the dynamics of spindle positioning. Some of these regulatory factors are shown to be different between budding yeasts and multicellular organisms (Fraschini *et al.* 2008, Neumuller and Knoblich 2009).

Nuclear envelope

The nuclear envelope (NE) is a hallmark of all eukaryotic cells. It is formed of an outer nuclear membrane (ONM) and an inner nuclear membrane (INM) (Figure 1.11) (Guttinger *et al.* 2009, Hetzer 2010). The outer membrane is in continuation with the endoplasmic reticulum (ER) and plays a major role in maintaining the integrity of the NE. The ONM also harbors ribosomes - the site for protein synthesis. The INM is in direct contact with chromosomes. In metazoans, chromatin is separated from the inner membrane by a layer of lamin proteins which are absent in yeast. The NE is a house of various proteins which play important roles in transport, genome maintenance and regulation of transcription. Most of the proteins involved in transport are assembled into nuclear pore complexes (NPCs) in the NE and are called as nucleoporins (Nups). The INM hosts a group of proteins, known as SUN domain proteins, which interact with lamins and chromatin. These proteins play roles in chromatin organization, chromatin dynamics, folding and replication of DNA. A group of proteins located on the ONM

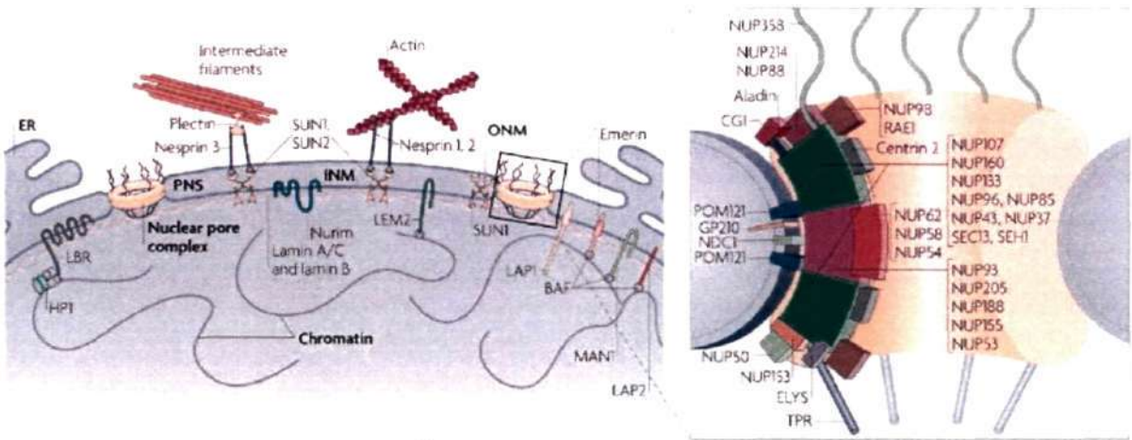

Figure 1.11 Connections between chromatin and the nuclear envelope. Key components of the NE are shown including the inner and outer nuclear membrane (INM and ONM), which enclose the perinuclear space (PNS). Nuclear pore complexes (NPCs) span the NE and are formed from several unique subcomplexes of nucleoporins (zoomed image). Linker of nucleoskeleton and cytoskeleton (LINC) complexes are made up of 'SUN' and 'KASH' domain containing proteins (described below). [Figure adapted from (Guttinger *et al.* 2009)]

interact with cytoskeletal proteins and maintain the nuclear positioning (Hetzer 2010). These proteins mainly include spectrin repeat containing proteins known as nesprins.

Nuclear pore complex (NPC)

The NPCs are structures formed by 30 distinct types of nucleoporins (Figure 1.11). The NPC is a transporter which selects and regulates the movement of many proteins across the NE. Electron microscopy imaging revealed the NPC as a cylindrical structure with 100-150 nm diameter and 50-70 nm thickness (Hoelz *et al.* 2011). The proteins present in the NPC are arranged in many layers to form this structure. The core proteins forming the luminal ring are in direct contact with INM and ONM and make the foundation of the NPC. The major proteins present in this layer are Ndc1, Pom152, and Pom34. This is followed by proteins arranged in two layers; the inner and the outer layer. The inner layer is mainly composed of the Nup170 or Nup155 sub-complex while the outer layer includes the Nup84 or Nup107 sub-complex. These two layers are connected to the linker Nups and the FG Nups. The FG Nups contain phenylalanine - glycine repeats and act as a direct mediator of transport as they are loosely hanging in the central pore area of the NPC. These proteins allow free

diffusion of small molecules like sugar, ions, and water. Larger molecules like proteins are transported using the active transport process in a regulated fashion. These NPCs are stable complexes but are reversibly disassembled during mitosis. The *de novo* assembly of NPCs takes place during interphase through ER which is in direct contact with the ONM (Wente and Rout 2010, Hoelz *et al.* 2011).

LINC complex

The linker of nucleoskeleton and cytoskeleton (LINC) complex forms a bridge across the NE in most eukaryotes and is responsible for force transfer between the cytoplasm and nucleoplasm (Simon and Wilson 2011, Chang *et al.* 2015). The LINC complex consists of KASH (Klarsicht, ANC-1, and Syne Homology) domain proteins present in the ONM and the SUN (Sad1 and UNC-84) domain proteins in the INM (Figure 1.12). The SUN domain is a highly conserved motif across evolution whereas the KASH domain is comprised of a highly variable stretch of 50-60 aa that typically ends with "PPPX" (Razafsky and Hodzic 2009, Zhou *et al.* 2015, Meier 2016). The KASH and the SUN domain interact with each other in the perinuclear space. The KASH proteins extend into the cytoplasm and interact with cytoskeletal elements and the SUN proteins interact with lamins, chromatin associated proteins in the nucleoplasm. Due to its capability of mechanical force transfer across the NE, the LINC complex plays important roles in the movement of the nucleus, signal transduction and chromatin organization (Starr 2009, Kim *et al.* 2015). Their role in nuclear anchorage and dynamics, nuclear structure maintenance is well studied in *C. elegans* (Bone *et al.* 2014, Cain *et al.* 2014). In yeasts, SUN-KASH proteins are closely associated with the SPB. In *S. pombe*, these proteins link the SPB with centromeres during mitosis and telomeres during meiosis and facilitate in centromere or telomere clustering (Fennell *et al.* 2015, Klutstein *et al.* 2015). In budding yeast, *S. cerevisiae*, the SUN protein, Mps3, interact with a sub-structure called the half-bridge. This interaction between Mps3 and the half-bridge is

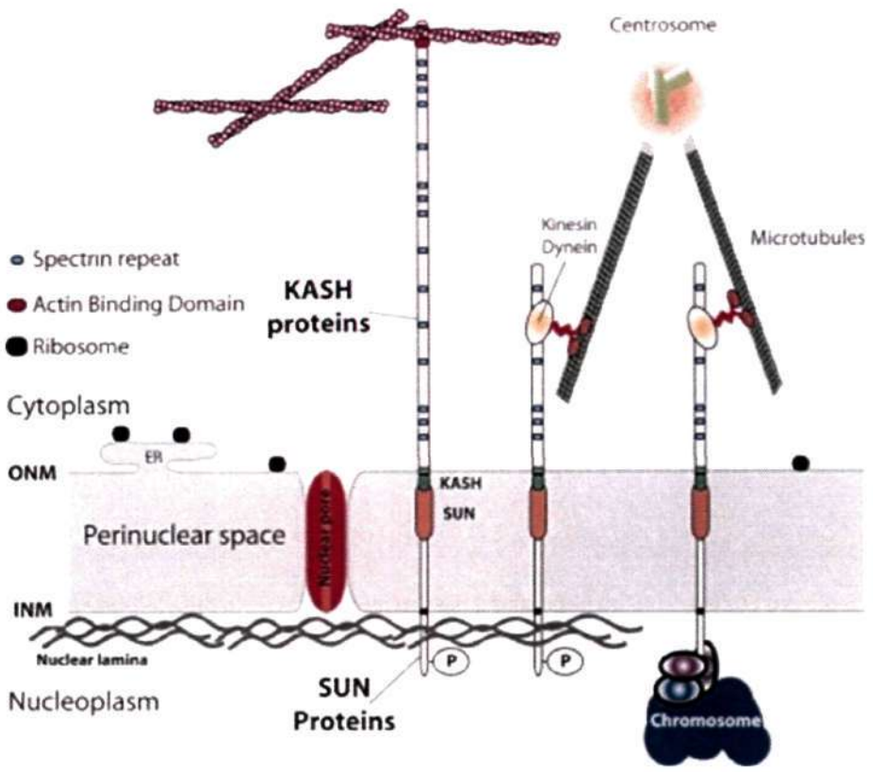

Figure 1.12 The Linker of Nucleoskeleton and Cytoskeleton (LINC) complex. The evolutionarily conserved interaction between SUN (orange) and KASH (green) domain–containing proteins physically interact to form the LINC in the perinuclear space. These proteins connects the nuclear lamina to essential cytoskeletal elements such as the actin and microtubule networks. [Figure adapted from (Razafsky and Hodzic 2009)]

essential for the SPB function, and play a role in the SPB duplication (Hagan and Yanagida 1995, Jaspersen *et al.* 2006). SUN-KASH proteins are also shown to play a critical role in meiotic chromosome pairing and synapsis formation in both yeast and mammals (Chikashige *et al.* 2006, Sato *et al.* 2009, Shibuya and Watanabe 2014). A recent study suggested their role in DNA repair as well (Swartz *et al.* 2014).

Types of mitosis

During mitosis, the NE undergoes remodelling to a great extent. Based on the dynamics of the NE, mitosis can be categorised broadly into two types: open and closed mitosis (Figure 1.13) (De Souza and Osmani 2007).

Open mitosis

Open mitosis is the type of mitosis where the NE breaks down completely and nucleoplasm mixes with the cytoplasm. This type of mitosis occurs mostly in metazoans. During mitosis, the NE undergoes dramatic changes beginning with disassembly of the NPCs. The linker layer disassembles first which is followed by the Nup107 complex. This reduces the integrity of the NE and facilitates its break down (Kutay and Hetzer 2008, De Souza and Osmani 2009). The lamin proteins are phosphorylated and removed from the NE. The disassembled NE is reserved into the ER in the form of small vesicles. This disassembly of the NE is well coordinated with the formation of a mitotic spindle. When mitosis is complete, the vesicles containing the NE interact with chromatin structures and starts fusing with each other to form the NE (Beck and Hurt 2017, Ungricht and Kutay 2017). The

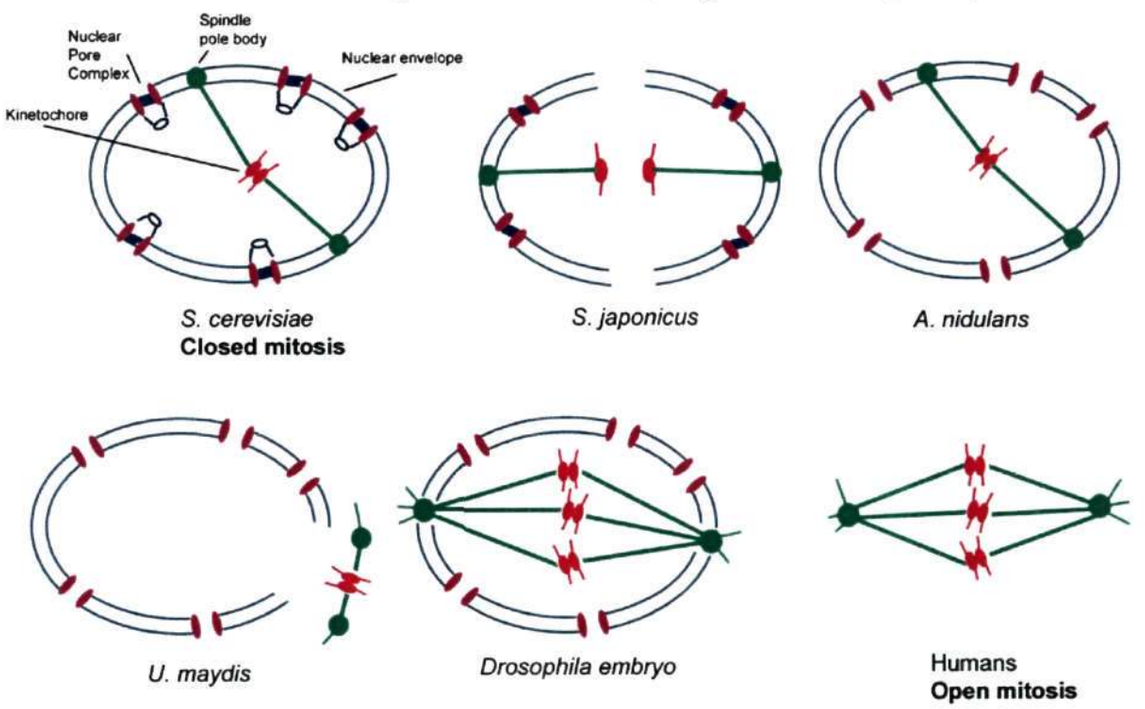

Figure 1.13 A diagram showing the types of mitosis observed in various organisms. The budding yeast, *S. cerevisiae*, undergoes completely closed mitosis where the nuclear envelope does not break during mitosis. On the contrary, humans undergo open mitosis where the nuclear envelope disintegrates completely during mitosis. Intermediate forms of mitosis are seen in other organisms where the nuclear envelope breaks during anaphase (*S. japonicus*), only the nuclear pore complexes disassemble (*A. nidulans*), the nuclear envelope breaks only at one locus (*U. maydis*) or near the two poles (*Drosophila* embryo) during mitosis. It is important to note that nuclear pore complexes are compromised either partially or completely in all cases except in the closed mitosis.

re-establishment of the NE is initiated with the reversal of phosphorylation of NE components followed by re-emergence of the INM proteins embedded in the ER. The cellular machinery ensures that the NE reassembly includes all chromosomes into the reforming nucleus. The compactness of anaphase chromosomes plays a key role in this process. The dense configuration of anaphase chromosomes helps in preventing invasion of membranes into chromatin, which could otherwise cause post-mitotic aberrations and in extreme cases, leads to deleterious micronucleus formation.

Closed mitosis

Closed mitosis refers to the type when the NE does not break down and chromosome segregation occurs inside the closed intact nucleus. The NE undergoes remodelling in its membrane structure to facilitate the transport of proteins required during mitosis. This occurs in budding yeast, *S. cerevisiae* and fission yeast *S. pombe* (De Souza and Osmani 2007). In *S. pombe,* the NE undergoes additional changes near the SPBs which allow the entry of SPBs into the nucleus without breaking the NE (Ding *et al.* 1997, Asakawa *et al.* 2010, Asakawa *et al.* 2011).

Divergent strategies of mitosis

Apart from the two conventional types of mitosis found in budding yeast, fission yeast and metazoans, various other strategies are adopted by various organisms to execute the process of mitotic division (Figure 1.13) (De Souza and Osmani 2009). The first example is the embryo of *D. melanogaster* where the NE breaks near centrosomes until chromosome segregation starts when it breaks down further (Kiseleva *et al.* 2001). A fungus, *A. nidulans*, undergoes another type of mitosis where FG repeats containing proteins from the NPCs disassemble. The rest of the NE remains intact during the whole process (De Souza *et al.* 2004). *Ustilago maydis* shows a different type of NE dynamics during mitosis. The NPCs disassemble completely and the NE breaks down near SPBs. After the NE breakdown, the

chromatin alone is pulled to the daughter cell by MTs. The nuclear division takes place in daughter cell which is followed by movement of half of the chromatin back to the mother cell while the remaining half is retained into the daughter cell. A new NE formation takes place around the daughter nuclear mass (Straube *et al.* 2005, Theisen *et al.* 2008). Recently, another type of mitotic process has been shown to occur in a fission yeast, *S. japonicus* (Aoki *et al.* 2011, Yam *et al.* 2011). In this fission yeast, the NE along with the NPCs remains intact during most of mitosis and breaks in the middle of the NE during anaphase. This variety in dynamics of the NE suggest that the basic process of chromosome segregation is conserved in all organisms but the strategies adopted to carry out the process have evolved.

Cryptococcus species complex

Cryptococcus species complex is a polyphyletic complex consisting of both pathogenic and non-pathogenic species. All the pathogenic species cluster together in *Filobasidiella* clade, proposed to have emerged from *Tremella* (Findley *et al.* 2012). These pathogenic species include *Cryptococcus neoformans* and *Cryptococcus gattii*. Other saprobic, non-pathogenic species are *Cryptococcus amylolentus*, *Filobasidiella depauperata*, and *Tsuchiyaea wingfieldii* (Figure 1.14A). The pathogenic species *C. neoformans* and *C. gattii* have been proposed to diverge approximately 37 million years ago (MYA) (Lin 2009). *C. neoformans* has been further split into two species, *C. neoformans* and *C. deneoformans*, estimated to have diverged from each other around 18.5 MYA. *C. gattii* has also been proposed to be a group of 5 species, *C. gattii, Cryptococcus bacillisporus, Cryptococcus deuterogattii, Cryptococcus tetragattii and Cryptococcus decagattii* (Hagen *et al.* 2015).

Life cycle of *Cryptococcus*

Cryptococcus species life cycle has been well understood with respect to *C. neoformans* (Figure 1.14 and 1.15). *C. neoformans* is a dimorphic fungus that switches

between two morphological forms - yeast and hyphal forms (Lin and Heitman 2006, Kozubowski and Heitman 2011). *Cryptococci* cells reside in a diverse ecological niche like plants and secondary hosts like amoeba or animals. It undergoes both sexual and asexual life cycle. The vegetative form is a single cellular yeast which is usually found in soil mixed with pigeon guano or decaying wood (Lin and Heitman 2006, Kozubowski and Heitman 2011). This form of *C. neoformans* grows by budding and usually found more frequently in the environment than its hyphal form (Figure 1.14B). It also forms pseudohyphal structures which are rarely found in the natural conditions (Lin 2009). The presence of **a** and α mating types in *C. neoformans* allows it to have a sexual cycle. *C. neoformans* shows both opposite as well as same sex mating leading to the formation of dikaryon, a characteristic feature of the Basidiomycota group (Figure 1.14C). The dikaryon develops into filaments and undergoes nuclear fusion in the clamp cell which is followed by meiosis and formation of spores. The spores are called as basidiospores and are the infectious propagules for the disease. The spores enter into the host body through the respiratory tract and infect lungs as the primary infection site (Kronstad *et al.* 2011). The spores can also stay in a dormant form in lungs and infect when the immunity of the host is compromised. These spores move to other parts of the body through the blood stream and cause infections (Figure 1.15). The spores can also pass through the blood-brain barrier and cause infection in the brain leading to cryptococcal meningitis. The transmission from human to human or animals to human is not observed in cryptococcal infections. Apart from spores, *C. neoformans* has many characteristic features which enhance its infectious capacity (Kronstad *et al.* 2011, Srikanta *et al.* 2014, May *et al.* 2016). These features include its ability to grow at high temperatures, the polysaccharide capsule which protects it within the host immune cells, morphological and phenotypic switches. While non-pathogenic species like *C. amylolentus* follow a similar life cycle except the infectious part, *F. depauperata* does not have any yeast form in its life cycle.

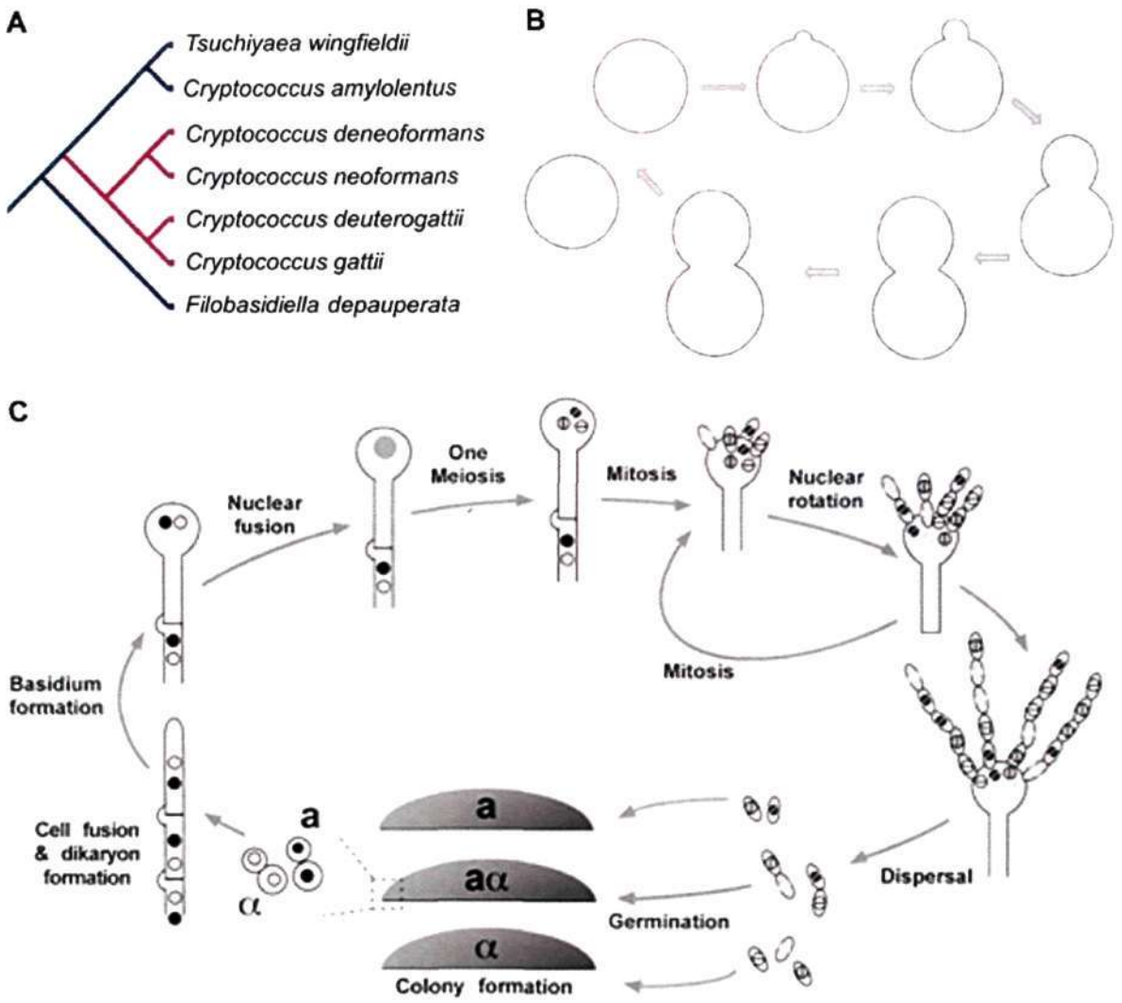

Figure 1.14 Life cycle of *Cryptococcus neoformans*. **(A)** A phylogram showing the number of species present in *Cryptococcus* species complex. The species marked with blue line are saprobic in nature while the ones marked in red are pathogenic in nature. **(B)** A cartoon depicting the asexual cell cycle of *C. neoformans*. *C. neoformans* grows by budding giving rise to the daughter cell. **(C)** A model describing the sexual life cycle of *C. neoformans*. Under starvation conditions, **a** and α cells undergo cell-cell fusion in response to pheromone signalling and form dikaryons. This triggers the filamentous growth which ultimately gives rise to basidium. The two nuclei fuse in the basidium giving rise to single diploid nucleus. The diploid nucleus undergoes meiosis and gives rise to 4 haploid nuclei which are then released in the form of spores. The spores germinate as yeast cells in favourable condition. [Figure adapted from (Idnurm 2010)]

Cryptococcosis

Infections of *Cryptococcus* species are known as Cryptococcosis and were identified in 1894. However, the human infections came to prominence with the onset of HIV infections in the 1980s. The severe form of *Cryptococcus* infection, Cryptococcal meningitis is the most common infection of the central nervous system (CNS) around the world. It is also the third

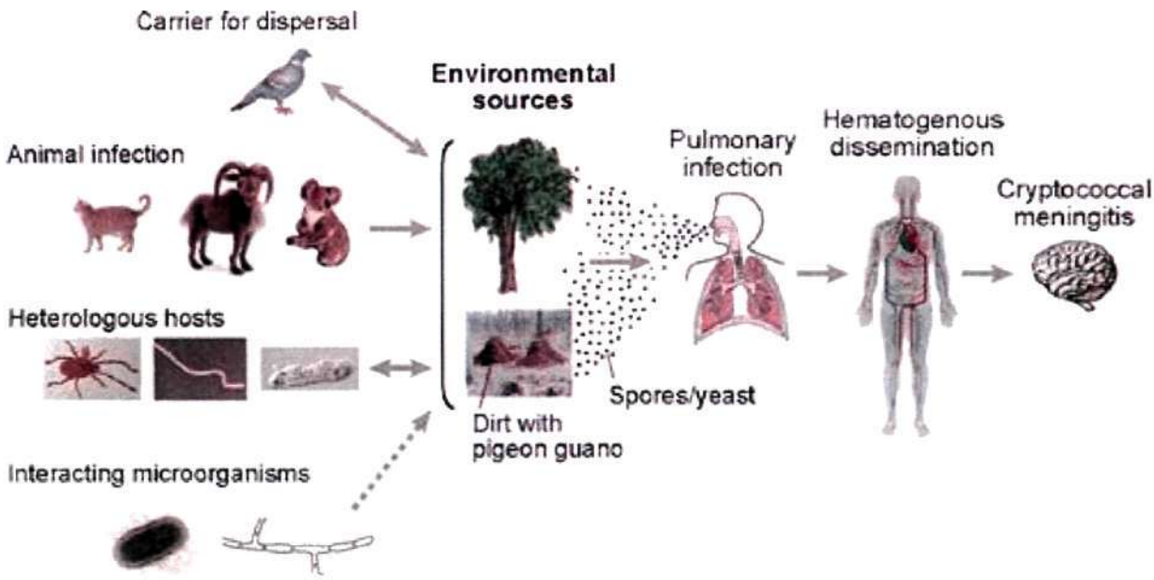

Figure 1.15 Infection cycle of *Cryptococcus neoformans*. The fungus survives in the environment within soil (commonly contaminated with bird guano) and trees. The fungus infects various animal hosts and can also survive environmental predators such as insects, worms, and amoeba. The fungus establishes a human pulmonary infection through inhalation of its spores or desiccated yeast cells from environmental sources. When the host becomes immunocompromised, the fungus can enter the central nervous system (CNS) causing the most severe form of human cryptococcosis. [Figure adapted from (Lin and Heitman 2006)]

most neurological complications in AIDS patients. A recent study estimated the number of deaths due to AIDS-related cryptococcal meningitis at a little more than 1,80,000 people per year, accounting for 15% of AIDS-related mortality (Rajasingham *et al.* 2017). However, the mortality rate can be as high as more than 75% in the Sub-Sahara African countries. The major reason for its more prevalence in African and South-East Asian countries is the lack of preventive measures in these countries. Although *Cryptococcus* infections are predominant in immunocompromised people like HIV-AIDS patients, they occasionally do infect immunocompetent patients. Cryptococcal infection is also prevalent in patients with solid organ transplants who are under steroid and immunosuppressive medication. Due to recent outbreak of Cryptococcosis in otherwise healthy individuals in North America and Canada (popularly known as Pacific Northwest outbreak), the focus has been shifted to certain lineages that may act as primary pathogens (Kidd *et al.* 2004). The main species involved in this outbreak was found to be *C. deuterogattii* (earlier known as *C. gattii* VGII).

Cryptococcus species complex in genomics era

The first species whose genome was sequenced from the *Cryptococcus* species complex was *C. deneoformans* (earlier known as *C. neoformans* var. *neoformans*) (Loftus *et al.* 2005). The sequencing data revealed that *C. deneoformans* has a 20 Mb haploid genome with over 6,500 genes which are rich in introns. The genome spans over 14 chromosomes of sizes ranging between 700 kb to 2.3 Mb. Approximately 5% of the genome is occupied with transposons, most of which were proposed to cluster near telomeres and putative centromeres. Based on the bioinformatics analysis, the centromeres in *C. deneoformans* are predicted to be large regional centromeres spanning a size range of 15-60 kb. Recently, genomes of *C. neoformans* (earlier known as *C. neoformans* var. *grubii*) and *C. gattii* (earlier known as *C. neoformans* var. *gattii*) were sequenced (D'Souza *et al.* 2011, Janbon *et al.* 2014). A comparison of *C. neoformans* and *C. deneoformans* genomes revealed 85-90% similarity and high level of collinearity. Comparison of *C. deneoformans* with *C. gattii* genome showed 85-87% similarity among these two species with few major rearrangement in the genome with respect to each other (D'Souza *et al.* 2011). The genome sequencing of the three *Cryptococcus* species revealed certain differences between these species. One of the main differences found was the absence of genes essential for functional RNAi in *C. deuterogattii* (Feretzaki *et al.* 2016). These genes are present in all other species of the *Cryptococcus* species complex. Genome level studies also revealed the presence of a tetrapolar mating type (*MAT)* locus in non-pathogenic species of *Cryptococcus* species complex and a bipolar *MAT* locus in pathogenic species (Findley *et al.* 2012). The tetrapolar mating system comprises of two *MAT* loci, one encoding pheromones and pheromone receptor genes (the *P/R* locus) and the other encoding transcription factors that govern sexual development (the *HD* locus). These two *MAT* loci are located on different chromosomes and segregate independently during sexual reproduction (Ni *et al.* 2011, Heitman *et al.* 2013). On

the other hand, in bipolar mating system, the two *MAT* loci (HD and P/R) are physically linked and located on the same chromosome.

Ustilago species complex

Ustilago species complex also belongs to the phylum Basidiomycota and consists of major plant pathogens like *Ustilago maydis*, *Ustilago hordei* and *Ustilago bromivora*. All these three species infect grass family plants (maize, barley etc.) causing smut diseases and are of considerable economic importance. Among the three species, *U. maydis* has been studied extensively with respect to its pathogenesis as well as the cell biology aspects (Perez-Martin *et al.* 2006, Brefort *et al.* 2009, Snetselaar and McCann 2017). The 20.5 Mb genome of *U. maydis* is distributed in 23 chromosomes and was sequenced in 2005 (Kamper *et al.* 2006). Unlike *Cryptococcus* species, the yeast-like form of *U. maydis* is unable to cause disease (Brefort *et al.* 2009, Lanver *et al.* 2017). The infectious stage is generated when two cells of opposite mating type (*a* and *b*) come together to form dikaryons. These dikaryons germinate into hyphae on maize leaves initiating the infection, and hence establish a biotrophic interaction with host. The genome of *U. hordei*, the fungus causing covered smut of barley, was sequenced in 2012 that revealed a number of differences with that of *U. maydis* (Laurie *et al.* 2012). One of the striking observations was the selective loss of the functional RNAi machinery genes in the *U. maydis* genome (Laurie *et al.* 2008, Laurie *et al.* 2012). The comparison also revealed that *U. maydis* has lost most of the transposons from its genome that are significantly enriched in the *U. hordei* genome (Laurie *et al.* 2012). More recently, the genome sequencing of *U. bromivora* (fungus infecting *Brachypodium* species of grass) was performed which suggested its evolutionary closeness to *U. hordei* than *U. maydis* (Rabe *et al.* 2016). Similar to *U. hordei*, *U. bromivora* was also found to harbour genes required for functional RNAi and a significant level of transposons. Thus, this group of three

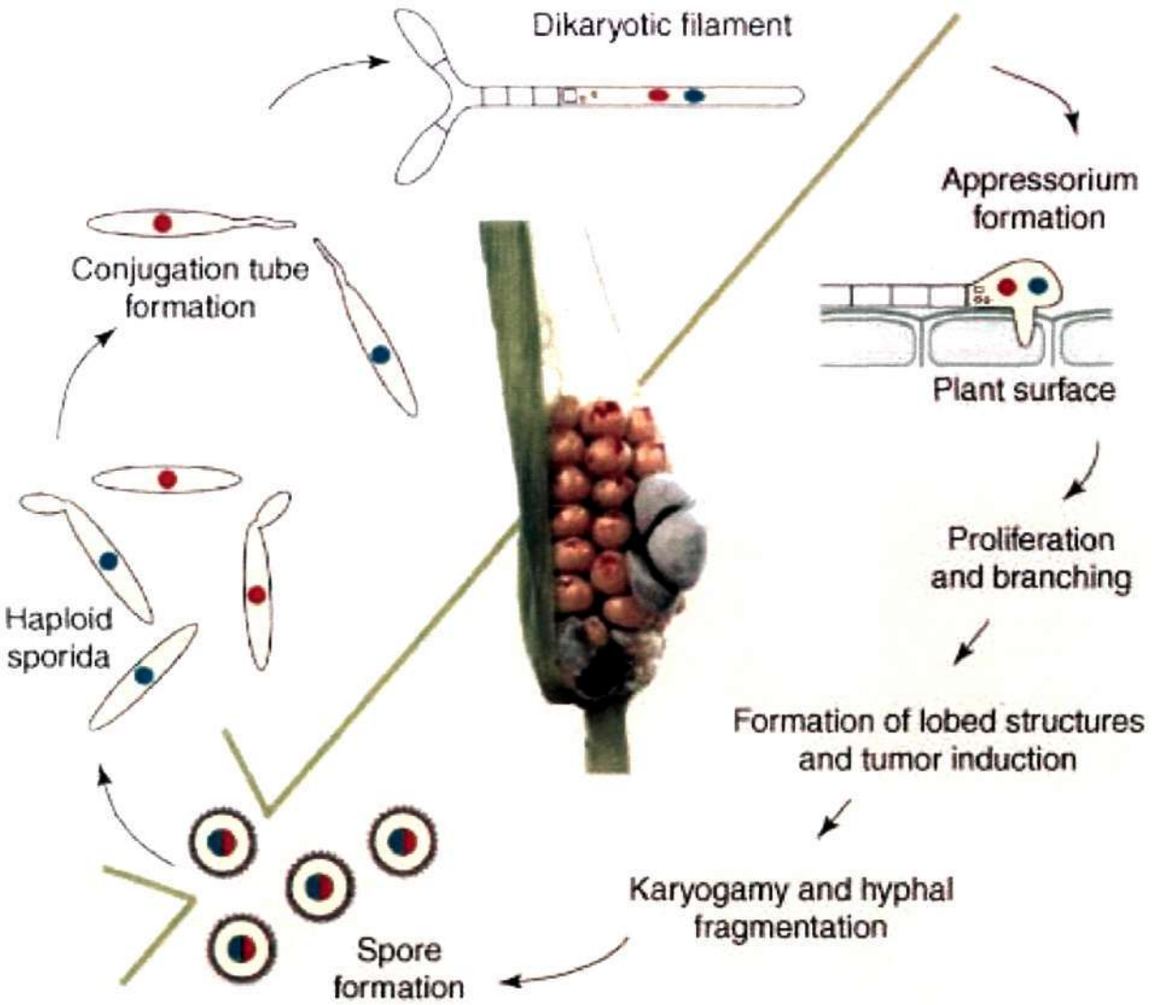

Figure 1.16 Life cycle of *Ustilago maydis*. The shaded area indicates processes that are absolutely dependent on the presence of the plant. The red and blue nuclei represents different mating types (*a* and *b*). After mating, *Ustilago* forms dikaryon structures which generates hyphae and invades the plant leaves. Karyogamy and meiosis takes place within the plant tissue. In the centre of the diagram an infected corn ear with typical disease symptoms is shown. In the lower part the tumour is ruptured and reveals massive amounts of black teliospores representing the diploid spores. These diploid spores germinate and undergo meiosis to produce haploid sporidia. [Figure adapted from (Feldbrugge *et al.* 2004)]

species presents a case where two species harbour functional RNAi machinery while it was lost in the third one, a scenario similar to *Cryptococcus* species complex.

Summary of the current work

In this work, we identified and characterized centromeres and studied their structural organization in a group of *Cryptococcus* species of the fungal phylum Basidiomycota.

Further, we examined the spatio-temporal dynamics of the centromere-kinetochore complex in one of these species, *Cryptococcus neoformans*, an opportunistic pathogen that infects immunocompromised as well as immunocompetent people worldwide.

Since centromeres have been shown to be evolving rapidly, we were interested in studying centromere evolution in closely related *Cryptococcus* species. Thus, we sought to identify centromeres in four species of the *Cryptococcus* species complex (Table 1.2). Chromatin immunoprecipitation (ChIP), with conserved kinetochore proteins CENP-A and CENP-C, followed by next generation sequencing (ChIP-seq) or qPCR was used to identify and/or validate the centromeres. This analysis led to the identification of large regional centromeres in all four *Cryptococcus* species. In all cases, each centromere resides in a long ORF-free and transcriptionally silent region on the respective chromosome. Sequence analysis of centromere DNA sequences revealed that they are enriched with retrotransposons. Retrotransposons present in the pathogenic species of the *Cryptococcus* species complex differ from those present in the non-pathogenic species hinting that centromeres are evolving rapidly in the *Cryptococcus* species complex.

Among the pathogenic species in *Cryptococcus* species complex, one of the species was known to be RNAi-deficient (R265) whereas the other two are RNAi-proficient (H99 and JEC21). We discovered a correlation between the presence of the RNAi machinery in the genome and the length of the centromere of the respective species - the centromere length in the RNAi-deficient species is significantly reduced as compared to the RNAi proficient strains. Comparison of retrotransposons present in centromeres of the three pathogenic species revealed that RNAi proficient species harbour a set of full-length retroelements; the RNAi-deficient species, on the other hand, completely lacks them. Using an experimental evolution based approach, we showed that in the RNAi mutants of H99, that usually possesses long retrotransposon-rich centromeres, undergo structural alterations across the

Species	Host	Genome size	Number of chromosomes	RNAi status
C. amylolentus	None	20.3 Mb	14	Present
C. neoformans	Human	18.9 Mb	14	Present
C. deneoformans	Human	18.5 Mb	14	Present
C. deuterogattii	Human	18.5 Mb	14	Absent
U. maydis	Maize	19.8 Mb	23	Absent
U. hordei	Barley	21.1 Mb	23	Present
U. bromivora	*Brachypodium* species	20.5 Mb	23	Present

Table 1.2 The fungal species under study. The fungal species studied in this report along with their hosts, genome size, number of chromosomes and status of RNAi is mentioned.

centromere regions. Using *in silico* analysis based on a specific set of properties of centromeres, we also identified centromeres in three *Ustilago* species - another basidiomycetous species complex which are major plant pathogens. Like *Cryptococcus*, RNAi is lost in one of the three species in *Ustilago* species complex. Comparison of putative centromere length in the three *Ustilago* species revealed that the RNAi-deficient species (*U. maydis*) has shorter centromeres than those of the RNAi-proficient species (*U. hordei* and *U. bromivora*). Taken together, we could identify centromeres in six pathogenic basidiomycetes belonging to two different species complexes. Both species complexes consist of one RNAi-deficient species with shorter centromeres compared to those of the RNAi-proficient species. Based on these observations, we conclude that RNAi components may be shaping up the structure of the centromere in basidiomycetous yeast species.

Subsequently, we explored the basic organization of components of the mitotic machinery in *C. neoformans*. Some of the evolutionarily conserved constituent proteins of the chromosome segregation machinery were chromosomally tagged with either GFP or mCherry

and their localization dynamics were studied using live-cell imaging. These experiments showed that in *C. neoformans* nuclear division occurs in the daughter bud unlike in other budding yeasts where it takes place in the mother cell. Our experiments also revealed that microtubules in *C. neoformans* are cytoplasmic during interphase but they were mostly nuclear localized during mitosis. Real-time imaging of multiple kinetochore proteins revealed a step-wise assembly of kinetochore complex in this organism. To understand the difference in the site of the nuclear division - at the mother cell in most ascomycetous budding yeasts (*S. cerevisiae*) versus the same in the daughter cell in a basidiomycetous yeast (*C. neoformans*), we developed a computational model to simulate mitosis in both fungal phyla using the published data. The model correctly predicted that the number of cytoplasmic microtubules (cMTs) defines the site of nuclear division in budding yeasts, which was validated experimentally by counting numbers of cMTs in both groups of fungi.

Kinetochores in *C. neoformans* were found to be unclustered during interphase and they begin to cluster as a cell begins to enter mitosis. The MT depolymerisation experiments indicated that microtubule integrity is essential for kinetochore clustering in this organism. However, the absence of nuclear microtubules during interphase hinted towards an indirect interaction between the kinetochores and microtubules. Hence, the possible role of the SUN-KASH protein complex, which forms a bridge across the nuclear envelope, was examined in kinetochore clustering. Co-localization of the SUN-domain protein, Sad1, with a kinetochore protein (CENP-A) revealed their close association at all stages of the cell cycle. A null mutant of Sad1 in *C. neoformans* could be generated but almost 50% of the *sad1* null cells remained inviable. These cells also showed gross chromosome segregation defects (in approximately 50% cells) and a significant delay in kinetochore clustering compared to the wild type. Together, these results uncover a novel function of the SUN domain proteins in mediating spatio-temporal dynamics of kinetochore clustering in *C. neoformans*.

RESULTS

2. Evolution of centromeres in the *Cryptococcus* species complex

Centromeres form the site of the kinetochore formation in all organisms. In most organisms, the site of kinetochore formation is defined by the presence of the centromere specific histone H3 variant, CENP-A. Hence, identification of CENP-A binding sites should reveal the centromere locations in an organism. Along with CENP-A, CENP-C is also known to localize at the functional centromeres in most organisms. Here, we identified centromeres in four different species of *Cryptococcus* species complex by performing chromatin immunoprecipitation (ChIP) using CENP-A or CENP-C or both. The species chosen include a non-pathogenic species, *Cryptococcus amylolentus* (CBS6039) and three pathogenic species – *Cryptococcus neoformans* (H99), *Cryptococcus deneoformans* (JEC21) and *Cryptococcus deuterogattii* (R265) (Figure 2.1). Once identified, the underlying DNA sequences were analysed for the presence of repeats or transposons in them. This study revealed that centromeres in *Cryptococcus* species are large regional and enriched with retrotransposons. The retroelements present in non-pathogenic species were found to be different from the one in pathogenic species.

Among the pathogenic species, R265 lost key components of the functional RNAi machinery (Feretzaki *et al.* 2016). We found that RNAi-deficient R265 harbours significantly shorter centromeres as compared to the RNAi-proficient species H99 or JEC21. We also predicted centromeres in the *Ustilago* species complex, a group of plant pathogens in

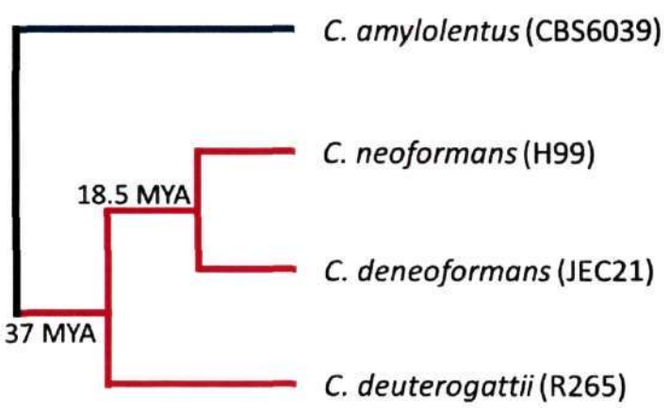

Figure 2.1 A phylogram showing the *Cryptococcus* species studied.

Basidiomycota, and observed a similar correlation between the loss of RNAi and shortening of centromeres. Overall, this study provides evidence of the structural evolution of the centromere in an RNAi-dependent manner in two groups of pathogenic species.

C. amylolentus harbours large regional centromeres

CENP-A is the centromere specific histone H3 variant and has been widely used to identify centromeres (Sanyal *et al.* 2004, Kapoor *et al.* 2015, Chatterjee *et al.* 2016). First, we performed CENP-A ChIP-seq analysis using strains derived from CBS6039 where CENP-A, a conserved kinetochore protein, was tagged with mCherry. Specifically, we identified CENP-A in *C. amylolentus* (Figure 2.2A) and then randomly inserted a genetic construct expressing an mCherry-CENP-A fusion protein into the CBS6039 genome. Live cell imaging at different stages of mitosis revealed that CENP-A localized as multiple puncta in unbudded cells and appears as a single puncta in dividing cells (Figure 2.2B). ChIP pull-down using anti-mCherry (CENP-A) antibodies in CBS6039, and subsequent sequencing of the ChIP DNA was performed using the Illumina platform. ChIP-Seq reads were then mapped back onto the CBS6039 genome. In most cases only one region of ~10-20 kb in length was found to be significantly enriched on each of the 14 chromosomes, suggesting that these regions are centromere regions on their respective chromosomes (Figure 2.2C and D). We observed a region with only modestly enriched ChIP-seq reads on CBS6039 chromosome 1. This is likely due to the fact that the chromosome 1 scaffold was artificially fused together from two individual scaffolds based on evidence from chromoblot analysis and the presence of repetitive elements at one end of each of the two initial scaffolds. Thus, it is possible that the centromere DNA sequence of chromosome 1 is not completely annotated in the current assembly of CBS6039. We also observed an additional minor CENP-A enrichment peak on

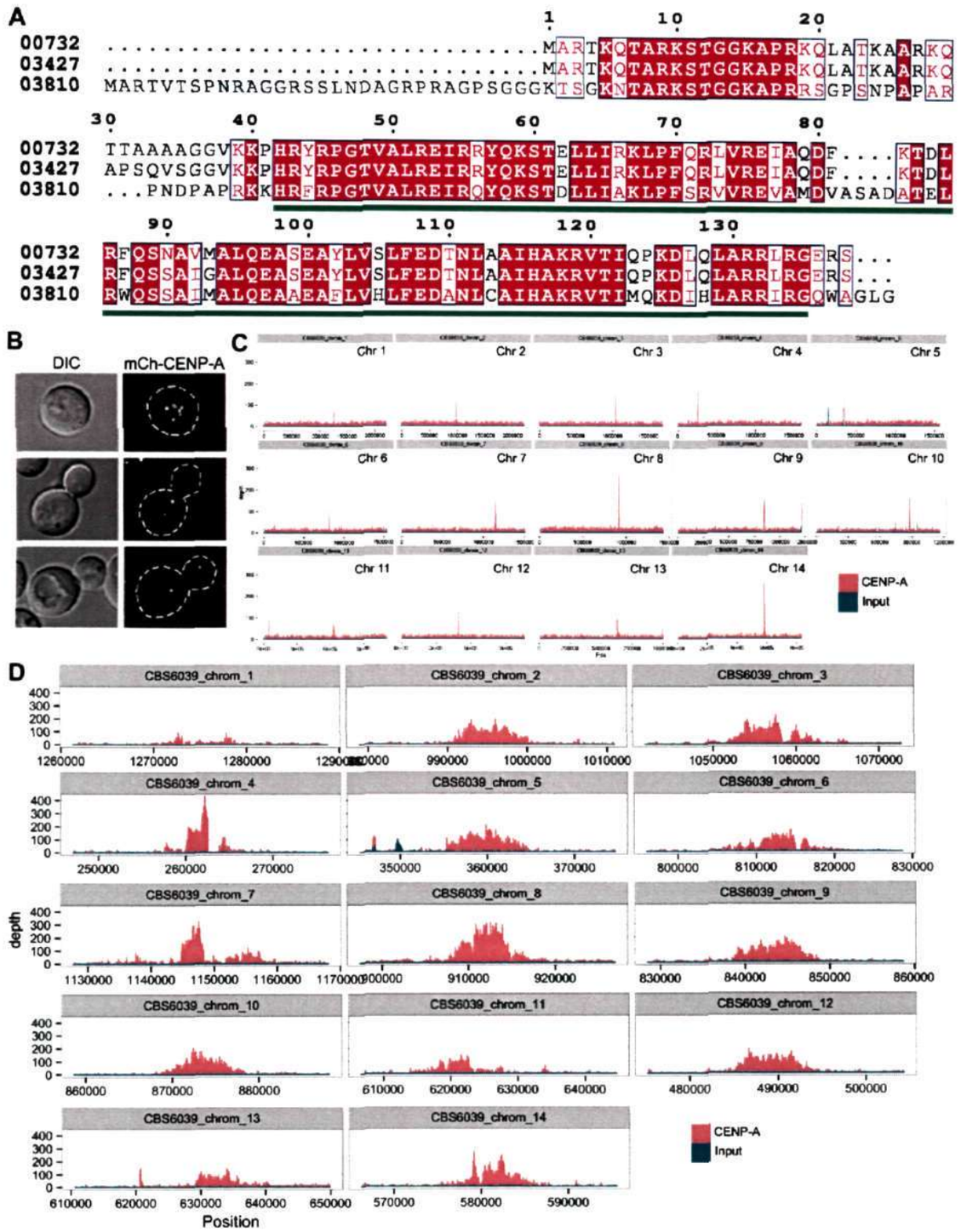

Figure 2.2 Identification of centromeric regions in the CBS6039 genome. **(A)** Sequence alignment of *C. amylolentus* CENP-A protein sequence with histone H3 sequences. **(B)** Live cell direct fluorescence microscopy images of centromere binding protein CENP-A at three different stages of the mitotic cycle. **(C)** Illustration of read depth of the mCherry-CENP-A ChIP-seq data along each of the 14 chromosomes in the CBS6039 genome. **(D)** Plots of read depths when mCherry-CENP-A ChIP-seq data were mapped against the CBS6039 genome assembly are presented. All of the centromeric regions identified in the CBS6039 genome (except for chromosome 1, see Results for more details) showed significantly enhanced read depth when compared to flanking non-centromeric regions. Red plots (chipD) are based on signals obtained from ChIP-seq analysis, while blue plots (contD) indicate the input DNA control.

chromosomes 9 and 10 (Figure 2.2C). However, the minor peak on chromosome 9 was located at the end of the chromosome, likely in the telomeric region. Additionally, in both cases the minor peaks overlapped with signal enrichments in the reads of total DNA controls, suggesting these peaks are likely false positives due to unique features of those chromosomal regions (e.g. telomeric repeats). Thus, our ChIP-seq data provide evidence that the centromeres in *C. amylolentus* are regional.

C. amylolentus centromeres contain centromere specific retrotransposons

To further define the *C. amylolentus* centromeric loci, we pursued a second approach to apply bioinformatics to identify the longest region on each of the chromosomes in the CBS6039 genome that is ORF-free and contains repetitive elements. One such region was identified on each of the 14 chromosomes in the CBS6039 genome. The length of these bioinformatically predicted centromeric regions ranged between 22,371 bp and 48,379 bp, and their locations overlapped with the chromosomal regions that showed the most significant enrichments in the ChIP-seq analysis, strengthening the assignment of these regions as centromeres (Table 2.1). We also identified six different retrotransposons in the CBS6039 genome that are specific for these centromeric regions, which are named as transposons in centromeres 1 – 6 (Tcen1 – Tcen6; Figure 2.3A). While Tcen1 contains only long terminal repeats, all of the other five Tcen elements (Tcen2 – Tcen6) contain genes typically found in retrotransposons, such as those encoding RNaseH, reverse transcriptase, and integrase (Figure 2.3A). Each of these six Tcen elements could be found in an apparently complete sequence in at least one centromere. Moreover, all of the centromeres contained multiple additional fragments of different Tcen elements (Figure 2.3B). We also examined the transcriptional status of centromeres by analysing the polyA RNA. The RNA-seq analysis

	CEN flanking Left ORF (coordinates)	ORF-free region (length in bp)	*CEN* flanking Right ORF (coordinates)
CEN1	CRAM_01_00527 1259704-1261928	1261929-1292020 (30,091)	CRAM_01_00532 1292021-1293761
CEN2	CRAM_02_01330 979876-981299	981300-1003798 (22,498)	CRAM_02_01332 1003799-1005713
CEN3	CRAM_03_02287 1036140-1037292	1037293-1069522 (32,229)	CRAM_03_02295 1069523-1072581
CEN4	CRAM_04_02687 227481-229236	229237-277616 (48,379)	CRAM_04_02698 277617-281635
CEN5	CRAM_05_03401 330603-332956	332957-371191 (38,234)	CRAM_05_03407 371192-372988
CEN6	CRAM_06_04254 787089-788876	788876-828761 (39,884)	CRAM_06_04263 828760-831955
CEN7	CRAM_07_05012 1122672-1123409	1123410-1157926 (34,516)	CRAM_07_05014 1157927-1159434
CEN8	CRAM_08_05536 894669-897481	897482-919853 (22,371)	CRAM_08_05544 919854-923991
CEN9	CRAM_09_06076 821096-822472	822473-859020 (36,547)	CRAM_09_06084 859021-860507
CEN10	CRAM_10_06607 864022-866478	866479-897364 (30,885)	CRAM_10_06614 897365-902058
CEN11	CRAM_11_06993 610980-612932	612543-649121 (36,578)	CRAM_11_07006 649122-650987
CEN12	CRAM_12_07424 467138-468905	468906-513539 (44,634)	CRAM_12_07432 513540-516248
CEN13	CRAM_13_07946 601369-603529	603530-642666 (39,136)	CRAM_13_07951 642667-654553
CEN14	CRAM_14_08367 567428-570174	570175-602631 (32,456)	CRAM_14_08371 602632-603681

Table 2.1 Coordinates of the centromere and its flanking ORFs in *C. amylolentus*. Some ORFs present in centromere regions were not considered for analysis due to their similarities with transposons or dubious nature of ORFs. ORFs which are < 200 aa long are not taken into consideration.

of the CBS6039 whole transcriptome revealed the absence of polyA RNA from all 14 centromeric regions identified in the CBS6039 genome (Figure 2.3C).

Combined together, we conclude that these are bona fide centromere regions on each chromosome in CBS6039. Each of these regions is the binding site of the centromeric histone CENP-A, is depleted of ORFs and enriched with retrotransposons and their remnants, and showed significantly reduced levels of transcription (Figures 2.2 and 2.3).

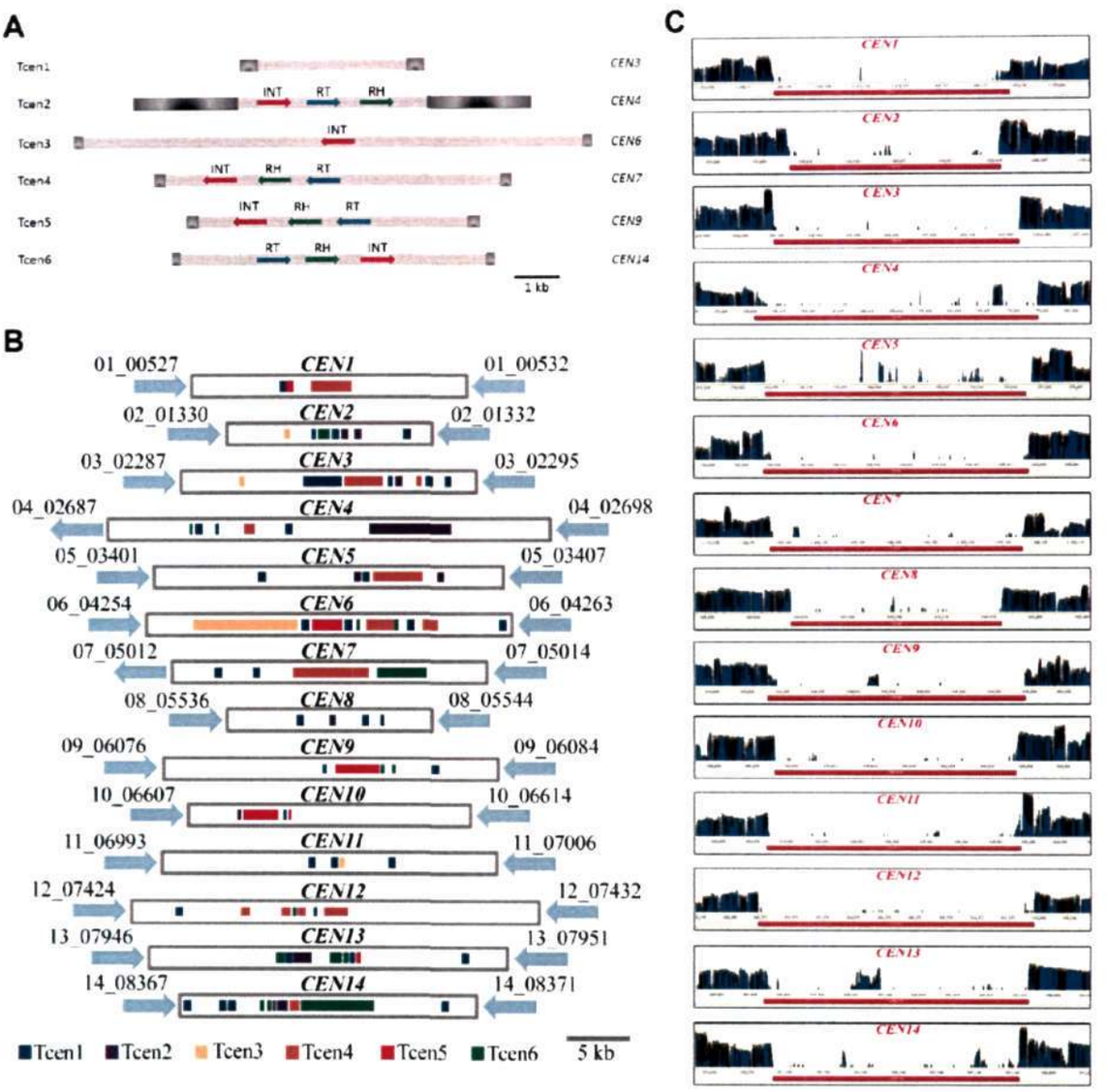

Figure 2.3 Identification and characterization of centromeric regions in the CBS6039 genome. **(A)** The diagram depicts the structures of the six unique centromere specific LTR retrotransposons, Tcen (Transposons in centromeres) 1 – 6, identified in the *C. amylolentus* centromeric regions. While Tcen1 contains only Long Terminal Repeats (LTRs, shown in grey), all of the other five Tcen elements consist of various genes/domains found in retrotransposons (RH, RNaseH; RT, Reverse Transcriptase; INT, Integrase). On the far right are the corresponding centromeres in the CBS6039 genome within which the full-length Tcen elements have been identified. **(B)** Schematic illustrating the distributions of the six Tcen elements, as well as their remnants, on the identified centromere regions in the CBS6039 genome. These intervals were defined as the longest ORF-free regions on the respective chromosomes and contain mostly retrotransposons or their remnants, and show enrichment of CENP-A binding based on ChIP-seq analyses. **(C)** RNA-seq analysis reveals that the identified CBS6039 centromere regions also had significantly reduced levels of transcriptional activity when compared to flanking non-centromeric regions. The blue bars indicate RNA-seq read depth.

Pathogenic *Cryptococcus* species harbour large regional centromeres

Next, we sought to identify the centromeres experimentally in three pathogenic species (represented by H99, JEC21, and R265) of the *Cryptococcus* species complex including verifying centromere locations predicted earlier in JEC21 (Loftus *et al.* 2005).

To achieve this goal, two of the evolutionarily conserved inner kinetochore proteins, CENP-A and CENP-C, were identified in each of the three species (Figure 2.4A and B). Both the proteins were tagged with mCherry and showed localization patterns same as *C. amylolentus* (Figure 2.4C and D). To identify functional centromeres in H99, we performed CENP-A and CENP-C chromatin immunoprecipitation (ChIP) followed by deep sequencing (ChIP-seq). ChIP-seq analysis revealed overlapping binding of both proteins at a single locus on each of the 14 chromosomes of H99 (Figure 2.4E). The binding patterns of both the proteins were identical and spanned across the ORF-free regions in most chromosomes (Figure 2.5A). The length of the CENP-A and CENP-C bound regions varied from 20 kb to 40 kb in H99 unlike centromeres of other fungi where the CENP-A-bound region remains nearly constant across chromosomes (Roy and Sanyal 2011). It is important to note here that centromeres in H99 are not yet completely assembled and contain a few sequence gaps in the current assembly. We attempted to close these gaps by PacBio as well as Sanger sequencing (see Materials and Methods for detail). This resulted in a significant improvement of the genome assembly as we could close the sequence gaps in 11 out of 14 centromeres leaving only *CEN3*, *CEN11*, and *CEN14* with remaining sequence gaps.

The H99 genome shares a high level of gene synteny with that of JEC21 (Figure 2.5B) (Janbon *et al.* 2014). By performing synteny analysis across centromere flanking regions of H99, we were able to predict putative centromeres in JEC21 (Table 2.2). The predicted regions were large ORF-free and map to regions earlier predicted as centromeres in JEC21. CENP-C ChIP-qPCR confirmed authenticity of each of these regions as functional

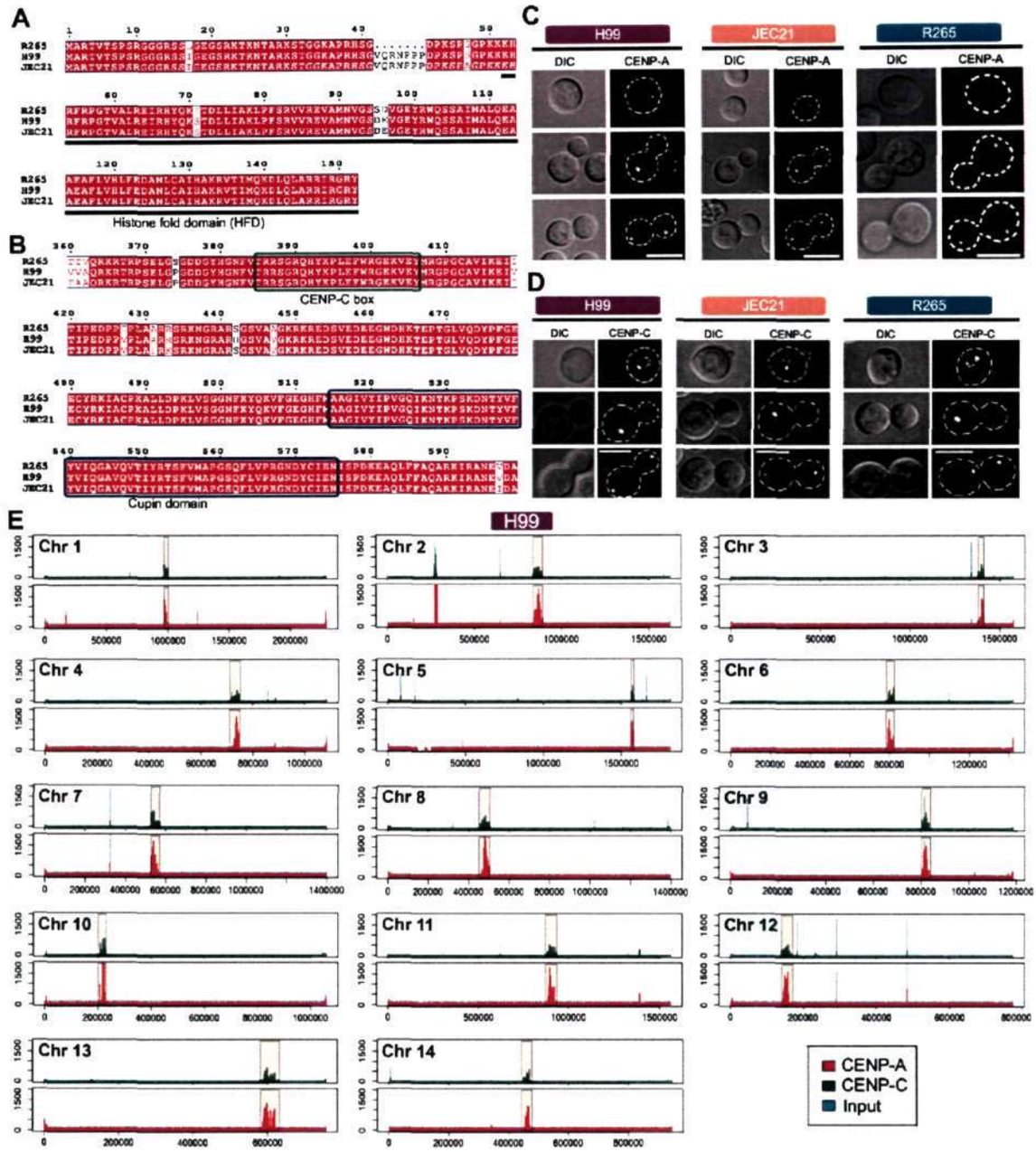

Figure 2.4 Identification of centromeres in H99. **(A)** Alignment of CENP-A proteins in R265 (ORF no. CNBG_0491), H99 (CNAG_00063), and JEC21 (CNA00540). The C-terminal region of CENP-A carries the conserved histone fold domain (HFD). **(B)** Multiple sequence alignment of CENP-C proteins in R265 (CNBG_4461), H99 (CNAG_05391) and JEC21 (CNH00580) revealed conservation of the CENP-C box and the DNA binding "Cupin" domain in these three species. **(C and D)** The sub-cellular localization patterns of two conserved kinetochore proteins, CENP-A and CENP-C, at various cell cycle stages in H99, JEC21, and R265. Bar, 5μm. **(E)** ChIP-seq analysis by CENP-A or CENP-C identified the location of the centromeres on each chromosome of H99. The additional CENP-A IP peak, appearing on chromosome 2, is probably an experimental artifact because any enrichment for CENP-C was not detected in the same region.

centromeres in all 14 chromosomes in JEC21 (Figure 2.5C). We obtained a significant enrichment of CENP-C using two distantly placed primers on each of the 14 centromeres

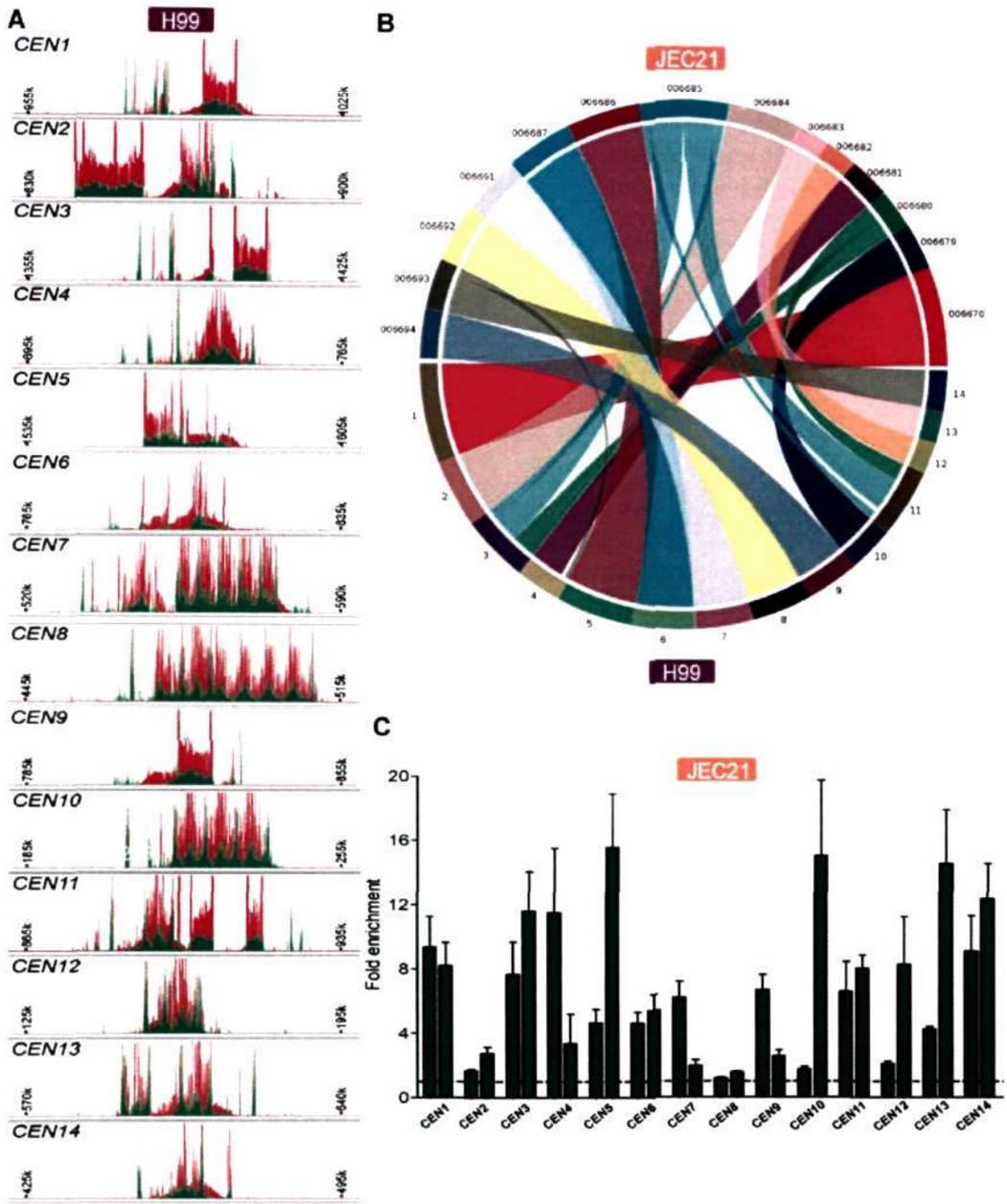

Figure 2.5 The *Cryptococcus* species complex has large regional type centromeres. (A) Overlapping binding of CENP-A (red) and CENP-C (green) on each of the 14 chromosomes of H99 as revealed by ChIP-seq analysis of these proteins. An 80 kb DNA sequence harbouring the centromere is shown here for each of the 14 chromosomes. **(B)** A circular map showing synteny between the H99 and JEC21 genomes. **(C)** CENP-C (mCherry)-ChIP-qPCR analysis confirmed enrichment of CENP-C on the predicted centromeres in JEC21. Fold enrichment was normalized to a non-*CEN* region, the level of which is marked by the dotted line in the graph. Error bars represent standard error of mean (SEM).

as compared to a non-centromeric locus.

R265 is the *C. deuterogattii* strain used as a representative of the third species in this study from the *Cryptococcus* pathogenic species complex (Lin and Heitman 2006). Although

CEN#	*C. neoformans* (H99)	*C. deneoformans* (JEC21)	*C. deuterogattii* (R265)*	
			GenBank assembly	*PacBio assembly*
1	Chr1: 970169-1006931 (36763)	NC_06670: 937505-998182 (60677)	SC2.1: 549793-562116 (12323)	tig00000008: 912944-925244 (12300)
2	Chr2: 835384-889427 (54044)	NC_06684: 855280-905374 (50094)	SC2.3: 1245675-1264837 (19162)	tig00000007: 703965-722663 (18698)
3	Chr3: 1378288-1409632 (31345)#	NC_06680: 139615-178627 (39012)	SC2.10: 161351-172304 (10953)	tig00000035: 163633-177826 (14193)
4	Chr4: 708804-752337 (43534)	NC_06681: 129330-176311 (46981)	SC2.12: 0-8787 + SC2.25: 0-9197 (17984)	tig00000001: 1470842-1484371 (13529)
5	Chr5: 1559983-1587231 (27248)	NC_06686: 220960-273717 (52757)	SC2.2:0-394 + SC2.21: 0-9330 (9724)	tig00000040: 198793-218003 (19210)
6	Chr6: 780649-821756 (41108)	NC_06687: 777728-854403 (76675)	SC2.9: 0-7641 + SC15:577279-579555 (9917)	tig00000020: 580177-593699 (13522)
7	Chr7: 525714-584338 (58625)	NC_06691: 863695-936334 (72639)	SC2.4: 804895-822827 (17932)	tig00000017: 487975-505882 (17907)
8	Chr8: 451162-512653 (61492)	NC_06692: 882181-912116 (29935)	SC2.5: 820773-828700 (7927)	tig00000023: 821976-830744 (8768)
9	Chr9: 801830-839446 (37617)	NC_06694: 323826-388577 (64751)	SC2.6: 400001-411645 (11644)	tig00000016: 814298-825988 (11690)
10	Chr10: 199434-243741 (44308)	NC_06679: 802162-882405 (80243)	SC2.17: 225860-239542 (13682)	tig00000031: 204951-218719 (13768)
11	Chr11: 868824-933658 (64835)#	NC_06685: 801507-911882 (110375)	SC2.7: 1115845-1125223 + SC2.8: 0-4505 (13883)	tig00000000: 1120186-1141240 (21054)
12	Chr12: 139633-171048 (31416)	NC_06682: 122048-182012 (59964)	SC2.13: 88902-104251 (15349)	tig00000022: 92971-107066 (14095)
13	Chr13: 579772-632362 (52591)	NC_06683: 569940-644450 (74510)	SC2.14: 98814-112148 (13334)	tig00000038: 105649-120839 (15190)
14	Chr14: 441845-477986 (36141)#	NC_06693: 706065-761098 (55033)	SC2.11: 341109-350585 (9476)	tig00000033: 360990-370343 (9353)

Table 2.2 The centromere coordinates in the H99, JEC21, and R265 isolates.
*in the absence of a chromosome-wise genome assembly of R265, supercontig (SC) numbers are noted for the GenBank assembly and scaffold numbers (tig…) are noted for the PacBio assembly. The numbers in brackets denote the length of the centromere in basepair (bp).
Centromeres with gaps and hence the actual length may be longer than estimated here.

there are 14 chromosomes, CENP-C (mCherry)-ChIP-seq analysis yielded 16 binding peaks in the publicly available genome assembly of 27 supercontigs in R265 (Figure 2.6A). In our

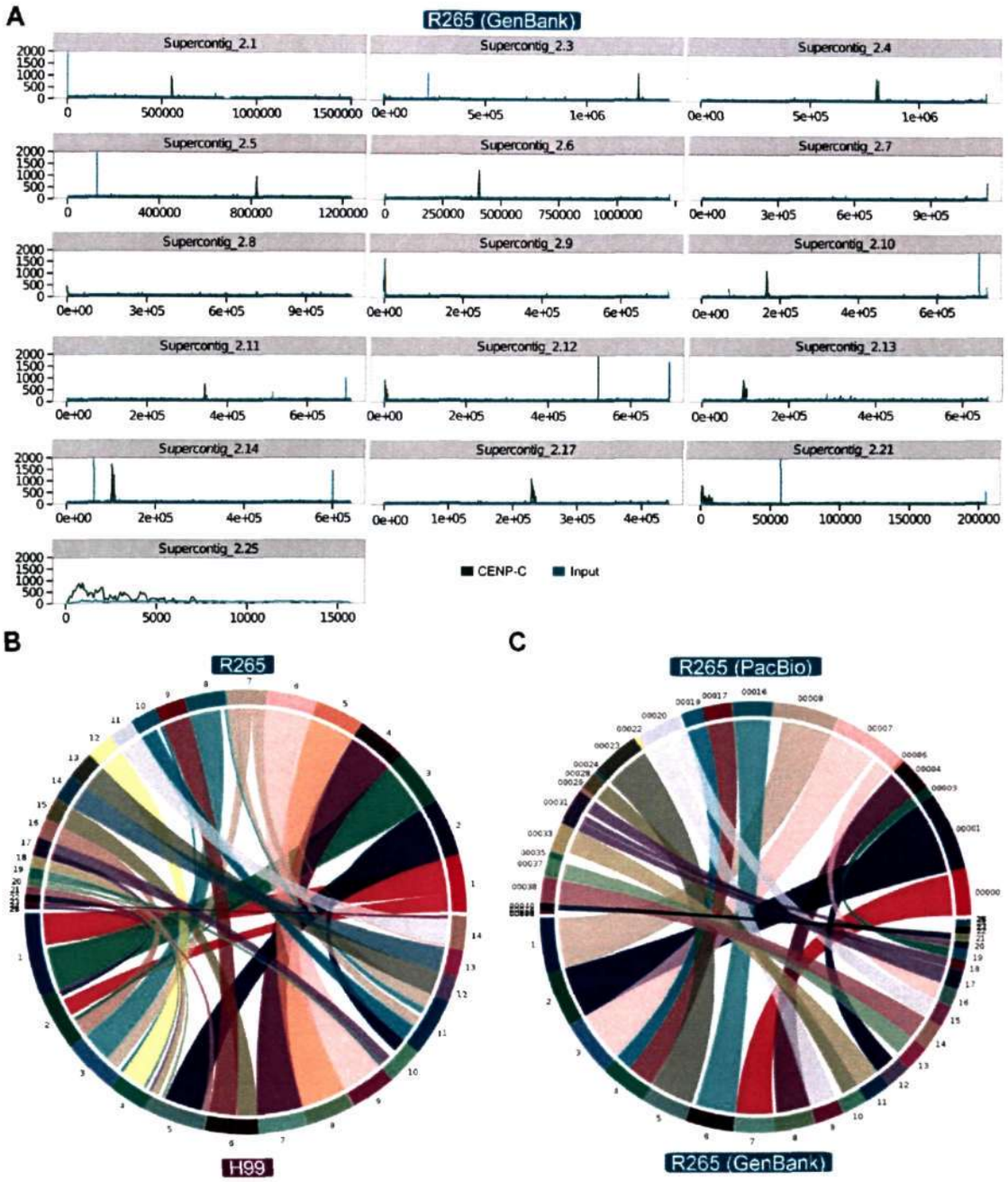

Figure 2.6 Identification of centromeres in R265. **(A)** CENP-C (mCherry)-ChIP-seq analysis identified locations of centromeres in R265. **(B)** Synteny analysis between the H99 and R265 assemblies showed a number of breaks in the current R265 assembly. As is evident, only 5 of the H99 orthologous chromosomes are entirely covered in the R265 assembly. **(C)** A synteny map showing a comparison of two R265 genome assemblies: one from GenBank and the other a *de novo* PacBio assembly.

analysis, we found that 4 centromeres were broken in the current assembly (Table 2.2). Whole genome comparison between H99 and R265 revealed a number of rearrangements, possibly due to poor assembly of R265 (Figure 2.6B). To improve the genome assembly for

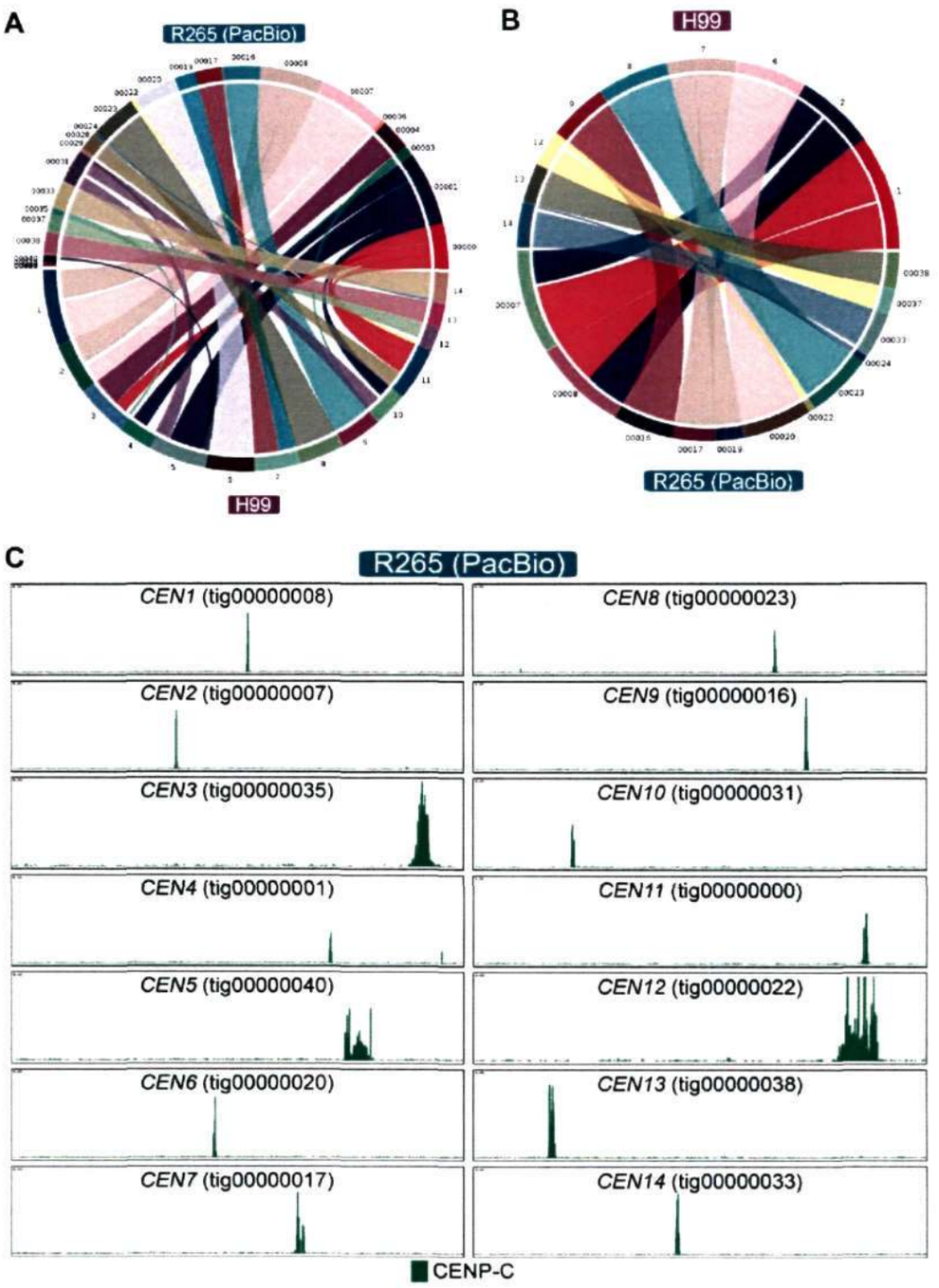

Figure 2.7 PacBio sequencing revealed 14 centromeres in R265. **(A)** A comparison of the R265 PacBio assembly with the H99 genome. **(B)** A diagram showing the 9 orthologous chromosomes of H99 that were completely assembled in the PacBio assembly of R265 with either no gap or a single gap. **(C)** CENP-C ChIP-seq analysis using the PacBio assembly revealed the locations of 14 centromeres in the R265 genome. Scaffold numbers are noted in the brackets.

R265, and also to obtain better coverage for centromeric regions, we performed PacBio sequencing for the R265 genome. The *de novo* assembly for R265 using PacBio sequencing

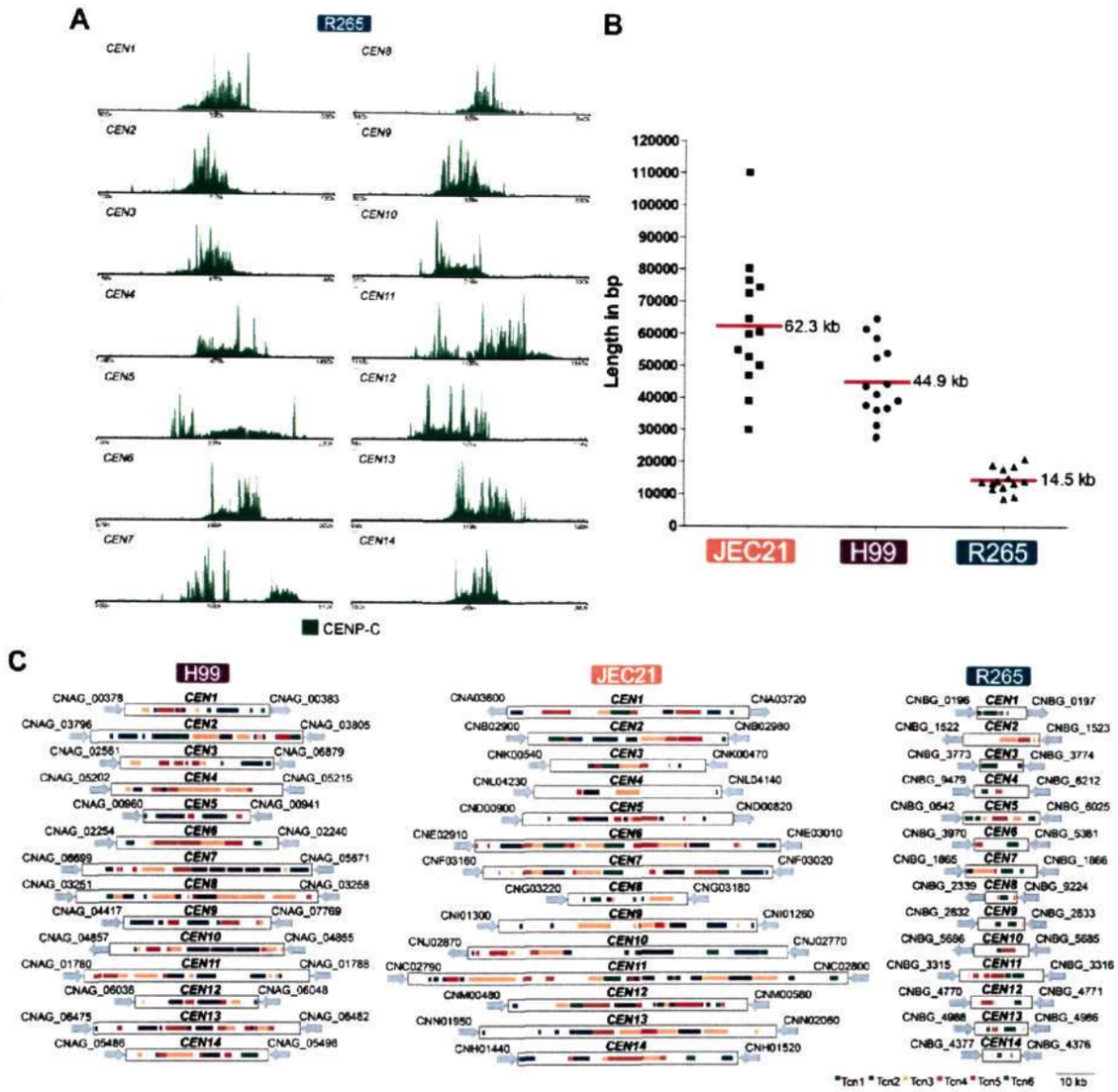

Figure 2.8 R265 harbours smaller centromeres than H99 and JEC21. **(A)** CENP-C (mCherry)-ChIP-seq identified 14 binding regions among 27 scaffolds in R265 PacBio assembly. Only scaffolds with significant CENP-C binding are shown. A 30 kb region spanning the CENP-C-bound region is shown for each scaffold. **(B)** The length of each centromere of the respective species was plotted. Each dot represents one centromere, and the horizontal red line depicts the mean centromere length of the corresponding species. **(C)** The presence of various retrotransposons across the centromeres in H99, JEC21, and R265. The diagrams are drawn to scale. Scale bar, 10 kb.

generated 27 scaffolds. However, these scaffolds exhibited a number of disagreements with the current GenBank assembly (Figure 2.6C). Further, a comparison with the H99 genome revealed a number of rearrangements, similar to what we obtained with H99 genome comparison to the GenBank assembly (Figure 2.7A). Nevertheless, the PacBio assembly yielded fewer rearrangements than the GenBank assembly and provided completely

assembled homologous chromosomes/scaffolds for 9 out of the14 H99 chromosomes (Figure 2.7B). Previously, a report predicted that the H99 and R265 genomes have undergone an arm exchange involving chromosomes 1 and 2 (Janbon *et al.* 2014). The new PacBio assembly provides compelling evidence towards the proposal (Figure 2.7A and B). Next, we analysed our CENP-C ChIP-seq data using the PacBio assembly and obtained 14 binding peaks that each lie on a scaffold (Figure 2.7C, 2.8A and Table 2.2). Similar to H99, all of the 14 peaks mapped to ORF-free regions in the R265 genome as well.

A comparative analysis revealed that the centromeres in R265 are significantly shorter with an average length of around 14 kb compared to those of H99 or JEC21, which have an average length of 44 kb and 62 kb respectively (Figure 2.8B and Table 2.2). Consequently, the CENP-C bound regions were also found to be shortened in R265 (5 to 15 kb) compared to H99 (20 to 40 kb). Thus, we conclude that the *Cryptococcus* species have CENP-A/CENP-C-rich regional centromeres of varying length.

Centromeric retrotransposons in pathogenic *Cryptococcus* species are different from *C. amylolentus*

C. amylolentus centromeres are found to be enriched with retrotransposons. A previous study had predicted presence of retrotransposons (Tcn1, Tcn5 and Tcn6) in putative centromeres of JEC21 (Goodwin and Poulter 2001, Loftus *et al.* 2005). Thus, we sought to analyse the centromeric sequences of the experimentally identified centromeres in the pathogenic *Cryptococcus* species. Sequence analysis of the CENP-A/CENP-C bound ORF-free centromere regions in all three species revealed the presence of retrotransposons, Tcn1-Tcn6, of the Ty1/Ty3 family (Figure 2.8C). Based on these results, we conclude that centromeres in the pathogenic *Cryptococcus* species are large regional and rich in same retroelements. Combined together with synteny conservation, these results suggest that

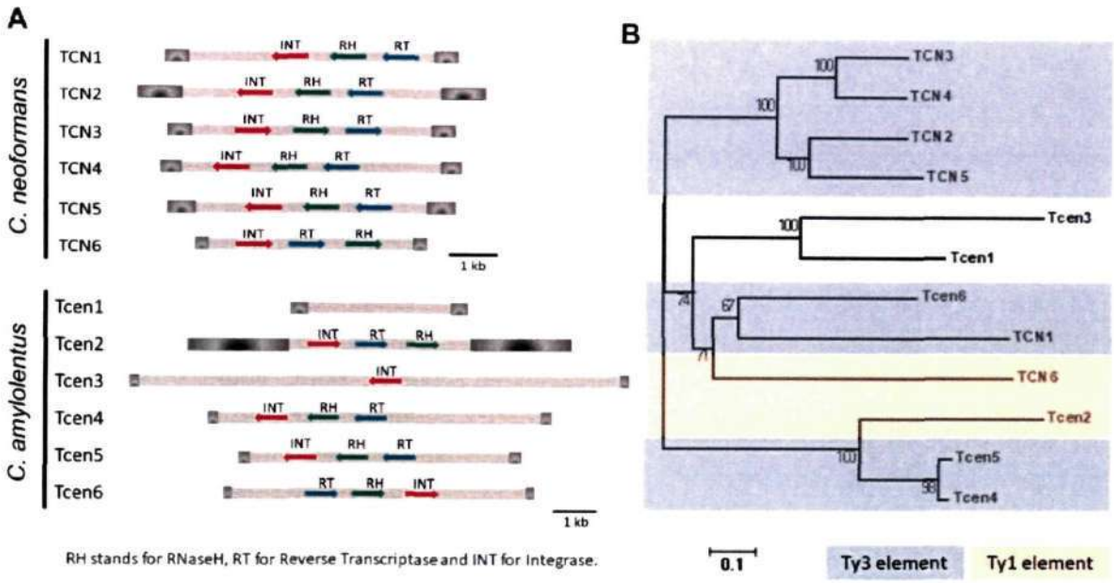

C

	Tcen1	Tcen2	Tcen3	Tcen4	Tcen5	Tcen6	TCN1	TCN2	TCN3	TCN4	TCN5	TCN6
Tcen1		27.20%	37.29%	27.51%	27.61%	36.11%	29.46%	29.01%	29.17%	30.56%	28.72%	30.68%
Tcen2	27.20%		25.17%	38.11%	39.96%	25.37%	25.96%	24.99%	25.05%	25.51%	24.84%	24.87%
Tcen3	37.29%	25.17%		25.16%	24.89%	27.55%	26.32%	26.55%	24.77%	26.15%	26.53%	25.30%
Tcen4	27.51%	38.11%	25.16%		79.92%	26.69%	25.62%	27.15%	33.87%	33.19%	27.35%	25.38%
Tcen5	27.61%	39.96%	24.89%	79.92%		27.03%	26.51%	27.31%	33.86%	33.20%	27.38%	25.46%
Tcen6	36.11%	25.37%	27.55%	26.69%	27.03%		31.33%	39.92%	35.64%	36.23%	38.68%	31.86%
TCN1	29.46%	25.96%	26.32%	25.62%	26.51%	31.33%		27.45%	25.22%	25.33%	26.73%	26.90%
TCN2	29.01%	24.99%	26.55%	27.15%	27.31%	39.92%	27.45%		42.06%	42.98%	45.95%	26.60%
TCN3	29.17%	25.05%	24.77%	33.87%	33.86%	35.64%	25.22%	42.06%		56.71%	40.38%	25.91%
TCN4	30.56%	25.51%	26.15%	33.19%	33.20%	36.23%	25.33%	42.98%	56.71%		42.04%	25.75%
TCN5	28.72%	24.84%	26.53%	27.35%	27.38%	38.68%	26.73%	45.95%	40.38%	42.04%		26.43%
TCN6	30.68%	24.87%	25.30%	25.38%	25.46%	31.86%	26.90%	26.60%	25.91%	25.75%	26.43%	

Figure 2.9 Centromeric retrotransposons are diverged between pathogenic and non-pathogenic *Cryptococcus* species. (A) Schematic showing the structural architecture of the retroelements present in centromeres of *C. neoformans* (TCN1-TCN6) and *C. amylolentus* (Tcen1-Tcen6). The maps are drawn to scale and some of the identified conserved ORFs are depicted. **(B)** Centromeric retrotransposons of *C. neoformans* (TCN1-TCN6) and that of *C. amylolentus* (Tcen1-Tcen6) were subjected to multiple sequence alignment and the evolutionary history was inferred using the Neighbor-Joining method. The percentage of replicate trees in which the associated taxa clustered together in the bootstrap test (1000 replicates) is shown next to the branch. The tree is drawn to scale, with branch lengths in the units of the number of base substitutions per site. **(C)** The sequences of the centromeric retroelements present in *C. neoformans* and *C. amylolentus* were subjected to multiple sequence alignment using Clustal and the identity matrix was generated.

neither the location nor the sequence elements of the centromeres diverged significantly among these closely related fungal species. However, these elements differ from the centromeric retroelements of *C. amylolentus* (Figure 2.9A). To further analyse the divergence among these retroelements, we performed multiple sequence alignment of six elements of each group. Both the groups (pathogenic and non-pathogenic species) contain elements belonging to Ty1 (INT-RT-RH) and Ty3 (INT-RH-RT) classes of retroelements. Two of the elements in *C. amylolentus*, Tcen1 and Tcen3, could not be classified as Ty1 or Ty3 since

they lack all the functional domains. While most of the elements of pathogenic species cluster together, two of them (Tcn1 and Tcn6) align closer to retroelements of *C. amylolentus* (Figure 2.9B). This could mean that these two elements evolved from a common ancestral element while the others were acquired later once the two species diverged from each other. A pairwise alignment of each of the 12 elements with each other revealed very limited identity among these elements with a few exceptions (Tcen4- Tcen5, Tcn3- Tcn4) (Figure 2.9C). We believe that this low level of identity corresponds to identity of conserved ORFs which are present in these retroelements. Overall, these results confirm that centromere sequences between the pathogenic and non-pathogenic species of the *Cryptococcus* species complex diverged significantly.

Loss of the RNAi machinery and shortening of centromere are correlated in R265

Ago, Dcr and Rdp - the key proteins of the RNAi machinery are all present in H99 and JEC21 but all are absent in R265 (Feretzaki *et al.* 2016). It was previously shown that RNAi suppresses transcription and transposition of retrotransposons including the Tcn elements in the RNAi-proficient species H99 and JEC21 (Janbon *et al.* 2010, Wang *et al.* 2010). A complete loss of RNAi in R265 might have led to an elevated level of transcription of retroelements leading to an increased transposition throughout its genome, including the centromeres. A recent study reported that putative centromeres of H99 are methylated at the DNA level (Huff and Zilberman 2014). Combining the available bisulfite sequencing results with our ChIP-seq results revealed that indeed centromeric DNA sequence of H99 is extensively methylated (Figure 2.10A). It was intriguing to find that the only DNA methylase coding gene, *DNMT5*, is found to be truncated in R265 (Figure 2.10B). To validate the absence of centromere DNA methylation, we performed genomic DNA restriction with

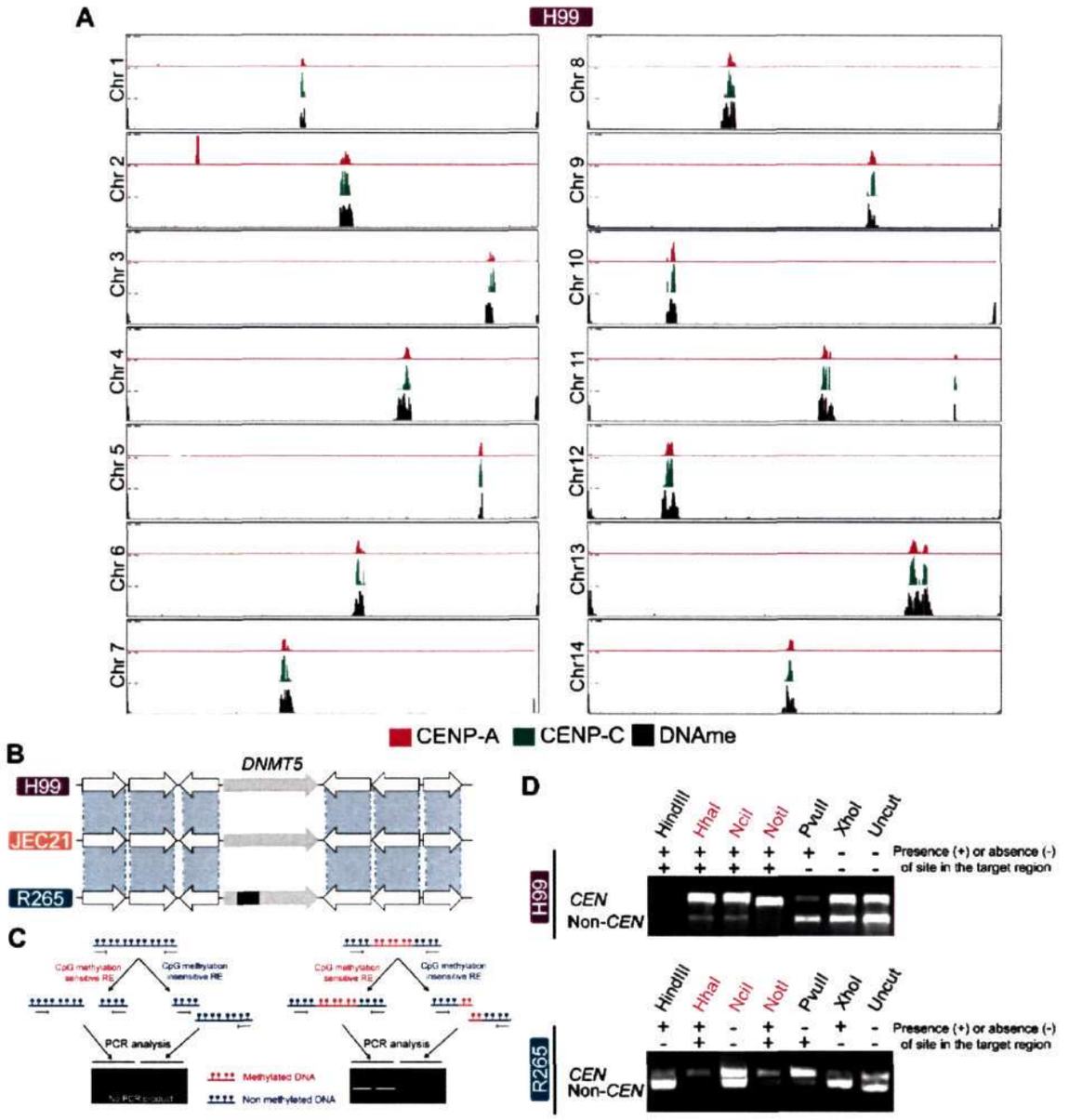

Figure 2.10 DNA methylation at the centromere is lost in R265. **(A)** Bisulfite sequencing analysis revealed DNA methylation at the centromeres of H99. Bisulfite sequencing data was obtained from a previous study (Huff and Zilberman 2014). **(B)** The *DNMT5* ORF is truncated in R265 at the syntenic locus to that of H99 and JEC21. **(C)** Diagram to show the rationale of the assay used to determine DNA methylation status at the centromere. **(D)** PCR analysis revealed a lack of methylation at the centromere DNA in R265 unlike that of H99. '+' or '-' refers to the presence or absence of the restriction site of a specific enzyme respectively. Enzymes in red letters are CpG methylation-sensitive while others are not. One centromeric region (*CEN6* for H99 and *CEN9* for R265) and one non-centromeric region (Chr1: 1726512-1727921 for H99 and SC6: 376524-377415 for R265) was subjected to the assay in H99 and R265.

methylation sensitive as well as non-sensitive enzymes followed by PCR amplification (Figure 2.10C). The methylation specific PCR results confirmed that DNA methylation is indeed absent at centromeres in R265 but present at H99 centromeres (Figure 2.10D). It is

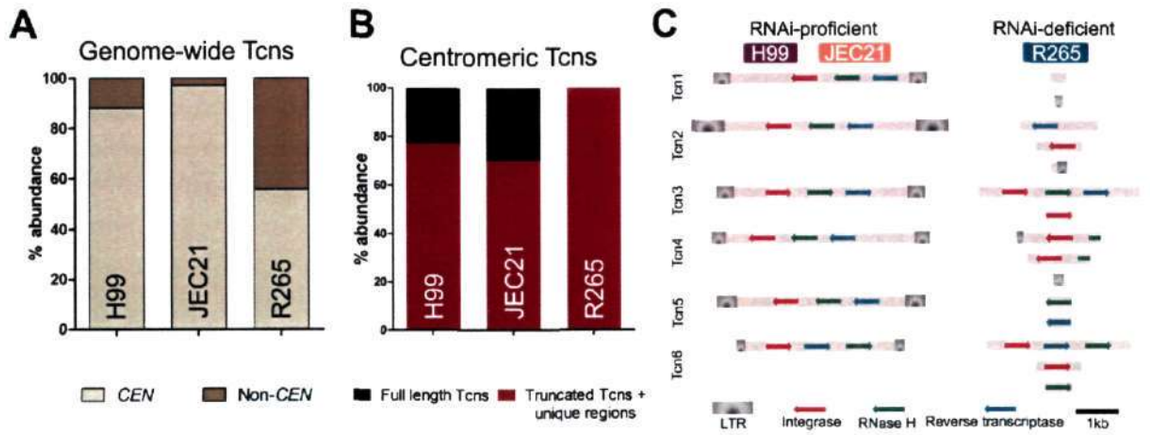

Figure 2.11 R265 harbours only truncated retroelements. (A) Distribution of retrotransposons, Tcn1- Tcn6, in centromeres and across the genome in H99, JEC21, and R265 is shown. **(B)** A bar diagram showing the distribution of full-length versus truncated retrotransposons at the centromeres in all three species. **(C)** A comparison of retrotransposon elements present in centromeres of RNAi-proficient and RNAi-deficient species. While both RNAi-proficient species (H99 and JEC21) possess a significant number of full-length retroelements, Tcn1- Tcn6, at the centromeres, the RNAi-deficient species (R265) harbours only truncated forms of the same in its genome.

important to note that DNA methylation is known to suppress recombination in some organisms (Maloisel and Rossignol 1998, Mirouze *et al.* 2012, Yelina *et al.* 2015).

To further investigate alterations in the centromere length observed, we performed a detailed analysis of the retrotransposons, Tcn1- Tcn6, in all three species. These retroelements are specifically enriched and mostly restricted (>95%) to centromeric regions in both H99 and JEC21 (Figure 2.11A). In contrast, while 50% of the retroelements lie within the centromeres, the rest are found across the length of the chromosomes in R265. The most striking observation is that the centromeres in H99 and JEC21 harbor a significant proportion of full-length retroelements (20-30%), whereas the R265 genome is completely devoid of such elements (Figure 2.11B). Instead, retroelements present in R265 are only remnants/footprints of transposons (Figure 2.11C). They lack one or more of the essential domains (LTRs, reverse transcriptase, integrase) required for transposition activity, rendering them non-functional for further transposition. Thus, this analysis reveals that loss of RNAi in

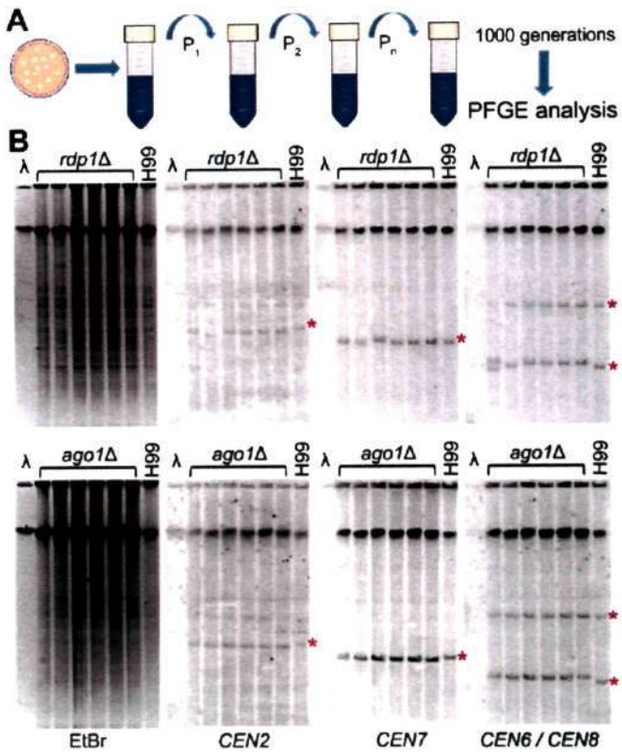

Figure 2.12 RNAi provides stability of retrotransposon-rich genomic loci. (A) Schematic of experimental evolution performed using H99 wild-type *(RDP1 AGO1)*, *rdp1*Δ and *ago1*Δ mutants. **(B)** Chromoblot analysis revealed genomic rearrangements at the centromeres when RNAi mutant (*rdp1*Δ and *ago1*Δ) strains were passaged for 1000 generations. Red stars indicate the length of NotI fragments expected in the wild-type strain H99. EtBr refers to ethidium bromide stained gels while *CEN2*, *CEN7*, *CEN6,* and *CEN8* refer to blots developed using probes against the corresponding centromere fragment.

R265 is correlated with the loss of full-length retrotransposons leading to an overall reduction in the length of the centromeres.

By comparison with H99, genome of R265 can be seem to have lost additional genes besides key enzymes in the RNAi pathway (D'Souza *et al.* 2011, Feretzaki *et al.* 2016). To address specifically the effect of RNAi on centromere length regulation, we performed experimental evolution experiments. H99 and its derived RNAi mutants (*rdp1*Δ or *ago1*Δ) were grown for 1000 generations under standard laboratory conditions (Figure 2.12A). Next, we probed alterations of the centromere length by Pulsed-Field Gel Electrophoresis (PFGE) of genomic DNA isolated from the passaged strains and digested by rare-cutting restriction enzymes followed by Southern hybridization (This part of the work was done in collaboration

with Sheng Sun in Joseph Heitman's lab, Duke University, USA). By using chromosome-specific probes, this analysis revealed frequent centromere length alterations in passaged RNAi mutants but not in the wild-type strain grown under similar conditions (Figure 2.12B). We analysed four different centromere regions and observed alterations in the centromere length in the independent single colonies isolated from the passaged mutants. Hence, the results of these experimental evolution studies suggest that centromeres are prone to structural alteration in the absence of regulatory factors, such as RNAi. Because centromeric transposons and RNAi are present in many organisms, it is possible that RNAi acts as a critical determinant of centromere evolution in other organisms as well.

Centromeres in *Ustilago* species complex also show evidence of RNAi mediated length regulation

To further strengthen our hypothesis towards the role of RNAi in the centromere evolution, we also identified centromeres in another basidiomycete species complex, the *Ustilago* species complex. Similar to the *Cryptococcus* species complex, the *Ustilago* species complex harbors three species where one species, *U. maydis*, has lost RNAi and *DNMT5* while *U. hordei* and *U. bromivora* harbour both the RNAi machinery as well as *DNMT5* (Laurie *et al.* 2012, Rabe *et al.* 2016). In *Cryptococcus*, centromeres are present in large ORF-free and poorly transcribed regions of the genome (Janbon *et al.* 2014). The centromeres in three *Cryptococcus* species are also syntenic with each other. Based on these parameters, we predicted centromeres in all three species of *Ustilago* complex by *in silico* analysis. A previous study in *U. maydis* has predicted its centromeres based on the presence of transposons and plasmid stability assays (Kamper *et al.* 2006). We combined those predictions with RNA-seq analysis and identified one ORF-free region in every chromosome

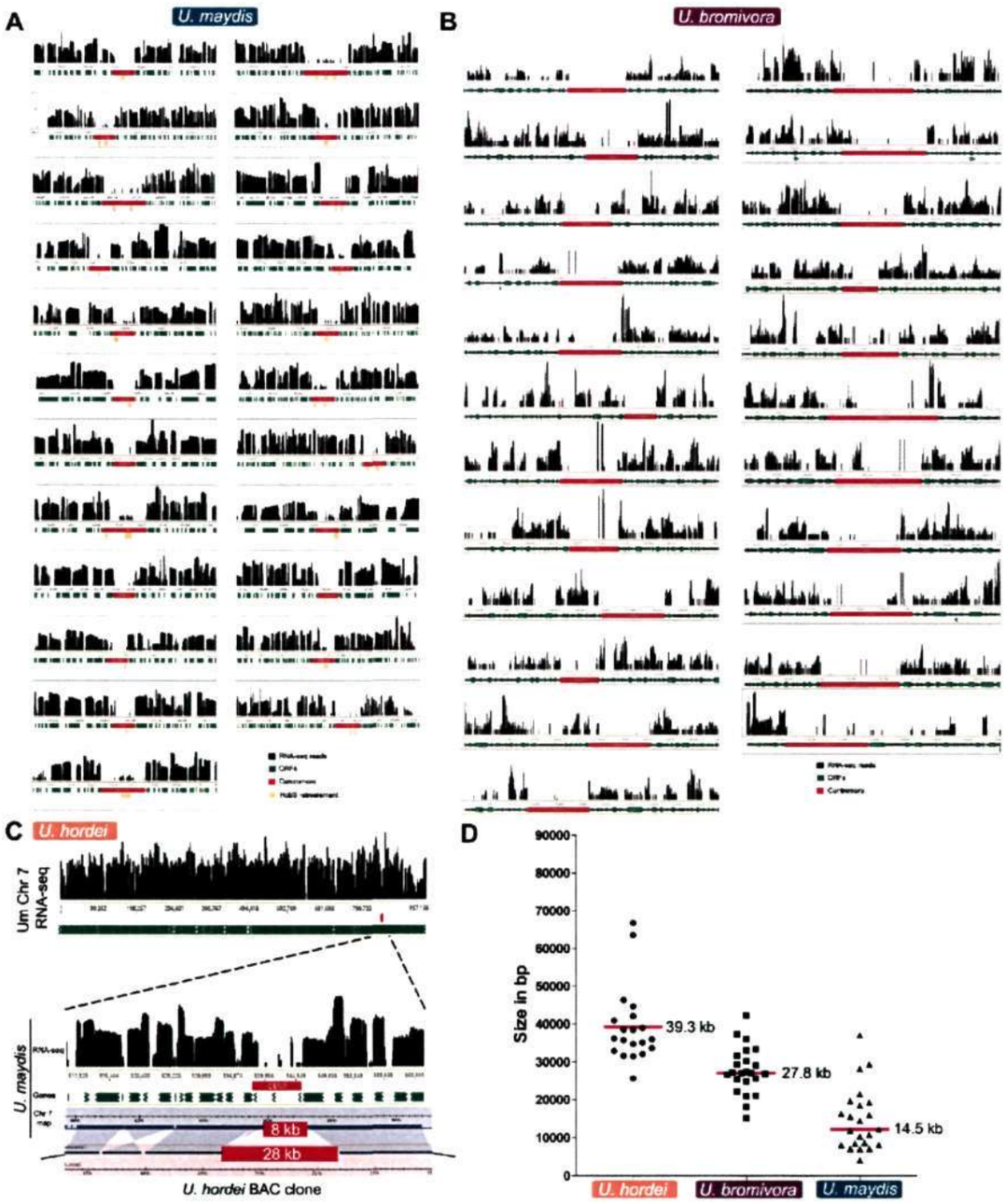

Figure 2.13 Centromeres in the *Ustilago* species complex. (A) Centromeres were predicted in *U. maydis* through parameters including the presence of transposons, lack of transcription and a long stretch of an ORF-free region. All the predicted centromeres are rich in HobS retroelements but poorly transcribed as revealed by the absence of polyA RNA. **(B)** Centromeres were identified in *U. bromivora* by synteny analysis with the *U. maydis* genome. The putative centromeres in *U. bromivora* are also poorly transcribed as shown by the lack of PolyA RNA from these regions. **(C)** The strategy adopted to estimate the length of centromeres in *U. hordei* was based on synteny with *U. maydis* centromere flanking regions. The synteny analysis was performed with the selected BAC clones of *U. hordei* since the current genome assembly is incomplete (See Materials and Methods for detail). The length of 18 of 23 centromeres was determined in the way as shown (*CEN7* is shown as an example here). **(D)** A comparison of the putative centromere length in *U. maydis, U. bromivora,* and *U. hordei.* Only 18 centromeres are plotted for *U. hordei* while all 23 are shown for both *U. maydis* and *U. bromivora.* Each dot represents one centromere, and the horizontal line depicts the mean value.

CEN #	*U. maydis* co-ordinates	*U. bromivora* co-ordinates	*U. hordei* co-ordinates*
1	Chr1: 672652-681079 (8428)	Chr2: 452858-488889 (36032)	Sc2: 1461689-1494602 (32914)
2	Chr2: 1723075-1739353 (16279)	Chr3: 1503289-1530560 (27272)	Sc3: 132303-174333 (42031)
3	Chr3: 446528-483667 (37140)	Chr4: 1374332-1396569 (22238)	N.D
4	Chr4: 67583-79380 (11798)	Chr5: 1889935-1915550 (25616)	Sc12: 396214-427879 (31666)
5	Chr5: 627251-639414 (12164)	Chr1: 480046-509128 (29083)	N.D.
6	Chr6: 921977-929042 (7066)	Chr6: 977201-998292 (21092)	Sc4: 1238539-1273654 (35116)
7	Chr7: 838836-845933 (7098)	Chr7: 76047-109059 (33013)	Sc6: 993198-1027945 (34748)
8	Chr8: 171427-191010 (19584)	Chr8: 705381-726397 (21017)	Sc14: 188704-229586 (40883)
9	Chr9: 142767-149931 (7165)	Chr10: 115367-133510 (18144)	Sc16: 576749-612953 (36205)
10	Chr10: 131074-139218 (8145)	Chr14: 100466-137856 (37391)	Sc12: 1237939-1276412 (38474)
11	Chr11: 258406-267040 (8635)	Chr15: 418425-445473 (27049)	Sc11: 1148546-1180655 (32110)
12	Chr12: 73829-95366 (21538)	Chr12: 26281-53109 (26829)	N.D.
13	Chr13: 368081-397514 (29434)	Chr11: 263218-289903 (26686)	N.D.
14	Chr14: 357506-373488 (15983)	Chr13: 352996-384709 (31714)	Sc10: 306600-340267 (33668)
15	Chr15: 262492-270546 (8055)	Chr19: 238674-268065 (29392)	Sc11: 259150-294933 (35784)
16	Chr16: 410262-420966 (10705)	Chr17: 109402-139667 (30266)	Sc29: 197725-223379 (25655)
17	Chr17: 90877-106428 (15552)	Chr16: 63155-78285 (15131)	Sc7: 138981-170485 (31505)
18	Chr18: 70385-89661 (19277)	Chr20: 55817-83227 (27411)	Sc15: 76204-115173 (38970)
19	Chr19: 526864-545420 (18557)	Chr18: 506603-548848 (42246)	Sc18: 503310-570065 (66756)
20	Chr20: 475200-479322 (4123)	Chr9: 707407-732237 (24831)	N.D.
21	Chr21: 321332-331632 (10301)	Chr21: 317190-350653 (33464)	Sc20: 385526-421512 (35987)
22	Chr22: 169493-183956 (14464)	Chr22: 160000-185505 (25506)	Sc22: 300552-345151 (44600)
23	Chr23: 232483-260749 (28267)	Chr23: 31187-58282 (27096)	Sc24: 324255-362781 (38527)

Table 2.3 The centromere coordinates in *U. maydis*, *U. bromivora* and *U. hordei*.
Um and Ub chromosome numbers are as per available in NCBI genome assemblies. Uh coordinates are as per our Pac-Bio assembly.
*in the absence of a chromosome-wise genome assembly of *U. hordei*, scaffold (Sc) numbers are mentioned. The numbers in brackets denote length of the centromere in basepair.
N.D., Not determined

as candidate centromere (Figure 2.13A, Table 2.3). The transcriptome data for *U. maydis* is available from a previous study (Kellner *et al.* 2014). For *U. bromivora*, we performed

synteny analysis with *U. maydis* genome and combined it with RNA-seq analysis of *U. bromivora* (Rabe *et al.* 2016). Both analyses revealed one region as putative centromere in each chromosome (Figure 2.13B). *U. hordei* BAC clone library along with PacBio sequencing was used to identify the centromeres and measure their length (Linning *et al.* 2004, Bakkeren *et al.* 2006). Both these approaches revealed locations and lengths of 18 putative centromeres in *U. hordei* (Figure 2.13C). Identification of centromeres in all three species revealed that RNAi-deficient *U. maydis* has shorter centromere (average length 12 kb) compared to RNAi-proficient *U. hordei* (average length 36 kb) and *U. bromivora* (average length 27 kb) (Figure 2.13D, Table 2.3). Previous studies have reported that *U. maydis* harbours a lesser number of transposons than *U. hordei* and *U. bromivora* (Laurie *et al.* 2012, Rabe *et al.* 2016). These observations further confirmed the correlation between the loss of RNAi and a reduction in the centromere length. Overall, our study provides strong evidence towards the role of RNAi in maintaining the structure of centromeres.

3. Organization of chromosome segregation machinery in *C. neoformans*

The process of chromosome segregation is poorly studied in basidiomycetes. To better understand this process in basidiomycetes, we explored the basic organization of components of the mitotic chromosome segregation machinery in *C. neoformans*. Two major components of this machinery are a large macromolecular complex the kinetochores that assemble on the centromere DNA and the microtubules (MTs) that originate from the microtubule organization centers (MTOCs). Some of the constituent proteins of the chromosome segregation machinery were chromosomally tagged with either GFP or mCherry and expressed as fusion proteins to study their localization dynamics by time-lapse imaging. To achieve better understanding of the process, we also developed a mathematical model to simulate mitosis in basidiomycetous budding yeasts and compared them with that of ascomycetous as well. The model successfully replicated the key mitotic events in both classes of fungi. Predictions obtained by simulating the model were successfully validated by performing relevant experiments.

Nuclear division in *C. neoformans* takes place in daughter cell

First, we studied the dynamics of nuclear division in *C. neoformans*. The nucleus was marked by an ectopically expressed GFP histone H4, and its subcellular localization was studied. Histones are a constitutive component of chromatin and hence tracking them through the stages of cell division allows one to investigate the dynamics of chromatin. Live cell imaging with GFP-H4 revealed that, during mitosis, GFP-H4 signals transitioned entirely from the mother into the daughter cell through the mother-daughter neck (Figure 3.1A). In the daughter cell, the area covered by the GFP-H4 signals was reduced by 66% as compared to the signals before GFP-H4 migrated through the neck suggesting significant chromatin condensation during mitosis. This was followed by the arrangement of the GFP-H4 signals in a double layered structure separated by a zone of no fluorescence (t= 25'20"). After staying

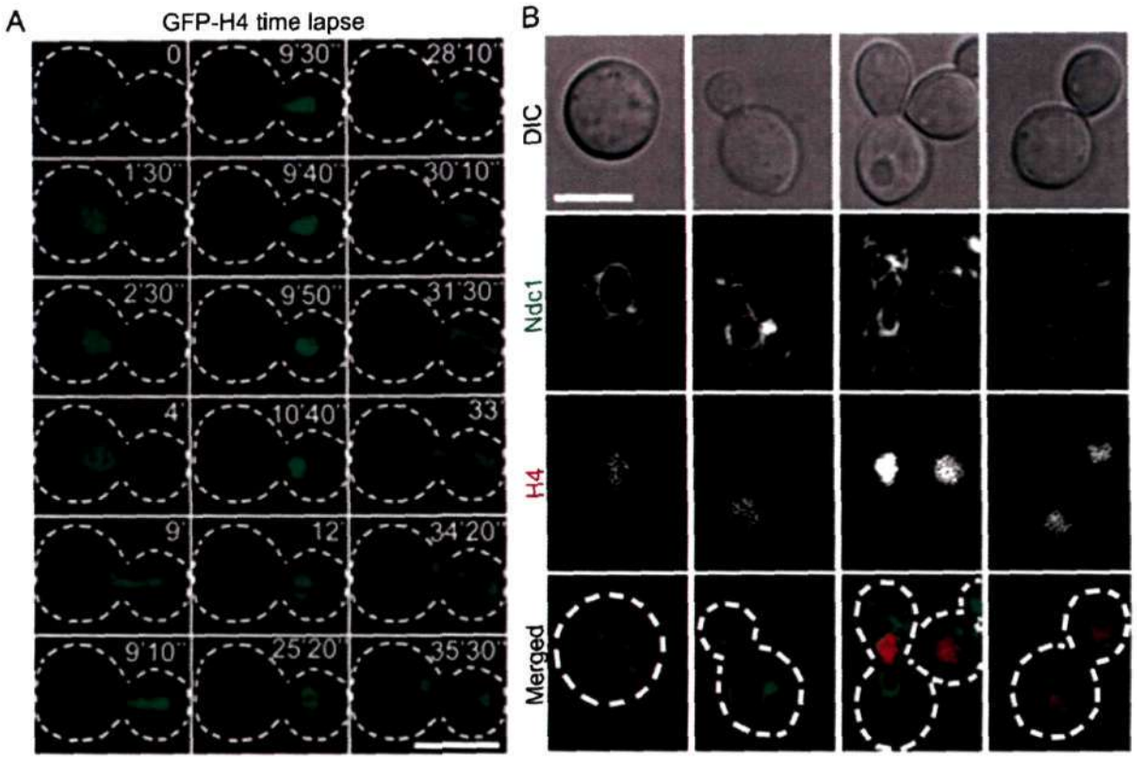

Figure 3.1 Chromatin dynamics in *C. neoformans*. **(A)** Dynamics of GFP-H4 in a live cell during the cell cycle. Initially, the signal was visible only in the mother cell. With progression of the cell cycle, the GFP-H4 moved to the daughter cell and arranged itself in a double layer structure which ultimately divided in two halves, one of which traversed back to mother cell and other half remained in the daughter cell. **(B)** Co-localization of the NE marked by GFP-Ndc1 with a chromatin marker H4-mCherry at different stages of cell cycle showed that chromatin was enclosed into the NE throughout the cell cycle. Bars, 5 μm.

in that arrangement for 5-10 min, the nuclear division took place in the daughter cell. One part moved back to the mother cell while the other remained in the daughter cell. To follow localization of the nuclear envelope (NE) and chromatin together, we co-expressed mCherry-tagged histone H4 and GFP-tagged Ndc1, a nuclear pore complex protein that localizes throughout the NE making it a tool to study dynamics of the nuclear membrane in most organisms (Stavru *et al.* 2006). In *C. neoformans*, GFP-Ndc1 signals localized primarily to the NE while a small fraction of the fusion protein localized to other organelles such as the endoplasmic reticulum (Figure 3.1B). We speculate that the extra cytoplasmic signals might be a consequence of overexpression of the fusion protein GFP-Ndc1. The co-localization of GFP-Ndc1 and H4-mCherry showed the presence of the NE encircling chromatin throughout

the cell cycle (Figure 3.1B). During mitosis, GFP-Ndc1 signals localized to both the mother and the daughter cell in a dumb-bell shaped structure. Thus, unlike chromatin, the nuclear envelope did not move entirely to the daughter cell, and half of it always remained in the mother cell itself. This observation is different with respect to another basidiomycetous yeast *U. maydis* where the NE does not surround chromatin during mitosis and chromatin alone moves to the daughter cell leaving behind the NE in the mother (Straube *et al.* 2005).

Microtubule dynamics in *C. neoformans*

Next, we sought to study the dynamics of MTs and MTOCs, two complexes essential for spindle formation during mitosis, in *C. neoformans*. We identified and epitope tagged α-tubulin to track MTs and Spc98, the γ-tubulin complex component, to study MTOCs in a strain in which chromatin was marked by H4. In interphase cells, MTs formed long strands in the cytoplasm and were seen to be excluded from the area covered by H4 (the nucleus) indicating that the MTs are absent from interphase nucleus. MT tips were arranged in an oriented direction towards the bud emergence site at the onset of mitosis (Figure 3.2A). This was followed by movement of both GFP-tubulin and H4-mCherry to the daughter cell. During mitosis, the MTs accumulated in the daughter cell and appeared as a bright rod-like structure in the middle of the chromatin doublet. With further progression of mitosis, the rod-like structure elongated to turn into a long spindle segregating chromatin into two halves (Figure 3.2A). MTOCs, marked by Spc98, showed similar localization patterns as puncta in the cytoplasm during interphase (Figure 3.2B). At the onset of mitosis, most of the Spc98 signals coalesced and partially co-localized with the nuclear mass. The clustering of the Spc98 signals at the nuclear periphery represents activation of the spindle pole body (SPB) in

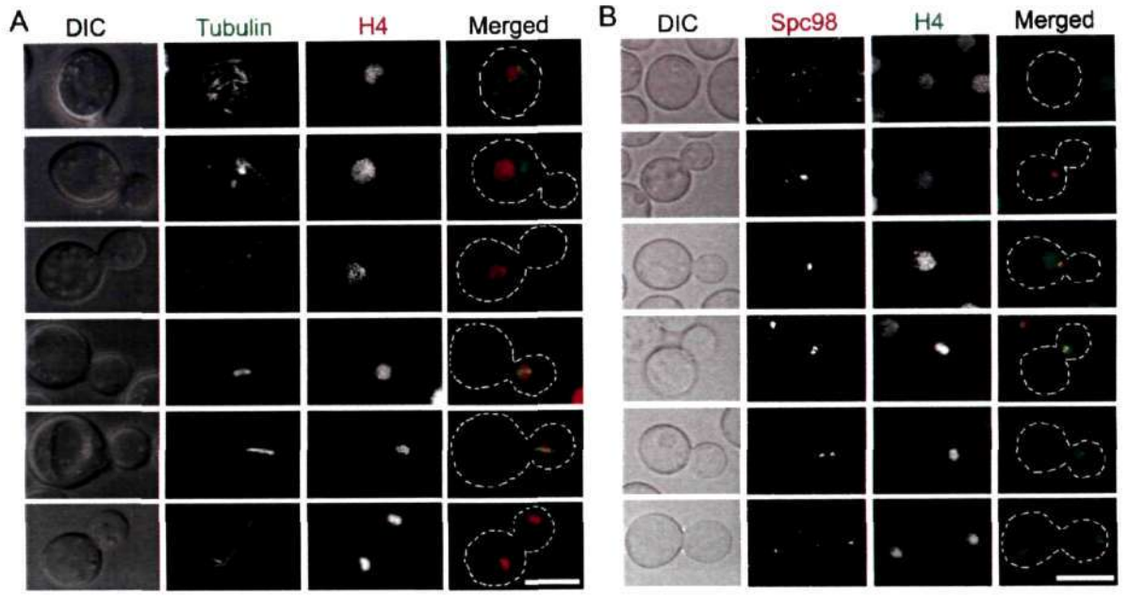

Figure 3.2 The dynamics of spindle structure in *C. neoformans*. (A) Snapshots showing relative dynamics of microtubules and chromatin at various cell stages of the cell cycle in *C. neoformans*. The microtubules, marked by tubulin, formed a mesh in cytoplasm in interphase cells and do not localize with the nucleus, marked by H4. During mitosis, the microtubules were not visible in cytoplasm and show close association with chromatin. The spindle elongates to divide the chromatin during anaphase. **(B)** Co-localization of Spc98-GFP and H4-mCherry at various stages of the cell cycle. Spc98-GFP signal is present as multiple puncta in cytoplasm during interphase and interacts with chromatin only during mitosis. Bars, 5 μm

this organism. In later stages, Spc98 signals clustered further onto the SPB and was seen leading the movement of the nuclear mass to the daughter cell. The Spc98 cluster then divided into two dots during mitosis, which further segregated during anaphase. Similar to chromatin, one clustered mass of Spc98 migrated back to the mother cell while the other half remained in the daughter cell. The dynamic localization patterns of MTs and MTOCs are similar to what has been reported in another basidiomycetous yeast, *U. maydis* (Steinberg *et al.* 2001, Straube *et al.* 2003).

Identification and localization of kinetochore proteins

To further study key mitotic events in this pathogenic basidiomycetous yeast, we identified and fluorescently tagged proteins with homology to known kinetochore subunits representing three functional layers of the kinetochore. The kinetochore proteins chosen for

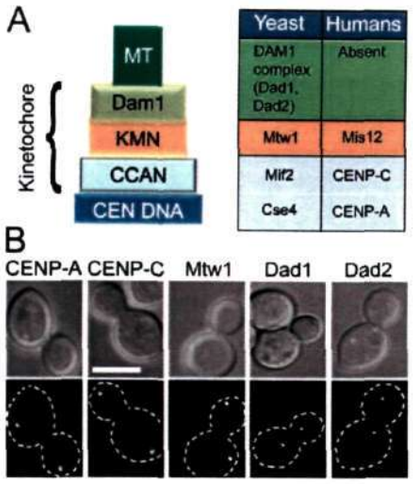

Figure 3.3 Localization of kinetochore proteins in *C. neoformans*. **(A)** Evolutionarily conserved proteins representing three layers of fungal kinetochores were identified in *C. neoformans*. **(B)** Representative kinetochore proteins indicated in A were fluorescently tagged with mCherry (CENP-A, CENP-C, Mtw1 and Dad2) or GFP (Dad1) and their localization was studied by confocal microscopy. Each protein shows typical kinetochore localization pattern as described previously in budding yeasts. Bar, 5 μm.

this analysis included: 1) two inner kinetochore components, the centromere-specific histone CENP-A/Cse4 and CENP-C/Mif2; 2) the outer kinetochore proteins Mis12/Mtw1 and two constituents, Dad1 and Dad2, of the Dam1 complex (Figure 3.3A). In large budded cells (with the budding index of 0.8-0.9) in which nuclear division would have already occurred, each of these five fluorescently tagged proteins exhibited typical localization signals of a yeast kinetochore protein - two single dots: one in the mother and one in the daughter cell – each representing clustered centromeres (Figure 3.3B). These results indicated that these proteins are indeed localized at the kinetochore in *C. neoformans*.

Kinetochore assembly is a step-wise process in *C. neoformans*

Next, we performed time-lapse imaging to follow the localization of the kinetochore proteins from all three kinetochore layers in *C. neoformans*. The persistent localization of the mCherry-CENP-A suggests that this protein is constitutively present at the centromere. CENP-C-mCherry showed nearly complete co-localization with GFP-CENP-A in all examined cells irrespective of the cell cycle stage (Figure 3.4A and B). Thus, the inner

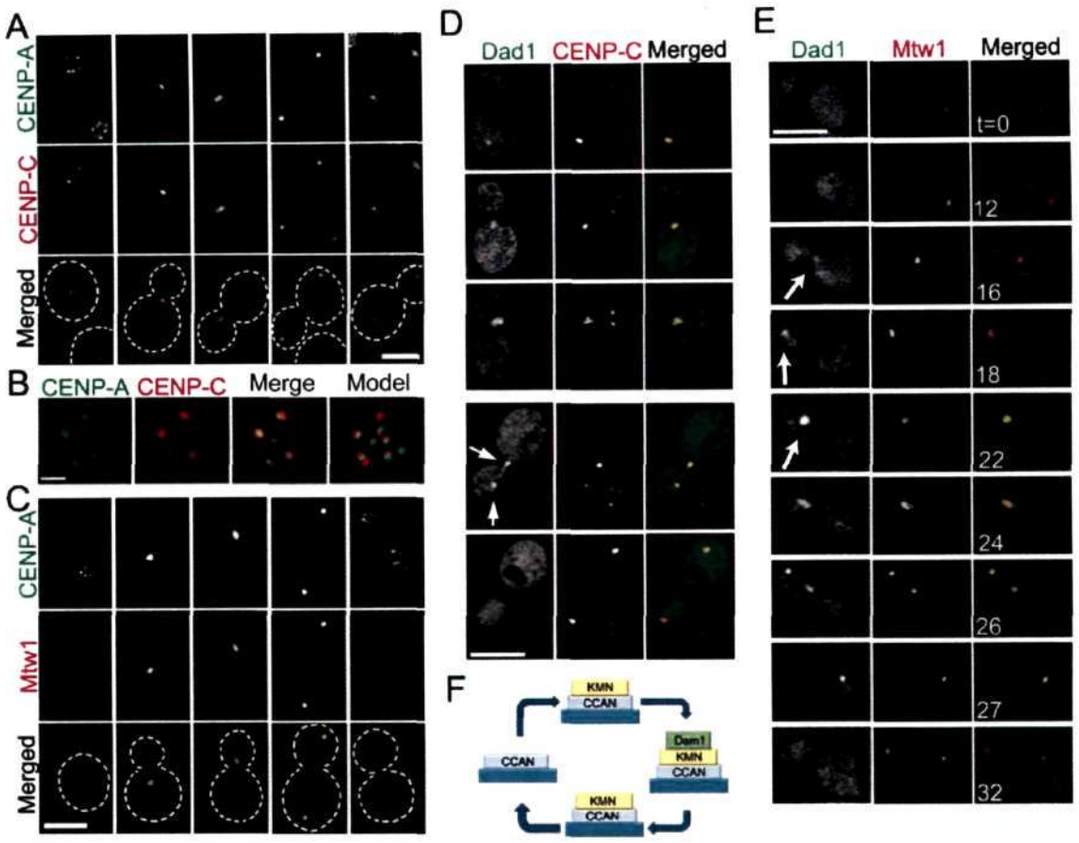

Figure 3.4 Ordered kinetochore assembly in *C. neoformans*. **(A)** Two inner kinetochore proteins, GFP-CENP-A and CENP-C-mCherry, co-localized at all stages of the cell cycle. Both proteins co-localized as separate dots in unbudded cells (first column), and soon after cytokinesis (last column) but remained clustered during mitosis (middle three columns). **(B)** A 3-D reconstruction based on Z-stack images of an unbudded cell shows a complete overlap of GFP-CENP-A and CENP-C-mCherry. **(C)** A middle kinetochore protein Mtw1-mCherry was not visible in cells where the inner kinetochore protein GFP-CENP-A was found as multiple non-clustered signals (the first and the last column). However, Mtw1-mCherry co-localized with clustered GFP-CENP-A (middle three columns). **(D)** An outer kinetochore component GFP-Dad1 became visible prior to mitosis when it co-localized with the inner kinetochore protein CENP-C-mCherry in a single cluster. **(E)** Co-localization of an outer (GFP-Dad1) and a middle (Mtw1-mCherry) kinetochore protein showed that GFP-Dad1 was loaded onto the kinetochore later than Mtw1-mCherry. GFP-Dad1 was visible during mitosis (t=16 to 27 min) and disappeared soon after chromosome segregation while Mtw1-mCherry remained present (t=32 min). **(F)** Schematic showing ordered assembly of kinetochore proteins. Bars, 5 μm (A, C, D, E) and 1 μm (B)

kinetochore in *C. neoformans* appeared to be centromere-associated throughout the cell cycle. In contrast, the outer kinetochore protein Mtw1-mCherry did not co-localize with GFP-CENP-A in cells that showed unclustered GFP-CENP-A (Figure 3.4C). The Mtw1-mCherry signals were visible and co-localized with GFP-CENP-A at the time when GFP-CENP-A signals became a single dot in the mother cell prior to mitosis and the two proteins remained

co-localized until telophase (Figure 3.4C). Examination of cells expressing the inner kinetochore component CENP-C-mCherry and the outer kinetochore protein GFP-Dad1 revealed that the timing of appearance of GFP-Dad1 was similar to that of Mtw1-mCherry and coincided with clustering of CENP-C-mCherry (Figure 3.4D). Further investigation of the relative localization of the GFP-Dad1 and the Mtw1-mCherry in the same cells revealed that the GFP-Dad1 signals became visible later as compared to the appearance of Mtw1-mCherry (Figure 3.4E). The signals of the GFP-Dad1 were visible as a single dot co-localizing first with Mtw1-mCherry in the mother cell, and remained until the division of the signals between the daughter and mother cell. Notably, while the Mtw1-mCherry dot signals were clearly visible in the mother and daughter cells later after nuclear division, GFP-Dad1 was no longer visible at this stage (Figure 3.4E). Taken together, these data suggest that the assembly of the kinetochore in *C. neoformans* is an ordered process in which the CCAN proteins are assembled throughout the entire cell cycle. Components of the KMN network are incorporated prior to mitosis concomitant with centromeric clustering. Final assembly of the Dam1 complex occurs after centromeres are clustered and are ready to translocate into the daughter cell for the subsequent division of the genetic material (Figure 3.4F). To further map the timing of the KMN network and the Dam1 complex proteins assembly, we calculated the budding index of cells when proteins of different complexes showed a single cluster in the mother cell. Comparison of the KMN and the Dam1 complex proteins showed a significant difference in the appearance of these two complexes (Figure 3.5). While both CENP-A and Mtw1, representing the CCAN and KMN complexes respectively, localized at the kinetochore when the budding index was around 0.4, Dad1, a Dam1 complex protein, was visible in cells only with a budding index of more than 0.6. This result along with microscopy shows that Mtw1 localizes earlier than Dad1 confirming that the kinetochore assembly in *C. neoformans* is a step-wise process.

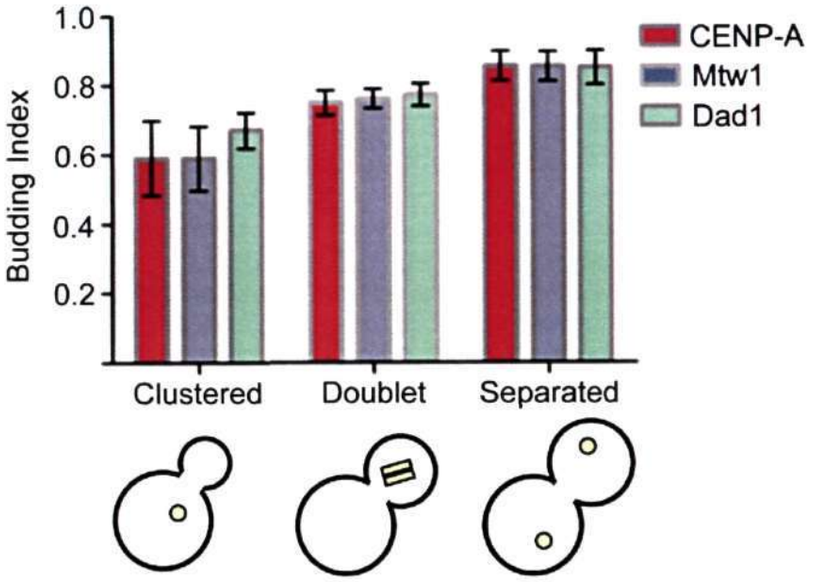

Figure 3.5 Budding index analysis revealed difference in loading of the outer kinetochore proteins. A Dam1 complex component GFP-Dad1 assembles at the kinetochore (B.I. 0.6) later than the KMN network protein Mtw1-mCherry (B.I. 0.4). Budding index was calculated for cells expressing either GFP-Dad1, Mtw1-mCherry or mCherry-CENP-A (n=100). In cells with the clustered kinetochore before mitosis budding index was significantly higher for GFP-Dad1 as compared to Mtw1-mCherry (p=0.0001).

The nuclear envelope partially disassembles during mitosis in *C. neoformans*

Ordered kinetochore assembly and open mitosis are hallmarks of the metazoan mitosis. In order to probe the status of mitosis (open versus closed) in *C. neoformans*, we employed several approaches to determine the structural integrity of the NE during mitosis in *C. neoformans*. First, we followed the localization of the fluorescently tagged core nuclear pore protein Nup107 (Boehmer *et al.* 2003) (This part of the work was done in collaboration with Lukasz Kozubowski in Joseph Heitman's lab, Duke University, USA). GFP-Nup107 showed dot-like punctate signals that outlined the NE (Figure 3.6A), similar to its localization as described in other fungal species but unlike the uniform dispersal of NPCs in metazoans (D'Angelo and Hetzer 2008, Theisen *et al.* 2008). Interestingly, in non-dividing cells fluorescent dots of mCherry-CENP-A were often observed at or near the NE, as determined based on their proximity to the GFP-Nup107 signals confirming that centromeres are

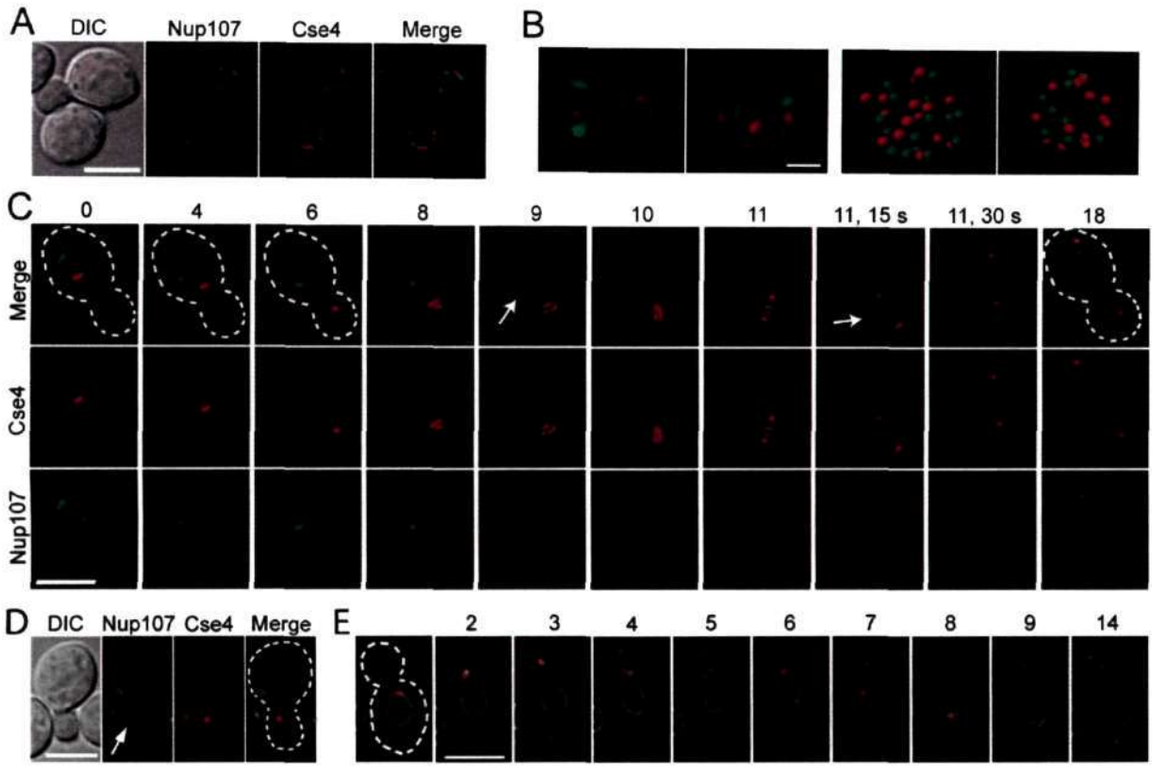

Figure 3.6 Dynamics of the nuclear envelope during mitosis in *C. neoformans*. **(A)** Localization of the nuclear pore complex protein Nup107 tagged with GFP and mCherry-CENP-A indicates that centromeres are present at the nuclear periphery. **(B)** A 3D reconstruction of images of two cells from A and the model show that GFP-Nup107 and mCherry-CENP-A do not co-localize at the NE. **(C)** Time-lapse analysis of GFP-Nup107 and mCherry-CENP-A revealed that GFP-Nup107 is not present on the NE during mitosis (time 9 to 11.15), suggesting that NPCs disassemble at the time of mitosis. After centromere separation, GFP-Nup107 is again visible on the NE marking the reassembly of NPCs after mitosis. **(D)** A discontinuous GFP-Nup107 signal (arrow), led by mCherry-CENP-A, invaginates into the daughter cell **(E)** GFP-Ndc1, a marker for the nuclear membrane, was used to examine nuclear membrane localization during the course of mitosis, which showed that it was present throughout the cell cycle. Bars, 5 μm (A, C, D and E) and 1 μm (B).

peripherally localized (Figure 3.6A). Strikingly, the dot signals of mCherry-CENP-A almost never co-localized with dots of GFP-Nup107 suggesting that NPCs and centromeres occupy different region of the NE (Figure 3.6A and B). Prior to mitosis mCherry-CENP-A was clustered primarily near or at the NE, and the final single bright dot of mCherry-CENP-A was always positioned closely associated with the NE (Figure 3.6C). During the initial transition of mCherry-CENP-A into the daughter cell, GFP-Nup107 formed a narrow invagination that appeared to be pulled by mCherry-CENP-A (Figure 3.6 C and D). Z-section time-lapse microscopy revealed that at the time when the mCherry-CENP-A single dot migrated into the

daughter cell, the signals of GFP-Nup107 that outlined the NE decreased gradually and were no longer visible after mCherry-CENP-A rearranged from a single dot into the doublet structure in the daughter cell (Figure 3.6C). This structural change was concomitant with a significant increase in the cytoplasmic signal of GFP-Nup107, such that the mean intensity of the GFP-Nup107 was nearly 3 times higher at 10 min as compared to at 4 min. When mCherry-CENP-A signals divided between the two cells, GFP-Nup107 appeared arch-like, closely surrounding a dot of mCherry-CENP-A (Figure 3.6C). Ultimately, GFP-Nup107 formed a circle with a few brighter dots that suggested a clustering of NPCs and reformation of the NE. Taken together, the analysis of the GFP-Nup107 dynamics suggests complete disassembly of the NPCs occurs during metaphase, consistent with possible disintegration of the NE during mitosis in *C. neoformans*.

Next, we followed the localization of the integral NE protein Ndc1, which is essential for the assembly of NPCs (Stavru *et al.* 2006, D'Angelo and Hetzer 2008). GFP-Ndc1 outlined the NE uniformly (Figure 3.6E). In striking contrast to GFP-Nup107, a bright GFP-Ndc1 signal largely persisted throughout the entire duration of nuclear division (Figure 3.6E). Similar to GFP-Nup107, during the initial movement of mCherry-CENP-A into the daughter cell, GFP-Ndc1 signals appeared as a stretched narrow invagination into the daughter cell that was pulled by the leading dot of mCherry-CENP-A (Figure 3.6E). The GFP-Ndc1 fluorescent signal immediately adjacent to mCherry-CENP-A appeared somewhat weaker or discontinuous in all of the stages (Figure 3.6E). A large portion of the GFP-Ndc1 signal that likely outlined the NE remained in the mother cell while mCherry-CENP-A rearranged into a doublet inside the daughter cell. During the subsequent chromosomal division, mCherry-CENP-A appeared to be continually surrounded by a membrane marked by GFP-Ndc1 in the daughter cell. These data suggest that the NE remains largely intact during mitosis in *C. neoformans* and only a partial breakage of the NE takes place near the clustered centromeres.

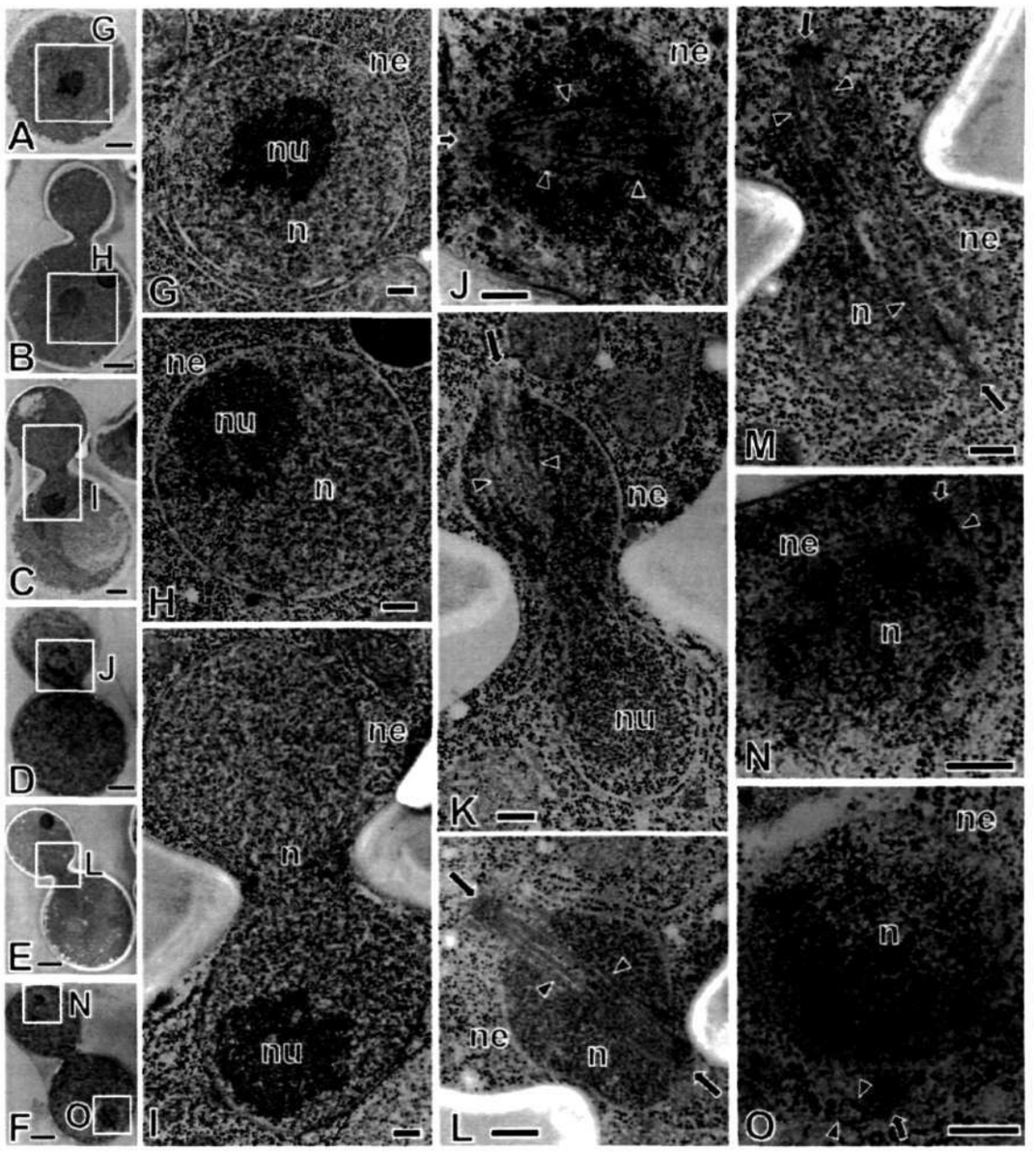

Figure 3.7 TEM analysis of mitosis in *C. neoformans*. **(A and G)** G1 - S phase, **(B and H)** G2 phase, **(C and I)** Prophase, **(D, J and K)** Prometaphase, **(E and L)** Metaphase, **(M)** Anaphase, **(F, N and O)** Telophase. The nuclear envelope (ne) was closed at G1 though prophase, broke near spindle pole body (arrow) at prometaphase, and closed at the end of telophase. Nucleolus (nu) was visible at G1 through prophase, stayed in the mother cell at prometaphase, disappeared at metaphase, and reappeared after telophase. Spindle pole body resided on the nuclear envelope as one duplicated form at G1 though G2 phase, separated into two at prophase, entered the nuclear region by breaking the nuclear envelope at prometaphase, located at the spindle poles at metaphase and anaphase, and was extruded back to the cytoplasm from the nuclear region at telophase. Microtubules (arrowheads) were distributed in the cytoplasm at G1 through prophase, appeared in the nucleus (n) at prometaphase through middle of telophase. Bars, 1 μm (A-F), 250 nm (G-O).

To investigate the NE status in even greater detail, we analysed mitotic events in *C. neoformans* using transmission electron microscopy (TEM) (Figure 3.7) (This work was done

in collaboration with Masashi Yamaguchi, Grand Fellow, Chiba University, Japan). TEM analysis revealed that while the NE stays largely intact during mitosis in *C. neoformans*, it did rupture at prometaphase, the point at which the spindle breaks through the NE during the migration of the spindle into the daughter cell (Figure 3.7). Taken together, our analyses of NE dynamics during mitosis strongly suggest that at prometaphase nearly half of the NE that surrounds chromatin migrates into the daughter cell and is led by clustered centromeres/SPBs. This pulling event appears to be preceded by a rupture of the NE by the spindle MTs already in the mother cell. The remainder of the NE persists in the mother cell, together with the nucleolus, and is devoid of chromatin. At metaphase, NPCs completely disassemble, the nucleolus disappears, and centromeres rearrange. At this step, the spindle breaks through the NE near SPBs/clustered centromeres. During spindle elongation, centromeres rearrange in the daughter cell and surround the spindle throughout its length. After the segregation of sister chromatids in the daughter cell and the migration of half of the nuclear mass from the daughter back to the mother cell, NPCs reassemble and the nucleolus reappears.

Nuclear/spindle dynamics depends on the number of cMTs and dynein activity

Our results on the nuclear segregation and MT dynamic in *C. neoformans*, a basidiomycete, revealed certain key differences from that of well-studied ascomycetous budding yeasts. The most significant difference is the site of nuclear division – the mother cell in ascomycetes and the daughter cell in basidiomycetes (Heath 1980, Straube *et al.* 2005, Gladfelter and Berman 2009, Kozubowski *et al.* 2013). To study the basis of this difference we developed a mathematical model for budding yeasts belonging to both ascomycetes and basidiomycetes (Sutradhar *et al.* 2015) (This part of the work was done in collaboration with Raja Paul's lab, IACS, Kolkata, and Shreyas Sridhar in my lab). Having developed the

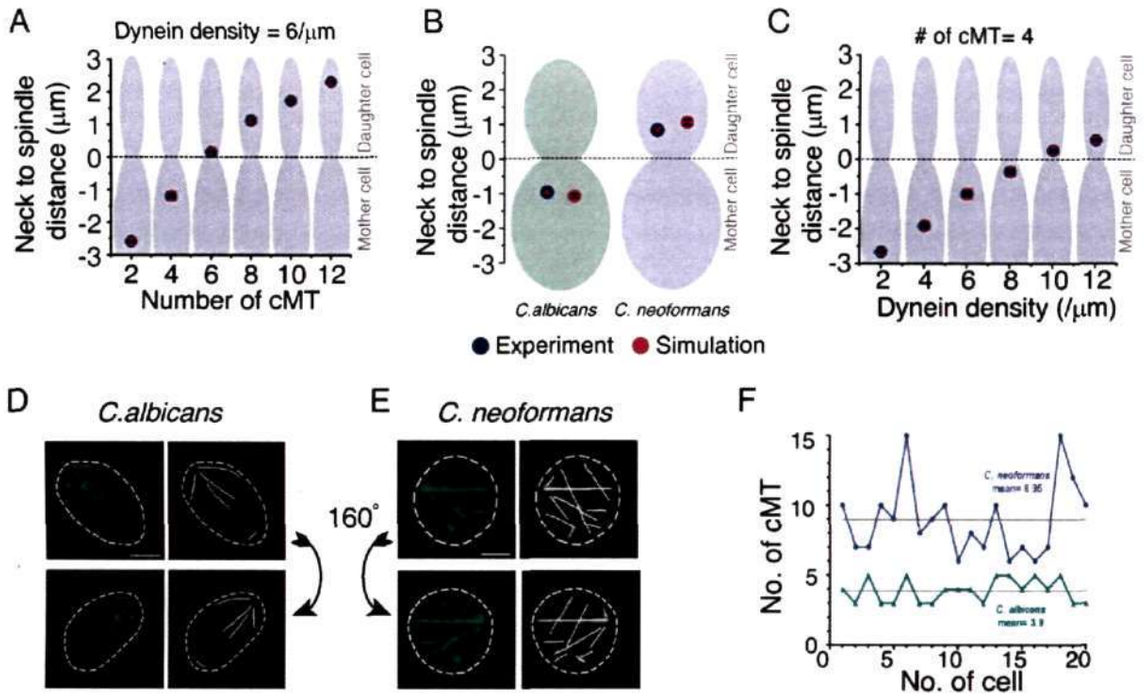

Figure 3.8 Dependence of nuclear migration on the number of cytoplasmic MTs and dyneins activity in ascomycetes and basidiomycetes. (A) *In silico* measurements of the neck to spindle distance upon altering cMT numbers per cell during mitosis. We observed that, for a fixed density of cortical dynein, a higher number of cMTs leads to a deeper penetration of the spindle into the daughter cell. **(B)** Mean distance of the spindle from neck is plotted as observed in simulation (n=100) and experiment (n=30) for both *C. albicans* and *C. neoformans*. Experimental measurements were carried out in a strain that had MTOCs tagged with GFP. DIC was used as a reference point for calculating spindle mid to neck distance. **(C)** The spindle migration can also be affected by an alternative pathway involving cortical dyneins. An increase in the cortical dynein density, for a fixed number of cMTs, results in similar nuclear dynamics obtained previously by altering the cMT number. Standard error of mean (SEM) is shown in red bars. **(D)** and **(E)** *C. albicans* and *C. neoformans* strains expressing Tub1-GFP were used to monitor and estimate cMTs. cMTs in all stacks were taken into consideration. Two different views over the y axis (0°, top panels, and 160°, bottom panels) of the 3D rendered images are shown to improve the visibility of cMTs that may be masked by others in a given orientation. Bar, 2μm. **(F)** The number of cMTs were counted in large number of cells of *C. albicans* and *C. neoformans*. These values were plotted and the calculated mean of cMTs per cell in each case was represented by a grey line.

model, we probed for the underlying variation in nuclear migration observed between ascomycetes and basidiomycetes. Differential migration patterns and a large deformation of the nucleus during migration suggested that the magnitude of force pulling SPBs towards the bud is greater in basidiomycetes as compared to ascomycetes (Straube *et al.* 2005, Fink *et al.* 2006, Kozubowski *et al.* 2013). The larger force generated could either be due to an increased population of cMTs and/or a higher dynein activity at the cortical region. It is widely believed that ascomycetes nucleate ~4 cMTs (Kosco *et al.* 2001), whereas the number of cMTs in

basidiomycetes was unknown. A previous study using *U. maydis* showed that the number of MTs in this organism is 10-15 indicating a higher number of cMTs in basidiomycetes (Straube *et al.* 2003). Considering a conserved cMT-cortex interaction, our model revealed that the size of the cMT population must be ≥ 8 for producing sufficient force to pull the nucleus into the daughter cell (Figure 3.8A). Assigning the number of cMTs as 4 for ascomycetes and 8 for basidiomycetes, simulations predicted the mean distances between the neck and the spindle as -0.90 μm and +0.83 μm, respectively. These values are close to the experimental measurements (Figure 3.8B). Further, an increase in the density of cortical dyneins engaged in pulling the cMTs also provided enough pulling force for the migration of the nucleus into the daughter cell in the basidiomycetes model when other parameters are kept constant (Figure 3.8C). To test the model's prediction of requiring a greater number of cMTs in basidiomycetes for migration of the nucleus into the daughter cell, we counted the number of cMTs in *C. albicans* (representative of ascomycetes, Figure 3.8D) and *C. neoformans* (representative of basidiomycetes, Figure 3.8E). Our experiments revealed that *C. neoformans* has approximately at least 2 times higher number of cMTs than the *C. albicans* (Figure 3.8, D- F). It was observed that approximately 6 – 15 cMTs formed a dense mesh-like network in *C. neoformans*, with an average number of cMTs per cell being ~9 (Figure 3.8F), while each *C. albicans* cell has 3-5 cMTs with an average of ~4 cMTs per cell (Figure 3.8F). The results presented above confirm the importance of cMT and dynein in positioning the spindle. Disruption of any of these components leads to severe mitotic defects (Markus and Lee 2011, Laan *et al.* 2012, Xiang 2012, Best *et al.* 2013). Thus, our model prediction supported by experimental validation confirms that an increased number of cMTs is required for migration of the nucleus/SPB into the daughter cell.

4. Kinetochore clustering in *C. neoformans* is mediated by a SUN domain protein, Sad1

Similar to many yeast species, kinetochores cluster together near the nuclear periphery throughout the mitotic cell cycle in *C. neoformans*. However, chromosomes are linearly aligned to form the metaphase plate in metazoans. During chromosome segregation, kinetochore clustering in yeast may facilitate their capture by the MTs and thus may play a function similar to that of the metaphase plate in metazoans. In *C. neoformans*, kinetochores are unclustered in interphase cells but they begin to cluster during mitosis. Thus the dynamics of kinetochore clustering is different in *C. neoformans* from other studied budding yeasts where kinetochores are clustered throughout the cell cycle. The unique kinetochore clustering dynamics prompted us to explore importance of this process in chromosome segregation in *C. neoformans*. As mentioned, live-cell imaging with the inner kinetochore proteins revealed that the kinetochore clustering occurs during the onset of mitosis. MT depolymerisation experiments revealed that the MTs are essential for the kinetochore clustering. However, localization dynamics of the kinetochore and MTs, when studied together in the same cell, indicated an indirect interaction of MTs with the kinetochores. We then examined the possible roles of the SUN-KASH protein complex, that is known to form a bridge across the nuclear envelope (Razafsky and Hodzic 2009, Kim *et al.* 2015), in spatio-temporal regulation of the kinetochore clustering in *C. neoformans*. This study identifies a novel role of the SUN domain protein Sad1 in mediating the kinetochore clustering at the right time and space during the mitotic cell cycle in *C. neoformans*.

Kinetochores cluster only during mitosis in *C. neoformans*

We examined the dynamics of kinetochores with respect to each other during the mitotic cycle by time-lapse imaging of cells expressing fluorescently tagged CENP-A,

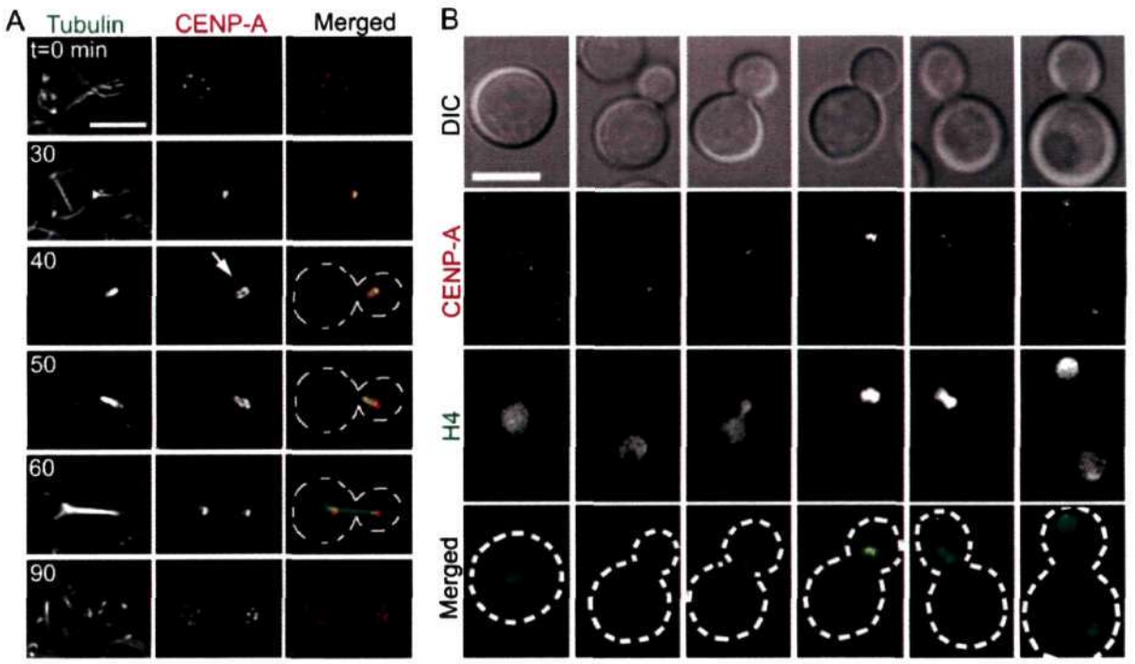

Figure 4.1 Kinetochore clustering in *C. neoformans*. **(A)** Cells expressing GFP-tubulin and the inner kinetochore protein mCherry-CENP-A were studied by time-lapse Z-section microscopy and single focal planes are shown. Initially non-clustered mCherry-CENP-A converges into a single dot in the mother cell. In the daughter cell, mCherry-CENP-A rearranges into a doublet that surrounds a single rod of GFP-tubulin, a putative spindle (t=40, arrow). At this stage cytoplasmic GFP-tubulin cables are no longer visible. After mCherry-CENP-A divides between the daughter and mother cell, mCherry-CENP-A unclusters and the GFP-tubulin cytoplasmic cables reappear (t=90). **(B)** Co-localization of CENP-A with histone H4 showing the nuclear peripheral localization of the kinetochore. During mitosis, the kinetochore is seen in between the two chromatin masses, also the place where spindle formation is observed. Bars, 5 μm.

mCherry-CENP-A. To better discern stages of the cell cycle, the spindle was visualized with GFP-tagged α-tubulin (GFP-tubulin). Signals of mCherry-CENP-A were punctate and appeared as multiple distinct dots in non-dividing cells, including unbudded cells and cells with small buds (budding index < 0.4) (Figure 4.1A). The circular arrangement of mCherry-CENP-A dot-like signals in most non-dividing cells suggested kinetochores localize adjacent to the nuclear periphery. Peripheral localization of kinetochores was further confirmed in cells that co-expressed GFP-H4 (Figure 4.1B). The number of dot-like signals of mCherry-CENP-A gradually decreased until ultimately in a subset of large budded cells (budding index = 0.4-0.55) the mCherry-CENP-A signals were visible as a single bright dot that subsequently migrated into the mother-daughter neck (Figure 4.1). Interestingly, when

clustering was nearly complete, mCherry-CENP-A signals appeared to contact a bundle of GFP-tubulin cables, suggesting that clustering of kinetochores and the attachment of MTs to the kinetochore cluster occur concomitantly (Figure 4.1A). The kinetochore cluster was always localized at the vicinity of the NE, similar to ascomycetous budding yeasts (Anderson *et al.* 2009, Duan *et al.* 2010, Thakur and Sanyal 2012, Thakur and Sanyal 2013). In the daughter cell, a dot-like signal of GFP-tubulin underwent a transition into an elongated rod which was surrounded by two bars of mCherry-CENP-A when observed at a single focal plane (Figure 4.1A). While the significance of this MT- kinetochore arrangement remains to be determined, it may be functionally analogous to the metaphase plate of metazoans. At this stage, the cytoplasmic MTs were no longer visible. Within ≤1 min after cytoplasmic/astral MTs became visible, the clustered kinetochore signal divided into two separate dots with one migrating back to the mother cell. After the division of the kinetochore cluster, cytoplasmic MTs reappeared, and the kinetochores began to uncluster forming dot-like signals like those observed in non-dividing cells.

Microtubules are necessary for clustering of the kinetochores prior to mitosis

The concomitant localization of kinetochores and tubulin when kinetochores were clustered prompted us to examine if MTs play a role in clustering of the kinetochores (This part of the work was done in collaboration with Lukasz Kozubowski in Joseph Heitman's lab, Duke University, USA). To test this, we used nocodazole (Noc) to depolymerize MTs in a strain that co-expressed mCherry-CENP-A (to assess the position of kinetochores) and GFP-Ndc1 (to assess the state of the NE and the stage during the cell cycle) (Figure 4.2A). First, we obtained a population of mostly unbudded cells (96% unbudded) by limiting oxygen during growth (Ohkusu *et al.* 2004). In this starting population, kinetochore signals were not

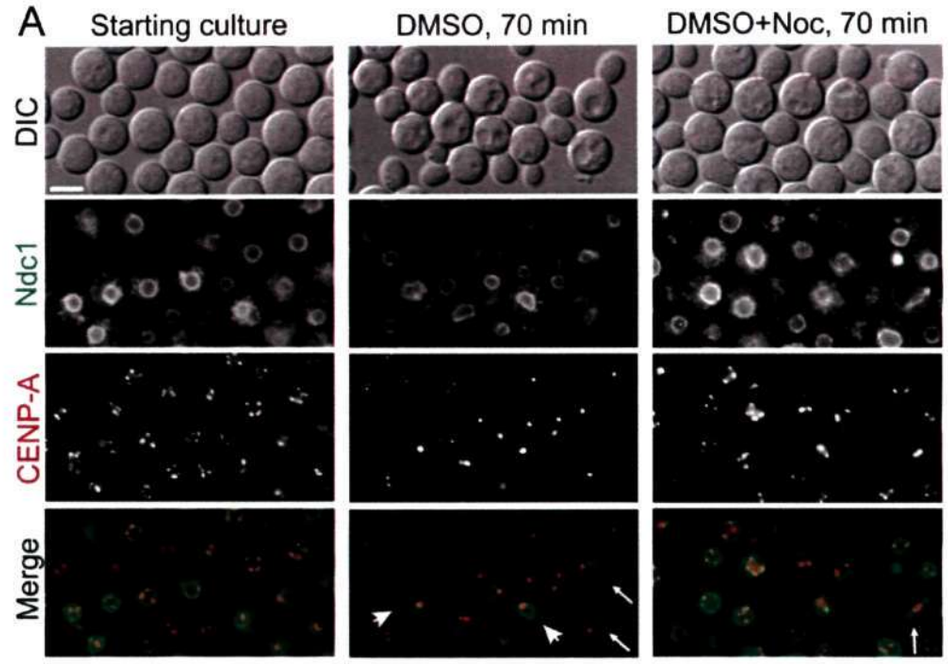

B

Time (min)	Sample	Budded	Cells in mitosis	CENP-A clustered cells not yet dividing	CENP-A unclustered	
					Small-budded	Large-budded
0	Control	3	0	0	3	0
	Nocod.	1	0	0	1	0
50	Control	66	5	20	41	0
	Nocod.	71	0	4*	49	18
70	Control	81	47	21	12	0
	Nocod.	68	0	9*	18	39

Numbers represent % (at least 100 cells were counted in each category)
* In these cells Ndc1 was delocalized

Figure 4.2 Clustering of kinetochores requires microtubules in *C. neoformans*. **(A)** Cells expressing mCherry-CENP-A and GFP-Ndc1 were synchronized in G1/G2 and released from the arrest in the presence of nocodazole (1 µg/ml) or DMSO as a control. At 70 min after the release the majority of nocodazole-treated cells showed non-clustered mCherry-CENP-A, while in the control sample, majority of cells either showed clustered kinetochores or progressed through mitosis. **(B)** The quantification of cells with respect to the stage of the cell cycle and % of kinetochore clustering. Bar, 5 µm.

clustered (Figure 4.2A). Approximately 70 min after the release from the arrest, both the control and nocodazole (Noc)-treated cells were mostly budded, indicating a resumption of synchronized growth and confirming that Noc treatment did not affect the establishment of cell polarity and the subsequent growth of the bud. While 47% of the control cells had the kinetochore signals either in the daughter cell or divided between the mother and the daughter, no such cells were found in the Noc-treated sample at 70 min (Figure 4.2B). As

expected, a significant portion of the control cells (21%) showed clustered kinetochores. The average ratio of the daughter/mother size in these cells was 0.6. Based on this information we examined Noc-treated cells with daughter/mother size ratio ≥0.62 for clustering of kinetochores. Strikingly, we found that 39% of all Noc-treated cells had the average daughter/mother size ratio of 0.72, and non-clustered kinetochores in the mother with no signal in the daughter. No Noc-treated cells with the clustered kinetochore signals were found at 70 min except for a small percentage (9%) of cells with aberrant localization of the NE. In these cells, the NE either formed a tight ring surrounding a small cluster of kinetochores and/or formed a bright cluster away from the kinetochore cluster (Figure 4.2A). We hypothesize that in these cells a process of chromatin condensation bypassed the requirement for MTs without hindering the formation of the tri-layered kinetochore structure and resulted in bringing centromeres in close proximity. These results suggest that MTs are involved in clustering of kinetochores prior to mitosis in *C. neoformans*.

Depletion of MTOCs lead to chromosome mis-segregation and aberrant kinetochore localization

MTs nucleate from MTOCs. Hence, disintegration of MTOCs in a cell will have impact on MT stability and may mimic the situation of nocodazole treatment. The effect of MTOC depletion can be examined by depleting a γ-tubulin complex protein using either the conditional knock-out or knock-down approach. In *C. neoformans*, one such method used is a conditional expression of genes by the *GAL7* promoter (Wickes and Edman 1995, Ruff *et al.* 2009). The *GAL7* promoter drives expression of the downstream gene in the presence of galactose as the carbon source and shuts down expression in the presence of glucose. Usage of the *GAL7* promoter thus allows one to study the effects of depletion of a protein just by changing the growth media from galactose to glucose. To investigate the effect of MTOC

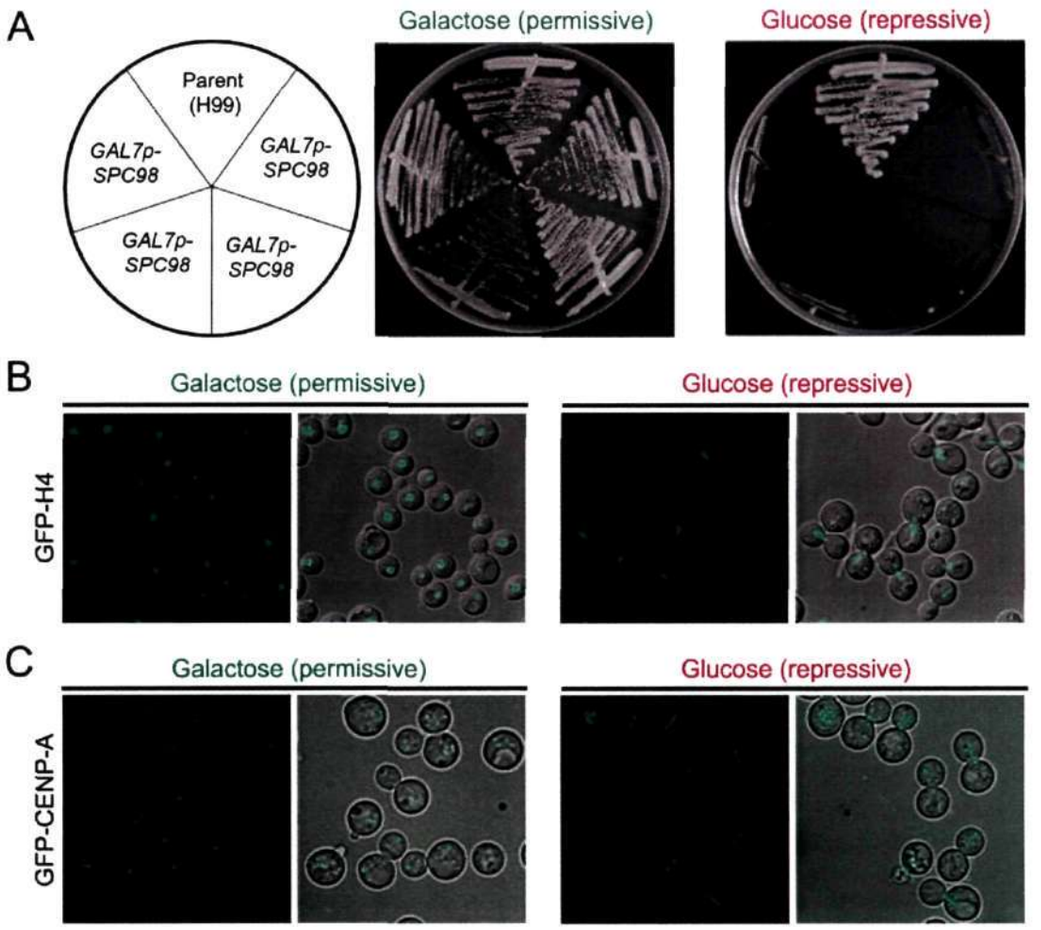

Figure 4.3 Depletion of a MTOC component leads to aberrant kinetochore localization. (A) Spc98, a component of MTOC, was placed under the *GAL7* promoter and the growth of this strain was determined in both permissive (galactose) and repressive (glucose) conditions. The strain grows in galactose containing media but not in glucose containing media hinting that Spc98 may be essential for viability. **(B)** Spc98 conditional mutant was grown in both permissive and repressive media for 12 h. The cells were harvested and studied for the status of chromatin (marked by GFP-H4) localization. The cells depleted of Spc98 showed massive chromosome segregation errors. **(C)** GFP-CENP-A localization revealed aberrant kinetochore localization pattern upon depletion of Spc98.

depletion, we replaced the native promoter of *SPC98*, which codes for a component of the γ-tubulin complex, with the *GAL7* promoter using homologous recombination. The resultant strain carrying *GAL7p-SPC98* did not grow in glucose containing media as expected but grew well in galactose (Figure 4.3A). This result shows that Spc98 is an essential protein in *C. neoformans* like other studied organisms (Lin *et al.* 2015). The conditional mutant cells were grown separately in either galactose or glucose containing media for 12 h and the status of chromatin and the kinetochore clustering was studied. The cells grown in glucose, i.e. the

absence of Spc98, showed mostly large budded cells with massive nuclear segregation defects as opposed to proper nuclear segregation observed in cells grown in galactose (Figure 4.3B). In most cells lacking Spc98, GFP-H4 signals marking chromatin was stretched and fragmented. The localization pattern of the kinetochores, marked by GFP-CENP-A, in the absence of Spc98 revealed a linear array of distinct GFP-CENP-A dots in large-budded cells instead of a single clustered dot seen in the presence of Spc98 (Figure 4.3C). Taken together, these results confirm that MTs play a major role in the kinetochore clustering and nuclear division. The presence of individual unclustered GFP-CENP-A dots in the absence of MTOCs suggests that the kinetochore clustering is affected in the absence of MT.

MTOCs localize close to the kinetochore

The kinetochores in *S. pombe* and *S. cerevisiae* are clustered and localized close to the SPB, which is embedded in the nuclear membrane (McIntosh and O'Toole 1999). The direct interaction of kinetochores with SPBs helps in holding the clustered kinetochores close to the NE. A previous report in *C. neoformans* suggested that SPBs are not embedded in the NE but are present in the cytoplasm, close to the outer nuclear membrane (Yamaguchi *et al.* 2009). To understand the association of MTOCs/SPBs with the kinetochores in *C. neoformans*, we localized Spc98-GFP, an MTOC marker, and mCherry-CENP-A, the kinetochore marker, in the same strain. In unbudded cells, MTOC puncta seem to be localized in the region excluded from the kinetochore localization area (Figure 4.4A). Upon detailed examination, we found that some of the Spc98 puncta localized very close to the CENP-A dots in interphase cells indicating that the kinetochores and MTOCs might be present in close proximity (Figure 4.4B). However, lack of colocalization between the two suggests that they probably do not have physical interaction. As the cell cycle progressed, the Spc98-GFP signals clustered and localized close to clustered kinetochores and moved to the daughter cell. Following this, both

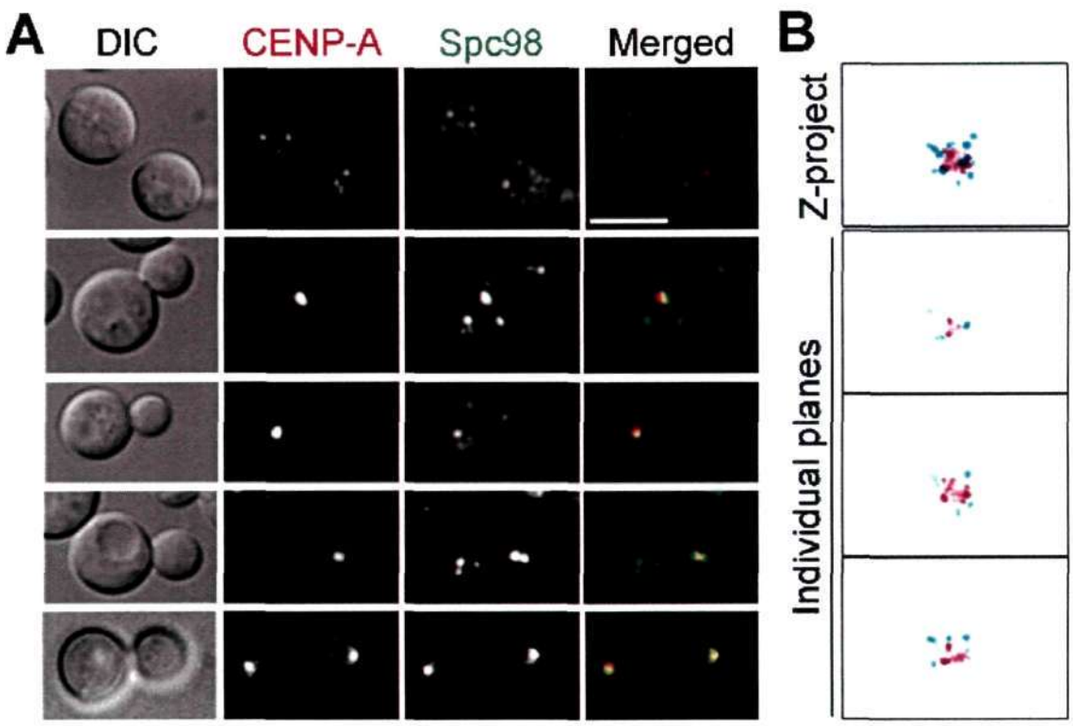

Figure 4.4 Kinetochores localize close to MTOCs in *C. neoformans*. **(A)** Cell cycle stages showing localization pattern of the kinetochore (CENP-A) and MTOC (Spc98) in *C. neoformans*. **(B)** The kinetochore (false coloured as purple) and MTOCs (false coloured as cyan), during interphase, show partial co-localization when visualized as the Z-projected image. However, they do not show any co-localization when observed as single plane images. While signals of Spc98-GFP are occasionally in close proximity to the kinetochore, often Spc98 signals are distinct indicating MTOCs presence throughout the cytoplasm. Bar, 5 µm.

MTOC and the kinetochore clusters segregated into two halves during mitosis, one of which then returned to the mother cell while the other is retained in the daughter cell. The concomitant clustering of MTOCs and kinetochores, along with MT depolymerisation suggests the existence of a possible indirect interaction between the kinetochore and MT/MTOCs in pre-mitotic cells. However, a direct interaction between these complexes during interphase is least expected due to the presence of the NE as a barrier. Thus, we hypothesize that the connection between MTOCs/MT and the kinetochores probably involves an active component of the NE.

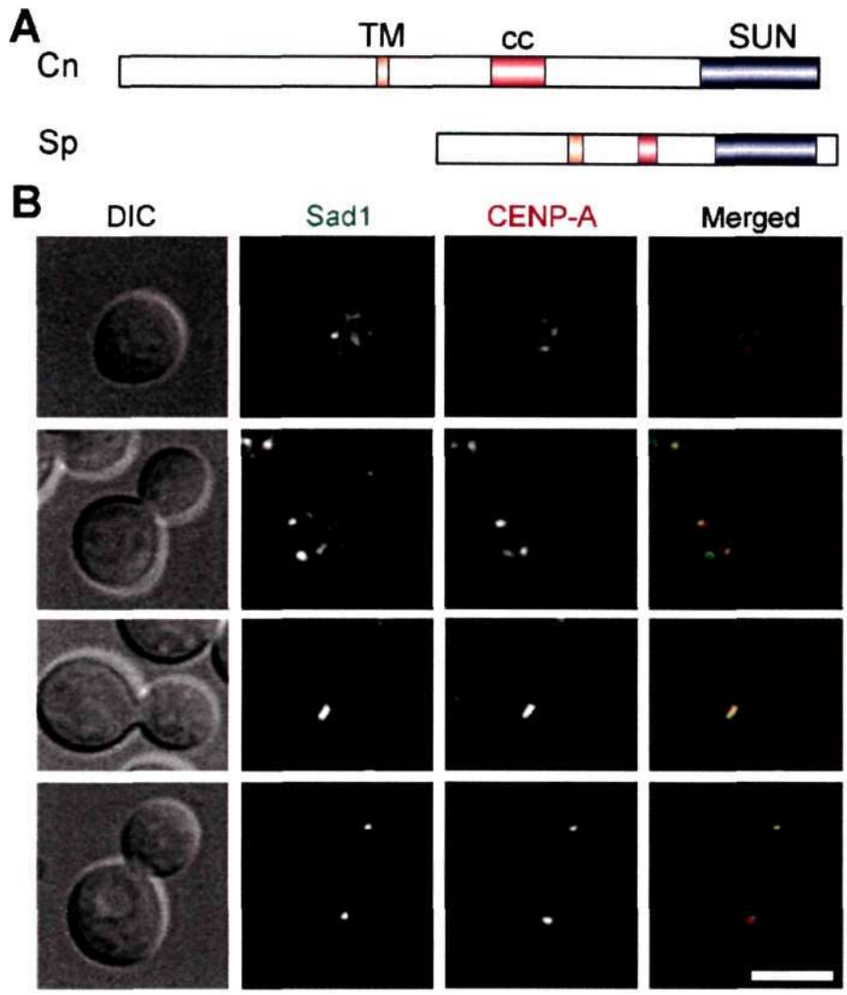

Figure 4.5 Sad1 localizes close to the kinetochore throughout the cell cycle in *C. neoformans*. **(A)** The domain architecture of *C. neoformans* Sad1 (CnSad1) and its comparison with *S. pombe* Sad1 (SpSad1). TM represents transmembrane domain, cc stands for coiled coil region and SUN represents SUN domain. **(B)** Co-localization of CnSad1 with CENP-A, a kinetochore marker, reveals close association between two proteins at all cell cycle stages. Bar, 5 μm.

Sad1, a SUN-domain protein in *C. neoformans*, localizes close to kinetochore

The linker of nucleoplasm and cytoplasm (LINC) complex, provide an ideal candidate for connecting the nuclear element to cytoplasmic counterparts. The LINC complex comprises of the SUN domain proteins localized at the inner nuclear membrane and the KASH domain proteins localized at the outer nuclear membrane. These two groups of proteins interact with each other in the nuclear lamina. KASH domain containing proteins interact with cytoskeletal elements, like MTOCs, in the cytoplasm and SUN domain proteins

interact with nuclear components, like lamins and chromatin present in the nucleoplasm (Chang *et al.* 2015, Kim *et al.* 2015). An *in silico* search through the BLAST analysis led to the identification of a well-conserved SUN domain containing protein, Sad1 in *C. neoformans*. However, no KASH domain protein was found in our analysis probably due to lack of an evolutionary conserved sequence motif among this group of proteins. *In silico* domain prediction for Sad1 revealed the presence of a coiled-coil region and a transmembrane domain along with the signature SUN domain, similar to *S. pombe* Sad1 (SpSad1) protein (Figure 4.5A). We tagged Sad1 with GFP and studied its relative localization with the kinetochore marker, mCherry-CENP-A, which revealed a close association between the two proteins in *C. neoformans* strain H99 (Figure 4.5B). During interphase, both proteins localized as multiple puncta close to each other. Unlike Spc98-GFP, localization of Sad1-GFP dot-like signals were restricted only to the nuclear periphery, close to kinetochore signals, and no cytoplasmic localization was observed. During mitosis, both the kinetochore and Sad1 signals clustered and partially co-localized until the nuclear division was completed. Based on these observations, we envisioned a possible mechanism where kinetochores connect with MT/MTOCs through a possible SUN-KASH link in interphase cells. It was suggested that SpSad1 might interact with outer kinetochore proteins through Csi1 and hence keeps the clustered kinetochore close to the NE in *S. pombe* (Hou *et al.* 2013, Fernandez-Alvarez *et al.* 2016). It is notable that the kinetochore is not entirely assembled in interphase cells in *C. neoformans* and only the inner kinetochore proteins are present.

Sad1 is required for timely clustering of kinetochores

The SUN domain proteins are essential for viability in most organisms studied including the fission yeast, *S. pombe* and the budding yeast, *S. cerevisiae* (Hagan and

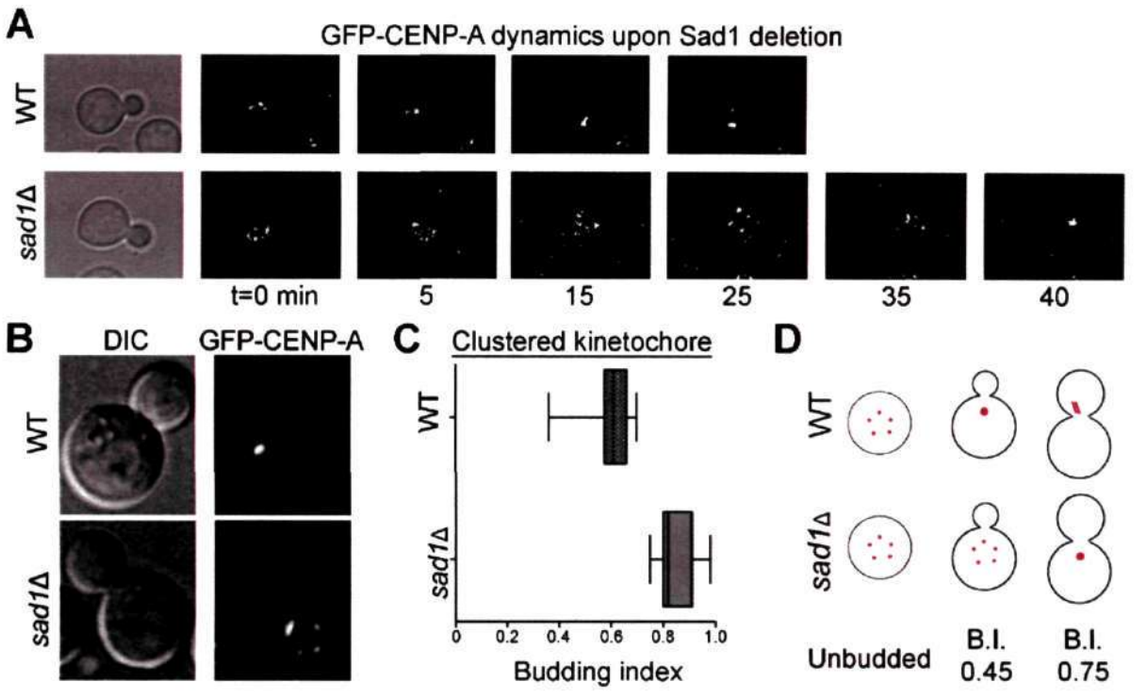

Figure 4.6 Kinetochore clustering is delayed in Sad1 null mutant. **(A)** A time-lapse image showing kinetochore clustering in both wild-type and *sad1*Δ mutant cells; n=5. **(B)** Snapshots displaying the status of kinetochore clustering in the mutant and wild-type cells of similar budding index. **(C)** The kinetochore clustering status was correlated with the bud size of the cells (B.I.) for both the wild-type and the mutant. The budding index was then plotted for cells with the clustered kinetochore signals; n=50. As seen, kinetochores clustered later in the mutant, i.e. when cells attained BI of 0.7. **(D)** A cartoon depicting the kinetochore clustering dynamics in both the wild-type and *sad1*Δ mutant.

Yanagida 1995, Jaspersen *et al.* 2006). The direct role of a SUN domain protein in the kinetochore dynamics is not explored in any organism. *C. neoformans*, with unique cell cycle stage dependent kinetochores clustering, provides an excellent model to study role of SUN proteins in kinetochore dynamics. To study this, we generated a null mutant for Sad1 to examine its role in the kinetochore clustering. Unlike *S. pombe* and *S. cerevisiae*, the Sad1 deletion mutant is viable in *C. neoformans*. Real-time live-cell imaging of GFP-CENP-A, a kinetochore marker, was performed in both the wild-type and the Sad1 null mutant cells with small bud size (budding index of 0.2). The wild-type cells showed complete kinetochore clustering ≤25 min, whereas the null mutant cells required ≥40 min for the same (Figure 4.6A). Earlier, we showed that CENP-A signals cluster by the time a cell attains the budding index of 0.4. This allowed us to quantify the extent of delay in kinetochore clustering in the

absence of Sad1. We measured the budding index of cells with clustered CENP-A signals in both wild-type and mutant cells. As expected, the wild-type cells with clustered kinetochore were observed with a minimum budding index of 0.4; the mutant cells on the other hand had clustered kinetochores with a budding index of ≥0.7 (Figure 4.6B and C). These results suggest that Sad1 plays an important role in timely clustering of kinetochores in *C. neoformans*. Interestingly, the kinetochore localization at the nuclear periphery in pre-mitotic cells was not altered in the mutant indicating that Sad1 may be dispensable for the kinetochore peripheral localization.

Sad1 is required for proper spindle localization to ensure equal nuclear division during mitosis

Defects in kinetochore clustering lead to abnormal chromosome segregation in most yeast species (Hou *et al.* 2012, Richmond *et al.* 2013). Sad1 null mutant cells suffer a significant delay in the kinetochore clustering in *C. neoformans*. To assess the effect of delay in kinetochore clustering on chromosome segregation, *sad1* mutant strain was generated where the nucleus is marked with GFP-H4. Analysis of GFP-H4 signals in the mutant revealed a high rate (~50%) of chromosome mis-segregation compared to the wild type cells (Figure 4.7A). The most common abnormal phenotype observed was the presence of multiple nuclear masses in a single cell. This result suggests that the nuclear dynamics is altered in the mutant cells leading to defective nuclear division. We previously demonstrated that the nuclear dynamics during mitosis in *C. neoformans* is dependent on the number and integrity of cMTs (Figure 3.8 and 4.2). In addition, the mutant cells exhibited a higher level of sensitivity to the microtubule-depolymerizing drug, benomyl, compared to the wild-type (Figure 4.7B) suggesting the role of Sad1 in a kinetochore-MT mediated process of chromosome segregation. Thus, we next studied the MT dynamics in the mutant.

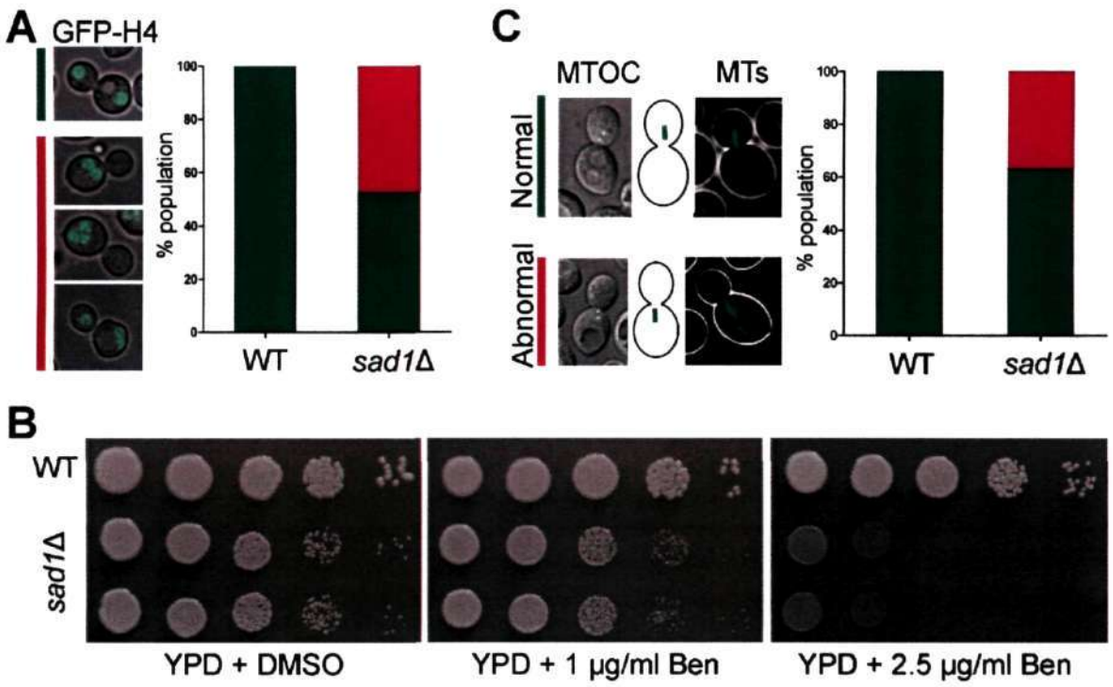

Figure 4.7 Sad1 null shows spindle mislocalization. **(A)** A graph showing the status of chromosome segregation (marked by GFP-H4) in the wild-type and *sad1*Δ mutant. Most of the phenotype observed in the mutant shows presence of two or more nuclei in the mother cell. **(B)** Plate images showing the sensitivity of *sad1*Δ mutant to a microtubule depolymerizing drug, benomyl (Ben), as compared to the wild-type cells. The mutant grows slower even in control (only DMSO) plate since a percent of cells lose viability in the mutant. **(C)** A graph depicting localization pattern of the mitotic spindle in *sad1*Δ mutant compared to the wild-type cells.

Examination of the mitotic spindle in the sad1 null mutant revealed a significant number of mutant cells (approx. 40%) with the mitotic spindle positioned in the mother cell (Figure 4.7C). The wild-type cells always showed the mitotic spindle formation in the daughter cell as expected. Also, the population of cells having the nuclear defect (~50%) and mitotic spindle defect is similar (~40%) (Figure 4.7A and C). These results also explain the slow growth of the *sad1* mutant in the control media, YPD with DMSO (Figure 4.7B). Based on these results, we concluded that abnormal chromosome segregation in *sad1* mutant arises due to improper nuclear migration to the daughter cell. A similar phenotype was observed in the *U. maydis* mutant of dynein, a motor protein, and the defect was attributed to a lack of force on chromatin that is exerted by the MTs through dynein (Fink *et al.* 2006). SUN-KASH proteins also interact with MTs through various motors including dynein (Luxton and Starr

2014). Thus, it is possible that, in the sad1 null mutant, chromatin fails to experience enough force required for its movement and cannot reach to the daughter cell which is the site of nuclear division. This would then lead to division of the nucleus in the mother cell giving rise to two nuclei in the same cell.

5. DISCUSSION

Centromeres are rapidly evolving in the *Cryptococcus* species complex

Centromeres are the rapidly changing loci in the genome despite having a conserved function, a phenomenon termed as the "centromere paradox" (Henikoff *et al.* 2001). A number of studies indicated that centromeres are evolving rapidly even among very closely related species. This process of rapid evolution of centromeres is well studied in ascomycetous fungal species (Bensasson *et al.* 2008, Padmanabhan *et al.* 2008, Rhind *et al.* 2011, Chatterjee *et al.* 2016). Multiple studies described the evolution of centromeric regions among closely related species of plants and animals as well (Giannuzzi *et al.* 2012, Melters *et al.* 2013, Zhang *et al.* 2014, Gao *et al.* 2015, Schneider *et al.* 2016). In this report, we identified centromeres in three pathogenic and one non-pathogenic species of the *Cryptococcus* species complex, the first experimental identification of centromeres in basidiomycetes.

We find that centromeres in all four species are rich with retrotransposons and they are large regional in nature. However, the retroelements present in the centromere show divergence between pathogenic versus non-pathogenic species. The three pathogenic species, *C. neoformans*, *C. deneoformans* and *C. deuterogattii* harbor retroelements Tcn1-6, whereas the non-pathogenic species, *C. amylolentus*, contains elements Tcen1-6 (Figure 5.1). All these elements are LTR-retrotransposons, but they share only 20-30% of identity between two groups, one each present in pathogenic and non-pathogenic species. Moreover, the conserved identity blocks are restricted to the conserved domains (like RT, RH and INT) found in these elements. These elements account for most of the centromeric DNA in *Cryptococcus* species. Thus, divergence in retroelements sequences suggests that centromere sequences in pathogenic *Cryptococcus* species have diverged from their non-pathogenic counterpart. The three pathogenic *Cryptococcus* species also provided an opportunity to test the role of RNAi in centromere evolution. We find that centromeres in the RNAi-deficient

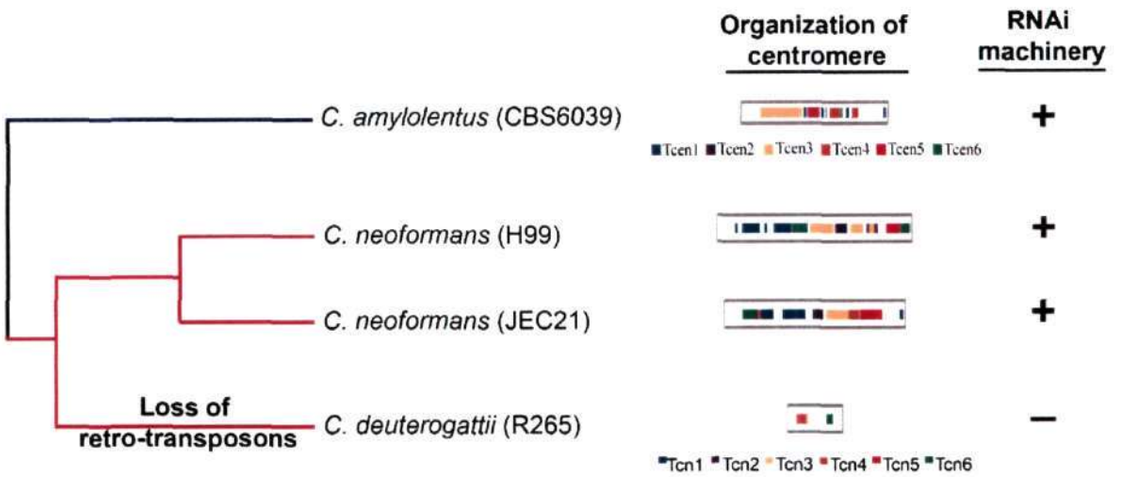

Figure 5.1 Schematic showing the length and composition of centromeres in various *Cryptococcus* species. Status of functional RNAi machinery of each strain is shown. The species marked with red lines are pathogenic while the one marked with blue is non-pathogenic in nature.

species are shorter as compared to the RNAi proficient species. Analysis of the centromere DNA sequence revealed that the RNAi-deficient species R265 possesses lesser and truncated retrotransposons than the RNAi-proficient species, H99 and JEC21 (Discussed below in detail). Taken together, our results reveal that centromeres evolve rapidly among closely related species in the fungal phylum of Basidiomycota.

RNAi-mediated evolution of centromeres in pathogenic *Cryptococcus* species

Transposons play a major role in shaping the evolution of genomes, including the centromere, in multiple ways (Fedoroff 2012, Biscotti *et al.* 2015, Chuong *et al.* 2017). It was proposed that the centromeric repeats present in fission yeast, maize and alpha-satellite repeats in human centromeres evolved from transposable elements (Dawe 2003, Wong and Choo 2004). Transposons also have been shown to play an active role in centromere evolution among closely related species in plants (Gao *et al.* 2015). Based on a study in the *Schizosaccharomyces* group, it was proposed that loss of transposons in *S. pombe* centromeres occurred due to recombination between LTRs of retrotransposons in the *S.*

japonicus genome (Rhind *et al.* 2011). The loss of retrotransposons was also correlated with a shift in transposon regulation from RNAi to Cbp1 (homolog of CENP-B). In this study, we show structural changes in centromeres mediated by retrotransposons. The centromeres in RNAi-proficient species, H99 and JEC21, harbor full-length retrotransposable elements, whereas RNAi-deficient R265 has centromeres that contain only footprints of the same. While these elements are present mostly in centromeres in both H99 and JEC21, they are spread throughout the genome in R265. We propose that the truncation of retrotransposons could have occurred due to recombination among retroelements rendering them inactive. One example of illegitimate recombination mediated retrotransposon truncation is reported in Angiosperms where it causes genome size reduction (Devos *et al.* 2002, Vitte and Panaud 2005).

The key proteins essential for a functional RNAi machinery were lost in R265 (Feretzaki *et al.* 2016), indicating that transposon regulation observed in RNAi-proficient species, H99 or JEC21, must have been lost in this species. Further, we find that centromere DNA is not methylated in R265 as the only DNA methylase coding gene, *DNMT5*, is found to be truncated in this species. It is important to note that DNA methylation is known to suppress recombination in some organisms (Maloisel and Rossignol 1998, Mirouze *et al.* 2012, Yelina *et al.* 2015). Based on these observations, we propose that loss of RNAi in these species might have led to amplification of retroelements which in turn would have integrated into the genome including the centromeres. Consequently, the presence of retroelements in close vicinity to each other would have enhanced the rate of recombination between these elements (Figure 5.2). Recombination would cause shortening of these regions and any illegitimate recombination event might render retrotransposons inactive. The absence of RNAi and DNA methylation can contribute to enhancing the rate of recombination between these elements (Maloisel and Rossignol 1998, Ellermeier *et al.* 2010, Mirouze *et al.* 2012,

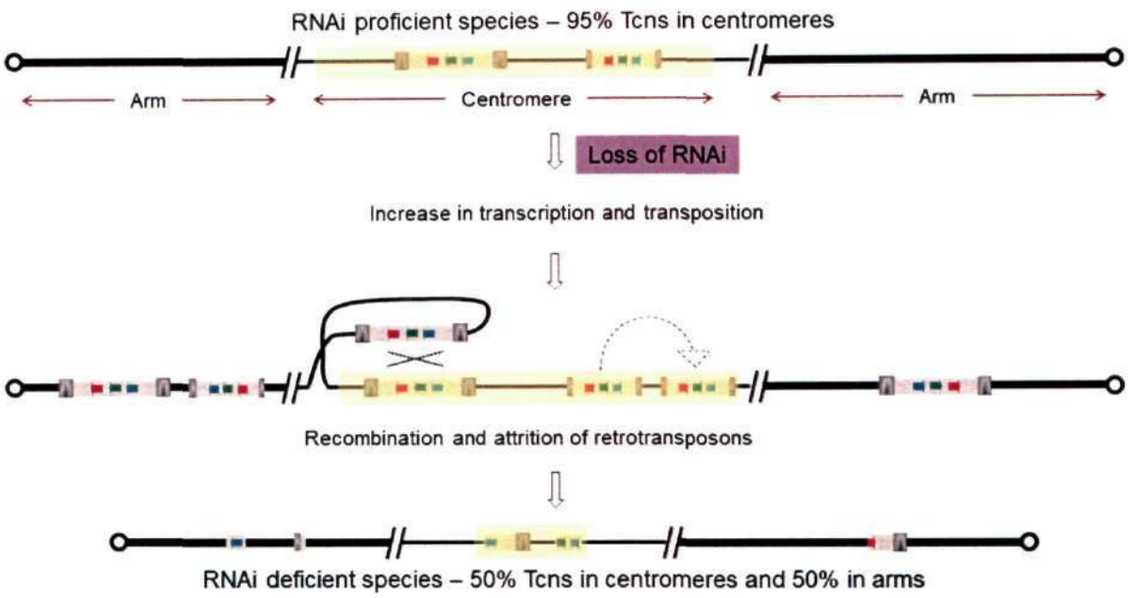

Figure 5.2 A model for centromere evolution in the *Cryptococcus* species complex. A possible sequence of events that might have occurred due to loss of RNAi machinery and/or DNA methylation in an RNAi-proficient strain (H99 or JEC21) that led to a genome with truncated retrotransposons that are unable to transpose in an RNAi-deficient strain (R265).

Yelina *et al.* 2015). Hence, we hypothesize that retrotransposon-rich centromeres in *Cryptococcus* species are prone to undergo expansion (transposition) and contraction (recombination) in the absence of a regulatory factor like RNAi (Figure 5.2). Both these events might have occurred in succession leading to alterations in the centromere length. Our experimental evolution with cells lacking key RNAi proteins in an otherwise RNAi-proficient species indicated that centromeres are indeed prone to undergo both increase as well as decrease in length upon loss of RNAi. It is notable that both transposition and recombination can be damaging to the genome if they associate with loss of essential genes or a chromosome fragment. Thus, only those cells with no essential region lost will survive. Since the partial loss of a centromere may not affect its function, the probability of such events being tolerated at the centromere will be higher. Illegitimate recombination may also cause truncation of retroelements accumulated in these regions. Thus, cells with a stabilized genome will probably have shorter centromeres with truncated retroelements, similar to R265, while the intermediate population during evolution might have possessed longer

centromeres. Overall, our study provides strong evidence towards the role of RNAi in maintaining the structure of centromeres.

Kinetochores in *C. neoformans* assemble in an ordered manner

The kinetochore assembly is a dynamic process that is required for timely execution of high fidelity chromosome segregation during mitosis. The kinetochore structure and its protein complexes are largely conserved from yeasts to humans but the process of its assembly has significantly diverged (Roy *et al.* 2012). The budding yeasts *S. cerevisiae* and *C. albicans* have a completely assembled kinetochore throughout the cell cycle (Meluh *et al.* 1998, Goshima and Yanagida 2000, Sanyal and Carbon 2002) while the fission yeast *S. pombe* recruits a part of the outer kinetochore only during mitosis (Liu *et al.* 2005, Sanchez-Perez *et al.* 2005). Metazoans follow a different pattern where the inner kinetochore, containing CENP-A, CENP-B, and CENP–C, is present throughout the cell cycle but the entire outer kinetochore only assemble during mitosis (Foltz *et al.* 2006, Liu *et al.* 2006, Przewloka *et al.* 2007). In *C. neoformans*, the inner kinetochore proteins (CENP-A and CENP-C) are constitutive and KMN network proteins localize only when clustering of centromeres begins (Figure 5.3). It is possible that bringing inner kinetochores of various chromosomes in close proximity is necessary for the outer kinetochore to assemble. The Dam1 complex, marked by Dad1 and Dad2, only assembles during mitosis and is probably concomitant with the initial disassembly of NPCs. In metazoans, the outer kinetochore assembles only during mitosis when the NE breaks down and chromosome congression occurs. In *C. neoformans*, though the NE remains largely, intact except for a transient opening near the SPBs, disassembly of the NPCs commences with the onset of mitosis. This disassembly of NPCs can facilitate entry of the outer kinetochore proteins into the nucleus, their recruitment on the kinetochore, and finally the interaction between the fully assembled

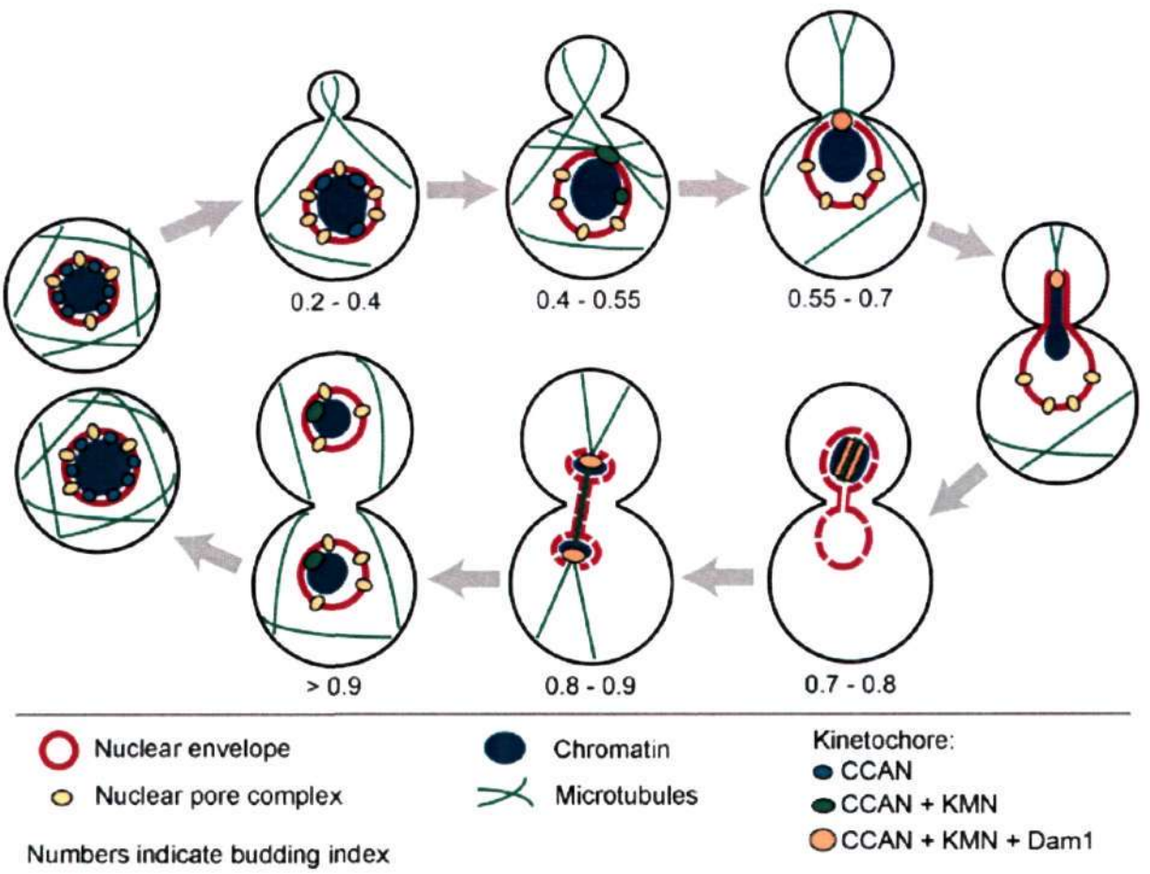

Figure 5.3 Key events during mitotic cell cycle in *C. neoformans*. A model showing clustering of centromeres, a gradual change in kinetochore architecture, and the nuclear envelope dynamics during the progression of the cell cycle in *C. neoformans*. The budding index at each stage was calculated by measuring relative bud sizes of at least 100 cells.

kinetochore and the newly formed mitotic spindle in a process that is strikingly similar to metazoans but not yet shown in any other yeast. Considering all our data, we propose that clustering of centromeres, disassembly of NPCs, and ordered assembly of kinetochores are highly coordinated events in *C. neoformans*.

C. neoformans undergoes semi-open mitosis

Two extreme variations in NE dynamics represent closed and open mitosis in ascomycetous budding yeasts and metazoans, respectively. In organisms where the NE only partially breaks down, classification of mitosis as open or closed is debatable. Our studies in *C. neoformans* demonstrate a breakdown of the NE near the SPBs during mitosis when the

nuclear spindle begins to appear (Figure 5.3). Moreover, localization of GFP-Nup107 suggests a complete disassembly of NPCs. Nup107 localized to the cytoplasm after disassembling from NPCs and the after some time, localizes to chromatin. This localization pattern of Nup107 is similar to *U. maydis,* where this complex localizes to chromatin before returning to the NE (Theisen *et al.* 2008). In mammals, NPCs disassemble and the Nup107-160 complex is almost entirely localized to kinetochores in mitosis (Belgareh *et al.* 2001, Loiodice *et al.* 2004). However, our study does not show such localization in *C. neoformans* indicating that it may be different from mammalian cells.

Though the NE remains intact, based on Ndc1 localization, it does undergo structural deformations. Complete breakdown of NPCs and partial disassembly of the NE have been reported in, *U. maydis,* and were classified as an open mitosis (Straube *et al.* 2005). Live cell imaging study in *C. neoformans* reveals stretching of the NE with a leading edge tipped by SPBs/clustered centromeres from the mother to the daughter cell. Therefore, it is possible that the NE breakdown in *C. neoformans* is a consequence of the stretching of the NE by SPBs, similar to the events described in *U. maydis*. Our data and previous studies suggest that partial opening of the NE during mitosis is common among all basidiomycetes. Recently semi-open mitosis was reported to occur in the fission yeast *S. japonicus* (Aoki *et al.* 2011, Yam *et al.* 2011), illustrating that various forms of NE breakdown may have evolved independently in different groups of fungi. The NE breakdown in *C. neoformans* may be more similar to metazoans in that it occurs early during mitosis, is accompanied by a complete disassembly of NPCs, and correlates with an ordered assembly of the kinetochore.

Number of cytoplasmic microtubules defines the site of nuclear division

In this study, we describe a model that accurately simulates the events of mitosis in distantly related budding yeasts belonging to the phyla Ascomycota and Basidiomycota. We

also sought to understand the basis behind the differences in mitotic events observed in these two phyla. A universal model was developed for the budding mode of division following which mitotic events were simulated and modeled both for ascomycetes and basidiomycetes by obtaining parameters either from literature or through experimental measurements. When compared, we observed that variations in the MT organization, orientation and dynamics account for most of the variations in mitotic events observed between these two classes of yeasts. The cytoskeletal elements, primarily MTs and their accessory network of proteins, have been shown to influence nuclear migration (Hwang *et al.* 2003, Straube *et al.* 2003, Martin *et al.* 2004, Fink *et al.* 2006, Gladfelter and Berman 2009, Markus *et al.* 2012, Kozubowski *et al.* 2013). Model simulations also predicted that at least 8 cMTs are required to provide the necessary force to migrate the entire nucleus to the daughter cell in basidiomycetes. This was in agreement with our experimental observations that show each *C. neoformans* cell nucleates an average of ~9 cMTs. Thus, a greater number of cMTs in basidiomycetes (~9 cMTs/cell) as compared to ascomycetes (~4 cMTs/cell) provides a larger pulling force on the SPB towards the emerging daughter cell resulting into a deeper penetration of the SPB in basidiomycetes. However, our model also predicts a redundant pathway in which an increased activity (population) of dynein motors present at the cortical region of the daughter cell could also provide sufficient force to pull the nucleus/SPB into the bud.

Although we focused solely on the role of MTs in this study, the model can also be used to address other contributing factors and their roles among these systems. For example, using this model we aim to further analyse the role of motor proteins during mitosis and define their roles more specifically. The model also has certain limitations which include consideration of only mechanical forces, absence of the nuclear envelope dynamics and lack of regulation by the mitotic checkpoint. DNA replication was considered as an instantaneous

process and MT dynamics was taken as constant throughout the cell cycle further adding to the model constraints. Nevertheless, this model lays the foundation for follow-up work which will help make a more refined and comprehensive model. It is important to mention here that the above said limitations/assumptions do not affect the quantitative conclusions presented in this study. The predictive nature and robustness also remain unaltered when model parameters were varied within a permissible window.

Sad1 mediates kinetochore clustering in *C. neoformans*

MTs play an important role in chromosome segregation by forming the spindle during mitosis. MTs are also known to affect clustering of kinetochores in *S. pombe* as well as in *S. cerevisiae* (Wargacki *et al.* 2010, Richmond *et al.* 2013). Perturbation of the kinetochore clustering in both these organisms has been shown to cause chromosome mis-segregation (Wargacki *et al.* 2010, Hou *et al.* 2012, Richmond *et al.* 2013). Our findings suggest that MTs are involved in clustering of kinetochores prior to mitosis in *C. neoformans.* In addition, MTs are not directly involved in the kinetochore clustering in this organism. The role of a SUN-domain protein, Sad1, was probed which revealed that Sad1 is required for the kinetochore clustering. Based on these results, we propose that an interaction between Sad1 and chromatin leads to kinetochore clustering and ensures nuclear dynamics is proper for high fidelity chromosome segregation (Figure 5.4). It is important to note that the nuclear division takes place after the entire nuclear mass is transferred to the daughter cell through a biased, directed dynamics of MTs in *C. neoformans* (Sutradhar *et al.* 2015). In a wild-type cell, MTs transfer their forces to chromatin through the centromere- kinetochore complex via Sad1, a part of the SUN-KASH bridge (Figure 5.4). In the absence of Sad1, the connection between chromatin and MTs is lost, and force is restricted to the NE and not transferred to the chromatin mass. This could give rise to multiple scenarios – i) the NE along with chromatin

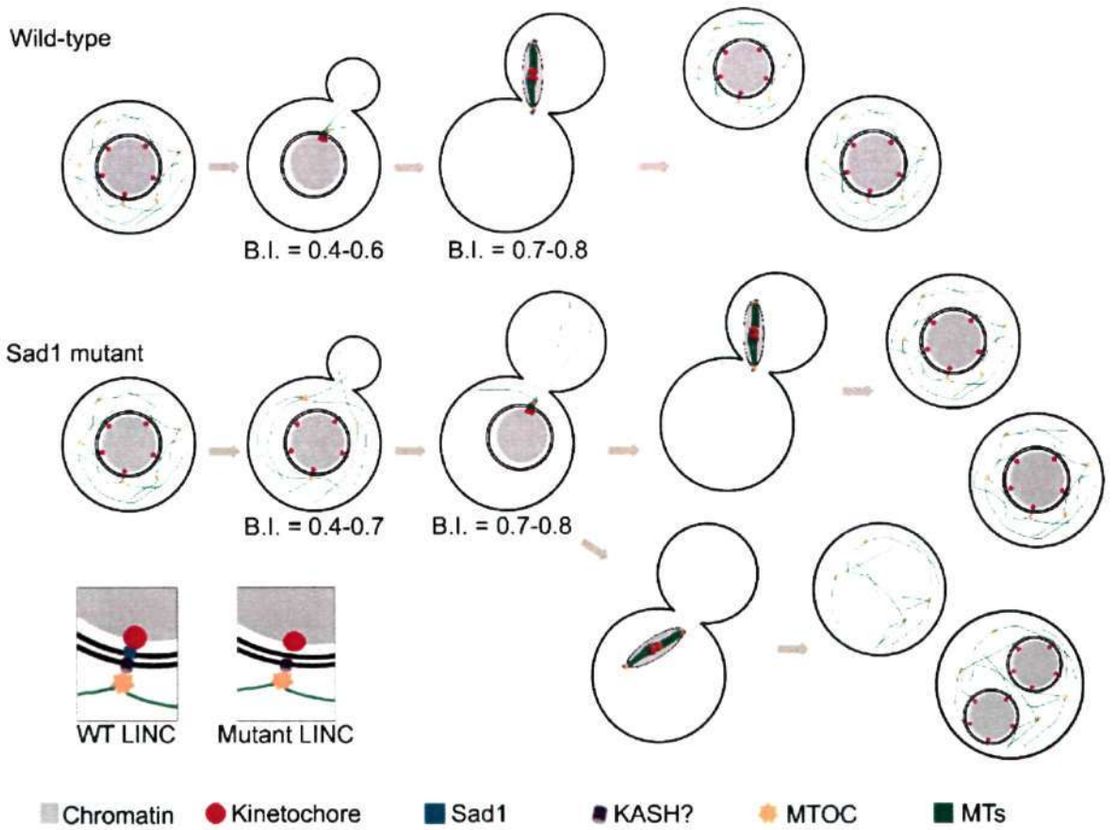

Figure 5.4 A model showing the role of Sad1 protein in the kinetochore clustering in *C. neoformans*. LINC, linker of nucleoskeleton and cytoskeleton; MTs, microtubules, MTOC, microtubule-organizing center.

migrates to the daughter cell, ii) the NE ruptures due to excess force, or iii) the nucleus is unable to move to the daughter cell due to lack of enough force. The experiments in *sad1* mutant revealed that approximately 50% of the mutant population harbours defects in nuclear migration and the spindle localization. These results reflect the occurrence of all the possible scenarios which could arise due to lack of Sad1. Overall, we describe a novel role for a SUN domain protein with respect to its role in the kinetochore dynamics. No KASH protein in this organism could be identified through *in silico* analysis and will require more biochemical studies.

A recent report in *S. pombe* also investigated the direct role of Sad1 in the kinetochore clustering and found that the Sad1- kinetochore interaction is required for the kinetochore cluster to be maintained (Fernandez-Alvarez *et al.* 2016). It was shown that in the absence of

this interaction, cells show defective spindle formation which was rescued when the SPB-kinetochore connection is restored artificially. Unlike *S. pombe*, kinetochores are unclustered in *C. neoformans* in interphase and cluster only during mitosis. However, in the absence of Sad1, kinetochores fail to cluster timely leading to chromosome mis-segregation. Also, in contrast to *S. pombe*, the mitotic spindle formation is not perturbed in *C. neoformans sad1* mutant; though the location of the spindle was altered in a large population in the mutant. Further, SpSad1 was proposed to interact with outer kinetochore complexes earlier (Asakawa *et al.* 2005, Hou *et al.* 2012). In *C. neoformans*, the outer kinetochore proteins are not present onto the kinetochore in interphase indicating that Sad1 may interact with some inner kinetochore proteins. Hence, though the process of kinetochore clustering is affected in both these organisms due to lack of Sad1 protein, the underlying mechanism varies. This may be attributed to fundamental differences in the process of mitotic division in these two organisms.

6. MATERIALS AND METHODS

Strains and primers

All yeast strains and plasmids used in this study are listed in Table 6.1. The oligonucleotide primers used in this study are listed in Table 6.2.

Media, growth conditions and transformation

Various *Cryptococcus* strains were grown in YPD (1% yeast extract, 2% peptone and 2% dextrose) media with shaking at 180 rpm, at 30°C unless specified. *Cryptococcus* cells were transformed using biolistic as described previously (Davidson *et al.* 2000) with certain modifications. Single colony of the strain was inoculated in 5 ml of YPD and grown at 30°C for 15-16 h. Cells were pelleted at 4,000 rpm for 5 min and media was discarded. The pellet was resuspended in 300-500 µl of autoclaved dH_2O and was plated on YPD agar media containing 1M sorbitol (recovery media). The plates were allowed to dry for 15-20 min in the laminar flow hood. Meanwhile, the DNA-gold particle mix was prepared by mixing 10 µl of 0.6 micron gold beads (BioRad, prepared in 50% glycerol as per the directions of manufacturer), 5 µl of DNA (equivalent to 1-3 µg of DNA), 10 µl of 2.5 M $CaCl_2$ and 2 µl of 1 M Spermidine free base (Sigma-Aldrich) in a 1.5 ml microfuge tube. The mixture was vortexed for 1 min and then allowed to stand at RT for 10 min. The gold beads were pelleted by centrifuging at 13,000 rpm for 10 s. The supernatant fraction was discarded and beads were washed with 500 µl of 100% ethanol by vortexing for 10 s. The beads were again pelleted down, supernatant was discarded. The beads were then resuspended in 10 µl of 100 % ethanol and spotted onto ethanol sterilized macrocarrier membrane. The spot was allowed to dry and used for biolistic transformation. The YPD sorbitol plate with cells was placed open at target distance of 6 cm with 1300 psi rupture disks. The DNA macrocarrier membrane was placed in biolistic delivery system and the setup was operated as per the manufacturer's instructions (BioRad). After bombarding with DNA, the plates were closed,

removed from the chamber and kept at 30°C for 5-6 h. The cells were then scrapped from the recovery plate and resuspended in 1 ml of dH_2O. The resuspension was plated onto the YPD agar media containing either 200 µg/ml of G-418 (Sigma-Aldrich), or 100 µg/ml nourseothricin (Werner BioAgents), or 200 µg/ml of hygromycin (Invitrogen). Transformants were obtained after 4-5 days which were then patched onto secondary plates with respective selection drugs. Only those colonies that grew on secondary selection plate were used to further experiments.

Construction of strains

CENP-A tagging with mCherry in H99, JEC21 and R265:

To tag CENP-A with mCherry at the N-terminus in *C. neoformans* (H99), *CENP-A* ORF followed by 477 bp of the 3' UTR was PCR amplified using primers VYP147 and VYP148. The PCR product was cloned into pLKB49 and pLKB55 using restriction enzymes, NheI and PacI to obtain pLKB70 and pLKB71, respectively. pLKB49 contains the neomycin resistance gene and pLKB55 harbours a gene that encodes for the hygromycin resistance protein. These plasmids are used to express mCherry-tagged chimeras from a constitutive *GPD1* promoter (Kozubowski *et al.* 2011). Subsequently, the *GPD1* promoter in pLKB70 and pLKB71 was replaced with the native *CENP-A* promoter to generate pLKB74 and pLKB75, respectively. For this purpose, *CENP-A* promoter region, a fragment of 530 bp upstream of *CENP-A* ORF, was amplified using primers, VYP149 and VYP150, and cloned into XhoI and FseI sites of pLKB70 and pLKB71. These constructs were utilized to generate strains CNVY101, CNVY184, CNVY501 and CNVY701. The strains were confirmed by western blot analysis using anti-mCherry antibody.

CENP-A tagging with mCherry in C. amylolentus:

To tag CENP-A with mCherry at N-terminus in *C. amylolentus*, the promoter region of the *CENP-A* ORF (784 bp), the mCherry gene sequence (708 bp) and the *CENP-A* ORF along with its 3' UTR as the terminator (1216 bp) were fused using the overlap PCR method (primers VYP901 - VYP906). The promoter, ORF, and terminator regions were amplified from the genomic DNA of *C. amylolentus* strain CBS6039 whereas the mCherry sequence was amplified from the pLK25 plasmid (Kozubowski and Heitman 2010). The full length PCR product was finally amplified using primers (VYP901 and VYP 906) containing flanking XbaI and XhoI restriction sites. The amplified product was cloned into pLK25 using XbaI and XhoI to generate pVY50. *C. amylolentus* strain, CBS6039, was then transformed with the plasmid DNA using biolistic transformation to generate strain CNVY902.

mCherry-tagging of CENP-C, Mtw1, Dad2 and H4:

C-terminal tagging with mCherry for CENP-C, Mtw1, Dad2 and H4 was done at the native locus by homologous recombination. The cassette for mCherry tagging was generated using the overlap PCR strategy (Kozubowski and Heitman 2010) as follows. Approximately 1 kb of the desired gene sequence up to the penultimate codon (US) and 1 kb sequence downstream of the stop codon (DS) was amplified from the respective genome. A 3.3 kb long sequence fragment containing mCherry along with neomycin gene (mCh-Neo) was amplified from a plasmid, pLK25 (Kozubowski and Heitman 2010). These three amplified DNA fragments (US, mCh-Neo, and DS) were purified separately and then mixed in an equimolar ratio. The mix was used as a template for the final overlap PCR. The overlap product of approximately 5 kb was used for transformation. The transformants were screened by PCR to confirm the integration of mCherry-encoding sequence at the 3' end of the target gene. This strategy was used to generate CNVY102 (CENP-C-mCherry), CNVY103 (Mtw1-mCherry), CNVY105(Dad2-mCherry) and CNVY109 (H4-mCherry), CNVY502 (CENP-C-

mCherry) and CNVY702 (CENP-C-mCherry) strains. Primers used in these experiments are listed in table 6.2.

GFP-tagging of CENP-A, H4, Dad1, Tubulin and Ndc1 under H3p:

N-terminal GFP fusion proteins expressing constructs (pVY1, pVY2, pVY3, pVY4 and pLKB35) were generated by cloning the corresponding ORF in vector pCN19 (Kozubowski and Heitman 2010). The ORF along with ~300 bp 3' UTR was amplified from the genome of *C. neoformans* strain H99 and cloned into the vector pCN19 using either BamHI alone or BamHI and SpeI. Transformation of the resulting plasmid in *C. neoformans* leads to expression of N-terminally GFP tagged protein under the constitutive histone H3 promoter. pVY1 was transformed to generate CNVY113 (GFP-CENP-A), CNVY115 (CENP-C-mCherry + GFP-CENP-A) and CNVY116 (Mtw1-mCherry + GFP-CENP-A). pVY2 was used to obtain CNVY104 (GFP-Dad1), CNVY117 (Mtw1-mCherry + GFP-Dad1) and CNVY118 (CENP-C-mCherry + GFP-Dad1) strains. pVY3 was used to generate strains CNVY108 (GFP-H4), CNVY114 (mCherry-CENP-A + GFP-Dad1). pVY4 was used to obtain CNVY110 (GFP-Ndc1), CNVY111(mCherry-CENP-A + GFP-Ndc1) and CNVY112(H4-mCherry + GFP-Ndc1). pLKB35 was transformed to get CNVY106 (GFP-Tubulin), CNVY107 (mCherry-CENP-A + GFP-Tubulin), , CNVY109 (H4-mCherry + GFP-Tubulin). The strains were confirmed by western blotting analysis using anti-GFP antibody.

GFP-tagging of CENP-A under native promoter:

To express GFP-CENP-A with its native promoter, *Sac*I-*Apa*I fragment containing from pVY1 was subcloned into pBlueScriptII KS (-) plasmid to generate pVY8. The *CENP-A* promoter (702 bp upstream of *CENP-A* ORF) was then amplified using VYP105 and VYP106 and cloned into *Sac*I-*Nco*I sites of pVY8 to generate pVY22. The plasmid was then transformed to generate CNVY156 and CNVY165.

GAL7-SPC98 strain construction:

The construct to replace the native promoter of *SPC98* with *GAL7* promoter was generated by overlap PCR. A 1 kb region from 5' UTR as upstream sequence or US (primers VYP123-VYP124) and 1 kb region of ORF, including ATG, as downstream sequence or DS (primers VYP127-VYP128) was amplified from H99 genome. The middle fragment, approximately 2 kb, containing hygromycin resistance gene and *GAL7* promoter region (~2 kb) was amplified from the plasmid pSHG7 using VYP125 and VYP126 (M.S. Thesis, Shreyas Sridhar, 2014). Three products were purified and used for overlap PCR using primers VYP129 and VYP130 to give rise to the full length cassette. The cassette was transformed and transformants were selected on YPG (1% yeast extract, 2% peptone and 2% galactose) containing 200 μg/ml of hygromycin to give rise to CNVY152, CNVY161 and CNVY175. The integration of the cassette in the genome was confirmed by PCR.

GFP tagging of Sad1 and Spc98:

Sad1 and Spc98 were tagged at C-terminal with GFP using the constructs generated by the overlap PCR strategy. For this purpose, 1 kb each of the 3' part of gene (without stop codon) and 3' UTR after stop codon was amplified from the H99 genome. A GFP-NAT fragment (approximately 3 kb) was amplified from pCN19 and all three fragments were fused by overlap PCR, generating the cassettes. The resulting cassettes were transformed in H99 using biolistics to genearate CNVY149 (Sad1-GFP), CNVY138 (mCherry-CENP-A + Sad1-GFP), CNVY176 (*GAL7p*-SPC98-GFP) and CNVY177 (*GAL7p*-SPC98-GFP + mCherry-CENP-A). The integrations were confirmed by PCR.

Generation of Sad1 null mutant:

Sad1 deletion cassette was generated by overlap PCR strategy. For this, 1 kb region upstream of ATG and 1 kb region downstream of stop codon were amplified separately using primer sets VYP138-VYP139 and VYP142-VYP137, respectively. Third fragment of 2 kb

containing Neomycin gene was amplified from pLK25 using primers, VYP140 and VYP141. The three parts were purified and fused together using primers, VYP143 and VYP144, to generate the final construct of 3.8 kb. The final construct was transformed to generate CNVY191, CNVY192, CNVY194, CNVY200 and CNVY210. The deletion mutants were confirmed by PCR.

Cryptococcus genomic DNA preparation

Overnight grown 5-10 ml *Cryptococcus* culture was pelleted and the pellet was resuspended in 0.5 ml extraction buffer (50mM Tris-Cl, pH 8.0/ 20mM EDTA, pH 8.0/1% SDS). The cell suspension was transferred to a 2 ml tube with 0.5 ml glass beads (Sigma-Aldrich). The tubes with cell-beads mix were subjected to either 3 rounds of vortexing of 2 min each with 1 min ice incubation in between or 15 min vortexing in cold room (4°C). The tubes were transferred to heating block at 65°C for 10 min followed by another round of vortexing for 2 min. Next, 200 µl 5 M potassium acetate and 150 µl 5 M NaCl were added to the tube, mixed by inverting and incubated on ice for 20 min. The tubes were centrifuged for 20 min at 13,000 rpm at room temperature (RT) and supernatant was transferred to a fresh 1.5 ml tube. Next, 450 µl chloroform was added, mixed by brief vortexing, and centrifuged at 13,000 rpm for 10 min at RT. The upper aqueous layer was transferred to a fresh 1.5 ml tube, 200 µl of 30% PEG8000 (Sigma-Aldrich) was added and mixed by inverting the tube. The tubes were incubated on ice for 10 min and centrifuged at 13,000 rpm for 10 min at RT. The supernatant was discarded, the pellet was resuspended in 50 µl sterile water containing 10 µg/ml RNase (Sigma-Aldrich) and incubated at 37°C for 30 min. After that, 5 µl 3 M sodium acetate (1/10th volume) and 150µl ethanol (3 volumes) were added and mix was incubated at -20°C for 30 min to 2 h. The tubes were centrifuged for 10 min at 13,000 rpm at 4°C to obtain

the DNA pellet. The supernatant was discarded, the pellet was air dried and finally resuspended in 50 µl sterile water.

Alternatively, a short protocol was also developed to isolate genomic DNA. Cells were pelleted and vortexed as described above. After vortexing, 500 µl phenol:chloroform:isoamylalcohol mix (HiMedia) was added into cell-beads mix. The mix was briefly vortexed to mix and centrifuged at 13,000 rpm for 10 min at RT. The upper aqueous layer was transferred to a fresh tube and 1 ml of 100% ethanol was added, mixed and incubated at -20°C for 1 h. The tubes were centrifuged at 13,000 rpm for 10 min at 4°C. The pellet was washed with 0.5 ml 70% ethanol, centrifuged at 13,000 rpm for 5 min at 4°C. The pellet was air dried and finally resuspended in 50 µl of sterile water containing 10 µg/ml RNase.

Western blot analysis

Cryptococcus strains were grown overnight in respective growth conditions as mentioned above and 3 OD_{600} corresponding cells were harvested by centrifugation at 4,000 rpm for 5 min. Cells were washed with 1 ml of dH_2O and resuspended in 400 µl of 15% Trichloroacetic acid (TCA) solution. The cell suspension was frozen in -20 overnight. Next day, the cells were thawed on ice and equal volume of glass beads were added. The cells were vortexed 3 times, 2 min each with 5 min interval. The liquid fraction was transferred to a fresh tube. The cells were pelleted at 13,000 rpm, 4°C for 15 min. The pellet was washed in 80% acetone solution followed by pelleting at 13,000 rpm for 5 min. After two rounds of washing, the pellet was air dried and resuspended in 50 µl of lysis buffer (1%SDS + 0.1N NaOH) with 1X loading dye. The lysates mix was incubated in boiling water bath for 10 min. A part of the lysates (15-20 µl) were electrophoresed on 12% or 15% SDS-PAGE and blotted onto a nitrocellulose membrane in a semi-dry apparatus (Bio-Rad). The blotted membranes were blocked by 5% skim milk containing PBS (pH 7.4) for 30 min at room temperature and

then, were incubated with 1:2000 dilutions in 2.5% skim milk containing PBS of anti-RFP (Chromotek) or anti-GFP (Roche) primary antibodies at 4°C overnight with constant shaking. Next, the membranes were washed thrice with PBST (0.1% Tween-20 in 1X PBS) solution. Anti-rat or anti-mouse HRP conjugated antibodies (Bangalore Genei) were added at a dilution of 1:5000 in 2.5% skim milk PBS solution and incubated for 1-2 h at RT. The membranes were then washed thrice with the PBST solution. Signals were detected using the chemiluminiscence method.

C. neoformans and *C. deuterogattii* PacBio sequencing and assembly update

The *C. neoformans* (H99) *and C. deuterogattii* (R265) genomes were sequenced using PacBio sequencing to improve sequence coverage for centromeric regions. The sequencing and PacBio analysis was performed in collaboration with Blake Billmyre and Sheng Sun in Joseph Heitman's lab, Duke University, USA. PacBio filtered subreads were used for a higher order scaffolding using SSPACE-LongRead v1-1 (Boetzer and Pirovano 2014), requiring 5 linking reads (-l 5) and a 200 base gap between scaffolds (-g 200). The *de novo* assembly of the PacBio reads led to generation of 20 and 27 scaffolds for H99 and R265, respectively. The centromere flanking gene sequences from the available GenBank assembly for H99 (GCA_000149245.3) and R265 (GCA_000149475.3) were searched using the BLAST analysis against the newly assembled PacBio assembly to identify the centromere locations. This analysis led to mapping of 10 centromeres (out of 14) in the newly assembled H99 genome with good read depth and no sequence gaps. These completely assembled 10 centromeres are *CEN1, CEN2, CEN4, CEN6, CEN7, CEN8, CEN9, CEN10, CEN12*, and *CEN13*. One of the four centromeres that remained incomplete even after using PacBio reads was *CEN5* with two sequence gaps. Using a chromosome walking approach followed by Sanger sequencing, both of these sequence gap regions were closed to obtain a complete

sequence coverage of *CEN5* as well. The sequences of these 11 centromere regions in the current GenBank assembly were replaced by the newly assembled sequences as described above. The updated assembly was used for all of the analysis conducted in this study. Similarly, the new PacBio assembly of R265 now covered all the 14 centromeres and was used for the genome analysis. The comparative synteny analysis was performed using "SyMAP".

Chromatin-immunoprecipitation (ChIP)

Desired *Cryptococcus* tagged strain was grown in 100 ml YPD until the exponential phase (OD_{600} = 1) and was cross-linked with 1% formaldehyde at room temperature for 30 min for CENP-A and 40 min for CENP-C tagged strain. The reaction was quenched by adding glycine to a final concentration of 125 mM. The cells were harvested and resuspended in 10 ml of distilled water containing 0.5 ml β-mercaptoethanol and incubated for 1 h in a shaker incubator at 150 rpm at 30°C. Cells were pelleted and resuspended in 10 ml spheroplasting buffer (1 M sorbitol/0.1 M sodium citrate, pH 5.8, and 0.01 M EDTA, pH 8.0) with 40 mg of lysing enzyme from *Trichoderma harzianum* (Sigma-Aldrich) and incubated for 4-5 h at 37°C. Spheroplasts were subsequently washed with ice-cold 1X PBS, Buffer I (0.25% TritonX-100, 10 mM EDTA, 0.5 mM EGTA, 10 mM Na-HEPES, pH 6.5), Buffer II (200 mM NaCl, 1 mM EDTA, 0.5 mM EGTA, 10 mM Na-HEPES) and finally resuspended in 1 ml of extraction buffer (50 mM HEPES, pH 7.5/140 mM NaCl/1 mM EDTA/0.1% Na-deoxycholate/1% Triton-X) containing 10 µl of protease inhibitor cocktail (Sigma-Aldrich). The lysates were sonicated using Bioruptor (Diagenode) for 17-24 cycles of 15 s on and 15 s off bursts at the high level intensity to obtain chromatin fragments of size of 300-500 bp. After centrifuging (13,000 rpm, 10 min, 4°C), chromatin fraction was distributed to obtain total and IP DNA (with or without antibodies) preparations as described below.

Total DNA (I):

Approximately 100 µl of lysate were added to 0.4 ml of elution buffer (1% SDS/0.1M $NaHCO_3$) with 20 µl of 5M NaCl. The reaction was incubated at 65°C overnight to reverse the crosslinking. DNA was isolated using phenol: chloroform extraction followed by ethanol precipitation and resuspended in 25 µl of MilliQ water containing 25 µg/ml RNase (Sigma-Aldrich).

Immunoprecipitated material (IP):

The remaining lysate (900 µl) was distributed into two 1.5-ml tubes (450 µl in each). In one of the tubes, 20 µl of RFP-TRAP beads (ChromoTek) were added and used as IP DNA with antibodies (+). In another tube, 20 µl of control beads were added to serve as a negative control (-). Both tubes were incubated overnight at 4°C on a roller. The IP materials were processed as described previously with some modifications (Dubin *et al.* 2010). The washing step with low salt buffer (0.1% SDS/ 1% Triton X-100/ 2 mM EDTA/ 20 mM Tris, pH 8.0/ 150 mM NaCl) and high salt buffer (0.1% SDS/ 1% Triton X-100/ 2 mM EDTA/ 20 mM Tris, pH 8.0/ 500 mM NaCl) were done twice, while the LiCl buffer (0.25 M LiCl/ 1% NP40/ 1% deoxycholate/ 1 mM EDTA/ 10 mM Tris, pH 8.0) washing was done only once. The beads were pelleted by centrifuging at 5,400 rpm for 2 min. Both the fractions (+ and -) were eluted in 500 µl of elution buffer, decrosslinked overnight and DNA was isolated using phenol: chloroform extraction followed by ethanol precipitation. The precipitated DNA was air dried and dissolved in 25 µl of MilliQ water containing 25 µg/ml RNase (Sigma-Aldrich).

The IP samples (I, + and -) were subjected to PCR amplification using primers from centromeric and non centromeric regions to determine the efficiency of ChIP experiment. Once confirmed, I and + samples were subjected to ChIP-sequencing (For mCherry-CENP-A, CENP-C-mCherry in H99; mCherry-CENP-A in CBS6039, and CENP-C-mCherry in R265) to identify centromere regions across the genome. For JEC21, all three samples (I, +

and -) were subjected to qPCR with centromere-specific primers along with a non-centromeric primer set. The fold enrichment for the same was calculated and plotted using GraphPad Prism. All the primers used for ChIP assays are mentioned in Table 6.2.

ChIP-sequencing, bisulfite sequencing and RNA-sequencing analysis

The ChIP-sequencing for H99 mCherry-CENP-A and CENP-C-mCherry was done at Genotypic Technology Pvt Ltd, Bangalore. Both Input and IP (+) samples from ChIP experiments were quantified using Qubit before processing for Library preparation. Library preparation was performed at Genotypic Technology's Genomics facility following certified protocols from NEXT Flex. ChIP-Seq libraries for sequencing were constructed according to the NEXTflex™ ChIP-Seq library protocol outlined in NEXTflex™ ChIP-Seq Kit - 5143-01. Briefly, DNA was subjected to a series of enzymatic reactions that repair frayed ends, phosphorylate the fragments, add a single nucleotide A overhang and ligate adaptors (NEXTflex ChIP Barcodes-48 kit). The libraries are enriched using PCR (5 cycles), fragments were size selected using a 2 % Low melting agarose gel and purified using MinElute Gel Extraction Kit (QIAGEN). The libraries were further enriched using PCR (13 cycles), post PCR cleanup was performed using Agencourt AMPURE XP beads (Beckman Coulter #A63881). The prepared libraries were quantified using Qubit fluorometer and validated for quality by running an aliquot on High Sensitivity Bioanalyzer Chip (Agilent). The DNA from prepared libraries was denatured and sequenced on the Illumina Genome Anayzer IIx by Sequencing by synthesis method to read 36 bases single end (CENP-C) or 100 bases paired end (CENP-A). Sequencing was performed by synthesis (SBS) technology using four fluorescently labelled nucleotides to sequence each cluster on the flow cell surface in parallel. During each sequencing cycle, a single labelled deoxynucleotide triphosphate (dNTP) was added and clusters were imaged. The fluorescent dye and blocker was cleaved

off and the next complementary base was added to the nucleic acid chain and imaged. Individual bases were called directly from signal intensity measurements during each cycle. Once sequencing was completed, the raw data was extracted from the server using the proprietary Illumina pipeline software to obtain FASTQ files. In total, 6 million single-end 36 nt reads (for CENP-C) or 10 million paired-end 100 nt reads (for CENP-A) were generated. Raw reads were processed using SeqQC (version 2.2). The processed reads were aligned to the target *C. neoformans* genome using Geneious R9 software (http://www.geneious.com) (Kearse *et al.* 2012). About 90% of the aligned reads were obtained per sample. All alignments for a particular read or pair were suppressed if more than 1000 reportable alignments exist for it. The alignments were further sorted into bam files.

For R265 CENP-C-mCherry and *C. amylolentus* mCherry-CENP-A ChIP-seq, the data was generated using a HiSeq 2500 instrument to perform a 48 bp paired-end run at Genomics sequencing facility at University of North Carolina, Chapel Hill, USA. Reads were then aligned to either R265 genome or *C. amylolentus* genome using the short read component of the BWA aligner (Li and Durbin 2009). The resulting alignment was converted, cleaned, and sorted using SAMtools (Li *et al.* 2009) and Picardtools (https://broadinstitute.github.io/picard/). Peaks were identified using the broad peaks setting of MACS2 (Zhang *et al.* 2008).

Bisulfite data of *C. neoformans*, acquired from a previously published study (PRJNA201680) (Huff and Zilberman 2014), was aligned to the H99 genome using Bismark v0.16.3 (Krueger and Andrews 2011) in order to determine the proportion of methylation present at sites across the genome. All the chromosome-wise read distribution and read depth graphs were generated using Integrative Genomics Viewer (IGV) (Robinson *et al.* 2011, Thorvaldsdottir *et al.* 2013).

The RNA-seq reads obtained for *C. amylolentus* (from Joseph Heitman's lab), *Ustilago maydis* (Kellner *et al.* 2014) and *Ustilago bromivora* (Rabe *et al.* 2016) were aligned to respective genomes by Geneious R9 software (http://www.geneious.com) (Kearse *et al.* 2012). The centromere regions with 10-30 kb flanking on each side were probed for the presence/absence of polyA RNA reads.

Methylation-specific PCR assay

Genomic DNA was isolated from overnight grown H99 and R265 using the glass beads method described earlier. The DNA was digested separately with CpG methylation-sensitive or insensitive enzymes overnight with a no enzyme control reaction. The digested DNA was diluted 1:40 and used for PCR amplification. For PCR, two pairs of primers were designed for each H99 and R265 - one pair amplifying centromere DNA (VYP75-VYP76 for H99 and VYP741-VYP742 for R265) and another one for non-centromeric (non-*CEN*) region (VYP79-VYP80 for H99 and VYP743-VYP744 for R265). The PCR products obtained were visualized by gel electrophoresis using 0.8% agarose gel.

Identification of intergenic regions and transposon mapping

The genomes of *C. neoformans* (H99), *C. deneoformans* (JEC21), and *C. deuterogattii* (R265) were scanned using the genome browser feature available in the FungiDB database (http://fungidb.org/fungidb/). The largest ORF-free regions with CENP-A or CENP-C binding on each chromosome were identified. For *Cryptococcus* species, the DNA sequence of each of the retrotransposons (Tcn1- Tcn6) has been previously reported (Goodwin and Poulter 2001). The nucleotide sequences of these Tcn elements were used as query sequences in a BLASTn analysis against *C. neoformans*, *C. deneoformans* and *C. deuterogattii* genomes at fungiDB database (http://fungidb.org/fungidb/) to identify the

transposable elements present in the genome. The BLAST hits against each of the transposons in all chromosomes were obtained and mapped on each of the identified ORF-free regions. Gene synteny analysis across the centromere regions among the three species was carried out using the synteny tool available in fungiDB (http://fungidb.org/fungidb/). Whole genome synteny analysis was carried out using SyMAP v4.2 (http://www.agcol.arizona.edu/software/symap/index.html).

For *C. amylolentus*, we scanned the genome of CBS6039 using the Geneious R9 software (http://www.geneious.com) (Kearse *et al.* 2012) to identify the intergenic regions. The largest intergenic (ORF-free) regions were identified on each chromosome. Some of the predicted ORFs were not considered authentic ORFs because they were either transposon-like or dubious in nature. The ORFs that were smaller than 200 amino acids were also not considered for this analysis. The LTR-retrotransposons in *C. amylolentus* centromeric regions were identified using the LTR-finder program (http://tlife.fudan.edu.cn/ltr_finder/, (Xu and Wang 2007)). Six LTR elements were identified in different centromeres. The sequences of these LTR elements were retrieved from the genome and subjected to sequence analysis for motif/domain analysis using CD-search (http://www.ncbi.nlm.nih.gov/Structure/cdd/wrpsb.cgi). Next, BLASTn analysis was performed to determine occurrence of full length/traces of these elements in the genome including centromeres. BLAST results were mapped onto the genome and we found that these elements clustered exclusively at the centromeres and hence these six elements were named Tcen1 through Tcen6.

Experimental evolution

Experimental evolution was performed using wild-type (H99) and RNAi mutant derivatives (*rdp1*Δ and *ago1*Δ mutants). The strains were inoculated in 5 ml of YPD broth

from a single colony and grown for 20-24 h at 30°C with shaking at 180 rpm. The next day, OD_{600} of the overnight culture was measured, and the required amount of cells were transferred into 5 ml of fresh YPD to achieve the initial OD_{600} of 0.1. The culture was then further grown for 20-24 h, following which OD_{600} was again measured. The number of generations was calculated for each of the strains from their initial (0.1) and final OD. On the next day, the overnight culture was again sub-cultured in fresh media starting with an initial OD_{600} of 0.1. Sub-culturing was continued on a daily basis until 1000 generations were completed for each strain. DMSO stocks of each of the passaged cultures were made at regular intervals of 2 weeks, i.e. every 80-90 generations

Pulsed-field gel electrophoresis and chromoblot analysis

For experimentally evolved strains, single colonies were streaked out from the starting culture, and 1000th generation passaged strains of wild type, *ago1*Δ, and *rdp1*Δ mutants. Plugs were prepared from single colonies as previously described (Findley *et al.* 2012), and two running conditions with different switching times were applied to separate large (200 – 400 s) and small (120 – 280 s) chromosomes, respectively. The electrophoresis was performed using 1% agarose gel in 0.5X TBE at 14°C with 120° fixed angle for 110 hours.

For chromoblot analysis, plugs prepared from single colonies were first digested overnight with restriction enzyme NotI-HF (NEB) and then run with switching time 7 – 60 s using a CHEF apparatus. The enzyme was chosen such that the entire centromere region is released as a single fragment along with flanking sequences that can be used as a probe. The DNA was then transferred to a membrane, and hybridized with probes targeting chromosomal regions flanking the centromeres, as previously described (Findley *et al.* 2012).

Centromere prediction in *Ustilago* species

A previous study in *U. maydis* has predicted its centromeres based on the presence of a transposon (HobS)-rich sequence as well as plasmid stability assays (Kamper *et al.* 2006). We performed RNA-seq analysis for *U. maydis* using the transcriptome data available from a previous study (Kellner *et al.* 2014). For RNA-seq analysis, the reads were aligned to the *U. maydis* reference genome using Geneious R9 software and plots for each chromosome were generated. Combining the earlier prediction with the lack of PolyA RNA reads, one region in each chromosome was identified as the putative centromere. Synteny with the *U. maydis* genome and RNA-seq (Rabe *et al.* 2016) analysis were performed using Geneious R9 software to predict putative centromeres in *U. bromivora* as well.

For *U. hordei*, both RNA-seq and synenty analysis could not be performed due to the lack of a suitable chromosome-wise assembly as well as RNA-seq data. Thus, as an alternative approach, the *U. hordei* BAC clone library was utilized to measure the length of putative centromeres (Linning *et al.* 2004, Bakkeren *et al.* 2006). First, a BLAST analysis with end sequences of BAC clones against *U. maydis* genome was performed. Considering that centromere flanking regions between all the three *Ustilago* species are syntenic, we identified the BAC clones that harbour the putative *U. hordei* centromeres. Based on the size of the BAC clones, the length of the cloned syntenic region in every BAC clone was estimated. The length of the sytenic region (based on BLAST hits) in *U. maydis* genome was also measured, and the difference between the length of syntenic regions from *U. maydis* and *U. hordei* was calculated. Since the genic content between two species is similar, the difference in length was attributed to increased centromere length in *U. hordei*. By this approach, the length of 17 centromeres out of 23 in *U. hordei* was predicted. Next, PacBio sequencing was performed for *U. hordei* and was followed by *de novo* assembly of *U. hordei* genome. Synteny analysis was performed using the refined genome, and 18 putative

centromeric regions were identified. Fifteen of these identified putative centromeres were the same as the ones predicted using BAC based approach and showed consensus on the centromere length. Two regions identified using the BAC clone approach are broken in our current PacBio assembly whereas three regions identified using PacBio approach lack equivalent BAC clones. Thus combining the data of BAC clone inserts and PacBio assembly, we could determine length of 18 centromeres in *U. hordei*.

Syntenic regions in *U. hordei* were identified using the synteny tool available in PEDANT public database (http://pedant.gsf.de/genomes.jsp?category=fungal) whereas we used Geneious tool to perform synteny analysis between *U. maydis* and *U. bromivora* genomes.

Fluorescence microscopy

Cells were grown in the YPD broth with shaking at 180 rpm for 14-16 h and pelleted at 4,000 rpm. Cells were then washed once with distilled water and finally resuspended in distilled water. Cells were observed under microscope.

For live cell imaging, an overnight YPD or synthetic complete medium-grown culture was diluted in fresh synthetic complete growth medium and grown for 3 h. Next, ~0.5 µl of cell suspension was placed on a slide containing a thin complete growth medium 2% agarose patch and a coverslip was placed on top. Images were captured at 100X using either confocal laser scanning microscope, LSM 510 META or LSM880 (Carl Zeiss, Germany) or the DeltaVision system (Applied Precision). The Image processing was done using either Zeiss image processing software LSM 5 Image Examiner, Image J, Image Pro-plus or Photoshop (Adobe Systems).

Counting of cytoplasmic microtubules

The number of cMTs per cell was determined by the method described previously (Kosco *et al.* 2001, Straube *et al.* 2003). The GFP tagged Tub1 strain of *Candida albicans* (YJB12856) or *C. neoformans* (CNVY106) was grown till log phase, harvested and mounted on an 2% agarose pad containing synthetic complete media (2% dextrose, 0.67% YNB w/o amino acids, 0.2% amino acid mix and 100 mg/l of uridine or uracil for *C. albicans* or *C. neoformans,* respectively). GFP-tagged tubulin images of *C. albicans* and *C. neoformans* cells were captured with identical settings using Carl Zeiss LSM 510 META confocal microscope (Carl Zeiss). Images were 3D rendered using Image J. cMTs were tracked manually using 3D rendered images across all planes. Bright clustered signals of Tub1-GFP which represented MTOCs were excluded from the counting. Subsequent processing was performed using Image J and Adobe Photoshop (Adobe systems). Cell number vs cMTs/cell was plotted using Prism (GraphPad Prism), with the calculated mean drawn for both *C. albicans* and *C. neoformans*.

Budding index calculation for kinetochore assembly

Budding index was calculated for 100 cells with respect to each kinetochore layer protein. The diameter of the mother cell (y, Figure 6.1) and the daughter cell (x, Figure 6.1)

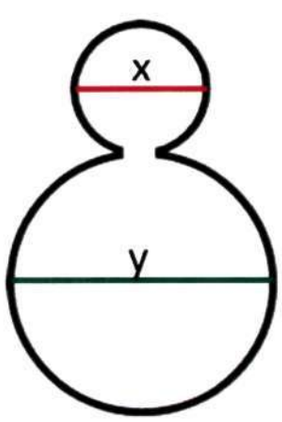

Figure 6.1 A cartoon to represent the budding index measurements.

was measured using either the Image Pro-plus software or LSM software. The diameter value of the daughter cell was then divided by the mother cell diameter value to obtain the ratio (x/y). This ratio was defined as the budding index.

Microtubule depolymerisation assays

To determine the effect of MT depolymerisation on the kinetochore clustering, the cells were grown overnight in YPD and synchronized to get unbudded cells as described previously (Ohkusu *et al.* 2004). The culture was divided in two halves. One part was treated with DMSO solution, and the remaining was treated with DMSO + nocodazole at the final concentration of 1 μg/ml. Initially cultures were treated for 1 h under low oxygen conditions to maintain the unbudded state. Subsequently, cultures were diluted into fresh medium and grown with aeration for 70 min either in the presence (DMSO+Noc) or absence (DMSO) of nocodazole. The cells were collected and placed on a 2% agarose patch (supplemented with either DMSO or DMSO+Noc) on the microscope slide and imaging was performed.

Table 6.1 Strains and Plasmids used in this study.

C. neoformans strains	
H99	α (Perfect *et al.* 1993)
KN99	a (Nielsen *et al.* 2003)
CNVY101	a KN99*::mCherry-CENP-A-NEO* (pLKB74)
CNVY102	a *CENP-C::CENP-C-mCherry-NEO*
CNVY103	a *MTW1::MTW1-mCherry:NEO*
CNVY104	α H99*::GFP-DAD1-NAT* (pVY2)
CNVY105	a *DAD2::DAD2-mCherry:NEO*
CNVY106	α H99*::GFP-TUBULIN-NAT* (pLKB35)
CNVY107	a KN99*::GFP-TUBULIN-NAT* (pLKB35) + *mCherry-CENP-A*-NEO (pLKB74)
CNVY108	α H99*::GFP-H4-NAT* (pVY3)
CNVY109	α *H4::H4-mCherry-NEO*, H99*::GFP-TUBULIN-NAT* (pLKB35)
CNVY110	α H99*::GFP-NDC1-NAT* (pVY4)
CNVY111	a KN99*::GFP-NDC1-NAT* (pVY4) + *mCherry-CENP-A-NEO* (pLKB74)
CNVY112	α *GFP-NDC1:NAT*/ pVY4, *H4::H4- mCherry-NEO*
CNVY113	α H99*::GFP-CENP-A:NAT* (pVY1)

CNVY114	a KN99*::mCherry-CENP-A-NEO* (pLKB74) + *GFP-H4-NAT* (pVY3)
CNVY115	a KN99*::GFP-CENP-A-NAT* (pVY1), *CENP-C::CENP-C- mCherry-NEO*
CNVY116	a KN99*::GFP-CENP-A-NAT* (pVY1), *MTW1::MTW1- mCherry-NEO*
CNVY117	a KN99*::GFP-DAD1-NAT* (pVY2), *MTW1::MTW1- mCherry-NEO*
CNVY118	a KN99*::GFP-DAD1-NAT* (pVY2), *CENP-C::CENP-C- mCherry-NEO*
CNVY138	a KN99*::mCherry-CENP-A-NEO* (pLKB74), *SAD1::SAD1-GFP-NAT*
CNVY149	α *SAD1::SAD1-GFP:NAT*
CNVY152	α *SPC98p::GAL7p-SPC98-HYG*
CNVY156	α H99*::CENP-Ap-GFP-CENP-A-NAT* (pVY8)
CNVY161	α *SPC98p::GAL7p-SPC98-HYG*, H99*::GFP-H4-NAT* (pVY3)
CNVY165	a KN99*::CENP-Ap-GFP-CENP-A-NAT* (pVY8)
CNVY175	α H99*::CENP-Ap-GFP-CENP-A-NAT* (pVY8), *SPC98p::GAL7p-SPC98-HYG*
CNVY176	α *SPC98p::GAL7p-SPC98-HYG, SPC98::SPC98-GFP-NAT*
CNVY177	α *SPC98p::GAL7p-SPC98-HYG, SPC98::SPC98-GFP-NAT*, H99*::mCherry-CENP-A-NEO* (pLKB74)
CNVY184	a KN99*::mCherry -CENP-A-HYG* (pLKB75)
CNVY191	α *SAD1::sad1-NEO*
CNVY192	a KN99*::mCherry -CENP-A-HYG* (pLKB75), *SAD1::sad1-NEO*
CNVY194	α H99*::GFP-TUBULIN-NAT* (pLKB35), *SAD1::sad1-NEO*
CNVY200	a KN99*::CENP-Ap-GFP-CENP-A-NAT* (pVY8), *SAD1::sad1-NEO*
CNVY210	α H99*::GFP-H4-NAT* (pVY3), *SAD1::sad1-NEO*
C. deneoformans strains	
JEC21	(Heitman *et al.* 1999)
CNVY501	α JEC21*::mCherry-CENP-A-HYG* (pLKB75)
CNVY502	α *CENP-C::CENP-C-mCherry-NEO*
C. deuterogattii strains	
R265	(Kidd *et al.* 2004)
CNVY701	α R265*::mCherry-CENP-A-NEO* (pLKB75)
CNVY702	α *CENP-C::CENP-C-mCherry-NEO*
C. amylolentus strains	
CBS6039	(Findley *et al.* 2009)
CNVY902	CBS6039*::mCherry-CENP-A-NEO* (pVY50)
Plasmids	
pVY1	pCN19 + CENP-A (BamHI-BamHI)
pVY2	pCN19 + Dad1 (BamHI-BamHI)
pVY3	pCN19 + H4 (BamHI-SpeI)
pVY4	pCN19 + Ndc1 (BamHI-SpeI)
pVY8	GFP-CENP-A-NAT from pVY1 into pBSII KS using SacI-ApaI
pVY50	CRAM CENP-A in pLK25
pVY22	*CENP-Ap* replaced *H3p* in pVY8
pLKB35	pCN19 + α-tubulin (BamHI-BamHI)
pLKB70	pXLI + mCherry-CENP-A (NEO)
pLKB71	pXLI + mCherry-CENP-A (HYG)
pLKB74	pXLI + *CENP-Ap*-mCherry-CENP-A (NEO)
pLKB75	pXLI + *CENP-Ap*-mCherry-CENP-A (HYG)

Table 6.2 Primers used in this study.

Primer name	Alias	Sequence (5'-3')	Purpose
H99 primers			
VYP1	CN-1 FP	GAACAATCCAGTCTCATCCATG	ChIP PCR
VYP2	CN-1 RP	GGAGATTAGATTAGTGAAGAGG	
VYP3	CN-2 FP	GGACTTCACCACGATCTGTG	
VYP4	CN-2 RP	GTTCGAGAATGCGTCGAGA	
VYP5	CN-3 FP	GGTGATGCTACCTCGGT	
VYP6	CN-3 RP	CCCGACGACTGTATCAGTTA	
VYP7	CN-4 FP	TGCTCTTCGTTGTAGTGGTC	
VYP8	CN-4 RP	GGTAGTTAACGAGGCCGAG	
VYP9	CN-5 FP	CATTACGTAACTCTCTCCTATG	
VYP10	CN-5 RP	CTCTGTCCTCGATCTTGAC	
VYP11	CN-6 FP	TTCCTTGCTTGACTACAATC	
VYP12	CN-6 RP	GTGTCAATTGCCAGAGATG	
VYP13	CN-7 FP	GCAAATGCAGGCAATATCA	
VYP14	CN-7 RP	GAGGGAAATCCAGTGATG	
VYP15	CN-8 FP	TGTCTGTGTTAGGCTTATG	
VYP16	CN-8 RP	GCTCTCGTCTTACCTTGCAC	
VYP17	CN-9 FP	GATTGTAGAATAGTTTCCATG	
VYP18	CN-9 RP	ATGCTTCAGGGTGTATGATC	
VYP19	CN-10 FP	ATTGCTCATGCTCTCTGTC	
VYP20	CN-10 RP	AAGGGAGAGGTGTCTTTGC	
VYP21	CN-11 FP	AATCAGAGATGTGGGTAGTC	
VYP22	CN-11 RP	TGAGCCAGAGCAGCTTG	
VYP23	CN-12 FP	GCTCAACGAACGCTGTCC	
VYP24	CN-12 RP	GACAACCACTAACCGCTCTG	
VYP25	CN-13 FP	AAAGGTGATAATACACCTTGG	
VYP26	CN-13 RP	CGGATTTGGTTGGGTTAGG	
VYP27	CN-14 FP	AAATGTCATGCATAGGACAG	
VYP28	CN-14 RP	GGTCGATGTGTAGATTGAAAC	
VYP29	CN-15 FP	CTCAAGCCATATGTCACCTC	
VYP30	CN-15 RP	CAGTTCGTCTGGTCCATC	
VYP31	CN-16 FP	GATGTCATCGAGGCAGCATC	
VYP32	CN-16 RP	TCTGCCCTGGATGAAGAGG	
VYP33	CN-17 FP	GTCTGGTATGAGTTAACCAG	
VYP34	CN-17 RP	GGTCAATGGCAGCATGG	
VYP35	CN-18 FP	CCATTGTCCATTCGCTCG	
VYP36	CN-18 RP	GGTGCGAGAATACAATTGTC	
VYP37	CN-19 FP	CGTGACAAATTCGACGATATTGC	
VYP38	CN-19 RP	TGTTTCTCCCATAGTGTTATCCAG	
VYP39	CN-20 FP	CGTGGTCGGTCATGACATG	
VYP40	CN-20 RP	CCTCTTTCCCATGATGCTGTTC	
VYP41	CN-21 FP	GGCAAGTGACCATGAGGAG	
VYP42	CN-21 RP	GCCTTTCTCGGCAGCATC	
VYP43	CN-22 FP	GGTACTCATTGTGCTTCTGTG	

VYP44	CN-22 RP	GCGCAGGAACTCATCGAC	
VYP45	CNLEU2 FP	TCAGCCGTTCTCAAGGATGAG	
VYP46	CNLEU2 RP	ACTTGAGATCAAGCTTGAGATCAG	
VYP47	CN CEN14R15 FP	TCCTGCCAACGGCAGAGC	
VYP48	CN CEN14R15 RP	CCTTTCTTCACACGATTCAC	
VYP49	CN CEN14L15 FP	TACACTACCGTCCATAACAC	
VYP50	CN CEN14L15 RP	AGGTTGTGGTTGCGTCAG	
VYP75	H99.CEN6.Me.FP	AGTCTCGTGTGGCTATGATT	Methylation-specific PCR
VYP76	H99.CEN6.Me.RP	GGATCTGCTTGACAGTGTCA	
VYP79	H99.Ctrl1.Me.FP	CCAACCGAAGCCCAAGACAA	
VYP80	H99.Ctrl1.Me.RP	TTGAAGGATGATCCGGCCGA	
VYP83	CN H4 FP	CGCGGATCCATGTCTGGTCGAGGAAAAGGTG	GFP-H4 tagging
VYP84	CN H4 RP	GGACTAGTAGAAGAAGGGGAAGAAGAAGTAGATAC	
VYP85	CN-H4 FP	GATCAGCAAATCCTCGTATGTACTTC	H4-mCherry tagging
VYP86	CN-H4-mCh RP	CTCGCCCTTGCTCACCATAGCACCGAAACCGTAAAGG	
VYP87	CN-H4-mCh FP	CCTTTACGGTTTCGGTGCTATGGTGAGCAAGGGCGAG	
VYP88	CN-Neo-H4 DS RP	GCTGCAAAAATCCACAAATGCCCAAGCTTGGTACCGAGCTC	
VYP89	CN-Neo-H4 DS FP	GAGCTCGGTACCAAGCTTGGGCATTTGTGGATTTTTGCAGC	
VYP90	CN-H4 DS RP	CCCGAAAATCTCCTCAAGG	
VYP91	CN Ndc1 FP	CGCGGATCCATGCCGGTACTACAACCACG	GFP-Ndc1 tagging
VYP92	CN Ndc1 RP	TCCATCAGCGGGTGATTGTATGCCTCAC	
VYP93	CN-Spc98 FP	ATTAGCCTCTACCGCCACCACC	Spc98-GFP/mCherry tagging
VYP94	CN-Spc98-mCh RP	CTCGCCCTTGCTCACCATAGCCCTCGCCGACCTTGATG	Spc98-mCherry tagging
VYP95	CN-Spc98-mCh FP	CATCAAGGTCGGCGAGGGCTATGGTGAGCAAGGGCGAG	
VYP96	CN-Neo-Spc98 DS RP	CAGCCACACGTATGAGGCCCCAAGCTTGGTACCGAGCTC	
VYP97	CN-Neo-Spc98 DS FP	GAGCTCGGTACCAAGCTTGGGGCCTCATACGTGTGGCTG	
VYP98	CN-Spc98 DS RP	CACACCCTTGTACAACAGGGACG	Spc98-GFP/mCherry tagging
VYP99	Spc98GFP.P2	CTCGCCCTTGCTCACCATAGCCCTCGCCGACCTTGATG	Spc98-GFP tagging
VYP100	Spc98GFP.P3	CATCAAGGTCGGCGAGGGCTATGGTGAGCAAGGGCGAG	
VYP101	Spc98GFP.P4	CAGCCACACGTATGAGGCCGCCTCTTCGCTATTACGC	
VYP102	Spc98GFP.P5	GCGTAATAGCGAAGAGGCGGCCTCATACGTGTGGCTG	
VYP103	CN Cse4-GFP FP	CAAGGATCCGCTATGGCAAGAACAGTAACGAG	GFP-CENP-A tagging
VYP104	CN Cse4-GFP RP	CTAGGATCCCATTGTCACCAAGCCTTGG	
VYP105	Cse4-GFP pr. FP	GCGCGAGCTCAGTAAGCGATTGTCAGCG	
VYP106	Cse4-GFP pr. RP	CATGCCATGGTATTCCTTCCGATTGTTTCGCG	
VYP107	CENP-C-mCh.P1	CCCGGTGACGACGGCTACCACGG	CENP-C-mCherry tagging
VYP108	CENP-C-mCh.P2	CTCGCCCTTGCTCACCATTCTCCTACTCTTCCCCTT	
VYP109	CENP-C-mCh.P3	AAGGGGAAGAGTAGGAGAATGGTGAGCAAGGGCGAG	
VYP110	CENP-C-mCh.P4	CTTCTTTCTCCTGCCAGCCCAAGCTTGGTACCGAGCTC	
VYP111	CENP-C-mCh.P5	GAGCTCGGTACCAAGCTTGGGCTGGCAGGAGAAAGAAG	
VYP112	CENP-C-mCh.P6	TCACCAGATAGAAAGAGTCTAGG	
VYP113	SBO54	GCATGATGCCCACAGGTAAATAAG	Mtw1-mCherry tagging
VYP114	SBO56	CTCGCCCTTGCTCACCATTTTATTATCCCTGAGTGACCC	
VYP115	SBO55	GGGTCACTCAGGGATAATAAAATGGTGAGCAAGGGCGAG	
VYP116	SBO58	CCTCCTAACATCGGCTATAATCCCAAGCTTGGTACCGAGCTC	
VYP117	SBO57	GAGCTCGGTACCAAGCTTGGGATTATAGCCGATGTTAGGAGG	

VYP118	SBO59	CGATCTCCGCCTGACCCTGACCTC	
VYP119	CnDAD1 FP	CAAGGATCCGCTATGTCTTTATCAAGACCATCG	GFP-Dad1 tagging
VYP120	CnDAD1 RP	CTAGGATCCTCGTCGAATGACAAATACG	
VYP123	CN Gal7-Spc98.P1	CGCGGATCCCGAGAGCGAATGTAGGGTG	Replacing SPC98p with GAL7p
VYP124	CN Gal7-Spc98.P2	GCAGATATCCATCACACTGTTCAGAGCGCACGTGTGC	
VYP125	CN Gal7-Spc98.P3	GCACACGTGCGCTCTGAACAGTGTGATGGATATCTGC	
VYP126	CN Gal7-Spc98.P4	CCTGACACCATTTCATCATCATTCTCAGGAGAGAATTGAGTGC	
VYP127	CN Gal7-Spc98.P5	GCACTCAATTCTCTCCTGAGAATGATGATGAAATGGTGTCAGG	
VYP128	CN Gal7-Spc98.P6	CGGGGTACCGTCAAGTTCATTTTGCGCAG	
VYP129	Gal7-Spc98 FP	CTTGGCAAGCTACGATAAGTGCAG	
VYP130	Gal7-Spc98 RP	CACTCCATCCTAGTGCCTGTCAGC	
VYP131	Gal7-FP (confirm)	ATACGCGAGTCCAACTTCGC	
VYP132	CN Sad1-GFP.P1	CACGAGCTCGATGAGCACAAGGTAGTGGA	Sad1-GFP tagging
VYP133	CN Sad1-GFP.P2	CTCGCCCTTGCTCACCATAGCATTCCCATGCACGCGAA	
VYP134	CN Sad1-GFP.P3	TTCGCGTGCATGGGAATGCTATGGTGAGCAAGGGCGAG	
VYP135	CN Sad1-GFP.P4	TCATGGTATCAAATCTGCCGCCTCTTCGCTATTACGC	
VYP136	CN Sad1-GFP.P5	GCGTAATAGCGAAGAGGCGGCAGATTTGATACCATGA	
VYP137	CN Sad1-GFP.P6	CCCATCGATCGGTGTCGCTGCTTCCATCT	Sad1-GFP tagging/deletion construct
VYP138	CN 3781 del P1	GCGCGGATCCGAAGAGAGAGGAGCATTCCG	Sad1 deletion construct
VYP139	CN 3781 del P2	GCACACTGGCGGCCGTTTGCTAATATGGGATGGAAGG	
VYP140	CN 3781 del P3	CCTTCCATCCCATATTAGCAAACGGCCGCCAGTGTGC	
VYP141	CN 3781 del P4	CACTATACATTGTGAAACCCCTGCAGAATTCGCCCTTGC	
VYP142	CN 3781 del P5	GCAAGGGCGAATTCTGCAGGGGTTTCACAATGTATAGTG	
VYP143	CN 3781 del final.FP	AGAACGAGGATGCTGCCTCTGC	
VYP144	CN 3781 del final.RP	CGGAACTACGTTCACCATGGC	
VYP145	CN 3781 del.conf FP	TTGTTGTTACCATCATCCTCTC	
VYP146	CN 3781 del.conf FP	CGGTGTCGCTGCTTCCATCT	
VYP147	NheI	GCAGCTAGCTATGGCAAGAACAGTAACGAG	mCherry-CENP-A tagging
VYP148	PacI	GACTTAATTAAGCTCAAATCGTAATCCTTC	
VYP149	XhoI	GTACTCGAGTCATGGAGAAGATAGATTG	
VYP150	FseI	CTAGGCCGGCCATTCCTTCCGATTGTTTCG	
VYP151	Cn DAD2 FP	GCTCTAGACTATCAATCGCCAATCGCTTC	Dad2-mCherry tagging
VYP152	Cn DAD2-mCh UP RP	CTCGCCCTTGCTCACCATTTGTTGTTTTGTTTTATCAGATGCG	
VYP153	Cn DAD2-mCh-Neo FP	CTGATAAAACAAAACAACAAATGGTGAGCAAGGGCGAG	
VYP154	Cn DAD2-mCh-Neo RP	CTATTGGTCGTCATCAGCAGGCCAAGCTTGGTACCGAGCTC	
VYP155	Cn DAD2-mCh down FP	GAGCTCGGTACCAAGCTTGGCCTGCTGATGACGACCAATAG	
VYP156	Cn DAD2 DS RP	CCCAAGCTTCTCCATATCGTGTCTCAATTTCATCTC	
VYP157	mCh-conf. RP	CTTGTACAGCTCGTCCATGC	mCherry tagging confirmation primer
VYP158	Full.P1	TAGCTTTCTGGATCCAAGAGGTTCC	CEN5 sequencing
VYP159	Full.P2	GAAAATATCATGCATAGGACAAAGGC	
VYP160	Full.P3	ATGCATAGGACCGGCAATTGC	
VYP161	Full.P4	TGCTGTGGGTCCATTGGAGGTC	
VYP162	Full.P5	CACATCCCCAATCCAAAAATGCACTC	
VYP163	Full.P6	CATCATCCACTAGTCTCCAAAGCC	
VYP164	P1.F2.N1.FP	ACTCTTGAGCTCAGCAATGTC	

VYP165	P1.N2.FP	ATGCCCACTGATGAGTGCATC	
VYP166	P1.N2.RP	GAACACAATCCGTCCATCAGCTG	
VYP167	P1.S4.FP	CACCTTGTGACCAATGTCG	
VYP168	P1.S5.FP	GTTGTTCGGTCTGTCTTAAC	
VYP169	P1.S6.FP	GCTATTCGCCTCAATAAACTCC	
VYP170	P1.S10.FP	CCTTCGCGATGAACAATACC	
VYP171	P1.S11.RP	CAAGTTCATAGTAACAGCCAC	
VYP172	P1.Tr.FP	GTGGCTGTTACTATGAACTTGATTTCC	
VYP173	P1.Tr.RP	GAGGAGTTTATTGAGGCGAATAGC	
VYP174	P2.N2.FP	CAATCATATTGCGAGACTTGAGC	
VYP175	P2.S6.FP	AGCTCTTGCAAGCTCTGCC	
VYP176	P2.S8.RP	GTTGCCTGCTGAGTTAAAC	
VYP177	P2.S11.FP	CAAGTTCATAGTAACAGCCAC	
VYP178	P2.Tr1.FP	GCACAGACAACCGAGGACCGTATAGAAGG	
VYP179	P2.Tr1.RP	CCTTCTATACGGTCCTCGGTTGTCTGTGC	
VYP180	P2.Tr2.FP	CCTCAGTAGAGTTCCTAGGTTTCATTGTCAGC	
VYP181	P2.Tr2.RP	GCTGACAATGAAACCTAGGAACTCTACTGAGG	
VYP182	P3.S12.RP	AGGTGCAAGAAGCTAATCCTGC	
JEC21 primers			
VYP501	JEC-Mif2-mCh.P1	GGATAGAGCAAGATCTGCTAGGTC	
VYP502	JEC-Mif2-mCh.P2	CTCGCCCTTGCTCACCATTCTCCTGCTCTTCCCCTTAC	
VYP503	JEC-Mif2-mCh.P3	GTAAGGGGAAGAGCAGGAGAATGGTGAGCAAGGGCGAG	
VYP504	JEC-Mif2-mCh.P4	GCTTCGTTACTGACAACAATATATCCCAAGCTTGGTACCGAGCTC	CENP-C mCherry tagging
VYP505	JEC-Mif2-mCh.P5	GAGCTCGGTACCAAGCTTGGGATATATTGTTGTCAGTAACGAAGC	
VYP506	JEC-Mif2-mCh.P6	TGAGGCAGGAATCATGTAGTC	
VYP507	JEC-Mif2-mCh.final FP	GGCTGCGCTGTTATCAAGGAGATC	
VYP508	JEC-Mif2-mCh.final RP	CTTGGGAGGGACGAATACATTGACCTG	
VYP509	JEC.CEN1.1.FP	GTGCAACTGCTATGTAGCTG	
VYP510	JEC.CEN1.1.RP	TGTGGAACGTCTGACAGTG	
VYP511	JEC.CEN1.2.FP	CTTATGCTCCTTCAAGTGC	
VYP512	JEC.CEN1.2.RP	ACCCAGCCTTGCTACTCAC	
VYP513	JEC.CEN2.1.FP	CTACCTTCTTCGACATTGGC	
VYP514	JEC.CEN2.1.RP	CCATCAAGTCGCCAAGTGC	
VYP515	JEC.CEN2.2.FP	ATCGGCAAGCACTAGTAGC	
VYP516	JEC.CEN2.2.RP	ACGTCATGACAGACCATGC	
VYP517	JEC.CEN3.1.FP	GTGGTCAATACGCAAGTCG	
VYP518	JEC.CEN3.1.RP	ACCGACCACTTCACTCTC	ChIP PCR
VYP519	JEC.CEN3.2.FP	CAGTAGACTGATCAGCAAGC	
VYP520	JEC.CEN3.2.RP	GCCACAATGACATACGAGC	
VYP521	JEC.CEN4.1.FP	CGTCTTCGCTATTCCAGTTC	
VYP522	JEC.CEN4.1.RP	CGTGACATTGTTCAGAGC	
VYP523	JEC.CEN4.2.FP	CAACAAGGGGAATAGGAAGG	
VYP524	JEC.CEN4.2.RP	GCTGATCGATGGACTCTTG	
VYP571	JEC.CEN5.1.qFP	TCGTCGAGCCGCATATGC	
VYP526	JEC.CEN5.1.RP	ACACTCCAGCGAAAATTGC	
VYP572	JEC.CEN5.2.qFP	GTGTTGCTTGCGTCGGTG	
VYP528	JEC.CEN5.2.RP	TGAAGGAAATGGTGGCACG	

VYP529	JEC.CEN6.1.FP	ACCAGCACCAGTCGCTTC	
VYP530	JEC.CEN6.1.RP	GTCTCAGACTTCATTCTCATC	
VYP531	JEC.CEN6.2.FP	CATAACTCGACTTCAACTCG	
VYP532	JEC.CEN6.2 RP	CCTTGACATCCGCACCAG	
VYP533	JEC.CEN7.1.FP	AACATCTTGGTGACTGTCG	
VYP534	JEC.CEN7.1.RP	AAACCATCTATCTTGAAGCAC	
VYP535	JEC.CEN7.2.FP	AGCACGGAAATCGCAGAC	
VYP536	JEC.CEN7.2.RP	TGAATGCAGGACGTCTTCG	
VYP537	JEC.CEN8.1.FP	TGCATCACATTGTGTCATGC	
VYP538	JEC.CEN8.1.RP	GTTTCAGGTCAATAGCAGAC	
VYP539	JEC.CEN8.2.FP	ACTCTTGCATGGAGTAGAATC	
VYP540	JEC.CEN8.2.RP	CATATGCATGACTTTCAACC	
VYP541	JEC.CEN9.1.FP	AATTGATAGGAACACTGATCAG	
VYP542	JEC.CEN9.1.RP	TACAGTCACAAGTACCTTGC	
VYP543	JEC.CEN9.2.FP	ACAACGCAGTAGTTCAAGTG	
VYP544	JEC.CEN9.2.RP	CCCCGAAGTACTAACCTTGC	
VYP545	JEC.CEN10.1.FP	TCAGACCCATCGTCAATCATG	
VYP546	JEC.CEN10.1.RP	CGAAGCCGATGCTGAGTAC	
VYP547	JEC.CEN10.2.FP	TCGGTTGAATTCCCTCCTG	
VYP548	JEC.CEN10.2.RP	ATGACTGTCTTGTTAGATCG	
VYP569	JEC.CEN11.1.qFP	TCACTGGATTCTTTGACAAGG	
VYP550	JEC.CEN11.1.RP	CTGCTCTTGGATGATATAGGAC	
VYP551	JEC.CEN11.2.FP	GTCTAGAGAGAGCTTGAGC	
VYP570	JEC.CEN11.2.qRP	CCAGAACACTTACAATATCGAAAC	
VYP553	JEC.CEN12.1.FP	GTCGAGTAGGCGAGGAAC	
VYP554	JEC.CEN12.1.RP	ACCTCAACACAGTCGACG	
VYP555	JEC.CEN12.2.FP	TAGGCGGTGTTGACGACAG	
VYP556	JEC.CEN12.2.RP	TCATTGGTGACACTACCTAC	
VYP557	JEC.CEN13.1.FP	AGTCACACGTCATACAAGTC	
VYP558	JEC.CEN13.1.RP	AACCTAGGAACTCTACTGAG	
VYP559	JEC.CEN13.2.FP	ACGACAATCGTAGCATCG	
VYP560	JEC.CEN13.2.RP	CTATGTCCTACTATCACGAC	
VYP561	JEC.CEN14.1.FP	CGTTCGTGGTATAGGTCTAGAG	
VYP567	JEC.CEN14.1.qRP	CCATTGCTAGTTTCGCATC	
VYP563	JEC.CEN14.2.FP	CATCCTTCCCCCATATGATG	
VYP568	JEC.CEN14.2.qRP	TCAACAGCGTCGCATTAATG	
VYP573	JEC.Ctrl..qFP	CTACTCATACAACGACACCTC	
VYP566	JEC.ChIP.ctrl.RP	TGAGTGAGCCACCTATAACG	
R265 primers			
VYP701	R265-Mif2-mCh.P1	ACGTCCGTCCGAACTTGG	CENP-C mCherry tagging
VYP702	R265-Mif2-mCh.P2	CTCGCCCTTGCTCACCATTCTCCTACTCTTCCCTTTACTTTTTCTC	
VYP703	R265-Mif2-mCh.P3	GAGAAAAAGTAAAGGGAAGAGTAGGAGAATGGTGAGCAAGGGCGAG	
VYP704	R265-Mif2-mCh.P4	CATCTTCCCCCTGCCAGTCCAAGCTTGGTACCGAGCTC	
VYP705	R265-Mif2-mCh.P5	GAGCTCGGTACCAAGCTTGGACTGGCAGGGGGAAGATG	
VYP706	R265-Mif2-mCh.P6	AGCCGCCAGGTAGATGAGG	
VYP707	R265-Mif2-mCh.final FP	CACTATCCCTGAAGATCCACCTATACC	

VYP708	R265-Mif2-mCh.final RP	CGATTGCCTGTTTCACTTCACTC	
VYP709	R265.CEN7.ChIP.1.FP	GTTTTGGATATAGTGGGAAAGTTC	ChIP PCR
VYP710	R265.CEN7.ChIP.1.RP	GGTTGTTAACGGATACAAATTCC	
VYP711	R265.CEN7.ChIP.2.FP	CTCTGCATTCCTGACATCG	
VYP712	R265.CEN7.ChIP.2.RP	AATCCAGGGTGATATCATCG	
VYP713	R265.CEN8.ChIP.1.FP	CGTGGCGTGAATACATACAC	
VYP714	R265.CEN8.ChIP.1.RP	TTGCAAAAGAAGGGAGGCTG	
VYP715	R265.CEN8.ChIP.2.FP	CTGAGTCCACAATGAAGGTG	
VYP716	R265.CEN8.ChIP.2.RP	CCAAGGTAACAAGCACAATG	
VYP717	R265.CEN14.ChIP.1.FP	GAATCAAGTCTGAGGCACTAC	
VYP718	R265.CEN14.ChIP.1.RP	GTAATCTGGTCTCCACAAGC	
VYP719	R265.CEN14.ChIP.2.FP	GCAGTTTCCATGTATAAGCTG	
VYP720	R265.CEN14.ChIP.2.RP	TAGACTACTGTAGGCACTGG	
VYP727	R265.ChIP.ctrl4.FP	GGACGGGCTGAGGAAAGTC	
VYP728	R265.ChIP.ctrl4.rP	GAAGCCCTATGAGGAACAAG	
VYP729	R265.ChIP.ctrl5.FP	CTCTCCTTTCCTTGCACCAGC	
VYP730	R265.ChIP.ctrl5.RP	ACTTTCTATCTGACCATTTCTCC	
VYP741	R265.CEN9.Me.FP	CTGACCTCTAGTTGCAGGAGC	Methylation specific PCR
VYP742	R265.CEN9.Me.RP	CCAGATGATGTGGCATTCAAG	
VYP743	R265.Ctrl.Me.FP	CTTGTCTCGGCGTCCCAAAC	
VYP744	R265.Ctrl.Me.RP	AAAACGCTCAAAGCCTCTACG	
***C. amylolentus* primers**			
VYP901	CRAM.mCh-CENP-A.P1	GACCTCTAGAGTTGCCTGTCGTTGCGAGTG	mCherry-CENP-A tagging
VYP902	CRAM.mCh-CENP-A.P2	CTCCTCGCCCTTGCTCACCATTGCGCTTGCTTCTCCTGTTCT	
VYP903	CRAM.mCh-CENP-A.P3	AGAACAGGAGAAGCAAGCGCAATGGTGAGCAAGGGCGAGGAG	
VYP904	CRAM.mCh-CENP-A.P4	GGACGTGACTGTTCGGGCCATCTTGTACAGCTCGTCCATGC	
VYP905	CRAM.mCh-CENP-A.P5	GCATGGACGAGCTGTACAAGATGGCCCGAACAGTCACGTCC	
VYP906	CRAM.mCh-CENP-A.P6	GACGCTCGAGCCAAATCGGTATCGTCCTTGCTG	
VYP907	CRAM_SC9.1.FP	GTCAAACCCGTTGCTCGTTC	ChIP PCR
VYP908	CRAM_SC9.1.new.RP	CCATTTTTGCAAACACCTTGC	
VYP909	CRAM_SC9.1.new.FP	GTTCATGAGAAGGAGCTCCTTG	
VYP910	CRAM_SC9.1.RP	GCCATACGCTCCAAGAACTCT	
VYP911	CRAM_SC9.2.FP	CTCGAAACGACCAAGTCGTG	
VYP912	CRAM_SC9.2.new.RP	GCATATACTTGTCACATAGACAGAC	
VYP913	CRAM_SC9.2.new.FP	GACGAGGATGGAAATGCTATCAC	
VYP914	CRAM_SC9.2.RP	AGCTCAGCTTGGTTGCGATG	
VYP915	CRAM_SC9.3.FP	CAGGAGTGTGGCATTGTTGG	
VYP916	CRAM_SC9.3.new.RP	ATGCTAGATTGGTCCTCTAACC	
VYP917	CRAM_SC9.3.new.FP	GATTACTTGTCAATAACCCATCC	
VYP918	CRAM_SC9.3.RP	TGGAAACTCTGGGGCTCAA	
VYP919	CRAM_SC9.4.FP	CTTCTCTTTTAGTAGGGCTGTCC	
VYP920	CRAM_SC9.4.RP	AAATAAGGGTACAAGTTGACCAG	
VYP921	CRAM_SC9.ctrl.FP	TCTCCCTCTCACAATCTACC	
VYP922	CRAM_SC9.ctrl.RP	GGTTGTAGAGAGCTTTCAGTG	

Appendix 1. Software, tools and websites used in this study.

S. no.	Name	Website	Purpose
1.	Geneious R9	http://www.geneious.com	For sequence alignments, synteny analysis, genome view
2.	FungiDB database	http://fungidb.org/fungidb/	For *Cryptococcus* sp. genome sequence retrieval and access
3.	LTR-finder program	http://tlife.fudan.edu.cn/ltr_finder/	For identification of LTR elements in the genome.
4.	CD-search	http://www.ncbi.nlm.nih.gov/Structure/cdd/wrpsb.cgi	For domain identification in proteins
5.	PEDANT public database	http://pedant.gsf.de/genomes.jsp?category=fungal	For *Ustilago* sp. genome sequence analysis
6.	Pfam	http://pfam.xfam.org/	For domain prediction in proteins
7.	Clustal Omega	http://www.ebi.ac.uk/Tools/msa/clustalo/	Multiple sequence alignment
8.	ESPript	http://espript.ibcp.fr/ESPript/ESPript/	For generating alignment figures
9.	SyMAP	http://www.agcol.arizona.edu/software/symap/index.html	For generating whole genome circular synteny maps

7. REFERENCES

Aleksenko, A., Nielsen, M. L. and Clutterbuck, A. J. (2001). "Genetic and physical mapping of two centromere-proximal regions of chromosome IV in *Aspergillus nidulans*." *Fungal Genet Biol* **32**(1): 45-54.

Alonso, A., Mahmood, R., Li, S., Cheung, F., Yoda, K. and Warburton, P. E. (2003). "Genomic microarray analysis reveals distinct locations for the CENP-A binding domains in three human chromosome 13q32 neocentromeres." *Hum Mol Genet* **12**(20): 2711-2721.

Ambesajir, A., Kaushik, A., Kaushik, J. J. and Petros, S. T. (2012). "RNA interference: A futuristic tool and its therapeutic applications." *Saudi J Biol Sci* **19**(4): 395-403.

Anders, A., Lourenco, P. C. and Sawin, K. E. (2006). "Noncore components of the fission yeast gamma-tubulin complex." *Mol Biol Cell* **17**(12): 5075-5093.

Anderson, M., Haase, J., Yeh, E. and Bloom, K. (2009). "Function and assembly of DNA looping, clustering, and microtubule attachment complexes within a eukaryotic kinetochore." *Mol Biol Cell* **20**(19): 4131-4139.

Aoki, K., Hayashi, H., Furuya, K., Sato, M., Takagi, T., Osumi, M., Kimura, A. and Niki, H. (2011). "Breakage of the nuclear envelope by an extending mitotic nucleus occurs during anaphase in *Schizosaccharomyces japonicus*." *Genes Cells.* **16**(9): 911-926.

Aoki, K., Nakaseko, Y., Kinoshita, K., Goshima, G. and Yanagida, M. (2006). "CDC2 phosphorylation of the fission yeast dis1 ensures accurate chromosome segregation." *Curr Biol* **16**(16): 1627-1635.

Arabidopsis Genome, I. (2000). "Analysis of the genome sequence of the flowering plant Arabidopsis thaliana." *Nature* **408**(6814): 796-815.

Aravin, A. A., Naumova, N. M., Tulin, A. V., Vagin, V. V., Rozovsky, Y. M. and Gvozdev, V. A. (2001). "Double-stranded RNA-mediated silencing of genomic tandem repeats and transposable elements in the *D. melanogaster* germline." *Curr Biol* **11**(13): 1017-1027.

Asakawa, H., Hayashi, A., Haraguchi, T. and Hiraoka, Y. (2005). "Dissociation of the Nuf2-Ndc80 complex releases centromeres from the spindle-pole body during meiotic prophase in fission yeast." *Mol Biol Cell* **16**(5): 2325-2338.

Asakawa, H., Hiraoka, Y. and Haraguchi, T. (2011). "Physical breakdown of the nuclear envelope is not necessary for breaking its barrier function." *Nucleus* **2**(6): 523-526.

Asakawa, H., Kojidani, T., Mori, C., Osakada, H., Sato, M., Ding, D. Q., Hiraoka, Y. and Haraguchi, T. (2010). "Virtual breakdown of the nuclear envelope in fission yeast meiosis." *Curr Biol* **20**(21): 1919-1925.

Bakkeren, G., Jiang, G., Warren, R. L., Butterfield, Y., Shin, H., Chiu, R., Linning, R., Schein, J., Lee, N., Hu, G., Kupfer, D. M., Tang, Y., Roe, B. A., Jones, S., Marra, M. and Kronstad, J. W. (2006). "Mating factor linkage and genome evolution in basidiomycetous pathogens of cereals." *Fungal Genet Biol* **43**(9): 655-666.

Barnhart, M. C., Kuich, P. H., Stellfox, M. E., Ward, J. A., Bassett, E. A., Black, B. E. and Foltz, D. R. (2011). "HJURP is a CENP-A chromatin assembly factor sufficient to form a functional *de novo* kinetochore." *J Cell Biol* **194**(2): 229-243.

Beck, M. and Hurt, E. (2017). "The nuclear pore complex: understanding its function through structural insight." *Nat Rev Mol Cell Biol* **18**(2): 73-89.

Belgareh, N., Rabut, G., Bai, S. W., van Overbeek, M., Beaudouin, J., Daigle, N., Zatsepina, O. V., Pasteau, F., Labas, V., Fromont-Racine, M., Ellenberg, J. and Doye, V. (2001). "An evolutionarily conserved NPC subcomplex, which redistributes in part to kinetochores in mammalian cells." *J Cell Biol* **154**(6): 1147-1160.

Bensasson, D., Zarowiecki, M., Burt, A. and Koufopanou, V. (2008). "Rapid evolution of yeast centromeres in the absence of drive." *Genetics* **178**(4): 2161-2167.

Best, H. A., Matthews, J. H., Heathcott, R. W., Hanna, R., Leahy, D. C., Coorey, N. V., Bellows, D. S., Atkinson, P. H. and Miller, J. H. (2013). "Laulimalide and peloruside A inhibit mitosis of *Saccharomyces cerevisiae* by preventing microtubule depolymerisation-dependent steps in chromosome separation and nuclear positioning." *Mol Biosyst* **9**(11): 2842-2852.

Bettencourt-Dias, M. (2013). "Q&A: Who needs a centrosome?" *BMC Biol* **11**: 28.

Biemont, C. (2010). "A brief history of the status of transposable elements: from junk DNA to major players in evolution." *Genetics* **186**(4): 1085-1093.

Billmyre, R. B., Calo, S., Feretzaki, M., Wang, X. and Heitman, J. (2013). "RNAi function, diversity, and loss in the fungal kingdom." *Chromosome Res* **21**(6-7): 561-572.

Biscotti, M. A., Olmo, E. and Heslop-Harrison, J. S. (2015). "Repetitive DNA in eukaryotic genomes." *Chromosome Res* **23**(3): 415-420.

Boehmer, T., Enninga, J., Dales, S., Blobel, G. and Zhong, H. (2003). "Depletion of a single nucleoporin, Nup107, prevents the assembly of a subset of nucleoporins into the nuclear pore complex." *Proc Natl Acad Sci U S A* **100**(3): 981-985.

Boetzer, M. and Pirovano, W. (2014). "SSPACE-LongRead: scaffolding bacterial draft genomes using long read sequence information." *BMC Bioinformatics* **15**(1): 211.

Bone, C. R., Tapley, E. C., Gorjanacz, M. and Starr, D. A. (2014). "The *Caenorhabditis elegans* SUN protein UNC-84 interacts with lamin to transfer forces from the cytoplasm to the nucleoskeleton during nuclear migration." *Mol Biol Cell* **25**(18): 2853-2865.

Bourc'his, D. and Bestor, T. H. (2004). "Meiotic catastrophe and retrotransposon reactivation in male germ cells lacking Dnmt3L." *Nature* **431**(7004): 96-99.

Bouzinba-Segard, H., Guais, A. and Francastel, C. (2006). "Accumulation of small murine minor satellite transcripts leads to impaired centromeric architecture and function." *Proc Natl Acad Sci U S A* **103**(23): 8709-8714.

Brefort, T., Doehlemann, G., Mendoza-Mendoza, A., Reissmann, S., Djamei, A. and Kahmann, R. (2009). "*Ustilago maydis* as a Pathogen." *Annu Rev Phytopathol* **47**: 423-445.

Brinkley BR and Stubblefield (1966). "The fine structure of the kinetochore of a mammalian cell *in vitro*." *Chromosoma.* **19**(1): 28-43.

Burrack, L. S., Applen, S. E. and Berman, J. (2011). "The requirement for the Dam1 complex is dependent upon the number of kinetochore proteins and microtubules." *Curr Biol* **21**(10): 889-896.

Buscaino, A., Allshire, R. and Pidoux, A. (2010). "Building centromeres: home sweet home or a nomadic existence?" *Curr Opin Genet Dev* **20**(2): 118-126.

Cai, Y., Yu, X., Hu, S. and Yu, J. (2009). "A brief review on the mechanisms of miRNA regulation." *Genomics Proteomics Bioinformatics* **7**(4): 147-154.

Cain, N. E., Tapley, E. C., McDonald, K. L., Cain, B. M. and Starr, D. A. (2014). "The SUN protein UNC-84 is required only in force-bearing cells to maintain nuclear envelope architecture." *J Cell Biol* **206**(2): 163-172.

Cam, H. P., Sugiyama, T., Chen, E. S., Chen, X., FitzGerald, P. C. and Grewal, S. I. (2005). "Comprehensive analysis of heterochromatin- and RNAi-mediated epigenetic control of the fission yeast genome." *Nat Genet* **37**(8): 809-819.

Camahort, R., Li, B., Florens, L., Swanson, S. K., Washburn, M. P. and Gerton, J. L. (2007). "Scm3 is essential to recruit the histone h3 variant cse4 to centromeres and to maintain a functional kinetochore." *Mol Cell* **26**(6): 853-865.

Cambareri, E. B., Aisner, R. and Carbon, J. (1998). "Structure of the chromosome VII centromere region in *Neurospora crassa*: degenerate transposons and simple repeats." *Mol Cell Biol* **18**(9): 5465-5477.

Castagnetti, S., Oliferenko, S. and Nurse, P. (2010). "Fission yeast cells undergo nuclear division in the absence of spindle microtubules." *PLoS Biol* **8**(10): e1000512.

Chan, F. L. and Wong, L. H. (2012). "Transcription in the maintenance of centromere chromatin identity." *Nucleic Acids Res* **40**(22): 11178-11188.

Chang, W., Worman, H. J. and Gundersen, G. G. (2015). "Accessorizing and anchoring the LINC complex for multifunctionality." *J Cell Biol* **208**(1): 11-22.

Chatterjee, G., Sankaranarayanan, S. R., Guin, K., Thattikota, Y., Padmanabhan, S., Siddharthan, R. and Sanyal, K. (2016). "Repeat-associated fission yeast-like regional centromeres in the ascomycetous budding yeast *Candida tropicalis*." *PLoS Genet* **12**(2): e1005839.

Cheeseman, I. M. (2014). "The kinetochore." *Cold Spring Harb Perspect Biol* **6**(7): a015826.

Cheeseman, I. M., Brew, C., Wolyniak, M., Desai, A., Anderson, S., Muster, N., Yates, J. R., Huffaker, T. C., Drubin, D. G. and Barnes, G. (2001). "Implication of a novel multiprotein Dam1p complex in outer kinetochore function." *J Cell Biol* **155**(7): 1137-1145.

Cheeseman, I. M. and Desai, A. (2008). "Molecular architecture of the kinetochore-microtubule interface." *Nat Rev Mol Cell Biol* **9**(1): 33-46.

Cheeseman, I. M., Enquist-Newman, M., Muller-Reichert, T., Drubin, D. G. and Barnes, G. (2001). "Mitotic spindle integrity and kinetochore function linked by the Duo1p/Dam1p complex." *J Cell Biol* **152**(1): 197-212.

Chen, E. S., Saitoh, S., Yanagida, M. and Takahashi, K. (2003). "A cell cycle-regulated GATA factor promotes centromeric localization of CENP-A in fission yeast." *Mol Cell* **11**(1): 175-187.

Chen, T., Ueda, Y., Dodge, J. E., Wang, Z. and Li, E. (2003). "Establishment and maintenance of genomic methylation patterns in mouse embryonic stem cells by Dnmt3a and Dnmt3b." *Mol Cell Biol* **23**(16): 5594-5605.

Cheng, Z., Dong, F., Langdon, T., Ouyang, S., Buell, C. R., Gu, M., Blattner, F. R. and Jiang, J. (2002). "Functional rice centromeres are marked by a satellite repeat and a centromere-specific retrotransposon." *Plant Cell* **14**(8): 1691-1704.

Cheng, Z. J. and Murata, M. (2003). "A centromeric tandem repeat family originating from a part of Ty3/gypsy-retroelement in wheat and its relatives." *Genetics* **164**(2): 665-672.

Chery, J. (2016). "RNA therapeutics: RNAi and antisense mechanisms and clinical applications." *Postdoc J* **4**(7): 35-50.

Chikashige, Y., Kinoshita, N., Nakaseko, Y., Matsumoto, T., Murakami, S., Niwa, O. and Yanagida, M. (1989). "Composite motifs and repeat symmetry in *S. pombe* centromeres: direct analysis by integration of NotI restriction sites." *Cell* **57**(5): 739-751.

Chikashige, Y., Tsutsumi, C., Yamane, M., Okamasa, K., Haraguchi, T. and Hiraoka, Y. (2006). "Meiotic proteins bqt1 and bqt2 tether telomeres to form the bouquet arrangement of chromosomes." *Cell* **125**(1): 59-69.

Choi, E. S., Stralfors, A., Castillo, A. G., Durand-Dubief, M., Ekwall, K. and Allshire, R. C. (2011). "Identification of noncoding transcripts from within CENP-A chromatin at fission yeast centromeres." *J Biol Chem* **286**(26): 23600-23607.

Chuong, E. B., Elde, N. C. and Feschotte, C. (2017). "Regulatory activities of transposable elements: from conflicts to benefits." *Nat Rev Genet* **18**(2): 71-86.

Ciferri, C., Pasqualato, S., Screpanti, E., Varetti, G., Santaguida, S., Dos Reis, G., Maiolica, A., Polka, J., De Luca, J. G., De Wulf, P., Salek, M., Rappsilber, J., Moores, C. A., Salmon, E. D. and Musacchio, A. (2008). "Implications for kinetochore-microtubule attachment from the structure of an engineered Ndc80 complex." *Cell* **133**(3): 427-439.

Clarke, L., Amstutz, H., Fishel, B. and Carbon, J. (1986). "Analysis of centromeric DNA in the fission yeast *Schizosaccharomyces pombe*." *Proc Natl Acad Sci U S A* **83**(21): 8253-8257.

Clarke, L. and Baum, M. P. (1990). "Functional analysis of a centromere from fission yeast: a role for centromere-specific repeated DNA sequences." *Mol Cell Biol* **10**(5): 1863-1872.

Clarke, L. and Carbon, J. (1980). "Isolation of a yeast centromere and construction of functional small circular chromosomes." *Nature* **287**(5782): 504-509.

Cleveland, D. W., Mao, Y. and Sullivan, K. F. (2003). "Centromeres and kinetochores: From epigenetics to mitotic checkpoint signaling." *Cell* **112**(4): 407-421.

Cuacos, M., FC, H. F. and Heckmann, S. (2015). "Atypical centromeres in plants-what they can tell us." *Front Plant Sci* **6**: 913.

Cumberledge, S. and Carbon, J. (1987). "Mutational analysis of meiotic and mitotic centromere function in *Saccharomyces cerevisiae*." *Genetics* **117**(2): 203-212.

D'Angelo, M. A. and Hetzer, M. W. (2008). "Structure, dynamics and function of nuclear pore complexes." *Trends Cell Biol* **18**(10): 456-466.

D'Souza, C. A., Kronstad, J. W., Taylor, G., Warren, R., Yuen, M., Hu, G., Jung, W. H., Sham, A., Kidd, S. E., Tangen, K., Lee, N., Zeilmaker, T., Sawkins, J., McVicker, G., Shah, S., Gnerre, S., Griggs, A., Zeng, Q., Bartlett, K., Li, W., Wang, X., Heitman, J., Stajich, J. E., Fraser, J. A., Meyer, W., Carter, D., Schein, J., Krzywinski, M., Kwon-Chung, K. J., Varma, A., Wang, J., Brunham, R., Fyfe, M., Ouellette, B. F., Siddiqui, A., Marra, M., Jones, S., Holt, R., Birren, B. W., Galagan, J. E. and Cuomo, C. A. (2011). "Genome variation in *Cryptococcus gattii*, an emerging pathogen of immunocompetent hosts." *mBio* **2**(1): e00342-00310.

Davidson, R. C., Cruz, M. C., Sia, R. A., Allen, B., Alspaugh, J. A. and Heitman, J. (2000). "Gene disruption by biolistic transformation in serotype D strains of *Cryptococcus neoformans*." *Fungal Genet Biol* **29**(1): 38-48.

Dawe, R. K. (2003). "RNA interference, transposons, and the centromere." *Plant Cell* **15**(2): 297-301.

Dawe, R. K. and Henikoff, S. (2006). "Centromeres put epigenetics in the driver's seat." *Trends Biochem Sci* **31**(12): 662-669.

De Souza, C. P., Osmani, A. H., Hashmi, S. B. and Osmani, S. A. (2004). "Partial nuclear pore complex disassembly during closed mitosis in *Aspergillus nidulans*." *Curr Biol* **14**(22): 1973-1984.

De Souza, C. P. and Osmani, S. A. (2007). "Mitosis, not just open or closed." *Eukaryot Cell* **6**(9): 1521-1527.

De Souza, C. P. and Osmani, S. A. (2009). "Double duty for nuclear proteins--the price of more open forms of mitosis." *Trends Genet* **25**(12): 545-554.

Devos, K. M., Brown, J. K. and Bennetzen, J. L. (2002). "Genome size reduction through illegitimate recombination counteracts genome expansion in *Arabidopsis*." *Genome Res* **12**(7): 1075-1079.

Ding, R., West, R. R., Morphew, D. M., Oakley, B. R. and McIntosh, J. R. (1997). "The spindle pole body of *Schizosaccharomyces pombe* enters and leaves the nuclear envelope as the cell cycle proceeds." *Mol Biol Cell* **8**(8): 1461-1479.

Djupedal, I., Kos-Braun, I. C., Mosher, R. A., Soderholm, N., Simmer, F., Hardcastle, T. J., Fender, A., Heidrich, N., Kagansky, A., Bayne, E., Wagner, E. G., Baulcombe, D. C., Allshire, R. C. and Ekwall, K. (2009).

"Analysis of small RNA in fission yeast; centromeric siRNAs are potentially generated through a structured RNA." *EMBO J* **28**(24): 3832-3844.

Drinnenberg, I. A., Fink, G. R. and Bartel, D. P. (2011). "Compatibility with killer explains the rise of RNAi-deficient fungi." *Science* **333**(6049): 1592.

Drinnenberg, I. A., Henikoff, S. and Malik, H. S. (2016). "Evolutionary turnover of kinetochore proteins: A ship of theseus?" *Trends in Cell Biology* **26**(7): 498-510.

Drinnenberg, I. A., Weinberg, D. E., Xie, K. T., Mower, J. P., Wolfe, K. H., Fink, G. R. and Bartel, D. P. (2009). "RNAi in budding yeast." *Science* **326**(5952): 544-550.

Duan, Z., Andronescu, M., Schutz, K., McIlwain, S., Kim, Y. J., Lee, C., Shendure, J., Fields, S., Blau, C. A. and Noble, W. S. (2010). "A three-dimensional model of the yeast genome." *Nature* **465**(7296): 363-367.

Dubin, M., Fuchs, J., Graf, R., Schubert, I. and Nellen, W. (2010). "Dynamics of a novel centromeric histone variant CenH3 reveals the evolutionary ancestral timing of centromere biogenesis." *Nucleic Acids Research* **38**: 7526-7537.

Dumesic, P. A. and Madhani, H. D. (2014). "Recognizing the enemy within: licensing RNA-guided genome defense." *Trends Biochem Sci* **39**(1): 25-34.

Earnshaw, W. C. and Rothfield, N. (1985). "Identification of a family of human centromere proteins using autoimmune sera from patients with scleroderma." *Chromosoma* **91**(3-4): 313-321.

Ellermeier, C., Higuchi, E. C., Phadnis, N., Holm, L., Geelhood, J. L., Thon, G. and Smith, G. R. (2010). "RNAi and heterochromatin repress centromeric meiotic recombination." *Proc Natl Acad Sci U S A* **107**(19): 8701-8705.

Enquist-Newman, M., Cheeseman, I. M., Van Goor, D., Drubin, D. G., Meluh, P. B. and Barnes, G. (2001). "Dad1p, third component of the Duo1p/Dam1p complex involved in kinetochore function and mitotic spindle integrity." *Mol Biol Cell* **12**(9): 2601-2613.

Fedoroff, N. V. (2012). "Presidential address. Transposable elements, epigenetics, and genome evolution." *Science* **338**(6108): 758-767.

Feldbrugge, M., Kamper, J., Steinberg, G. and Kahmann, R. (2004). "Regulation of mating and pathogenic development in *Ustilago maydis*." *Curr Opin Microbiol* **7**(6): 666-672.

Fellmann, C. and Lowe, S. W. (2014). "Stable RNA interference rules for silencing." *Nat Cell Biol* **16**(1): 10-18.

Fennell, A., Fernandez-Alvarez, A., Tomita, K. and Cooper, J. P. (2015). "Telomeres and centromeres have interchangeable roles in promoting meiotic spindle formation." *J Cell Biol* **208**(4): 415-428.

Feretzaki, M., Billmyre, R. B., Clancey, S. A., Wang, X. and Heitman, J. (2016). "Gene network polymorphism illuminates loss and retention of novel rnai silencing components in the *Cryptococcus* pathogenic species complex." *PLoS Genet* **12**(3): e1005868.

Fernandez-Alvarez, A., Bez, C., O'Toole, E. T., Morphew, M. and Cooper, J. P. (2016). "Mitotic nuclear envelope breakdown and spindle nucleation are controlled by interphase contacts between centromeres and the nuclear envelope." *Dev Cell* **39**(5): 544-559.

Ferri, F., Bouzinba-Segard, H., Velasco, G., Hube, F. and Francastel, C. (2009). "Non-coding murine centromeric transcripts associate with and potentiate Aurora B kinase." *Nucleic Acids Res* **37**(15): 5071-5080.

Findley, K., Rodriguez-Carres, M., Metin, B., Kroiss, J., Fonseca, A., Vilgalys, R. and Heitman, J. (2009). "Phylogeny and phenotypic characterization of pathogenic *Cryptococcus* species and closely related saprobic taxa in the Tremellales." *Eukaryot Cell* **8**(3): 353-361.

Findley, K., Sun, S., Fraser, J. A., Hsueh, Y.-P., Averette, A. F., Li, W., Dietrich, F. S. and Heitman, J. (2012). "Discovery of a modified tetrapolar sexual cycle in *Cryptococcus amylolentus* and the evolution of *MAT* in the *Cryptococcus* species complex." *PLoS Genetics* **8**(2): e1002528.

Findley, K., Sun, S., Fraser, J. A., Hsueh, Y. P., Averette, A. F., Li, W., Dietrich, F. S. and Heitman, J. (2012). "Discovery of a modified tetrapolar sexual cycle in *Cryptococcus amylolentus* and the evolution of MAT in the *Cryptococcus* species complex." *PLoS Genet* **8**(2): e1002528.

Fink, G., Schuchardt, I., Colombelli, J., Stelzer, E. and Steinberg, G. (2006). "Dynein-mediated pulling forces drive rapid mitotic spindle elongation in *Ustilago maydis*." *EMBO J* **25**(20): 4897-4908.

Fitzgerald-Hayes, M., Clarke, L. and Carbon, J. (1982). "Nucleotide sequence comparisons and functional analysis of yeast centromere DNAs." *Cell* **29**(1): 235-244.

Flemming, W. (1882). *Zellsubstanz, Kern und Zelltheilung*, F. C. W. Vogel, Leipzig.

Foley, E. A. and Kapoor, T. M. (2013). "Microtubule attachment and spindle assembly checkpoint signalling at the kinetochore." *Nat Rev Mol Cell Biol* **14**(1): 25-37.

Foltz, D. R., Jansen, L. E., Black, B. E., Bailey, A. O., Yates, J. R., 3rd and Cleveland, D. W. (2006). "The human CENP-A centromeric nucleosome-associated complex." *Nat Cell Biol* **8**(5): 458-469.

Fournier, P., Abbas, A., Chasles, M., Kudla, B., Ogrydziak, D. M., Yaver, D., Xuan, J. W., Peito, A., Ribet, A. M., Feynerol, C. and et al. (1993). "Colocalization of centromeric and replicative functions on autonomously replicating sequences isolated from the yeast *Yarrowia lipolytica*." *Proc Natl Acad Sci U S A* **90**(11): 4912-4916.

Fraschini, R., Venturetti, M., Chiroli, E. and Piatti, S. (2008). "The spindle position checkpoint: how to deal with spindle misalignment during asymmetric cell division in budding yeast." *Biochem Soc Trans* **36**(Pt 3): 416-420.

Freitag, M. (2016). "The kinetochore interaction network (KIN) of ascomycetes." *Mycologia* **108**(3): 485-505.

Fukagawa, T. (2017). "Critical histone post-translational modifications for centromere function and propagation." *Cell Cycle*: 1-7.

Fukagawa, T. and Earnshaw, W. C. (2014). "The centromere: chromatin foundation for the kinetochore machinery." *Dev Cell* **30**(5): 496-508.

Fukagawa, T., Nogami, M., Yoshikawa, M., Ikeno, M., Okazaki, T., Takami, Y., Nakayama, T. and Oshimura, M. (2004). "Dicer is essential for formation of the heterochromatin structure in vertebrate cells." *Nat Cell Biol* **6**(8): 784-791.

Gao, D., Jiang, N., Wing, R. A., Jiang, J. and Jackson, S. A. (2015). "Transposons play an important role in the evolution and diversification of centromeres among closely related species." *Front Plant Sci* **6**: 216.

Ghildiyal, M. and Zamore, P. D. (2009). "Small silencing RNAs: an expanding universe." *Nat Rev Genet* **10**(2): 94-108.

Giam, M. and Rancati, G. (2015). "Aneuploidy and chromosomal instability in cancer: a jackpot to chaos." *Cell Div* **10**: 3.

Giannuzzi, G., Catacchio, C. R. and Ventura, M. (2012). *Centromere Evolution: Digging Into Mammalian Primary Constriction*, INTECH Open Access Publisher.

Gieni, R. S., Chan, G. K. and Hendzel, M. J. (2008). "Epigenetics regulate centromere formation and kinetochore function." *J Cell Biochem* **104**(6): 2027-2039.

Gladfelter, A. and Berman, J. (2009). "Dancing genomes: fungal nuclear positioning." *Nat Rev Microbiol* **7**(12): 875-886.

Gong, Z., Wu, Y., Koblizkova, A., Torres, G. A., Wang, K., Iovene, M., Neumann, P., Zhang, W., Novak, P., Buell, C. R., Macas, J. and Jiang, J. (2012). "Repeatless and repeat-based centromeres in potato: implications for centromere evolution." *Plant Cell* **24**(9): 3559-3574.

Goodier, J. L. and Kazazian, H. H., Jr. (2008). "Retrotransposons revisited: the restraint and rehabilitation of parasites." *Cell* **135**(1): 23-35.

Goodwin, T. J. and Poulter, R. T. (2001). "The diversity of retrotransposons in the yeast *Cryptococcus neoformans*." *Yeast* **18**(9): 865-880.

Goshima, G., Saitoh, S. and Yanagida, M. (1999). "Proper metaphase spindle length is determined by centromere proteins Mis12 and Mis6 required for faithful chromosome segregation." *Genes Dev* **13**(13): 1664-1677.

Goshima, G. and Yanagida, M. (2000). "Establishing Biorientation Occurs with Precocious Separation of the Sister Kinetochores, but Not the Arms, in the Early Spindle of Budding Yeast." *Cell* **100**(6): 619-633.

Grewal, S. I. and Klar, A. J. (1997). "A recombinationally repressed region between mat2 and mat3 loci shares homology to centromeric repeats and regulates directionality of mating-type switching in fission yeast." *Genetics* **146**(4): 1221-1238.

Gunawardane, R. N., Martin, O. C., Cao, K., Zhang, L., Dej, K., Iwamatsu, A. and Zheng, Y. (2000). "Characterization and reconstitution of *Drosophila* gamma-tubulin ring complex subunits." *J Cell Biol* **151**(7): 1513-1524.

Guttinger, S., Laurell, E. and Kutay, U. (2009). "Orchestrating nuclear envelope disassembly and reassembly during mitosis." *Nat Rev Mol Cell Biol* **10**(3): 178-191.

Hagan, I. and Yanagida, M. (1995). "The product of the spindle formation gene sad1+ associates with the fission yeast spindle pole body and is essential for viability." *J Cell Biol* **129**(4): 1033-1047.

Hagen, F., Khayhan, K., Theelen, B., Kolecka, A., Polacheck, I., Sionov, E., Falk, R., Parnmen, S., Lumbsch, H. T. and Boekhout, T. (2015). "Recognition of seven species in the *Cryptococcus gattii/Cryptococcus neoformans* species complex." *Fungal Genet Biol* **78**: 16-48.

Hall, I. M., Shankaranarayana, G. D., Noma, K., Ayoub, N., Cohen, A. and Grewal, S. I. (2002). "Establishment and maintenance of a heterochromatin domain." *Science* **297**(5590): 2232-2237.

Hall, L. E., Mitchell, S. E. and O'Neill, R. J. (2012). "Pericentric and centromeric transcription: a perfect balance required." *Chromosome Res* **20**(5): 535-546.

Hanisch, A., Sillje, H. H. and Nigg, E. A. (2006). "Timely anaphase onset requires a novel spindle and kinetochore complex comprising Ska1 and Ska2." *EMBO J* **25**(23): 5504-5515.

He, L. and Hannon, G. J. (2004). "MicroRNAs: small RNAs with a big role in gene regulation." *Nat Rev Genet* **5**(7): 522-531.

Heath, I. B. (1980). "Variant mitoses in lower eukaryotes: indicators of the evolution of mitosis." *Int Rev Cytol* **64**: 1-80.

Heikkinen, E., Launonen, V., Muller, E. and Bachmann, L. (1995). "The pvB370 BamHI satellite DNA family of the *Drosophila virilis* group and its evolutionary relation to mobile dispersed genetic pDv elements." *J Mol Evol* **41**(5): 604-614.

Heitman, J., Allen, B., Alspaugh, J. A. and Kwon-Chung, K. J. (1999). "On the origins of congenic MATalpha and MATa strains of the pathogenic yeast *Cryptococcus neoformans*." *Fungal Genet Biol* **28**(1): 1-5.

Heitman, J., Sun, S. and James, T. Y. (2013). "Evolution of fungal sexual reproduction." *Mycologia* **105**(1): 1-27.

Hemmerich, P., Stoyan, T., Wieland, G., Koch, M., Lechner, J. and Diekmann, S. (2000). "Interaction of yeast kinetochore proteins with centromere-protein/transcription factor Cbf1." *Proc Natl Acad Sci U S A* **97**(23): 12583-12588.

Henikoff, S., Ahmad, K. and Malik, H. S. (2001). "The centromere paradox: Stable inheritance with rapidly evolving DNA." *Science* **293**(5532): 1098-1102.

Henikoff, S. and Dalal, Y. (2005). "Centromeric chromatin: what makes it unique?" *Curr Opin Genet Dev* **15**(2): 177-184.

Hetzer, M. W. (2010). "The nuclear envelope." *Cold Spring Harb Perspect Biol* **2**(3): a000539.

Heus, J. J., Bloom, K. S., Zonneveld, B. J., Steensma, H. Y. and Van den Berg, J. A. (1993). "Chromatin structures of *Kluyveromyces lactis* centromeres in *K. lactis* and *Saccharomyces cerevisiae*." *Chromosoma* **102**(9): 660-667.

Heus, J. J., Zonneveld, B. J., de Steensma, H. Y. and van den Berg, J. A. (1993). "The consensus sequence of *Kluyveromyces lactis* centromeres shows homology to functional centromeric DNA from *Saccharomyces cerevisiae*." *Mol Gen Genet* **236**(2-3): 355-362.

Hieter, P., Mann, C., Snyder, M. and Davis, R. W. (1985). "Mitotic stability of yeast chromosomes: a colony color assay that measures nondisjunction and chromosome loss." *Cell* **40**(2): 381-392.

Hoelz, A., Debler, E. W. and Blobel, G. (2011). "The structure of the nuclear pore complex." *Annu Rev Biochem* **80**: 613-643.

Hofmann, C., Cheeseman, I. M., Goode, B. L., McDonald, K. L., Barnes, G. and Drubin, D. G. (1998). "*Saccharomyces cerevisiae* Duo1p and Dam1p, novel proteins involved in mitotic spindle function." *J Cell Biol* **143**(4): 1029-1040.

Horvitz, H. R. and Herskowitz, I. (1992). "Mechanisms of asymmetric cell division: two Bs or not two Bs, that is the question." *Cell* **68**(2): 237-255.

Hou, H., Kallgren, S. P. and Jia, S. (2013). "Csi1 illuminates the mechanism and function of Rabl configuration." *Nucleus* **4**(3).

Hou, H., Zhou, Z., Wang, Y., Wang, J., Kallgren, S. P., Kurchuk, T., Miller, E. A., Chang, F. and Jia, S. (2012). "Csi1 links centromeres to the nuclear envelope for centromere clustering." *J Cell Biol* **199**(5): 735-744.

Hua-Van, A., Le Rouzic, A., Maisonhaute, C. and Capy, P. (2005). "Abundance, distribution and dynamics of retrotransposable elements and transposons: similarities and differences." *Cytogenet Genome Res* **110**(1-4): 426-440.

Huff, J. T. and Zilberman, D. (2014). "Dnmt1-independent CG methylation contributes to nucleosome positioning in diverse eukaryotes." *Cell* **156**(6): 1286-1297.

Hwang, E., Kusch, J., Barral, Y. and Huffaker, T. C. (2003). "Spindle orientation in *Saccharomyces cerevisiae* depends on the transport of microtubule ends along polarized actin cables." *J Cell Biol* **161**(3): 483-488.

Idnurm, A. (2010). "A tetrad analysis of the basidiomycete fungus *Cryptococcus neoformans*." *Genetics* **185**(1): 153-163.

Iwasaki, Y. W., Siomi, M. C. and Siomi, H. (2015). "Piwi-interacting rna: Its biogenesis and functions." *Annu Rev Biochem* **84**: 405-433.

Jackson, A. P., Gamble, J. A., Yeomans, T., Moran, G. P., Saunders, D., Harris, D., Aslett, M., Barrell, J. F., Butler, G., Citiulo, F., Coleman, D. C., de Groot, P. W., Goodwin, T. J., Quail, M. A., McQuillan, J., Munro, C. A., Pain, A., Poulter, R. T., Rajandream, M. A., Renauld, H., Spiering, M. J., Tivey, A., Gow, N. A., Barrell, B., Sullivan, D. J. and Berriman, M. (2009). "Comparative genomics of the fungal pathogens *Candida dubliniensis* and *Candida albicans*." *Genome Res* **19**(12): 2231-2244.

Jakopec, V., Topolski, B. and Fleig, U. (2012). "Sos7, an essential component of the conserved *Schizosaccharomyces pombe* NDC80-MIND-Spc7 complex, identifies a new family of fungal kinetochore proteins." *Mol Cell Biol* **32**(16): 3308-3320.

Janbon, G., Maeng, S., Yang, D. H., Ko, Y. J., Jung, K. W., Moyrand, F., Floyd, A., Heitman, J. and Bahn, Y. S. (2010). "Characterizing the role of RNA silencing components in *Cryptococcus neoformans*." *Fungal Genet Biol* **47**(12): 1070-1080.

Janbon, G., Ormerod, K. L., Paulet, D., Byrnes, E. J., 3rd, Yadav, V., Chatterjee, G., Mullapudi, N., Hon, C. C., Billmyre, R. B., Brunel, F., Bahn, Y. S., Chen, W., Chen, Y., Chow, E. W., Coppee, J. Y., Floyd-Averette, A., Gaillardin, C., Gerik, K. J., Goldberg, J., Gonzalez-Hilarion, S., Gujja, S., Hamlin, J. L., Hsueh, Y. P., Ianiri, G., Jones, S., Kodira, C. D., Kozubowski, L., Lam, W., Marra, M., Mesner, L. D., Mieczkowski, P. A., Moyrand, F., Nielsen, K., Proux, C., Rossignol, T., Schein, J. E., Sun, S., Wollschlaeger, C., Wood, I. A., Zeng, Q., Neuveglise, C., Newlon, C. S., Perfect, J. R., Lodge, J. K., Idnurm, A., Stajich, J. E., Kronstad, J. W., Sanyal, K., Heitman, J., Fraser, J. A., Cuomo, C. A. and Dietrich, F. S. (2014). "Analysis of the genome and transcriptome of *Cryptococcus neoformans* var. *grubii* reveals complex RNA expression and microevolution leading to virulence attenuation." *PLoS Genet* **10**(4): e1004261.

Jaspersen, S. L., Martin, A. E., Glazko, G., Giddings, T. H., Jr., Morgan, G., Mushegian, A. and Winey, M. (2006). "The Sad1-UNC-84 homology domain in Mps3 interacts with Mps2 to connect the spindle pole body with the nuclear envelope." *J Cell Biol* **174**(5): 665-675.

Jin, Q. W., Fuchs, J. and Loidl, J. (2000). "Centromere clustering is a major determinant of yeast interphase nuclear organization." *J Cell Sci* **113 (Pt 11)**: 1903-1912.

Jin, W., Lamb, J. C., Zhang, W., Kolano, B., Birchler, J. A. and Jiang, J. (2008). "Histone modifications associated with both A and B chromosomes of maize." *Chromosome Res* **16**(8): 1203-1214.

Kadotani, N., Nakayashiki, H., Tosa, Y. and Mayama, S. (2003). "RNA silencing in the phytopathogenic fungus *Magnaporthe oryzae*." *Mol Plant Microbe Interact* **16**(9): 769-776.

Kamper, J., Kahmann, R., Bolker, M., Ma, L. J., Brefort, T., Saville, B. J., Banuett, F., Kronstad, J. W., Gold, S. E., Muller, O., Perlin, M. H., Wosten, H. A., de Vries, R., Ruiz-Herrera, J., Reynaga-Pena, C. G., Snetselaar, K., McCann, M., Perez-Martin, J., Feldbrugge, M., Basse, C. W., Steinberg, G., Ibeas, J. I., Holloman, W., Guzman, P., Farman, M., Stajich, J. E., Sentandreu, R., Gonzalez-Prieto, J. M., Kennell, J. C., Molina, L., Schirawski, J., Mendoza-Mendoza, A., Greilinger, D., Munch, K., Rossel, N., Scherer, M., Vranes, M., Ladendorf, O., Vincon, V., Fuchs, U., Sandrock, B., Meng, S., Ho, E. C., Cahill, M. J., Boyce, K. J., Klose, J., Klosterman, S. J., Deelstra, H. J., Ortiz-Castellanos, L., Li, W., Sanchez-Alonso, P., Schreier, P. H., Hauser-Hahn, I., Vaupel, M., Koopmann, E., Friedrich, G., Voss, H., Schluter, T., Margolis, J., Platt, D., Swimmer, C., Gnirke, A., Chen, F., Vysotskaia, V., Mannhaupt, G., Guldener, U., Munsterkotter, M., Haase, D., Oesterheld, M., Mewes, H. W., Mauceli, E. W., DeCaprio, D., Wade, C. M., Butler, J., Young, S., Jaffe, D. B., Calvo, S., Nusbaum, C., Galagan, J. and Birren, B. W. (2006). "Insights from the genome of the biotrophic fungal plant pathogen *Ustilago maydis*." *Nature* **444**(7115): 97-101.

Kanellopoulou, C., Muljo, S. A., Kung, A. L., Ganesan, S., Drapkin, R., Jenuwein, T., Livingston, D. M. and Rajewsky, K. (2005). "Dicer-deficient mouse embryonic stem cells are defective in differentiation and centromeric silencing." *Genes Dev* **19**(4): 489-501.

Kapitonov, V. V. and Jurka, J. (1999). "Molecular paleontology of transposable elements from *Arabidopsis thaliana*." *Genetica* **107**(1-3): 27-37.

Kapoor, S., Zhu, L., Froyd, C., Liu, T. and Rusche, L. N. (2015). "Regional centromeres in the yeast *Candida lusitaniae* lack pericentromeric heterochromatin." *Proc Natl Acad Sci U S A* **112**(39): 12139-12144.

Kearse, M., Moir, R., Wilson, A., Stones-Havas, S., Cheung, M., Sturrock, S., Buxton, S., Cooper, A., Markowitz, S., Duran, C., Thierer, T., Ashton, B., Meintjes, P. and Drummond, A. (2012). "Geneious Basic: An integrated and extendable desktop software platform for the organization and analysis of sequence data." *Bioinformatics* **28**(12): 1647-1649.

Kellner, N., Heimel, K., Obhof, T., Finkernagel, F. and Kamper, J. (2014). "The SPF27 homologue Num1 connects splicing and kinesin 1-dependent cytoplasmic trafficking in *Ustilago maydis*." *PLoS Genet* **10**(1): e1004046.

Kidd, S. E., Hagen, F., Tscharke, R. L., Huynh, M., Bartlett, K. H., Fyfe, M., Macdougall, L., Boekhout, T., Kwon-Chung, K. J. and Meyer, W. (2004). "A rare genotype of *Cryptococcus gattii* caused the cryptococcosis outbreak on Vancouver Island (British Columbia, Canada)." *Proc Natl Acad Sci U S A* **101**(49): 17258-17263.

Kim, D. and Rossi, J. (2008). "RNAi mechanisms and applications." *Biotechniques* **44**(5): 613-616.

Kim, D. I., Birendra, K. C. and Roux, K. J. (2015). "Making the LINC: SUN and KASH protein interactions." *Biol Chem* **396**(4): 295-310.

Kipling, D. and Warburton, P. E. (1997). "Centromeres, CENP-B and Tigger too." *Trends Genet* **13**(4): 141-145.

Kiseleva, E., Rutherford, S., Cotter, L. M., Allen, T. D. and Goldberg, M. W. (2001). "Steps of nuclear pore complex disassembly and reassembly during mitosis in early *Drosophila* embryos." *J Cell Sci* **114**(Pt 20): 3607-3618.

Klutstein, M., Fennell, A., Fernandez-Alvarez, A. and Cooper, J. P. (2015). "The telomere bouquet regulates meiotic centromere assembly." *Nat Cell Biol* **17**(4): 458-469.

Knoblich, J. A. (2008). "Mechanisms of asymmetric stem cell division." *Cell* **132**(4): 583-597.

Kobayashi, N., Suzuki, Y., Schoenfeld, L. W., Muller, C. A., Nieduszynski, C., Wolfe, K. H. and Tanaka, T. U. (2015). "Discovery of an unconventional centromere in budding yeast redefines evolution of point centromeres." *Curr Biol* **25**(15): 2026-2033.

Kollman, J. M., Polka, J. K., Zelter, A., Davis, T. N. and Agard, D. A. (2010). "Microtubule nucleating gamma-TuSC assembles structures with 13-fold microtubule-like symmetry." *Nature* **466**(7308): 879-882.

Kollman, J. M., Zelter, A., Muller, E. G., Fox, B., Rice, L. M., Davis, T. N. and Agard, D. A. (2008). "The structure of the gamma-tubulin small complex: implications of its architecture and flexibility for microtubule nucleation." *Mol Biol Cell* **19**(1): 207-215.

Koo, D. H., Han, F., Birchler, J. A. and Jiang, J. (2011). "Distinct DNA methylation patterns associated with active and inactive centromeres of the maize B chromosome." *Genome Res* **21**(6): 908-914.

Kosco, K. A., Pearson, C. G., Maddox, P. S., Wang, P. J., Adams, I. R., Salmon, E. D., Bloom, K. and Huffaker, T. C. (2001). "Control of microtubule dynamics by Stu2p is essential for spindle orientation and metaphase chromosome alignment in yeast." *Mol Biol Cell* **12**(9): 2870-2880.

Kozubowski, L., Aboobakar, E. F., Cardenas, M. E. and Heitman, J. (2011). "Calcineurin colocalizes with P-bodies and stress granules during thermal stress in *Cryptococcus neoformans*." *Eukaryot Cell* **10**(11): 1396-1402.

Kozubowski, L. and Heitman, J. (2010). "Septins enforce morphogenetic events during sexual reproduction and contribute to virulence of *Cryptococcus neoformans*." *Mol Microbiol* **75**(3): 658-675.

Kozubowski, L. and Heitman, J. (2011). "Profiling a killer, the development of *Cryptococcus neoformans*." *FEMS Microbiol Rev* **36**(1): 78-94.

Kozubowski, L., Yadav, V., Chatterjee, G., Sridhar, S., Yamaguchi, M., Kawamoto, S., Bose, I., Heitman, J. and Sanyal, K. (2013). "Ordered kinetochore assembly in the human-pathogenic basidiomycetous yeast *Cryptococcus neoformans*." *mBio* **4**(5): e00614-00613.

Kronstad, J. W., Attarian, R., Cadieux, B., Choi, J., D'Souza, C. A., Griffiths, E. J., Geddes, J. M., Hu, G., Jung, W. H., Kretschmer, M., Saikia, S. and Wang, J. (2011). "Expanding fungal pathogenesis: *Cryptococcus* breaks out of the opportunistic box." *Nat Rev Microbiol* **9**(3): 193-203.

Krueger, F. and Andrews, S. R. (2011). "Bismark: a flexible aligner and methylation caller for Bisulfite-Seq applications." *Bioinformatics* **27**(11): 1571-1572.

Kutay, U. and Hetzer, M. W. (2008). "Reorganization of the nuclear envelope during open mitosis." *Curr Opin Cell Biol* **20**(6): 669-677.

Kwon-Chung, K. J. and Chang, Y. C. (2012). "Aneuploidy and drug resistance in pathogenic fungi." *PLoS Pathog* **8**(11): e1003022.

Laan, L., Pavin, N., Husson, J., Romet-Lemonne, G., van Duijn, M., Lopez, M. P., Vale, R. D., Julicher, F., Reck-Peterson, S. L. and Dogterom, M. (2012). "Cortical dynein controls microtubule dynamics to generate pulling forces that position microtubule asters." *Cell* **148**(3): 502-514.

Lanver, D., Tollot, M., Schweizer, G., Lo Presti, L., Reissmann, S., Ma, L. S., Schuster, M., Tanaka, S., Liang, L., Ludwig, N. and Kahmann, R. (2017). "*Ustilago maydis* effectors and their impact on virulence." *Nat Rev Microbiol* **15**(7): 409-421.

Lara-Gonzalez, P., Westhorpe, F. G. and Taylor, S. S. (2012). "The spindle assembly checkpoint." *Curr Biol* **22**(22): R966-980.

Laurie, J. D., Ali, S., Linning, R., Mannhaupt, G., Wong, P., Guldener, U., Munsterkotter, M., Moore, R., Kahmann, R., Bakkeren, G. and Schirawski, J. (2012). "Genome comparison of barley and maize smut fungi reveals targeted loss of RNA silencing components and species-specific presence of transposable elements." *Plant Cell* **24**(5): 1733-1745.

Laurie, J. D., Linning, R. and Bakkeren, G. (2008). "Hallmarks of RNA silencing are found in the smut fungus *Ustilago hordei* but not in its close relative *Ustilago maydis*." *Curr Genet* **53**(1): 49-58.

Lechner, J. and Carbon, J. (1991). "A 240 kd multisubunit protein complex, CBF3, is a major component of the budding yeast centromere." *Cell* **64**(4): 717-725.

Lee, H. C., Aalto, A. P., Yang, Q., Chang, S. S., Huang, G., Fisher, D., Cha, J., Poranen, M. M., Bamford, D. H. and Liu, Y. (2010). "The DNA/RNA-dependent RNA polymerase QDE-1 generates aberrant RNA and dsRNA for RNAi in a process requiring replication protein A and a DNA helicase." *PLoS Biol* **8**(10).

Lee, L., Tirnauer, J. S., Li, J., Schuyler, S. C., Liu, J. Y. and Pellman, D. (2000). "Positioning of the mitotic spindle by a cortical-microtubule capture mechanism." *Science* **287**(5461): 2260-2262.

Li, H. and Durbin, R. (2009). "Fast and accurate short read alignment with Burrows-Wheeler transform." *Bioinformatics* **25**(14): 1754-1760.

Li, H., Handsaker, B., Wysoker, A., Fennell, T., Ruan, J., Homer, N., Marth, G., Abecasis, G., Durbin, R. and Genome Project Data Processing, S. (2009). "The Sequence Alignment/Map format and SAMtools." *Bioinformatics* **25**(16): 2078-2079.

Lin, T. C., Neuner, A. and Schiebel, E. (2015). "Targeting of gamma-tubulin complexes to microtubule organizing centers: conservation and divergence." *Trends Cell Biol* **25**(5): 296-307.

Lin, T. C., Neuner, A., Schlosser, Y. T., Scharf, A. N., Weber, L. and Schiebel, E. (2014). "Cell-cycle dependent phosphorylation of yeast pericentrin regulates gamma-TuSC-mediated microtubule nucleation." *eLife* **3**: e02208.

Lin, X. (2009). "*Cryptococcus neoformans*: morphogenesis, infection, and evolution." *Infect Genet Evol* **9**(4): 401-416.

Lin, X. and Heitman, J. (2006). "The biology of the *Cryptococcus neoformans* species complex." *Annu Rev Microbiol* **60**: 69-105.

Linning, R., Lin, D., Lee, N., Abdennadher, M., Gaudet, D., Thomas, P., Mills, D., Kronstad, J. W. and Bakkeren, G. (2004). "Marker-based cloning of the region containing the UhAvr1 avirulence gene from the basidiomycete barley pathogen *Ustilago hordei*." *Genetics* **166**(1): 99-111.

Liu, S. T., Rattner, J. B., Jablonski, S. A. and Yen, T. J. (2006). "Mapping the assembly pathways that specify formation of the trilaminar kinetochore plates in human cells." *J Cell Biol* **175**(1): 41-53.

Liu, X., McLeod, I., Anderson, S., Yates, J. R., 3rd and He, X. (2005). "Molecular analysis of kinetochore architecture in fission yeast." *EMBO J* **24**(16): 2919-2930.

Lo, A. W., Magliano, D. J., Sibson, M. C., Kalitsis, P., Craig, J. M. and Choo, K. H. (2001). "A novel chromatin immunoprecipitation and array (CIA) analysis identifies a 460-kb CENP-A-binding neocentromere DNA." *Genome Res* **11**(3): 448-457.

Loftus, B. J., Fung, E., Roncaglia, P., Rowley, D., Amedeo, P., Bruno, D., Vamathevan, J., Miranda, M., Anderson, I. J., Fraser, J. A., Allen, J. E., Bosdet, I. E., Brent, M. R., Chiu, R., Doering, T. L., Donlin, M. J., D'Souza, C. A., Fox, D. S., Grinberg, V., Fu, J., Fukushima, M., Haas, B. J., Huang, J. C., Janbon, G., Jones, S. J., Koo, H. L., Krzywinski, M. I., Kwon-Chung, J. K., Lengeler, K. B., Maiti, R., Marra, M. A., Marra, R. E., Mathewson, C. A., Mitchell, T. G., Pertea, M., Riggs, F. R., Salzberg, S. L., Schein, J. E., Shvartsbeyn, A., Shin, H., Shumway, M., Specht, C. A., Suh, B. B., Tenney, A., Utterback, T. R., Wickes, B. L., Wortman, J. R., Wye, N. H., Kronstad, J. W., Lodge, J. K., Heitman, J., Davis, R. W., Fraser, C. M. and Hyman, R. W. (2005). "The genome of the basidiomycetous yeast and human pathogen *Cryptococcus neoformans*." *Science* **307**(5713): 1321-1324.

Loiodice, I., Alves, A., Rabut, G., Van Overbeek, M., Ellenberg, J., Sibarita, J. B. and Doye, V. (2004). "The entire Nup107-160 complex, including three new members, is targeted as one entity to kinetochores in mitosis." *Mol Biol Cell* **15**(7): 3333-3344.

Luders, J. and Stearns, T. (2007). "Microtubule-organizing centres: a re-evaluation." *Nat Rev Mol Cell Biol* **8**(2): 161-167.

Luxton, G. W. and Starr, D. A. (2014). "KASHing up with the nucleus: novel functional roles of KASH proteins at the cytoplasmic surface of the nucleus." *Curr Opin Cell Biol* **28**: 69-75.

Lynch, D. B., Logue, M. E., Butler, G. and Wolfe, K. H. (2010). "Chromosomal G + C content evolution in yeasts: systematic interspecies differences, and GC-poor troughs at centromeres." *Genome Biol Evol* **2**: 572-583.

Malik, H. S. and Henikoff, S. (2003). "Phylogenomics of the nucleosome." *Nat Struct Biol* **10**(11): 882-891.

Mallik, R. and Gross, S. P. (2004). "Molecular motors: strategies to get along." *Curr Biol* **14**(22): R971-982.

Maloisel, L. and Rossignol, J. L. (1998). "Suppression of crossing-over by DNA methylation in *Ascobolus*." *Genes Dev* **12**(9): 1381-1389.

Mandrioli, M. and Manicardi, G. C. (2012). "Unlocking holocentric chromosomes: new perspectives from comparative and functional genomics?" *Curr Genomics* **13**(5): 343-349.

Markus, S. M., Kalutkiewicz, K. A. and Lee, W.-L. (2012). "Astral microtubule asymmetry provides directional cues for spindle positioning in budding yeast." *Experimental Cell Research* **318**(12): 1400-1406.

Markus, S. M. and Lee, W. L. (2011). "Microtubule-dependent path to the cell cortex for cytoplasmic dynein in mitotic spindle orientation." *Bioarchitecture* **1**(5): 209-215.

Marques, A., Ribeiro, T., Neumann, P., Macas, J., Novak, P., Schubert, V., Pellino, M., Fuchs, J., Ma, W., Kuhlmann, M., Brandt, R., Vanzela, A. L., Beseda, T., Simkova, H., Pedrosa-Harand, A. and Houben, A. (2015). "Holocentromeres in *Rhynchospora* are associated with genome-wide centromere-specific repeat arrays interspersed among euchromatin." *Proc Natl Acad Sci U S A* **112**(44): 13633-13638.

Marshall, W. F., Dernburg, A. F., Harmon, B., Agard, D. A. and Sedat, J. W. (1996). "Specific interactions of chromatin with the nuclear envelope: positional determination within the nucleus in *Drosophila melanogaster*." *Mol Biol Cell* **7**(5): 825-842.

Martin, R., Walther, A. and Wendland, J. (2004). "Deletion of the dynein heavy-chain gene DYN1 leads to aberrant nuclear positioning and defective hyphal development in *Candida albicans*." *Eukaryot Cell* **3**(6): 1574-1588.

Masumoto, H., Nakano, M. and Ohzeki, J. (2004). "The role of CENP-B and alpha-satellite DNA: de novo assembly and epigenetic maintenance of human centromeres." *Chromosome Res* **12**(6): 543-556.

Matzke, M. A. and Birchler, J. A. (2005). "RNAi-mediated pathways in the nucleus." *Nat Rev Genet* **6**(1): 24-35.

Matzke, M. A. and Mosher, R. A. (2014). "RNA-directed DNA methylation: an epigenetic pathway of increasing complexity." *Nat Rev Genet* **15**(6): 394-408.

May, R. C., Stone, N. R., Wiesner, D. L., Bicanic, T. and Nielsen, K. (2016). "*Cryptococcus*: from environmental saprophyte to global pathogen." *Nat Rev Microbiol* **14**(2): 106-117.

McAinsh, A. D., Tytell, J. D. and Sorger, P. K. (2003). "Structure, function, and regulation of budding yeast kinetochores." *Annu Rev Cell Dev Biol* **19**: 519-539.

McGrew, J., Diehl, B. and Fitzgerald-Hayes, M. (1986). "Single base-pair mutations in centromere element III cause aberrant chromosome segregation in *Saccharomyces cerevisiae*." *Mol Cell Biol* **6**(2): 530-538.

McIntosh, J. R. and O'Toole, E. T. (1999). "Life cycles of yeast spindle pole bodies: getting microtubules into a closed nucleus." *Biol Cell* **91**(4-5): 305-312.

Meier, I. (2016). "LINCing the eukaryotic tree of life - towards a broad evolutionary comparison of nucleocytoplasmic bridging complexes." *J Cell Sci* **129**(19): 3523-3531.

Melters, D. P., Bradnam, K. R., Young, H. A., Telis, N., May, M. R., Ruby, J. G., Sebra, R., Peluso, P., Eid, J., Rank, D., Garcia, J. F., DeRisi, J. L., Smith, T., Tobias, C., Ross-Ibarra, J., Korf, I. and Chan, S. W. (2013). "Comparative analysis of tandem repeats from hundreds of species reveals unique insights into centromere evolution." *Genome Biol* **14**(1): R10.

Melters, D. P., Paliulis, L. V., Korf, I. F. and Chan, S. W. (2012). "Holocentric chromosomes: convergent evolution, meiotic adaptations, and genomic analysis." *Chromosome Res* **20**(5): 579-593.

Meluh, P. B. and Koshland, D. (1995). "Evidence that the *MIF2* gene of *Saccharomyces cerevisiae* encodes a centromere protein with homology to the mammalian centromere protein CENP-C." *Mol Biol Cell* **6**(7): 793-807.

Meluh, P. B., Yang, P., Glowczewski, L., Koshland, D. and Smith, M. M. (1998). "Cse4p Is a component of the core centromere of *Saccharomyces cerevisiae*." *Cell* **94**(5): 607-613.

Meraldi, P., McAinsh, A. D., Rheinbay, E. and Sorger, P. K. (2006). "Phylogenetic and structural analysis of centromeric DNA and kinetochore proteins." *Genome Biol* **7**(3): R23.

Milks, K. J., Moree, B. and Straight, A. F. (2009). "Dissection of CENP-C-directed centromere and kinetochore assembly." *Mol Biol Cell* **20**(19): 4246-4255.

Miranda, J. J., De Wulf, P., Sorger, P. K. and Harrison, S. C. (2005). "The yeast DASH complex forms closed rings on microtubules." *Nat Struct Mol Biol* **12**(2): 138-143.

Mirouze, M., Lieberman-Lazarovich, M., Aversano, R., Bucher, E., Nicolet, J., Reinders, J. and Paszkowski, J. (2012). "Loss of DNA methylation affects the recombination landscape in *Arabidopsis*." *Proc Natl Acad Sci U S A* **109**(15): 5880-5885.

Moroi, Y., Peebles, C., Fritzler, M. J., Steigerwald, J. and Tan, E. M. (1980). "Autoantibody to centromere (kinetochore) in scleroderma sera." *Proc Natl Acad Sci U S A* **77**(3): 1627-1631.

Mouyna, I., Henry, C., Doering, T. L. and Latge, J. P. (2004). "Gene silencing with RNA interference in the human pathogenic fungus *Aspergillus fumigatus*." *FEMS Microbiol Lett* **237**(2): 317-324.

Murchison, E. P., Partridge, J. F., Tam, O. H., Cheloufi, S. and Hannon, G. J. (2005). "Characterization of Dicer-deficient murine embryonic stem cells." *Proc Natl Acad Sci U S A* **102**(34): 12135-12140.

Murphy, S. M., Preble, A. M., Patel, U. K., O'Connell, K. L., Dias, D. P., Moritz, M., Agard, D., Stults, J. T. and Stearns, T. (2001). "GCP5 and GCP6: two new members of the human gamma-tubulin complex." *Mol Biol Cell* **12**(11): 3340-3352.

Musacchio, A. and Desai, A. (2017). "A Molecular View of Kinetochore Assembly and Function." *Biology (Basel)* **6**(1).

Muszewska, A., Hoffman-Sommer, M. and Grynberg, M. (2011). "LTR retrotransposons in fungi." *PLoS ONE* **6**(12): e29425.

Nagaki, K., Cheng, Z., Ouyang, S., Talbert, P. B., Kim, M., Jones, K. M., Henikoff, S., Buell, C. R. and Jiang, J. (2004). "Sequencing of a rice centromere uncovers active genes." *Nat Genet* **36**(2): 138-145.

Nakagawa, H., Lee, J. K., Hurwitz, J., Allshire, R. C., Nakayama, J., Grewal, S. I., Tanaka, K. and Murakami, Y. (2002). "Fission yeast CENP-B homologs nucleate centromeric heterochromatin by promoting heterochromatin-specific histone tail modifications." *Genes Dev* **16**(14): 1766-1778.

Nakano, M., Cardinale, S., Noskov, V. N., Gassmann, R., Vagnarelli, P., Kandels-Lewis, S., Larionov, V., Earnshaw, W. C. and Masumoto, H. (2008). "Inactivation of a human kinetochore by specific targeting of chromatin modifiers." *Dev Cell* **14**(4): 507-522.

Nakayashiki, H. (2005). "RNA silencing in fungi: mechanisms and applications." *FEBS Lett* **579**(26): 5950-5957.

Nakayashiki, H., Kadotani, N. and Mayama, S. (2006). "Evolution and diversification of RNA silencing proteins in fungi." *J Mol Evol* **63**(1): 127-135.

Nekrasov, V. S., Smith, M. A., Peak-Chew, S. and Kilmartin, J. V. (2003). "Interactions between centromere complexes in *Saccharomyces cerevisiae*." *Mol Biol Cell* **14**(12): 4931-4946.

Neumann, P., Navratilova, A., Koblizkova, A., Kejnovsky, E., Hribova, E., Hobza, R., Widmer, A., Dolezel, J. and Macas, J. (2011). "Plant centromeric retrotransposons: a structural and cytogenetic perspective." *Mob DNA* **2**(1): 4.

Neumuller, R. A. and Knoblich, J. A. (2009). "Dividing cellular asymmetry: asymmetric cell division and its implications for stem cells and cancer." *Genes Dev* **23**(23): 2675-2699.

Ng, R. and Carbon, J. (1987). "Mutational and in vitro protein-binding studies on centromere DNA from *Saccharomyces cerevisiae*." *Mol Cell Biol* **7**(12): 4522-4534.

Ni, M., Feretzaki, M., Sun, S., Wang, X. and Heitman, J. (2011). "Sex in fungi." *Annu Rev Genet* **45**: 405-430.

Nielsen, K., Cox, G. M., Wang, P., Toffaletti, D. L., Perfect, J. R. and Heitman, J. (2003). "Sexual cycle of *Cryptococcus neoformans* var. *grubii* and virulence of congenic a and alpha isolates." *Infect Immun* **71**(9): 4831-4841.

Nielsen, M. L., Hermansen, T. D. and Aleksenko, A. (2001). "A family of DNA repeats in *Aspergillus nidulans* has assimilated degenerated retrotransposons." *Mol Genet Genomics* **265**(5): 883-887.

Nishino, T., Takeuchi, K., Gascoigne, K. E., Suzuki, A., Hori, T., Oyama, T., Morikawa, K., Cheeseman, I. M. and Fukagawa, T. (2012). "CENP-T-W-S-X forms a unique centromeric chromatin structure with a histone-like fold." *Cell* **148**(3): 487-501.

Obbard, D. J., Gordon, K. H., Buck, A. H. and Jiggins, F. M. (2009). "The evolution of RNAi as a defence against viruses and transposable elements." *Philos Trans R Soc Lond B Biol Sci* **364**(1513): 99-115.

Ohkuma, M., Kobayashi, K., Kawai, S., Hwang, C. W., Ohta, A. and Takagi, M. (1995). "Identification of a centromeric activity in the autonomously replicating TRA region allows improvement of the host-vector system for *Candida maltosa*." *Mol Gen Genet* **249**(4): 447-455.

Ohkuni, K. and Kitagawa, K. (2011). "Endogenous transcription at the centromere facilitates centromere activity in budding yeast." *Curr Biol* **21**(20): 1695-1703.

Ohkusu, M., Raclavsky, V. and Takeo, K. (2004). "Induced synchrony in *Cryptococcus neoformans* after release from G2-arrest." *Antonie Van Leeuwenhoek* **85**(1): 37-44.

Ortiz, J., Stemmann, O., Rank, S. and Lechner, J. (1999). "A putative protein complex consisting of Ctf19, Mcm21, and Okp1 represents a missing link in the budding yeast kinetochore." *Genes Dev* **13**(9): 1140-1155.

Padeken, J., Mendiburo, M. J., Chlamydas, S., Schwarz, H. J., Kremmer, E. and Heun, P. (2013). "The nucleoplasmin homolog NLP mediates centromere clustering and anchoring to the nucleolus." *Mol Cell* **50**(2): 236-249.

Padmanabhan, S., Thakur, J., Siddharthan, R. and Sanyal, K. (2008). "Rapid evolution of Cse4p-rich centromeric DNA sequences in closely related pathogenic yeasts, *Candida albicans* and *Candida dubliniensis*." *Proc Natl Acad Sci U S A* **105**(50): 19797-19802.

Pagliuca, C., Draviam, V. M., Marco, E., Sorger, P. K. and De Wulf, P. (2009). "Roles for the conserved spc105p/kre28p complex in kinetochore-microtubule binding and the spindle assembly checkpoint." *PLoS ONE* **4**(10): e7640.

Perez-Martin, J., Castillo-Lluva, S., Sgarlata, C., Flor-Parra, I., Mielnichuk, N., Torreblanca, J. and Carbo, N. (2006). "Pathocycles: *Ustilago maydis* as a model to study the relationships between cell cycle and virulence in pathogenic fungi." *Mol Genet Genomics* **276**(3): 211-229.

Perfect, J. R., Ketabchi, N., Cox, G. M., Ingram, C. W. and Beiser, C. L. (1993). "Karyotyping of *Cryptococcus neoformans* as an epidemiological tool." *J Clin Microbiol* **31**(12): 3305-3309.

Petrovic, A., Keller, J., Liu, Y., Overlack, K., John, J., Dimitrova, Y. N., Jenni, S., van Gerwen, S., Stege, P., Wohlgemuth, S., Rombaut, P., Herzog, F., Harrison, S. C., Vetter, I. R. and Musacchio, A. (2016). "Structure of the MIS12 complex and molecular basis of its interaction with CENP-C at human kinetochores." *Cell* **167**(4): 1028-1040 e1015.

Pidoux, A. L. and Allshire, R. C. (2004). "Kinetochore and heterochromatin domains of the fission yeast centromere." *Chromosome Res* **12**(6): 521-534.

Pidoux, A. L., Choi, E. S., Abbott, J. K., Liu, X., Kagansky, A., Castillo, A. G., Hamilton, G. L., Richardson, W., Rappsilber, J., He, X. and Allshire, R. C. (2009). "Fission yeast Scm3: A CENP-A receptor required for integrity of subkinetochore chromatin." *Mol Cell* **33**(3): 299-311.

Piegu, B., Bire, S., Arensburger, P. and Bigot, Y. (2015). "A survey of transposable element classification systems - a call for a fundamental update to meet the challenge of their diversity and complexity." *Mol Phylogenet Evol* **86**: 90-109.

Potapova, T. and Gorbsky, G. J. (2017). "The Consequences of Chromosome Segregation Errors in Mitosis and Meiosis." *Biology (Basel)* **6**(1).

Przewloka, M. R., Zhang, W., Costa, P., Archambault, V., D'Avino, P. P., Lilley, K. S., Laue, E. D., McAinsh, A. D. and Glover, D. M. (2007). "Molecular analysis of core kinetochore composition and assembly in *Drosophila melanogaster*." *PLoS ONE* **2**(5): e478.

Rabe, F., Bosch, J., Stirnberg, A., Guse, T., Bauer, L., Seitner, D., Rabanal, F. A., Czedik-Eysenberg, A., Uhse, S., Bindics, J., Genenncher, B., Navarrete, F., Kellner, R., Ekker, H., Kumlehn, J., Vogel, J. P., Gordon, S. P., Marcel, T. C., Munsterkotter, M., Walter, M. C., Sieber, C. M., Mannhaupt, G., Guldener, U., Kahmann, R. and Djamei, A. (2016). "A complete toolset for the study of *Ustilago bromivora* and *Brachypodium* sp. as a fungal-temperate grass pathosystem." *eLife* **5:e20522**.

Rajasingham, R., Smith, R. M., Park, B. J., Jarvis, J. N., Govender, N. P., Chiller, T. M., Denning, D. W., Loyse, A. and Boulware, D. R. (2017). "Global burden of disease of HIV-associated cryptococcal meningitis: an updated analysis." *Lancet Infect Dis*.

Razafsky, D. and Hodzic, D. (2009). "Bringing KASH under the SUN: the many faces of nucleo-cytoskeletal connections." *J Cell Biol* **186**(4): 461-472.

Reinhart, B. J. and Bartel, D. P. (2002). "Small RNAs correspond to centromere heterochromatic repeats." *Science* **297**(5588): 1831.

Rhind, N., Chen, Z., Yassour, M., Thompson, D. A., Haas, B. J., Habib, N., Wapinski, I., Roy, S., Lin, M. F., Heiman, D. I., Young, S. K., Furuya, K., Guo, Y., Pidoux, A., Chen, H. M., Robbertse, B., Goldberg, J. M., Aoki, K., Bayne, E. H., Berlin, A. M., Desjardins, C. A., Dobbs, E., Dukaj, L., Fan, L., FitzGerald, M. G., French, C., Gujja, S., Hansen, K., Keifenheim, D., Levin, J. Z., Mosher, R. A., Muller, C. A., Pfiffner, J., Priest, M., Russ, C., Smialowska, A., Swoboda, P., Sykes, S. M., Vaughn, M., Vengrova, S., Yoder, R., Zeng, Q., Allshire, R., Baulcombe, D., Birren, B. W., Brown, W., Ekwall, K., Kellis, M., Leatherwood, J., Levin, H., Margalit, H., Martienssen, R., Nieduszynski, C. A., Spatafora, J. W., Friedman, N., Dalgaard, J. Z., Baumann, P., Niki, H., Regev, A. and Nusbaum, C. (2011). "Comparative functional genomics of the fission yeasts." *Science* **332**(6032): 930-936.

Richmond, D., Rizkallah, R., Liang, F., Hurt, M. M. and Wang, Y. (2013). "Slk19 clusters kinetochores and facilitates chromosome bipolar attachment." *Mol Biol Cell* **24**(5): 566-577.

Robinson, J. T., Thorvaldsdottir, H., Winckler, W., Guttman, M., Lander, E. S., Getz, G. and Mesirov, J. P. (2011). "Integrative genomics viewer." *Nat Biotechnol* **29**(1): 24-26.

Romano, N. and Macino, G. (1992). "Quelling: transient inactivation of gene expression in *Neurospora crassa* by transformation with homologous sequences." *Mol Microbiol* **6**(22): 3343-3353.

Roy, B., Burrack, L. S., Lone, M. A., Berman, J. and Sanyal, K. (2011). "CaMtw1, a member of the evolutionarily conserved Mis12 kinetochore protein family, is required for efficient inner kinetochore assembly in the pathogenic yeast *Candida albicans*." *Mol Microbiol* **80**(1): 14-32.

Roy, B. and Sanyal, K. (2011). "Diversity in requirement of genetic and epigenetic factors for centromere function in fungi." *Eukaryot Cell* **10**(11): 1384-1395.

Roy, B., Varshney, N., Yadav, V. and Sanyal, K. (2013). "The process of kinetochore assembly in yeasts." *FEMS Microbiol Lett* **338**(2): 107-117.

Ruff, J. A., Lodge, J. K. and Baker, L. G. (2009). "Three galactose inducible promoters for use in *C. neoformans* var. *grubii*." *Fungal Genet Biol* **46**(1): 9-16.

Saffery, R., Sumer, H., Hassan, S., Wong, L. H., Craig, J. M., Todokoro, K., Anderson, M., Stafford, A. and Choo, K. H. (2003). "Transcription within a functional human centromere." *Mol Cell* **12**(2): 509-516.

Sanchez-Perez, I., Renwick, S. J., Crawley, K., Karig, I., Buck, V., Meadows, J. C., Franco-Sanchez, A., Fleig, U., Toda, T. and Millar, J. B. (2005). "The DASH complex and Klp5/Klp6 kinesin coordinate bipolar chromosome attachment in fission yeast." *EMBO J* **24**(16): 2931-2943.

Sansregret, L. and Swanton, C. (2017). "The role of aneuploidy in cancer evolution." *Cold Spring Harb Perspect Med* **7**(1).

Sanyal, K., Baum, M. and Carbon, J. (2004). "Centromeric DNA sequences in the pathogenic yeast *Candida albicans* are all different and unique." *Proc Natl Acad Sci U S A.* **101**(31): 11374-11379.

Sanyal, K. and Carbon, J. (2002). "The CENP-A homolog CaCse4p in the pathogenic yeast *Candida albicans* is a centromere protein essential for chromosome transmission." *Proc Natl Acad Sci U S A.* **99**(20): 12969-12974.

Sato, A., Isaac, B., Phillips, C. M., Rillo, R., Carlton, P. M., Wynne, D. J., Kasad, R. A. and Dernburg, A. F. (2009). "Cytoskeletal forces span the nuclear envelope to coordinate meiotic chromosome pairing and synapsis." *Cell* **139**(5): 907-919.

Schmidt, J. C., Arthanari, H., Boeszoermenyi, A., Dashkevich, N. M., Wilson-Kubalek, E. M., Monnier, N., Markus, M., Oberer, M., Milligan, R. A., Bathe, M., Wagner, G., Grishchuk, E. L. and Cheeseman, I. M. (2012). "The kinetochore-bound Ska1 complex tracks depolymerizing microtubules and binds to curved protofilaments." *Dev Cell* **23**(5): 968-980.

Schnable, P. S., Ware, D., Fulton, R. S., Stein, J. C., Wei, F., Pasternak, S., Liang, C., Zhang, J., Fulton, L., Graves, T. A., Minx, P., Reily, A. D., Courtney, L., Kruchowski, S. S., Tomlinson, C., Strong, C., Delehaunty, K., Fronick, C., Courtney, B., Rock, S. M., Belter, E., Du, F., Kim, K., Abbott, R. M., Cotton, M., Levy, A., Marchetto, P., Ochoa, K., Jackson, S. M., Gillam, B., Chen, W., Yan, L., Higginbotham, J., Cardenas, M., Waligorski, J., Applebaum, E., Phelps, L., Falcone, J., Kanchi, K., Thane, T., Scimone, A., Thane, N., Henke, J., Wang, T., Ruppert, J., Shah, N., Rotter, K., Hodges, J., Ingenthron, E., Cordes, M., Kohlberg, S., Sgro, J., Delgado, B., Mead, K., Chinwalla, A., Leonard, S., Crouse, K., Collura, K., Kudrna, D., Currie, J., He, R., Angelova, A., Rajasekar, S., Mueller, T., Lomeli, R., Scara, G., Ko, A., Delaney, K., Wissotski, M., Lopez, G., Campos, D., Braidotti, M., Ashley, E., Golser, W., Kim, H., Lee, S., Lin, J., Dujmic, Z., Kim, W., Talag, J., Zuccolo, A., Fan, C., Sebastian, A., Kramer, M., Spiegel, L., Nascimento, L., Zutavern, T., Miller, B., Ambroise, C., Muller, S., Spooner, W., Narechania, A., Ren, L., Wei, S., Kumari, S., Faga, B., Levy, M. J., McMahan, L., Van Buren, P., Vaughn, M. W., Ying, K., Yeh, C. T., Emrich, S. J., Jia, Y., Kalyanaraman, A., Hsia, A. P., Barbazuk, W. B., Baucom, R. S., Brutnell, T. P., Carpita, N. C., Chaparro, C., Chia, J. M., Deragon, J. M., Estill, J. C., Fu, Y., Jeddeloh, J. A., Han, Y., Lee, H., Li, P., Lisch, D. R., Liu, S., Liu, Z., Nagel, D. H., McCann, M. C., SanMiguel, P., Myers, A. M., Nettleton, D., Nguyen, J., Penning, B. W., Ponnala, L., Schneider, K. L., Schwartz, D. C., Sharma, A., Soderlund, C., Springer, N. M., Sun, Q., Wang, H., Waterman, M., Westerman, R., Wolfgruber, T. K., Yang, L., Yu, Y., Zhang, L., Zhou, S., Zhu, Q., Bennetzen, J. L., Dawe, R. K., Jiang, J., Jiang, N., Presting, G. G., Wessler, S. R., Aluru, S., Martienssen, R. A., Clifton, S. W., McCombie, W. R., Wing, R. A. and Wilson, R. K. (2009). "The B73 maize genome: complexity, diversity, and dynamics." *Science* **326**(5956): 1112-1115.

Schneider, K. L., Xie, Z., Wolfgruber, T. K. and Presting, G. G. (2016). "Inbreeding drives maize centromere evolution." *Proc Natl Acad Sci U S A* **113**(8): E987-996.

Scott, K. C. (2013). "Transcription and ncRNAs: at the cent(rome)re of kinetochore assembly and maintenance." *Chromosome Res* **21**(6-7): 643-651.

Scott, K. C. and Bloom, K. S. (2014). "Lessons learned from counting molecules: how to lure CENP-A into the kinetochore." *Open Biol* **4**(12).

Servant, G. and Deininger, P. L. (2015). "Insertion of retrotransposons at chromosome ends: Adaptive response to chromosome maintenance." *Front Genet* **6**: 358.

Shang, W. H., Hori, T., Martins, N. M., Toyoda, A., Misu, S., Monma, N., Hiratani, I., Maeshima, K., Ikeo, K., Fujiyama, A., Kimura, H., Earnshaw, W. C. and Fukagawa, T. (2013). "Chromosome engineering allows the efficient isolation of vertebrate neocentromeres." *Dev Cell* **24**(6): 635-648.

Shang, W. H., Hori, T., Toyoda, A., Kato, J., Popendorf, K., Sakakibara, Y., Fujiyama, A. and Fukagawa, T. (2010). "Chickens possess centromeres with both extended tandem repeats and short non-tandem-repetitive sequences." *Genome Res* **20**(9): 1219-1228.

Shibuya, H. and Watanabe, Y. (2014). "The meiosis-specific modification of mammalian telomeres." *Cell Cycle* **13**(13): 2024-2028.

Shiu, P. K., Raju, N. B., Zickler, D. and Metzenberg, R. L. (2001). "Meiotic silencing by unpaired DNA." *Cell* **107**(7): 905-916.

Simon, D. N. and Wilson, K. L. (2011). "The nucleoskeleton as a genome-associated dynamic 'network of networks'." *Nat Rev Mol Cell Biol* **12**(11): 695-708.

Simon, L., Voisin, M., Tatout, C. and Probst, A. V. (2015). "Structure and function of centromeric and pericentromeric heterochromatin in *Arabidopsis thaliana*." *Front Plant Sci* **6**: 1049.

Sinzelle, L., Izsvak, Z. and Ivics, Z. (2009). "Molecular domestication of transposable elements: from detrimental parasites to useful host genes." *Cell Mol Life Sci* **66**(6): 1073-1093.

Smith, K. M., Phatale, P. A., Sullivan, C. M., Pomraning, K. R. and Freitag, M. (2011). "Heterochromatin is required for normal distribution of *Neurospora crassa* CenH3." *Mol Cell Biol* **31**(12): 2528-2542.

Snetselaar, K. and McCann, M. (2017). "*Ustilago maydis*, the corn smut fungus, has an unusual diploid mitotic stage." *Mycologia* **109**(1): 140-152.

Srikanta, D., Santiago-Tirado, F. H. and Doering, T. L. (2014). "*Cryptococcus neoformans*: historical curiosity to modern pathogen." *Yeast* **31**(2): 47-60.

Starr, D. A. (2009). "A nuclear-envelope bridge positions nuclei and moves chromosomes." *J Cell Sci* **122**(Pt 5): 577-586.

Starr, D. A., Saffery, R., Li, Z., Simpson, A. E., Choo, K. H., Yen, T. J. and Goldberg, M. L. (2000). "HZwint-1, a novel human kinetochore component that interacts with HZW10." *J Cell Sci* **113 (Pt 11)**: 1939-1950.

Stavru, F., Hulsmann, B. B., Spang, A., Hartmann, E., Cordes, V. C. and Gorlich, D. (2006). "NDC1: a crucial membrane-integral nucleoporin of metazoan nuclear pore complexes." *J Cell Biol* **173**(4): 509-519.

Steinberg, G., Wedlich-Soldner, R., Brill, M. and Schulz, I. (2001). "Microtubules in the fungal pathogen *Ustilago maydis* are highly dynamic and determine cell polarity." *J Cell Sci* **114**(Pt 3): 609-622.

Steiner, F. A. and Henikoff, S. (2014). "Holocentromeres are dispersed point centromeres localized at transcription factor hotspots." *eLife* **3**: e02025.

Steiner, N. C., Hahnenberger, K. M. and Clarke, L. (1993). "Centromeres of the fission yeast *Schizosaccharomyces pombe* are highly variable genetic loci." *Mol Cell Biol* **13**(8): 4578-4587.

Stoler, S., Rogers, K., Weitze, S., Morey, L., Fitzgerald-Hayes, M. and Baker, R. E. (2007). "Scm3, an essential *Saccharomyces cerevisiae* centromere protein required for G2/M progression and Cse4 localization." *Proc Natl Acad Sci U S A* **104**(25): 10571-10576.

Straube, A., Brill, M., Oakley, B. R., Horio, T. and Steinberg, G. (2003). "Microtubule organization requires cell cycle-dependent nucleation at dispersed cytoplasmic sites: polar and perinuclear microtubule organizing centers in the plant pathogen *Ustilago maydis*." *Mol Biol Cell* **14**(2): 642-657.

Straube, A., Weber, I. and Steinberg, G. (2005). "A novel mechanism of nuclear envelope break-down in a fungus: nuclear migration strips off the envelope." *EMBO J* **24**(9): 1674-1685.

Sullivan, B. A. and Karpen, G. H. (2004). "Centromeric chromatin exhibits a histone modification pattern that is distinct from both euchromatin and heterochromatin." *Nat Struct Mol Biol* **11**(11): 1076-1083.

Sullivan, K. F. and Glass, C. A. (1991). "CENP-B is a highly conserved mammalian centromere protein with homology to the helix-loop-helix family of proteins." *Chromosoma* **100**(6): 360-370.

Sultana, T., Zamborlini, A., Cristofari, G. and Lesage, P. (2017). "Integration site selection by retroviruses and transposable elements in eukaryotes." *Nat Rev Genet* **18**(5): 292-308.

Sun, X., Wahlstrom, J. and Karpen, G. (1997). "Molecular structure of a functional *Drosophila* centromere." *Cell* **91**(7): 1007-1019.

Sutradhar, S., Yadav, V., Sridhar, S., Sreekumar, L., Bhattacharyya, D., Ghosh, S. K., Paul, R. and Sanyal, K. (2015). "A comprehensive model to predict mitotic division in budding yeasts." *Mol Biol Cell* **26**(22): 3954-3965.

Suzuki, A., Badger, B. L., Haase, J., Ohashi, T., Erickson, H. P., Salmon, E. D. and Bloom, K. (2016). "How the kinetochore couples microtubule force and centromere stretch to move chromosomes." *Nat Cell Biol* **18**(4): 382-392.

Swartz, R. K., Rodriguez, E. C. and King, M. C. (2014). "A role for nuclear envelope-bridging complexes in homology-directed repair." *Mol Biol Cell* **25**(16): 2461-2471.

Taddei, A. and Gasser, S. M. (2012). "Structure and function in the budding yeast nucleus." *Genetics* **192**(1): 107-129.

Taddei, A., Schober, H. and Gasser, S. M. (2010). "The budding yeast nucleus." *Cold Spring Harb Perspect Biol* **2**(8): a000612.

Takahashi, K., Chen, E. S. and Yanagida, M. (2000). "Requirement of Mis6 centromere connector for localizing a CENP-A-like protein in fission yeast." *Science* **288**(5474): 2215-2219.

Takeo, S., Lake, C. M., Morais-de-Sa, E., Sunkel, C. E. and Hawley, R. S. (2011). "Synaptonemal complex-dependent centromeric clustering and the initiation of synapsis in *Drosophila* oocytes." *Curr Biol* **21**(21): 1845-1851.

Talbert, P. B., Bayes, J. J. and Henikoff, S. (2009). Evolution of Centromeres and Kinetochores: A Two-Part Fugue. *The Kinetochore:: From Molecular Discoveries to Cancer Therapy*. P. De Wulf and W. C. Earnshaw. New York, NY, Springer New York: 1-37.

Tanaka, K., Chang, H. L., Kagami, A. and Watanabe, Y. (2009). "CENP-C functions as a scaffold for effectors with essential kinetochore functions in mitosis and meiosis." *Dev Cell* **17**(3): 334-343.

Tanaka, K., Kitamura, E. and Tanaka, T. U. (2010). "Live-cell analysis of kinetochore-microtubule interaction in budding yeast." *Methods* **51**(2): 206-213.

Tanaka, T. U. (2010). "Kinetochore-microtubule interactions: steps towards bi-orientation." *EMBO J* **29**(24): 4070-4082.

Tanneti, N. S., Landy, K., Joyce, E. F. and McKim, K. S. (2011). "A pathway for synapsis initiation during zygotene in *Drosophila* oocytes." *Curr Biol* **21**(21): 1852-1857.

Teixido-Travesa, N., Roig, J. and Luders, J. (2012). "The where, when and how of microtubule nucleation - one ring to rule them all." *J Cell Sci* **125**(Pt 19): 4445-4456.

Ten Hoopen, R., Cepeda-Garcia, C., Fernandez-Arruti, R., Juanes, M. A., Delgehyr, N. and Segal, M. (2012). "Mechanism for astral microtubule capture by cortical Bud6p priming spindle polarity in *S. cerevisiae*." *Curr Biol* **22**(12): 1075-1083.

Thakur, J. and Sanyal, K. (2011). "The essentiality of the fungus-specific Dam1 complex is correlated with a one-kinetochore-one-microtubule interaction present throughout the cell cycle, independent of the nature of a centromere." *Eukaryot Cell* **10**(10): 1295-1305.

Thakur, J. and Sanyal, K. (2012). "A coordinated interdependent protein circuitry stabilizes the kinetochore ensemble to protect CENP-A in the human pathogenic yeast *Candida albicans*." *PLoS Genet* **8**(4): e1002661.

Thakur, J. and Sanyal, K. (2013). "Efficient neocentromere formation is suppressed by gene conversion to maintain centromere function at native physical chromosomal loci in *Candida albicans*." *Genome Res* **23**(4): 638-652.

Theisen, U., Straube, A. and Steinberg, G. (2008). "Dynamic rearrangement of nucleoporins during fungal "open" mitosis." *Mol Biol Cell* **19**(3): 1230-1240.

Thorvaldsdottir, H., Robinson, J. T. and Mesirov, J. P. (2013). "Integrative Genomics Viewer (IGV): high-performance genomics data visualization and exploration." *Brief Bioinform* **14**(2): 178-192.

Topp, C. N., Zhong, C. X. and Dawe, R. K. (2004). "Centromere-encoded RNAs are integral components of the maize kinetochore." *Proc Natl Acad Sci U S A* **101**(45): 15986-15991.

Torres-Martinez, S. and Ruiz-Vazquez, R. M. (2016). "RNAi pathways in *Mucor*: A tale of proteins, small RNAs and functional diversity." *Fungal Genet Biol* **90**: 44-52.

Ungricht, R. and Kutay, U. (2017). "Mechanisms and functions of nuclear envelope remodelling." *Nat Rev Mol Cell Biol* **18**(4): 229-245.

Vagin, V. V., Sigova, A., Li, C., Seitz, H., Gvozdev, V. and Zamore, P. D. (2006). "A distinct small RNA pathway silences selfish genetic elements in the germline." *Science* **313**(5785): 320-324.

Valverde, R., Ingram, J. and Harrison, S. C. (2016). "Conserved tetramer junction in the kinetochore Ndc80 complex." *Cell Rep* **17**(8): 1915-1922.

Varma, D. and Salmon, E. D. (2012). "The KMN protein network--chief conductors of the kinetochore orchestra." *J Cell Sci* **125**(Pt 24): 5927-5936.

Venkei, Z., Przewloka, M. R. and Glover, D. M. (2011). "*Drosophila* Mis12 complex acts as a single functional unit essential for anaphase chromosome movement and a robust spindle assembly checkpoint." *Genetics* **187**(1): 131-140.

Vernis, L., Poljak, L., Chasles, M., Uchida, K., Casaregola, S., Kas, E., Matsuoka, M., Gaillardin, C. and Fournier, P. (2001). "Only centromeres can supply the partition system required for ARS function in the yeast *Yarrowia lipolytica*." *J Mol Biol* **305**(2): 203-217.

Villalobos-Escobedo, J. M., Herrera-Estrella, A. and Carreras-Villasenor, N. (2016). "The interaction of fungi with the environment orchestrated by RNAi." *Mycologia* **108**(3): 556-571.

Vissel, B. and Choo, K. H. (1989). "Mouse major (gamma) satellite DNA is highly conserved and organized into extremely long tandem arrays: implications for recombination between nonhomologous chromosomes." *Genomics* **5**(3): 407-414.

Vitte, C. and Panaud, O. (2005). "LTR retrotransposons and flowering plant genome size: emergence of the increase/decrease model." *Cytogenet Genome Res* **110**(1-4): 91-107.

Volpe, T. and Martienssen, R. A. (2011). "RNA interference and heterochromatin assembly." *Cold Spring Harb Perspect Biol* **3**(9): a003731.

Volpe, T., Schramke, V., Hamilton, G. L., White, S. A., Teng, G., Martienssen, R. A. and Allshire, R. C. (2003). "RNA interference is required for normal centromere function in fission yeast." *Chromosome Res* **11**(2): 137-146.

Volpe, T. A., Kidner, C., Hall, I. M., Teng, G., Grewal, S. I. and Martienssen, R. A. (2002). "Regulation of heterochromatic silencing and histone H3 lysine-9 methylation by RNAi." *Science* **297**(5588): 1833-1837.

Wade, R. H. (2009). "On and around microtubules: an overview." *Mol Biotechnol* **43**(2): 177-191.

Wang, H., Oliferenko, S. and Balasubramanian, M. K. (2003). "Cytokinesis: relative alignment of the cell division apparatus and the mitotic spindle." *Curr Opin Cell Biol* **15**(1): 82-87.

Wang, K., Wu, Y., Zhang, W., Dawe, R. K. and Jiang, J. (2014). "Maize centromeres expand and adopt a uniform size in the genetic background of oat." *Genome Res* **24**(1): 107-116.

Wang, X., Hsueh, Y. P., Li, W., Floyd, A., Skalsky, R. and Heitman, J. (2010). "Sex-induced silencing defends the genome of *Cryptococcus neoformans* via RNAi." *Genes Dev* **24**(22): 2566-2582.

Wargacki, M. M., Tay, J. C., Muller, E. G., Asbury, C. L. and Davis, T. N. (2010). "Kip3, the yeast kinesin-8, is required for clustering of kinetochores at metaphase." *Cell Cycle* **9**(13): 2581-2588.

Wei, R. R., Al-Bassam, J. and Harrison, S. C. (2007). "The Ndc80/HEC1 complex is a contact point for kinetochore-microtubule attachment." *Nat Struct Mol Biol* **14**(1): 54-59.

Weick, E. M. and Miska, E. A. (2014). "piRNAs: from biogenesis to function." *Development* **141**(18): 3458-3471.

Wente, S. R. and Rout, M. P. (2010). "The nuclear pore complex and nuclear transport." *Cold Spring Harb Perspect Biol* **2**(10).

Wertheimer, N. B., Stone, N. and Berman, J. (2016). "Ploidy dynamics and evolvability in fungi." *Philos Trans R Soc Lond B Biol Sci* **371**(1709).

Westermann, S. and Schleiffer, A. (2013). "Family matters: structural and functional conservation of centromere-associated proteins from yeast to humans." *Trends Cell Biol* **23**(6): 260-269.

Westhorpe, F. G. and Straight, A. F. (2013). "Functions of the centromere and kinetochore in chromosome segregation." *Curr Opin Cell Biol* **25**(3): 334-340.

Westhorpe, F. G. and Straight, A. F. (2014). "The centromere: epigenetic control of chromosome segregation during mitosis." *Cold Spring Harb Perspect Biol* **7**(1): a015818.

Wickes, B. L. and Edman, J. C. (1995). "The *Cryptococcus neoformans GAL7* gene and its use as an inducible promoter." *Mol Microbiol* **16**(6): 1099-1109.

Wienholds, E. and Plasterk, R. H. (2005). "MicroRNA function in animal development." *FEBS Lett* **579**(26): 5911-5922.

Wigge, P. A. and Kilmartin, J. V. (2001). "The Ndc80p complex from *Saccharomyces cerevisiae* contains conserved centromere components and has a function in chromosome segregation." *J Cell Biol* **152**(2): 349-360.

Williams, J. S., Hayashi, T., Yanagida, M. and Russell, P. (2009). "Fission yeast Scm3 mediates stable assembly of Cnp1/CENP-A into centromeric chromatin." *Mol Cell* **33**(3): 287-298.

Wong, A. K. and Rattner, J. B. (1988). "Sequence organization and cytological localization of the minor satellite of mouse." *Nucleic Acids Res* **16**(24): 11645-11661.

Wong, L. H., Brettingham-Moore, K. H., Chan, L., Quach, J. M., Anderson, M. A., Northrop, E. L., Hannan, R., Saffery, R., Shaw, M. L., Williams, E. and Choo, K. H. (2007). "Centromere RNA is a key component for the assembly of nucleoproteins at the nucleolus and centromere." *Genome Res* **17**(8): 1146-1160.

Wong, L. H. and Choo, K. H. (2004). "Evolutionary dynamics of transposable elements at the centromere." *Trends Genet* **20**(12): 611-616.

Wood, V., Gwilliam, R., Rajandream, M. A., Lyne, M., Lyne, R., Stewart, A., Sgouros, J., Peat, N., Hayles, J., Baker, S., Basham, D., Bowman, S., Brooks, K., Brown, D., Brown, S., Chillingworth, T., Churcher, C., Collins, M., Connor, R., Cronin, A., Davis, P., Feltwell, T., Fraser, A., Gentles, S., Goble, A., Hamlin, N., Harris, D., Hidalgo, J., Hodgson, G., Holroyd, S., Hornsby, T., Howarth, S., Huckle, E. J., Hunt, S., Jagels, K., James, K., Jones, L., Jones, M., Leather, S., McDonald, S., McLean, J., Mooney, P., Moule, S., Mungall, K., Murphy, L., Niblett, D., Odell, C., Oliver, K., O'Neil, S., Pearson, D., Quail, M. A., Rabbinowitsch, E., Rutherford, K., Rutter, S., Saunders, D., Seeger, K., Sharp, S., Skelton, J., Simmonds, M., Squares, R., Squares, S., Stevens, K., Taylor, K., Taylor, R. G., Tivey, A., Walsh, S., Warren, T., Whitehead, S., Woodward, J., Volckaert, G., Aert, R., Robben, J., Grymonprez, B., Weltjens, I., Vanstreels, E., Rieger, M., Schafer, M., Muller-Auer, S., Gabel, C., Fuchs, M., Dusterhoft, A., Fritzc, C., Holzer, E., Moestl, D., Hilbert, H., Borzym, K., Langer, I., Beck, A., Lehrach, H., Reinhardt, R., Pohl, T. M., Eger, P., Zimmermann, W., Wedler, H., Wambutt, R., Purnelle, B., Goffeau, A., Cadieu, E., Dreano, S., Gloux, S., Lelaure, V., Mottier, S., Galibert, F., Aves, S. J., Xiang, Z., Hunt, C., Moore, K., Hurst, S. M., Lucas, M., Rochet, M., Gaillardin, C., Tallada, V. A., Garzon, A., Thode, G., Daga, R. R., Cruzado, L., Jimenez, J., Sanchez, M., del Rey, F., Benito, J., Dominguez, A., Revuelta, J. L., Moreno, S., Armstrong, J., Forsburg, S. L., Cerutti, L., Lowe, T., McCombie, W. R., Paulsen, I., Potashkin, J., Shpakovski, G. V., Ussery, D., Barrell, B. G. and Nurse, P. (2002). "The genome sequence of *Schizosaccharomyces pombe*." *Nature* **415**(6874): 871-880.

Xiang, X. (2012). "Nuclear positioning: dynein needed for microtubule shrinkage-coupled movement." *Curr Biol* **22**(12): 044.

Xu, Z. and Wang, H. (2007). "LTR_FINDER: an efficient tool for the prediction of full-length LTR retrotransposons." *Nucleic Acids Res* **35**(Web Server issue): W265-268.

Yam, C., He, Y., Zhang, D., Chiam, K. H. and Oliferenko, S. (2011). "Divergent strategies for controlling the nuclear membrane satisfy geometric constraints during nuclear division." *Curr Biol* **21**(15): 1314-1319.

Yamagata, K., Yamazaki, T., Miki, H., Ogonuki, N., Inoue, K., Ogura, A. and Baba, T. (2007). "Centromeric DNA hypomethylation as an epigenetic signature discriminates between germ and somatic cell lineages." *Dev Biol* **312**(1): 419-426.

Yamaguchi, M., Biswas, S. K., Ohkusu, M. and Takeo, K. (2009). "Dynamics of the spindle pole body of the pathogenic yeast *Cryptococcus neoformans* examined by freeze-substitution electron microscopy." *FEMS Microbiol Lett* **296**(2): 257-265.

Ye, A. A. and Maresca, T. J. (2013). "Cell division: kinetochores SKAdaddle." *Curr Biol* **23**(3): R122-124.

Yelina, N. E., Lambing, C., Hardcastle, T. J., Zhao, X., Santos, B. and Henderson, I. R. (2015). "DNA methylation epigenetically silences crossover hot spots and controls chromosomal domains of meiotic recombination in *Arabidopsis*." *Genes Dev* **29**(20): 2183-2202.

Zeng, K., de las Heras, J. I., Ross, A., Yang, J., Cooke, H. and Shen, M. H. (2004). "Localisation of centromeric proteins to a fraction of mouse minor satellite DNA on a mini-chromosome in human, mouse and chicken cells." *Chromosoma* **113**(2): 84-91.

Zhang, H., Koblizkova, A., Wang, K., Gong, Z., Oliveira, L., Torres, G. A., Wu, Y., Zhang, W., Novak, P., Buell, C. R., Macas, J. and Jiang, J. (2014). "Boom-bust turnovers of megabase-sized centromeric DNA in *solanum* species: Rapid evolution of DNA sequences associated with centromeres." *Plant Cell* **26**(4): 1436-1447.

Zhang, W., Lee, H. R., Koo, D. H. and Jiang, J. (2008). "Epigenetic modification of centromeric chromatin: hypomethylation of DNA sequences in the CENH3-associated chromatin in *Arabidopsis thaliana* and maize." *Plant Cell* **20**(1): 25-34.

Zhang, X., Yazaki, J., Sundaresan, A., Cokus, S., Chan, S. W., Chen, H., Henderson, I. R., Shinn, P., Pellegrini, M., Jacobsen, S. E. and Ecker, J. R. (2006). "Genome-wide high-resolution mapping and functional analysis of DNA methylation in arabidopsis." *Cell* **126**(6): 1189-1201.

Zhang, Y., Liu, T., Meyer, C. A., Eeckhoute, J., Johnson, D. S., Bernstein, B. E., Nusbaum, C., Myers, R. M., Brown, M., Li, W. and Liu, X. S. (2008). "Model-based analysis of ChIP-Seq (MACS)." *Genome Biol* **9**(9): R137.

Zhong, C. X., Marshall, J. B., Topp, C., Mroczek, R., Kato, A., Nagaki, K., Birchler, J. A., Jiang, J. and Dawe, R. K. (2002). "Centromeric retroelements and satellites interact with maize kinetochore protein CENH3." *Plant Cell* **14**(11): 2825-2836.

Zhou, J., Fu, Y., Xie, J., Li, B., Jiang, D., Li, G. and Cheng, J. (2012). "Identification of microRNA-like RNAs in a plant pathogenic fungus *Sclerotinia sclerotiorum* by high-throughput sequencing." *Mol Genet Genomics* **287**(4): 275-282.

Zhou, Q., Wang, Z., Zhang, J., Meng, H. and Huang, B. (2012). "Genome-wide identification and profiling of microRNA-like RNAs from *Metarhizium anisopliae* during development." *Fungal Biol* **116**(11): 1156-1162.

Zhou, X., Graumann, K. and Meier, I. (2015). "The plant nuclear envelope as a multifunctional platform LINCed by SUN and KASH." *J Exp Bot* **66**(6): 1649-1659.

Zhou, Z., Feng, H., Zhou, B. R., Ghirlando, R., Hu, K., Zwolak, A., Miller Jenkins, L. M., Xiao, H., Tjandra, N., Wu, C. and Bai, Y. (2011). "Structural basis for recognition of centromere histone variant CenH3 by the chaperone Scm3." *Nature* **472**(7342): 234-237.

Zimmer, C. and Fabre, E. (2011). "Principles of chromosomal organization: lessons from yeast." *J Cell Biol* **192**(5): 723-733.

8. LIST OF PUBLICATIONS

Publications related to the thesis work

1. Roy, B., Varshney, N., **Yadav, V.** and Sanyal, K. (2013). "The process of kinetochore assembly in yeasts." *FEMS Microbiol Lett* **338**(2): 107-117.

2. Kozubowski*, L., **Yadav*, V.**, Chatterjee, G., Sridhar, S., Yamaguchi, M., Kawamoto, S., Bose, I., Heitman, J. and Sanyal, K. (2013). "Ordered kinetochore assembly in the human-pathogenic basidiomycetous yeast *Cryptococcus neoformans*." *mBio* **4**(5): e00614-00613. (cover page article)

3. Janbon, G., Ormerod, K. L., Paulet, D., Byrnes, E. J., 3rd, **Yadav, V.**, Chatterjee, G., Mullapudi, N., Hon, C. C., Billmyre, R. B., Brunel, F., Bahn, Y. S., Chen, W., Chen, Y., Chow, E. W., Coppee, J. Y., Floyd-Averette, A., Gaillardin, C., Gerik, K. J., Goldberg, J., Gonzalez-Hilarion, S., Gujja, S., Hamlin, J. L., Hsueh, Y. P., Ianiri, G., Jones, S., Kodira, C. D., Kozubowski, L., Lam, W., Marra, M., Mesner, L. D., Mieczkowski, P. A., Moyrand, F., Nielsen, K., Proux, C., Rossignol, T., Schein, J. E., Sun, S., Wollschlaeger, C., Wood, I. A., Zeng, Q., Neuveglise, C., Newlon, C. S., Perfect, J. R., Lodge, J. K., Idnurm, A., Stajich, J. E., Kronstad, J. W., Sanyal, K., Heitman, J., Fraser, J. A., Cuomo, C. A. and Dietrich, F. S. (2014). "Analysis of the genome and transcriptome of *Cryptococcus neoformans* var. *grubii* reveals complex RNA expression and microevolution leading to virulence attenuation." *PLoS Genet* **10**(4): e1004261.

4. Sutradhar*, S., **Yadav*, V.**, Sridhar*, S., Sreekumar, L., Bhattacharyya, D., Ghosh, S. K., Paul, R. and Sanyal, K. (2015). "A comprehensive model to predict mitotic division in budding yeasts." *Mol Biol Cell* **26**(22): 3954-3965. (cover page article)

5. Sun, S., **Yadav, V.**, Billmyre, R. B., Cuomo, C. A., Nowrousian, M., Wang, L., Souciet, J. L., Boekhout, T., Porcel, B., Wincker, P., Granek, J. A., Sanyal, K. and Heitman, J. (2017). "Fungal genome and mating system transitions facilitated by chromosomal translocations involving intercentromeric recombination." *PLoS Biol* **15**(8): e2002527.

6. **Yadav, V.**, Sun, S., Billmyre, B., Bakkeren, G., Heitman, J. and Sanyal, K. (2017). "RNAi-dependent accelerated centromere evolution in closely related fungal species." *Proc Natl Acad Sci U S A* (under revision).

7. **Yadav, V.** and Sanyal K. (2017). "Spatio-temporal regulation of kinetochore clustering by the SUN domain protein Sad1 in *Cryptococcus neoformans*." (manuscript under preparation)

*, equal contribution

Publications from other collaborative work

1. Hoque, J., Akkapeddi, P., **Yadav, V.**, Manjunath, G. B., Uppu, D. S., Konai, M. M., Yarlagadda, V., Sanyal, K. and Haldar, J. (2015). "Broad spectrum antibacterial and antifungal polymeric paint materials: synthesis, structure-activity relationship, and membrane-active mode of action." *ACS Appl Mater Interfaces* **7**(3): 1804-1815.

2. Datta*, A., **Yadav*, V.**, Ghosh, A., Choi, J., Bhattacharyya, D., Kar, R. K., Ilyas, H., Dutta, A., An, E., Mukhopadhyay, J., Lee, D., Sanyal, K., Ramamoorthy, A. and Bhunia, A. (2016). "Mode of Action of a Designed Antimicrobial Peptide: High Potency against *Cryptococcus neoformans*." *Biophys J* **111**(8): 1724-1737.

3. Hoque, J., Adhikary, U., **Yadav, V.**, Samaddar, S., Konai, M. M., Prakash, R. G., Paramanandham, K., Shome, B. R., Sanyal, K. and Haldar, J. (2016). "Chitosan Derivatives Active against Multidrug-Resistant Bacteria and Pathogenic Fungi: In Vivo Evaluation as Topical Antimicrobials." *Mol Pharm* **13**(10): 3578-3589.

4. Ghosh, C., **Yadav, V.**, Younis, W., Mohammad, H., Hegazy, Y. A., Seleem, M. N., Sanyal, K. and Haldar, J. (2017). "Aryl-alkyl-lysines: Membrane-Active Fungicides That Act against Biofilms of *Candida albicans*." *ACS Infect Dis* **3**(4): 293-301.

*, equal contribution

MINIREVIEW

The process of kinetochore assembly in yeasts

Babhrubahan Roy, Neha Varshney, Vikas Yadav & Kaustuv Sanyal

Molecular Mycology Laboratory, Molecular Biology and Genetics Unit, Jawaharlal Nehru Centre for Advanced Scientific Research, Bangalore, India

Correspondence: Kaustuv Sanyal, Molecular Mycology Laboratory, Molecular Biology and Genetics Unit, Jawaharlal Nehru Centre for Advanced Scientific Research, Jakkur Post, Bangalore 560 064, India. Tel: +91 80 2208 2878; fax: +91 80 2208 2766; e-mail: sanyal@jncasr.ac.in

Received 1 September 2012; revised 29 September 2012; accepted 1 October 2012. Final version published online 29 October 2012.

DOI: 10.1111/1574-6968.12019

Editor: Derek Sullivan

Keywords
centromere; evolution; kinetochore recruitment; spindle; microtubules; yeast.

Abstract

High fidelity chromosome segregation is essential for efficient transfer of the genetic material from the mother to daughter cells. The kinetochore (KT), which connects the centromere DNA to the spindle apparatus, plays a pivotal role in this process. In spite of considerable divergence in the centromere DNA sequence, basic architecture of a KT is evolutionarily conserved from yeast to humans. However, the identification of a large number of KT proteins paved the way of understanding conserved and diverged regulatory steps that lead to the formation of a multiprotein KT super-complex on the centromere DNA in different organisms. Because it is a daunting task to summarize the entire spectrum of information in a minireview, we focus here on the recent understanding in the process of KT assembly in three yeasts: *Saccharomyces cerevisiae*, *Schizosaccharomyces pombe* and *Candida albicans*. Studies in these unicellular organisms suggest that although the basic process of KT assembly remains the same, the dependence of a conserved protein for its KT localization may vary in these organisms.

Introduction

The precise transmission of the genetic information from one generation to the next during the mitotic cell cycle is extremely important for a eukaryotic organism. This process involves faithful duplication of the whole genome during S phase followed by segregation of the duplicated genome with high fidelity during mitosis. The molecular mechanisms that ensure equal distribution of duplicated chromosomes in mitosis require proper assembly of a large multiprotein complex at the centromere (*CEN*), known as the kinetochore (KT). The primary function of a KT is to attach the chromosome to the dynamic plus ends of spindle microtubules (MTs), a crucial step in segregation of chromosomes. KTs are also associated with the formation of heterochromatin at the centromeric/pericentric regions and maintenance of cohesion between sister chromatids till anaphase onset (Cleveland *et al.*, 2003; Cheeseman & Desai, 2008). Additionally, a KT is involved in the recruitment of the spindle assembly checkpoint machinery that monitors the KT-MT attachment and initiates signals to prevent cell cycle progression if an error persists. Once all the chromosomes are bi-orientated, separation of two sister chromatids marks the onset of anaphase. Any defect in the KT structure can disrupt KT–MT interaction that may result in an unequal distribution of chromosomes leading to aneuploidy.

Cellular events associated with the mitotic cell cycle

In metazoan cells, the nuclear envelope breaks down during mitosis that allows KT–MT interaction to facilitate bi-oriented chromosomes to arrange on a plane known as the metaphase plate (Nasmyth, 2001; Guttinger *et al.*, 2009). In contrast, the nuclear envelope never breaks down in budding yeasts and thus cells undergo closed mitosis without formation of a metaphase plate (Straight *et al.*, 1997; Sazer, 2005; De Souza & Osmani, 2007). Existence of a metaphase plate is unlikely in *Schizosaccharomyces pombe* and *Candida albicans* as well. Interestingly, a semi-open mitosis has been reported recently in fission yeast *Schizosaccharomyces japonicus* (Aoki *et al.*, 2011; Yam *et al.*, 2011). The nuclear envelope breaks down only during anaphase in this organism. The nuclear envelope virtually breaks down by increasing its permeability during both mitosis and meiosis in *S. pombe* as well (Asakawa *et al.*, 2010, 2011). These studies indicate

FEMS MICROBIOLOGY LETTERS

RESEARCH ARTICLE

Ordered Kinetochore Assembly in the Human-Pathogenic Basidiomycetous Yeast *Cryptococcus neoformans*

Lukasz Kozubowski,[a,b] Vikas Yadav,[c] Gautam Chatterjee,[c] Shreyas Sridhar,[c] Masashi Yamaguchi,[d] Susumu Kawamoto,[d] Indrani Bose,[e] Joseph Heitman,[b] Kaustuv Sanyal[c]

Division of Infectious Diseases, Department of Medicine, Duke University Medical Center, Durham, North Carolina, USA[a]; Department of Molecular Genetics and Microbiology, Duke University Medical Center, Durham, North Carolina, USA[b]; Molecular Mycology Laboratory, Molecular Biology and Genetics Unit, Jawaharlal Nehru Centre for Advanced Scientific Research, Bangalore, India[c]; Medical Mycology Research Center, Chiba University, Chiba, Japan[d]; Department of Biology, Western Carolina University, Cullowhee, North Carolina, USA[e]

L.K. and V.Y. contributed equally to this work

ABSTRACT **Kinetochores facilitate interaction between chromosomes and the spindle apparatus. The formation of a metazoan trilayered kinetochore is an ordered event in which inner, middle, and outer layers assemble during disassembly of the nuclear envelope during mitosis. The existence of a similar strong correlation between kinetochore assembly and nuclear envelope breakdown in unicellular eukaryotes is unclear. Studies in the hemiascomycetous budding yeasts *Saccharomyces cerevisiae* and *Candida albicans* suggest that an ordered kinetochore assembly may not be evolutionarily conserved. Here, we utilized high-resolution time-lapse microscopy to analyze the localization patterns of a series of putative kinetochore proteins in the basidiomycetous budding yeast *Cryptococcus neoformans*, a human pathogen. Strikingly, similar to most metazoa but atypical of yeasts, the centromeres are not clustered but positioned adjacent to the nuclear envelope in premitotic *C. neoformans* cells. The centromeres gradually coalesce to a single cluster as cells progress toward mitosis. The mitotic clustering of centromeres seems to be dependent on the integrity of the mitotic spindle. To study the dynamics of the nuclear envelope, we followed the localization of two marker proteins, Ndc1 and Nup107. Fluorescence microscopy of the nuclear envelope and components of the kinetochore, along with ultrastructure analysis by transmission electron microscopy, reveal that in *C. neoformans*, the kinetochore assembles in an ordered manner prior to mitosis in concert with a partial opening of the nuclear envelope. Taken together, the results of this study demonstrate that kinetochore dynamics in *C. neoformans* is reminiscent of that of metazoans and shed new light on the evolution of mitosis in eukaryotes.**

IMPORTANCE **Successful propagation of genetic material in progeny is essential for the survival of any organism. A proper kinetochore-microtubule interaction is crucial for high-fidelity chromosome segregation. An error in this process can lead to loss or gain of chromosomes, a common feature of most solid cancers. Several proteins assemble on centromere DNA to form a kinetochore. However, significant differences in the process of kinetochore assembly exist between unicellular yeasts and multicellular metaozoa. Here, we examined the key events that lead to formation of a proper kinetochore in a basidiomycetous budding yeast, *Cryptococcus neoformans*. We found that, during the progression of the cell cycle, nonclustered centromeres gradually clustered and kinetochores assembled in an ordered manner concomitant with partial opening of the nuclear envelope in this organism. These events have higher similarity to mitotic events of metazoans than to those previously described in other yeasts.**

Received 2 August 2013 **Accepted** 11 September 2013 **Published** 1 October 2013

Citation Kozubowski L, Yadav V, Chatterjee G, Sridhar S, Yamaguchi M, Kawamoto S, Bose I, Heitman J, Sanyal K. 2013. Ordered kinetochore assembly in the human-pathogenic basidiomycetous yeast *Cryptococcus neoformans*. mBio 4(5):e00614-13. doi:10.1128/mBio.00614-13.

Editor Judith Berman, University of Minnesota, GCD

Address correspondence to Kaustuv Sanyal, sanyal@jncasr.ac.in, and Lukasz Kozubowski, lukasz.kozubowski@duke.edu/lkozubo@clemson.edu.

High-fidelity chromosome segregation is essential for faithful propagation of genetic information. The process of chromosome segregation is powered by the dynamic interaction between the chromosomes and the spindle microtubules. The chromosomal attachment site of spindle microtubules is a multimeric proteinaceous structure formed on the centromere DNA, termed the kinetochore (KT) (1). An error in the KT-microtubule interaction can result in improper chromosome segregation, leading to aneuploidy, a hallmark of several cancers (2, 3).

While the trilaminar architecture of the KT is conserved from yeast to humans, structural and functional evolution of some of the KT proteins is evident (4). Among the three layers of the KT, the components of the inner layer that interact directly with DNA are conserved in organisms with regional centromeres (centromere DNA is >3 kb in length) (5). The centromere-specific histone H3 of the CENP-A/Cse4 family and CENP-C/Mif2 are two such evolutionarily conserved inner KT proteins (6). Several middle KT proteins, such as Mis12/Mtw1 and Nuf2, are present in most

AMERICAN SOCIETY FOR MICROBIOLOGY

mBio®

An ASM Access® Publication

PRODUCED IN ASSOCIATION WITH THE AMERICAN ACADEMY OF MICROBIOLOGY

SEPTEMBER/OCTOBER 2013 VOLUME 4 | ISSUE 5

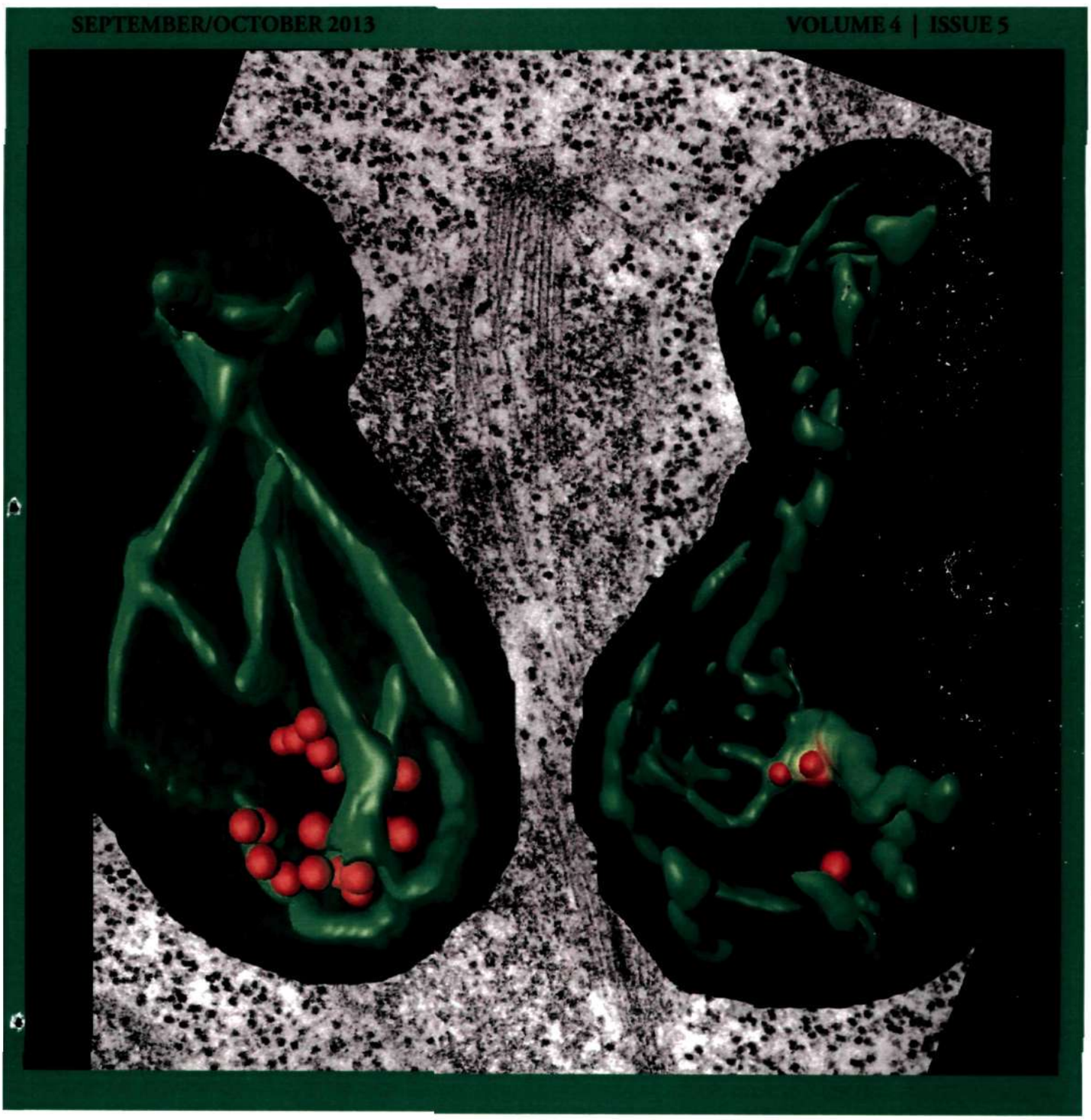

OPEN ACCESS Freely available online

PLOS | GENETICS

Analysis of the Genome and Transcriptome of *Cryptococcus neoformans* var. *grubii* Reveals Complex RNA Expression and Microevolution Leading to Virulence Attenuation

Guilhem Janbon[1,2]*, Kate L. Ormerod[3], Damien Paulet[4], Edmond J. Byrnes III[5¤], Vikas Yadav[6], Gautam Chatterjee[6], Nandita Mullapudi[7], Chung-Chau Hon[8], R. Blake Billmyre[5], François Brunel[9], Yong-Sun Bahn[10], Weidong Chen[11], Yuan Chen[5], Eve W. L. Chow[3], Jean-Yves Coppée[4], Anna Floyd-Averette[5], Claude Gaillardin[9], Kimberly J. Gerik[12], Jonathan Goldberg[13], Sara Gonzalez-Hilarion[1,2], Sharvari Gujja[13], Joyce L. Hamlin[14], Yen-Ping Hsueh[5,15], Giuseppe Ianiri[16], Steven Jones[17], Chinnappa D. Kodira[13], Lukasz Kozubowski[18], Woei Lam[12], Marco Marra[17], Larry D. Mesner[14], Piotr A. Mieczkowski[19], Frédérique Moyrand[1,2], Kirsten Nielsen[5,20], Caroline Proux[4], Tristan Rossignol[9], Jacqueline E. Schein[17], Sheng Sun[5], Carolin Wollschlaeger[1,2], Ian A. Wood[21], Qiandong Zeng[13], Cécile Neuvéglise[9], Carol S. Newlon[11], John R. Perfect[22], Jennifer K. Lodge[12], Alexander Idnurm[16], Jason E. Stajich[5,23], James W. Kronstad[24], Kaustuv Sanyal[6], Joseph Heitman[5]*, James A. Fraser[3], Christina A. Cuomo[13]*, Fred S. Dietrich[5]*

1 Institut Pasteur, Unité Biologie et Pathogénicité Fongiques, Département Génomes et Génétique, Paris, France, **2** INRA, USC2019, Paris, France, **3** University of Queensland, School of Chemistry and Molecular Biosciences, Brisbane, Queensland, Australia, **4** Institut Pasteur, Plate-forme Transcriptome et Epigénome, Département Génomes et Génétique, Paris, France, **5** Duke University Medical Center, Department of Molecular Genetics and Microbiology, Durham, North Carolina, United States of America, **6** Jawaharlal Nehru Centre for Advanced Scientific Research, Molecular Biology and Genetics Unit, Bangalore, India, **7** Genotypic Technology Private Limited, Bangalore, India, **8** Institut Pasteur, Unité Biologie Cellulaire du Parasitisme, Département Biologie Cellulaire et Infection, Paris, France, **9** INRA, UMR 1319 Micalis, Jouy-en-Josas, France, **10** Yonsei University, Center for Fungal Pathogenesis, Department of Biotechnology, Seoul, Republic of Korea, **11** Rutgers New Jersey Medical School, Department of Microbiology and Molecular Genetics, Newark, New Jersey, United States of America, **12** Washington University School of Medicine, Department of Molecular Microbiology, St. Louis, Missouri, United States of America, **13** Broad Institute of MIT and Harvard, Cambridge, Massachusetts, United States of America, **14** University of Virginia, Department of Biochemistry and Molecular Genetics, Charlottesville, Virginia, United States of America, **15** California Institute of Technology, Division of Biology, Pasadena, California, United States of America, **16** University of Missouri-Kansas City, School of Biological Sciences, Division of Cell Biology and Biophysics, Kansas City, Missouri, United States of America, **17** Canada's Michael Smith Genome Sciences Centre, BC Cancer Agency, Vancouver, British Columbia, Canada, **18** Clemson University, Department of Genetics and Biochemistry, Clemson, South Carolina, United States of America, **19** University of North Carolina, Department of Genetics, Chapel Hill, North Carolina, United States of America, **20** University of Minnesota, Microbiology Department, Minneapolis, Minnesota, United States of America, **21** University of Queensland, School of Mathematics and Physics, Brisbane, Queensland, Australia, **22** Duke University Medical Center, Duke Department of Medicine and Molecular Genetics and Microbiology, Durham, North Carolina, United States of America, **23** University of California, Department of Plant Pathology & Microbiology, Riverside, California, United States of America, **24** Michael Smith Laboratories, Department of Microbiology and Immunology, Vancouver, British Columbia, Canada

Abstract

Cryptococcus neoformans is a pathogenic basidiomycetous yeast responsible for more than 600,000 deaths each year. It occurs as two serotypes (A and D) representing two varieties (i.e. *grubii* and *neoformans*, respectively). Here, we sequenced the genome and performed an RNA-Seq-based analysis of the *C. neoformans* var. *grubii* transcriptome structure. We determined the chromosomal locations, analyzed the sequence/structural features of the centromeres, and identified origins of replication. The genome was annotated based on automated and manual curation. More than 40,000 introns populating more than 99% of the expressed genes were identified. Although most of these introns are located in the coding DNA sequences (CDS), over 2,000 introns in the untranslated regions (UTRs) were also identified. Poly(A)-containing reads were employed to locate the polyadenylation sites of more than 80% of the genes. Examination of the sequences around these sites revealed a new poly(A)-site-associated motif (AUGHAH). In addition, 1,197 miscRNAs were identified. These miscRNAs can be spliced and/or polyadenylated, but do not appear to have obvious coding capacities. Finally, this genome sequence enabled a comparative analysis of strain H99 variants obtained after laboratory passage. The spectrum of mutations identified provides insights into the genetics underlying the micro-evolution of a laboratory strain, and identifies mutations involved in stress responses, mating efficiency, and virulence.

Citation: Janbon G, Ormerod KL, Paulet D, Byrnes EJ III, Yadav V, et al. (2014) Analysis of the Genome and Transcriptome of *Cryptococcus neoformans* var. *grubii* Reveals Complex RNA Expression and Microevolution Leading to Virulence Attenuation. PLoS Genet 10(4): e1004261. doi:10.1371/journal.pgen.1004261

Editor: Michael Freitag, Oregon State University, United States of America

Received September 19, 2013; **Accepted** February 7, 2014; **Published** April 17, 2014

A comprehensive model to predict mitotic division in budding yeasts

Sabyasachi Sutradhar[a,*], Vikas Yadav[b,*], Shreyas Sridhar[b,*], Lakshmi Sreekumar[b], Dibyendu Bhattacharyya[c], Santanu Kumar Ghosh[d], Raja Paul[a], and Kaustuv Sanyal[b]

[a]Department of Solid State Physics, Indian Association for the Cultivation of Science, Kolkata 700032, India; [b]Molecular Mycology Laboratory, Molecular Biology and Genetics Unit, Jawaharlal Nehru Centre for Advanced Scientific Research, Jakkur, Bangalore 560064, India; [c]Tata Memorial Centre, Advanced Centre for Treatment Research and Education in Cancer, Kharghar, Navi Mumbai 410210, India; [d]Department of Biosciences and Bioengineering, Indian Institute of Technology, Bombay, Powai, Mumbai 400076, India

ABSTRACT **High-fidelity chromosome segregation during cell division depends on a series of concerted interdependent interactions. Using a systems biology approach, we built a robust minimal computational model to comprehend mitotic events in dividing budding yeasts of two major phyla: Ascomycota and Basidiomycota. This model accurately reproduces experimental observations related to spindle alignment, nuclear migration, and microtubule (MT) dynamics during cell division in these yeasts. The model converges to the conclusion that biased nucleation of cytoplasmic microtubules (cMTs) is essential for directional nuclear migration. Two distinct pathways, based on the population of cMTs and cortical dyneins, differentiate nuclear migration and spindle orientation in these two phyla. In addition, the model accurately predicts the contribution of specific classes of MTs in chromosome segregation. Thus we present a model that offers a wider applicability to simulate the effects of perturbation of an event on the concerted process of the mitotic cell division.**

Monitoring Editor
Alex Mogilner
University of California, Davis

Received: Apr 23, 2015
Revised: Aug 13, 2015
Accepted: Aug 14, 2015

INTRODUCTION

Mitosis is a fundamental cellular process that enables faithful transmission of genetic material to the subsequent generation in eukaryotes. This process is well coordinated and requires the cumulative effort of several macromolecular machineries, including the centromere–kinetochore complex, the mitotic spindle, microtubule organizing centers (MTOCs), molecular motors, and microtubule-associated proteins (MAPs). The foundation for this process of chromosome segregation is provided by a specialized chromatin structure, the centromere, upon which 60–80 proteins assemble to form the kinetochore (KT). The KT connects centromeric chromatin to the mitotic spindle. The mitotic spindle, nucleated by MTOCs, is a bipolar array of microtubules (MTs) that provides the force required to segregate chromosomes. This mitotic spindle is synergistically modulated by motor proteins (Mallik and Gross, 2004), the plus end–directed kinesins and the minus end–directed dyneins, and MAPs, which dynamically alter the rate of MT stability. The unequal rate of MT polymerization and depolymerization provides the push–pull forces that mediate poleward movement of segregated chromosomes into two daughter cells. Apart from requiring the assembly of the segregation machinery on the centromere and push–pull forces to enable chromosomes to segregate, proper spindle positioning and orientation is crucial for carrying out faithful segregation of chromosomes (Segal and Bloom, 2001; Kusch *et al.*, 2002).

In most organisms, MTs are largely localized to the cytoplasm until spindle formation begins during mitosis. These cytoplasmic MTs (cMTs) emanate from either multiple cytoplasmic MTOCs, as in metazoans, or from a single nuclear envelope (NE)-embedded MTOC, as in the budding yeast *Saccharomyces cerevisiae*. The cMTs, along with motor proteins, influence nuclear positioning and

This article was published online ahead of print in MBoC in Press (http://www.molbiolcell.org/cgi/doi/10.1091/mbc.E15-04-0236) on August 26, 2015.

*These authors contributed equally to this work.

Address correspondence to: Kaustuv Sanyal (sanyal@jncasr.ac.in) or Raja Paul (ssprp@iacs.res.in).

Abbreviations used: cMT, cytoplasmic microtubule; DAPI, 4′,6-diamidino-2-phenylindole; GFP, green fluorescent protein; ipMT, interpolar microtubule; kMT, kinetochore microtubule; KT, kinetochore; MAP, microtubule-associated protein; MBC, methyl benzimidazole carbamate; MT, microtubule; MTOC, microtubule organizing center; NE, nuclear envelope; SPB, spindle pole body; SPOC, spindle positioning checkpoint.

Supplemental Material can be found at:
http://www.molbiolcell.org/content/suppl/2015/08/24/mbc.E15-04-0236v1.DC1.html

ascb
an international forum for cell biology

MBoC

MOLECULAR BIOLOGY OF THE CELL

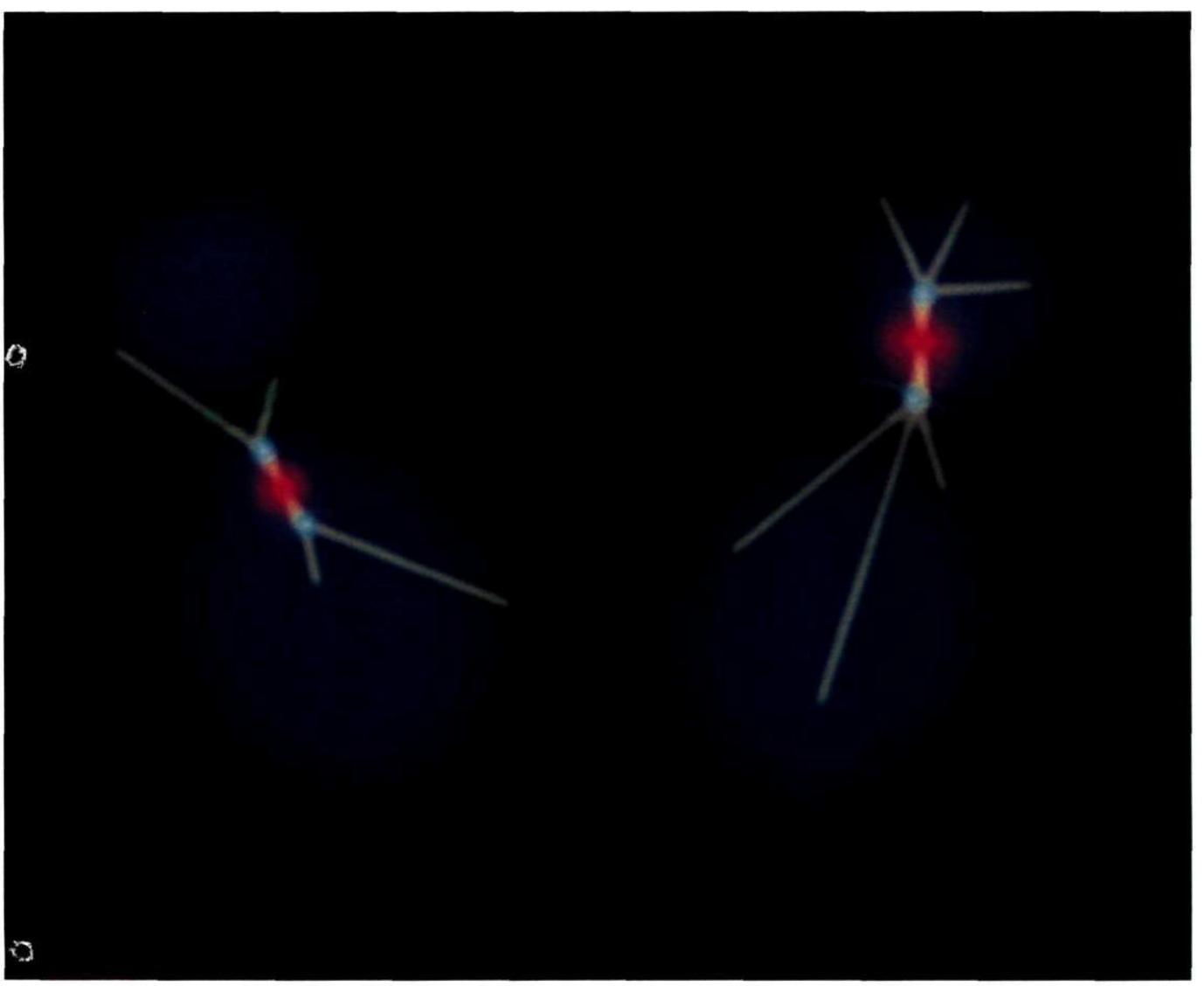

VOLUME 26 • NUMBER 22 • NOVEMBER 5, 2015

SECOND SPECIAL ISSUE ON QUANTITATIVE CELL BIOLOGY

PLOS | BIOLOGY

RESEARCH ARTICLE

Fungal genome and mating system transitions facilitated by chromosomal translocations involving intercentromeric recombination

Sheng Sun[1], Vikas Yadav[2], R. Blake Billmyre[1], Christina A. Cuomo[3], Minou Nowrousian[4], Liuyang Wang[1], Jean-Luc Souciet[5], Teun Boekhout[6,7], Betina Porcel[8,9,10], Patrick Wincker[8,9,10], Joshua A. Granek[1], Kaustuv Sanyal[2], Joseph Heitman[1]*

1 Department of Molecular Genetics and Microbiology, Duke University Medical Center, Durham, North Carolina, United States of America, **2** Molecular Biology and Genetics Unit, Jawaharlal Nehru Centre for Advanced Scientific Research, Bangalore, India, **3** Broad Institute of MIT and Harvard, Cambridge, Massachusetts, United States of America, **4** Lehrstuhl für Allgemeine und Molekulare Botanik, Ruhr-Universität Bochum, Bochum, Germany, **5** Université de Strasbourg, CNRS UMR7156, Strasbourg, France, **6** Westerdijk Fungal Biodiversity Institute, Utrecht, The Netherlands, **7** Institute for Biodiversity and Ecosystem Dynamics (IBED), University of Amsterdam, Amsterdam, The Netherlands, **8** Commissariat à l'Energie Atomique (CEA), Institut de Génomique (IG), Genoscope, Evry, France, **9** Université d'Evry, UMR 8030, Evry, France, **10** Centre National de Recherche Scientifique (CNRS), UMR 8030, Evry, France

* heitm001@duke.edu

Citation: Sun S, Yadav V, Billmyre RB, Cuomo CA, Nowrousian M, Wang L, et al. (2017) Fungal genome and mating system transitions facilitated by chromosomal translocations involving intercentromeric recombination. PLoS Biol 15(8): e2002527. https://doi.org/10.1371/journal.pbio.2002527

Academic Editor: Kenneth Wolfe, University College Dublin, Ireland

Received: March 23, 2017

Accepted: July 25, 2017

Published: August 11, 2017

.ta Availability Statement: All relevant data can e accessed through NCBI BioProject accession o. PRJNA200571 and EBI accession no. ?RJEB1993.

Funding: Senior Research Fellow of Council of Scientific and Industrial Research (CSIR), Govt. of India (grant number 09/733(0179)/2012/EMR-I) received by VY. The funder had no role in study design, data collection and analysis, decision to publish, or preparation of the manuscript.

Abstract

Species within the human pathogenic *Cryptococcus* species complex are major threats to public health, causing approximately 1 million annual infections globally. *Cryptococcus amylolentus* is the most closely known related species of the pathogenic *Cryptococcus* species complex, and it is non-pathogenic. Additionally, while pathogenic *Cryptococcus* species have bipolar mating systems with a single large mating type (*MAT*) locus that represents a derived state in Basidiomycetes, *C. amylolentus* has a tetrapolar mating system with 2 *MAT* loci (*P/R* and *HD*) located on different chromosomes. Thus, studying *C. amylolentus* will shed light on the transition from tetrapolar to bipolar mating systems in the pathogenic *Cryptococcus* species, as well as its possible link with the origin and evolution of pathogenesis. In this study, we sequenced, assembled, and annotated the genomes of 2 *C. amylolentus* isolates, CBS6039 and CBS6273, which are sexual and interfertile. Genome comparison between the 2 *C. amylolentus* isolates identified the boundaries and the complete gene contents of the *P/R* and *HD MAT* loci. Bioinformatic and chromatin immunoprecipitation sequencing (ChIP-seq) analyses revealed that, similar to those of the pathogenic *Cryptococcus* species, *C. amylolentus* has regional centromeres (*CEN*s) that are enriched with species-specific transposable and repetitive DNA elements. Additionally, we found that while neither the *P/R* nor the *HD* locus is physically closely linked to its centromere in *C. amylolentus*, and the regions between the *MAT* loci and their respective centromeres show overall synteny between the 2 genomes, both *MAT* loci exhibit genetic linkage to their respective centromere during meiosis, suggesting the presence of recombinational suppressors and/or epistatic gene interactions in the *MAT-CEN* intervening regions. Furthermore,